AN INVESTIGATION OF LARGE-SCALE HEAT TRANSFER PROCESSES AND SEA-SURFACE TEMPERATURE FLUCTUATIONS IN THE NORTH PACIFIC OCEAN

by

NATHAN EDWARD CLARK

Sc.B., Brown University
(1962)

WITHDRAWN FROM MIT LIBRARIES
LINDGREN

SUBMITTED IN PARTIAL FULFILLMENT
OF THE REQUIREMENTS FOR THE
DEGREE OF DOCTOR OF
PHILOSOPHY
at the

MASSACHUSETTS INSTITUTE OF
TECHNOLOGY
May, 1967

Signature of Author.....
Department of Meteorology, May 12, 1967

Certified by.....
Thesis Supervisor

Accepted by.....
Chairman, Departmental Committee
on Graduate Students

AN INVESTIGATION OF LARGE-SCALE HEAT TRANSFER PROCESSES AND SEA-SURFACE TEMPERATURE FLUCTUATIONS IN THE NORTH PACIFIC OCEAN

by

Nathan Edward Clark

Submitted to the Department of Meteorology on May 12, 1967, in partial fulfillment of the requirement for the degree of Doctor of Philosophy.

ABSTRACT

The atmospheric and oceanic parameters of sea-surface temperature, air temperature, wet-bulb temperature, cloud cover, and wind speed are used to compute monthly average values of the incoming radiation, the effective back radiation, the latent and sensible heat transfers, and the total heat transfer across the sea surface over the North Pacific Ocean from 20°N to 55°N for the period extending from 1951 through 1957.

The yearly average of the total heat flux across the surface is integrated over the ocean from 15°N to 60°N, and it is found that the ocean loses 7×10^{14} cal/sec in this area on a yearly average basis.

The 12 monthly 7-year mean or normal values for each heating term are Fourier analyzed, and it is found that each term has a regular yearly cycle with maxima and minima separated by 6-month intervals. The yearly cycles of the sea-surface temperature are compared to the yearly cycles of the total heat transfer across the ocean surface, and it is found that the sea-surface temperatures have their maximum values near the end of the heating cycle (August or September) and have their minimum values at the end of the cooling cycle (February or March). These results agree with the theoretical results of a one-dimensional model of the seasonal thermocline.

The normal values of the 12 monthly means of the heat advection in the surface layer of the ocean are determined as residuals from the surface layer heat balance equation. The results obtained agree fairly well with what is known about current patterns of the North Pacific and also with the results of another independent investigation.

The departures of each monthly value from the normal values, i.e. the monthly anomalies, are computed for each of the heating terms and also for the sea-surface and air temperatures

for all 84 months. It is found that the sea-surface temperature anomaly patterns are geographically coherent, that they can be fairly extensive in geographic size, and that on the average they persist in time to about three months or slightly longer. The air temperature anomalies are greater in magnitude but are closely related in time to those of the sea-surface temperature. The persistence of sea-surface temperature anomalies is related to the dynamics of forced and free convection within the upper mixed layer of the ocean and to the transfer of heat through the seasonal thermocline.

The anomaly patterns of the heating terms also show geographic coherence but have little month-to-month persistence.

Correlation studies between the anomaly series of the month-to-month change in sea-surface temperature and those of the total heat transfer across the sea surface and also those of the horizontal temperature advection due to wind drift show that there are statistically significant relations between these quantities. The positive correlation is improved by adding the temperature change due to surface heat transfer to the temperature change due to horizontal advection and correlating the results with the observed sea surface temperature changes.

A multiple linear correlation analysis between the three terms, (1) the observed change in sea-surface temperature, (2) the sum of temperature change due to surface heat transfer and that due to horizontal advection, and (3) the vertical velocity induced beneath the Ekman layer, shows that the percentage of variance of the first term accounted for by relation to other variables is increased from 20 to 25 per cent in winter, 13 to 18 per cent in spring, 12 to 18 per cent in summer, and 13 to 19 per cent in fall by including the effects of the third term as well as the second.

A statistically significant positive correlation is found between the anomaly series of the sea-surface temperature and those of the specific humidity of the air, indicating that the amount of moisture in the surface layer of the atmosphere over the ocean is a function of the sea-surface temperature.

A statistically significant positive correlation is also found between the anomaly series of the latent heat transfer between ocean and atmosphere and those of the atmospheric water vapor divergence field. It is felt that this type of analysis, if applied to a smaller area with better data, would be helpful in obtaining a better transfer formula for the latent heat flux.

Thesis Supervisor: Hurd C. Willett
Title: Professor of Meteorology

TABLE OF CONTENTS

List of Figures

List of Tables

I. Introduction

A. Review of Sea-Surface Temperature Fluctuation Studies

In 1920 Helland-Hansen and Nansen conducted their pioneering investigation into the causes of large-scale fluctuations in sea-surface temperatures. Since then numerous studies have been made concerning this intriguing and elusive problem. In each case, an attempt was made to relate large-scale anomalies of sea-surface temperature to fluctuations in space and time of various meteorological and oceanographic parameters, wind speed, surface drift currents, solar radiation, etc. Helland-Hansen and Nansen began by correlating sea-surface temperature changes in the North Atlantic Ocean with anomalies of the north-south component of the geostrophic wind. Their results indicated that the temperature anomalies were strongly related to the wind anomalies and that they were not transported to any great degree by the motion of sea-surface currents. These results were supported by the work done by Neumann, Fisher, Pandolfo and Pierson (1958) and by J. Bjerknes (1962) in the same region.

Bjerknes demonstrated that it is probably the interplay between the time changes in Q_a, the net transfer of heat to the atmosphere including both latent and sensible heat, and those of Q_v and Q_d, the advective heat supply and heat supply due to up-welling, that regulates the trends of sea-surface temperature. He found that a long trend of cooling north of

50°N extending from the 1890's to the early 1920's is accompanied by a strengthening of the Icelandic low, and the warming trend of sea-surface temperatures until the early 1940's is accompanied by a weakening of the Icelandic low. Superposed on the long cooling trend, rising and falling trends of 2 to 5 years durations were found. In these trends the ocean always cooled when the prevailing west wind strengthened and warmed up when the wind weakened. During the long trend of northern cooling from the 1890's to the early 1920's, the surface water warmed up west and north of the subtropical high pressure zone, presumably because of increased wind and Gulf Stream advection.

The statistics presented by Bjerknes indicate only that increased wind speed is accompanied by a cooling of the underlying surface waters and vice versa in some regions of the North Atlantic. The other mechanisms postulated for the strengthening or reversal of these trends must depend upon physical explanations which are based upon experience obtained from further investigations. At present, there is no way to test the hypothesis that the trend of cooling of the sea surface due to increased west winds is reversed by an increase in Gulf Stream advection, since heat transport cannot be determined from the mean mass flow, which is the only quantity that can be computed from wind-driven current theory.

The results obtained by Neumann et al indicate that the

same negative correlation exists between the zonal index of atmospheric circulation over the North Atlantic and the surface temperature anomaly on a monthly time scale. Their work also supports the idea that the temperature anomalies are not advected to any great extent by surface drift. Correlations between anomalies (departure from a normal value for a given month) of sea-surface temperature for adjacent areas at time lags in 2-month increments from 0 to 24 months were computed. The coefficients were significantly highest when simultaneous anomalies were correlated. This indicates that processes causing simultaneous changes over large areas, such as evaporation and surface divergence, are probably more important than advection.

Namias (1959) has attempted to explain the warming of the surface waters of the Eastern North Pacific Ocean during 1957 and 1958 by relating it to the abnormal velocity components of the atmospheric circulation. Although he obtained some of the gross features of the observed temperature distribution, his method is open to at least two objections. The first is that he considered a normal (time average) state of the atmosphere for a particular region to correspond to a normal state of the sea-surface temperature distribution for the same region. From the anomalous wind components, he computed the anomalous surface water displacements which, when placed over the normal

pattern of sea-surface temperature for the period in question, enabled him to compute the anomalies of temperature due to advection of the surface water. The second objection is that of using only the surface water advection term from the heat budget equation for a local surface layer (see Chapter II).

Namias (1965) modified this procedure somewhat and computed the anomalous drift of surface water as before but used an observed set of isotherms instead of the normal set in order to compute the advection of temperature anomalies. His correlation coefficients were improved somewhat over those of the previous work. However, the horizontal advection term was still the only term evaluated, although he did mention the possible effects of up-welling associated with the divergence of the wind field and the transfer of latent and sensible heat across the sea surface.

Arthur (1966) has extended Namias' work to include the effects of the normal and anomalous wind drift currents on the anomalous temperature gradients that occur within a specified period of time. His method thus takes account of all terms in the horizontal temperature advection equation,

$$\theta'(t_2) = \theta'(t_1) - \int_{t_1}^{t_2} \left[(U+u') \frac{\partial \theta'}{\partial x} + (V+v') \frac{\partial \theta'}{\partial y} \right] dt \qquad \text{(I.1)}$$

$$- \int_{t_1}^{t_2} \left[u' \frac{\partial \bar{\theta}}{\partial x} + v' \frac{\partial \bar{\theta}}{\partial y} \right] dt \,,$$

where the capital letters denote the basic or normal values, the primes denote the anomalies, and t_1 and t_2 denote the beginning and end of the period in question. The first and third terms on the right-hand side of the equation are identified as the steps in Namias' method, while the second term represents Arthur's extension. Again, both the effects of local changes in surface heat transfer and of vertical velocities are neglected. In fact, the assumption is made that

$$\frac{\partial \Theta}{\partial t} = -U\frac{\partial \Theta}{\partial x} - V\frac{\partial \Theta}{\partial y} - W\frac{\partial \Theta}{\partial z} + Q \qquad \text{(I.2)}$$

in which the normal change in sea-surface temperature is balanced by the effects of the normal surface heat transfer, Q. At present, evaluations of the extension are being carried out at the Extended Forecast Division of the U. S. Weather Bureau.

A much more rigorous approach was adopted by Berson (1962) in which he attempted to determine from both theory and data the two major effects on the heat balance in the surface layer of the ocean, the effect on latent and sensible heat transfer from the ocean, and the effect on the intensity of vertical mixing and on horizontal transport within the upper mixed layer from variable large-scale surface wind systems. His results

(determined from data for a middle latitude zone of the North Pacific Ocean during September 1959 through August 1960) indicate that in the central longitudes and during autumn and winter when anomalies of net radiation are small, a large proportion of the anomalous evaporation and turbulent heat conduction is generally tapped from the accumulation of heat due to the effect of wind stress anomalies on advection. He also developed a numerical method, including both advection and surface heat transfer, for computing sea-surface temperature anomaly changes when the wind stresses are given.

Berson concluded that feedback from ocean to atmosphere can be treated numerically by subtracting the thermal energy equation of the troposphere from the thermal energy equation of the active layer of the ocean and obtaining a differential equation expressing the exchange of heat across their common boundary. The main problem in this method is in determining the changes in the depth of the mixed layer or seasonal thermocline of the sea. Since very little data on this quantity exists, he is forced to use a linear relationship between wind speed and layer depth determined from various ocean stations in the North Pacific. This relationship holds only for the monthly changes during a particular year and not for changes in the same month over many years. During the study presented below, data from ocean station PAPA (50°N-145°W) was looked at and it was found that the linear relationship

varies from year to year and that no simple relationship holds for changes from year to year for a particular month.

Roden (1962, 1963) has made a number of studies on the power spectra of various meteorological and oceanographic variables. In his 1962 paper, he investigated records of sea-surface temperature, cloudiness and wind speed for eight ocean areas between Europe and South America. He looked at the frequency range between zero and six cycles per year and found that most of the power of temperature anomalies is concentrated at low frequencies and that there are no periodicities, that a significant and inverse relation exists between temperature and wind anomalies in the NE trade wind regions, and that along the Brazilian coast there is a direct relation between temperature and north wind anomalies and an inverse relation between temperature and east wind anomalies. He found no relation between temperature and cloud cover, implying that solar radiation anomalies are not important in determining sea-surface temperature changes.

Probably the most ambitious program being conducted at present is that of the Fleet Numerical Weather Facility (FNWF) at Monterey, California. Based on the theoretical work of Laevastu (1960) and data collected on a world-wide basis from naval vessels, analyses and forecasts are made of wave structure, surface currents, thermal structure, surface heat transfer, mixed layer depth, and sound channels. The analyses are made

twice daily at 00Z and 12Z and 24-hour forecasts are made on a daily basis. The results are sent out via high-speed computer data links to the Fleet Weather Centrals where they are plotted on local area charts and transmitted in facsimile or message form to fleet users.

The synoptic oceanographic analyses made at Monterey show that pronounced changes in the surface layers of the ocean are quite common. The sea-surface temperature (SST) changes can frequently be of the order of half the annual range and, in some areas, can even exceed the total annual range. The studies indicate that the average period of the SST changes is shorter (a few days) in higher latitudes, the areas of passing cyclones, than in the lower latitudes where semi-permanent anticyclones predominate. The magnitudes of the changes are usually largest near the stronger gradients of SST (current boundaries) and smallest in areas of small horizontal gradients. The explanation of these synoptic changes can, in most cases, be found in the atmospheric driving forces affecting both the dynamics of the ocean surface layer and the surface heat transfer.

The advective changes by surface currents, computed according to a method derived by Whitting in 1909 and described in Chapter V, are quite apparent on the analyzed charts and account for a major part of the SST anomalies in some areas. Changes caused by surface heat exchange and vertical velocities in the mixed layer can be as large as 1.5°F in a 24-hour period, and

as large as 5°F at middle and high latitudes during the summer season. These driving forces change in the same way as the weather conditions at the surface. Thus, the changes in the surface layers of the sea normally change at least as rapidly as does the surface weather, and it is concluded that oceanographic analyses and forecasts should be carried out with the same frequency as those of the surface weather.

In working with their data, the FNWF define three types of SST anomalies: (1) a deviation in a given region at a specified time from the normal or long-period average for the same region, (2) the difference between a temperature actually observed and some reference temperature, and (3) deviations of SST values at given places from smoothed latitudinal values for the same period of time. Some conclusions drawn regarding the first type of anomaly are that they are relatively large in horizontal extent, that some of them can be persistent over long periods while some appear and disappear quite rapidly, and that some of the anomalies migrate with the average surface current.

The computation of the third type of anomaly is done numerically by scale and pattern separation. The method consists of repeated application of a smoothing operator which reduces first the amplitudes of the shortest wave lengths and gradually affects longer and longer wave lengths. Removal

of small-scale disturbances from the initial analysis leaves the large-scale pattern; finally, removing the zonal portion of the large-scale pattern gives the large-scale anomalies.

The large-scale anomalies change slowly from season to season with fluctuations occurring as the surface weather changes over the areas, while the small-scale anomalies can be classified into two additional groups. The first of these corresponds to changes induced by local up-welling, heat exchange, and mixing. The second group consists of those caused by advection and meanders along current boundaries and eddies; analysis of the advection anomalies at major current boundaries shows that they are persistent to the extent that changes occur according to the prevailing local winds. In general, warming occurs ahead of cold fronts (when southwesterly winds are prevalent), and cooling occurs after frontal passages (when northerly winds prevail).

In addition to oceanographic analyses and forecasts, surface weather forecasts are also made on a daily basis which take into account the exchange of heat between the ocean and atmosphere. Thus, we have an operational system that uses the information obtained from detailed studies of air-sea interaction processes.

B. Review of Ocean Surface Layer Heat Transfer Studies

An extensive review of this subject is given by Malkus in Volume I of The Sea, Chapter 4. The following will briefly touch on the works mentioned in this review as a background to the description of air-sea interaction studies that have been conducted since the publication of The Sea in 1962.

The transfer of heat between ocean and atmosphere by turbulent conduction and the flux of water vapor may be determined indirectly by two independent methods. The first is that of using energy and mass budget requirements, while the second method depends upon the use of exchange formulas that have been developed from the laws of small-scale molecular and turbulent transfer.

In the energy budget method of determining the heat flux, the following equation is used to express the balance between the amount of heat absorbed by the sea surface due to radiation, the amount of this heat transported by ocean currents, and the amount of heat supplied to the atmosphere:

$$R = Q_s + Q_e + S + Q_v \ , \qquad \text{(I.3)}$$

where R is the radiation surplus and equals the solar radiation minus that which is reflected from the surface and that which is reradiated back into space; Q_s is the amount of sensible heat

that is transferred between ocean and atmosphere; Q_e is the amount of latent heat given up by the sea due to evaporation; S is the amount of heat stored in the ocean; and Q_v is the amount of heat advected by ocean currents. The total exchange, $Q_s + Q_e$, between ocean and atmosphere may then be computed from the relation,

$$Q_s + Q_e = R - S - Q_v \qquad (I.4)$$

The main studies using this procedure have been conducted by Sverdrup (1942), Jacobs (1951), Budyko (1956), London (1957) and Houghton (1954), each of whom attempted to evaluate $Q_s + Q_e$ using various methods of computing R. The critical variable affecting R is the amount and type of cloud cover in the area under investigation. In his work, Budyko showed that the incoming radiation is approximately a linear relation of the mean cloudiness, while the long-wave back radiation decreases in a non-linear fashion with the mean cloudiness. For annual averages, the storage S and the flux-divergence Q_v were considered negligible in comparison to the other terms.

According to Malkus (1960),the most important demonstration in marine meteorology of the past twenty years (Jacobs, 1951; Montgomery, 1940; Bunker, 1960; Riehl et al, 1951) is that the

transfer of latent and sensible heat and momentum from sea to air is governed largely by two parameters, the air-sea property difference of temperature or vapor pressure and the prevailing wind speed averaged over some time period. Thus, while the average air-sea fluxes over long periods and large regions are computable from planetary heat and mass budget requirements, the fluctuations which build this picture and give rise to the enormous departures from it are directly related to transient atmosphere phenomena.

The basic premise underlying this development is that turbulent exchange is the dominant mechanism affecting the vertical distribution of a property from the air-sea interface to a distance of several tens of meters above it, so that the fluxes obey the equation,

$$F_p = -K_p \frac{dp}{dz} , \qquad (I.5)$$

where F_p is the flux of the property p, dp/dz is the vertical gradient of the property, and K_p is the eddy transfer coefficient which is many orders of magnitude larger than the corresponding molecular transfer coefficient. Thus, using the above equation and making several assumptions about the nature of the turbulence, equations can be derived relating the flux of momentum, water vapor and sensible heat to a wind speed at

some height and the difference between the property at that height and at the sea surface (see Chapter II).

The main works using this method that are reviewed by Malkus are those of Budyko (1955, 1956), Drozdov (1953), Jacobs (1951, 1951a), Sverdrup (1957), London (1957) and Houghton (1954). The annual mean distribution of Q_e and Q_s and the other heat-balance components of the sea surface are presented. The resulting annual heat budget of the ocean forms a foundation for discussing the global heat and water budgets, the climatological picture of air-sea heat exchange, and the average seasonal variation in several regions of this exchange. She also reviews a study done by Colon (1960) in which he used both the energy budget method and the transfer equation method to investigate the monthly and seasonal distribution of the various components of the surface layer heat balance equation for the Caribbean Sea.

As a result of the observations of solar radiation made during the International Geophysical Year, Budyko (1963) has completed a new Atlas of the heat balance of the earth. The Atlas contains 69 world charts including the annual means of solar radiation reaching the earth's surface, the radiation balance of the earth's surface, and the heat exchange between ocean and atmosphere due to evaporation and turbulent heat conduction. It also contains charts of the mean annual con-

ditions of the redistribution of the heat in the oceans due to ocean currents, of the radiation balance of the surface atmosphere, of the heat of condensation, and of the redistribution of heat in the atmosphere due to atmospheric motion. The charts are considered to be more accurate and are more detailed than those presented in the Atlas prepared in 1956.

Some of the results obtained from this study are that the meridional transfer of heat in the world oceans is about 60 per cent of the heat transfer of the atmosphere, that the components of heat balance of the Atlantic, Pacific, and Indian Oceans differ slightly from each other, and that for each ocean the main part of the heat of the radiation balance is expended on evaporation. It was also determined that the earth absorbs 168 kcal/cm^2 annually. Two-thirds of this amount, 112 kcal/cm^2/yr, is absorbed at the earth's surface, while the rest is absorbed by the atmosphere. The earth's surface loses 40 kcal/cm^2 per year by effective long-wave radiation, and, as a result, its average radiation balance is equal to 72 kcal/cm^2/yr. Of this amount, 59 kcal/cm^2/yr is expended on evaporation, and 13 kcal/cm^2/yr is expended on the turbulent loss of heat to the atmosphere.

Wyrtki (1965, 1966) has used climatic data obtained from the U. S. Bureau of Commercial Fisheries to calculate the heat exchange at the surface of the Pacific Ocean north of 20°S

for the period 1947 to 1960. In the 1965 study, the average annual components of the surface heat transfer are given along with the implications of their distribution with regard to ocean circulation. It was found that the North Pacific gains heat at a rate of 3×10^{14} cal/sec. The heat gain occurs mainly along the eastern side of the ocean and south of 25°N, while the main heat loss occurs in the region of the Kuroshio Current. From a simple theoretical model, Wyrtki found that the average temperature distribution in the range of the subtropical anticyclone is maintained in the presence of these heat sources and sinks by a horizontal circulation of the order of 10 million m^3/sec in a shallow surface layer.

The 1966 study is an atlas of the monthly variation of heat exchange and surface temperature north of 20°S in the North Pacific Ocean. He used the same data as that of the 1965 study and averaged them over two-degree latitude-longitude squares and by months for the 1947 to 1960 period. For each ten degree square, the seasonal variation of the heat transfer components, the total heat exchange at the surface, and the sea-surface temperature were presented.

The U. S. Bureau of Commercial Fisheries at La Jolla, California, began to publish monthly charts of meteorological variables and heat transfer at the air-sea interface in 1965 (Johnson, Flittner and Cline; 1965). The data are collected

from synoptic marine radio weather reports from ships at sea and analyzed by electronic computer. The analyzed results are prepared in chart form covering the entire North Pacific Ocean and distributed to participating and interested agencies.

In 1965 Garstang reported the results of a project designed to study the role of diurnal variations of sensible and latent heat over the tropical ocean. The transfer equations used incorporate a drag coefficient that is linearly dependent upon wind speed and atmospheric stability. It was found that pronounced diurnal variations in sensible heat transfer occur along with semi-diurnal oscillations in cloudiness and precipitation. Within synoptic scale disturbances the transfer of either sensible or latent heat may increase by an order of magnitude. Integrated over the entire disturbance, the energy flux is found to double the undisturbed values. Since the role of the energy input to the systems is fundamental to understanding the structure and behavior of both synoptic and mesoscale systems, he concludes that emphasis should be placed on including these variable quantities in prediction schemes.

Due to the fact that the distribution of energy transfer is strongly dependent upon the frequency of synoptic scale systems, mean maps based on climatological data bear little relation to the actual synoptic maps of energy flux. The transfers also differ in magnitude in the tropical regions

from the values given by previous investigations (e.g. Budyko, 1956) and indicate that a revision may need to be made on the current estimates of the heat balance of the world oceans.

Kraus and Morrison (1966) have conducted a statistical analysis of wind, air, dew-point, and sea-surface temperature records from all nine weather ships in the North Atlantic Ocean. The study showed that local variations between years are highly significant when compared to variations within months. The fluctuations show a consistent pattern of more that 500 miles in the atmosphere and a persistence over several months. The horizontal extent of sea-surface temperature anomalies appears to be small; however, they tend to be more persistent than the air temperature anomalies. It was also found that short-period variations in the flux of latent and sensible heat are due predominantly to atmospheric variations. This effect is greatest in the winter; during the summer the effect of sea-surface temperature anomalies is somewhat greater. The values obtained for the heat fluxes were higher than those given by Jacobs (1951) and may be due to the different record periods used or the absence of a correction term in Jacobs' work due to the covariance between the meteorological variables of wind speed and air-sea temperature difference and between wind speed and air-sea vapor pressure difference on a daily basis.

C. Purpose of Thesis

The purpose of this work is to determine what relationships, if any, exist between the atmospheric parameters of wind speed, water vapor content, cloud cover and radiation and the monthly and seasonal fluctuations of sea-surface temperature and of heat transfer between the ocean and atmosphere. The data used in this study are much more extensive (7 years, 1951-1957, of data covering the North Pacific Ocean from 20°N to 55°N) than any that have been analyzed previously, and it is felt that much information has been obtained concerning the interaction of the two media.

It is obvious from the review of previous studies that it is necessary to include the effects of both surface advection and local heat transfer in order to account for fluctuations in time and space of the sea-surface temperature. An attempt is made in this report to relate fluctuations in the transfer of heat between ocean and atmosphere and fluctuations in the surface advection of heat due to wind-drift to fluctuations in the sea-surface temperature.

Chapter II of the report outlines the theoretical considerations behind the transfer formulas used in the study. Chapter III describes the type of data available and the procedures used to put the data into a workable form. Chapter IV discusses the results of the heat transfer computations and also the relations between the yearly cycle of the total

heat transfer across the sea surface and the yearly cycles of the sea-surface and air temperatures. Chapter V describes the spatial and temporal scales of anomaly patterns (an anomaly is the monthly departure of a value from some calculated mean or normal value) of the heat transfer terms and of the sea-surface and air temperatures; it also discusses the results of correlation studies made between the time series of the heat transfer term anomalies and those of the sea-surface temperature anomalies. Chapter VI describes the results of further correlation studies made between other atmospheric and oceanic paramteres. Finally, Chapter VII summarizes the results of the previous chapters and discusses areas of possible future studies of this and other types.

II. Theory

A. Development of Surface Layer Heat Balance Equation

For a column of water of unit cross-sectional area and of depth -D (z positive upwards), the heat balance equation may be written as

$$\rho c \int_0^t \int_{-D}^{0} \frac{dT_s}{dt} dz\, dt = \int_0^t Q_r\, dt - \int_0^t Q_a\, dt + \int_0^t \int_{-D}^{0} Q_v\, dz\, dt + \int_0^t Q_D\, dt, \quad \text{(II.I)}$$

where T_s is the temperature of a unit volume of water, Q_r is the radiation surplus, Q_a is the sum of latent and sensible heat transfer between ocean and atmosphere, Q_v is the horizontal advection of heat into the column, and Q_D is the vertical flux of heat into the column at the depth -D. This equation expresses the relationship that exists over the time interval t between the storage of heat in the column of water and the total exchange of heat energy between the column and its environment.

B. Development of Heat Transfer Formulas

1. The radiation balance Q_r may be broken up into three terms, Q_i, Q_R and Q_b where

$$Q_r = Q_i - Q_R - Q_b, \text{ and} \quad \text{(II.2)}$$

Q_i is the incoming solar radiation reaching the earth's surface, and Q_b is the effective back radiation equal to the difference

between the long wave radiation from the sea surface and the long wave radiation from the atmosphere.

The incoming radiation Q_i (cal/cm^2/day) is determined from the following equation proposed by Berliand (1960),

$$Q_i = Q_{io} (1 - ac - bc^2) , \qquad \text{(II.3)}$$

where Q_{io} is the incoming solar radiation with a clear sky, c is the fractional cloud cover, b is a constant equal to .38, and a is a function of latitude varying from .37 at 20° to .41 at 55°. The values of Q_{io} are taken from a table given by Berliand (1960) as a function of latitude and month.

The amount of radiation reflected from the sea surface Q_R is determined from

$$Q_R = Q_i \cdot r , \qquad \text{(II.4)}$$

where r is the percentage of radiation reflected and given in a table by Budyko (1965) as a function of latitude and month. Cox and Munk (1955) have calculated r taking into account the effect of wind speed on the nature of the reflecting sea surface. However, between 20°N and 55°N their values do not differ significantly from those of Budyko.

2. The effective back radiation Q_b (cal/cm^2/day) is determined from the semi-empirical equation proposed by Berliand

and Berliand (1952),

$$Q_b = S\sigma\theta_s^4(.39-.050\sqrt{e})(1-kc^2)+4\sigma S\theta_s^3(\theta_s-\theta_a) \quad \text{(II.5)}$$

where S = .97 is the ratio of the radiation of the sea to that of a black body;

$\sigma = 1.75 \times 10^{-7}$ is the Stefan-Boltzmann constant;

θ_{sea}, θ_{air} are the absolute temperatures(^oC) ;

e is vapor pressure of the air in mb;

c is the fractional cloud cover; and

k is a function of the latitude.

The first term, which takes into account the effect of sea-surface temperature, humidity, and cloudiness, varies between 20 and 200 cal/cm^2/day. The constant k has been evaluated considering the vertical extent of clouds as well as the height of the cloud base from the earth's surface; it varies from .51 at the equator to .75 at 55°N due to the decrease in cloud base height in the polar regions. The second term represents the effect of stability on the back radiation and varies between -20 and 20 cal/cm^2/day.

3. The exchange of latent and sensible heat between ocean and atmosphere may be determined from the theory of turbulent transfer and some assumptions about the nature of the wind field just above the sea surface.

If turbulent exchange is the dominant mechanism affecting the vertical distribution of a property near the surface, then the vertical flux of the property p obeys the equation

$$Fp = -Kp \frac{dp}{dz}, \tag{II.6}$$

where Kp is the eddy transfer coefficient. For heat and water vapor, Fp is constant in the vertical in a thin boundary layer in which heat and water vapor are not accumulating. In the lowest few tens of meters over the sea surface, the air is well-stirred, shear-turbulence dominated, neutrally stable and barotropic. Under these conditions, the following exchange formulas may be used to determine the flux of momentum τ, sensible heat Q_s and latent heat Q_e:

$$\tau = Km \frac{du}{dz}, \tag{II.7}$$

$$Q_s = -cpKs \frac{dT}{dz}, \text{ and} \tag{II.8}$$

$$Q_e = LE = -LK_e \frac{dq}{dz}, \tag{II.9}$$

where Km, Ks and Ke are the eddy exchange coefficients of momentum, sensible heat and water vapor, u is the wind speed, T is the temperature of the air, and q is the specific

humidity of the air.

When turbulent shear flow is the dominant process, the assumption that Km = Ks = Ke = K is made, and

$$K = \tau / \frac{du}{dz} \tag{II.7a}$$

may be substituted into (II.8) and (II.9). In addition, the relation

$$\tau_o = \rho C_D u_a^2 \tag{II.10}$$

may be obtained from either observations or from the work on turbulence done by Rossby and Montgomery (1935). In this equation, the drag coefficient C_D is a function of surface roughness, anemometer height, and von Karman's constant.

If the vertical derivatives of (II.7) -- (II.9) are expressed in terms of finite differences between the heights z_a and o,

$$\begin{aligned} u &= u_a - o = u_a \ , \\ T &= T_a - T_s \ , \text{ and} \\ q &= q_a - q_s , \end{aligned} \tag{II.11}$$

then the transfer equations may be written as

$$\tau_o = \rho C_D u_a^2 \quad , \tag{II.12}$$

$$Q_s = \rho c_p C_D (T_s - T_a) u_a \quad , \text{ and} \tag{II.13}$$

$$Q_e = LE = \rho L C_D (q_s - q_a) u_a \quad . \tag{II.14}$$

The drag coefficient C_D depends upon the wind speed close to the sea surface and is, therefore, not a constant. Deacon and Webb (1962) have derived a linear relationship between the drag coefficient and wind speed measured at a height of 10 meters above the sea surface from the observational results of various investigations. This relationship,

$$c_{10} = (1.00 + 0.07 u_{10}) \times 10^{-3} \tag{II.15}$$

is applicable for near neutral stability conditions and shows a comparatively slow increase of drag coefficient with wind speed.

Since winds are measured at heights of around 10 meters, the drag coefficient is dependent upon the effect of atmospheric stability. For a wind speed at 1 meter above the surface, the 10 meter speed will be greater under stable than under unstable conditions. Therefore, the drag coefficient should be smaller for stable conditions than that determined from (II.15) and larger for unstable conditions. In his study on heat transfer between ocean and atmosphere over a tropical ocean, Garstang (1965) used some theory of Monin and Obukov

(1954) to obtain a relationship between the drag coefficient at 6 meters C_6, the wind speed u_6, and the bulk Richardson number R_B,

$$C_6 = (1.46 + 0.07\mathcal{U}_6 - 4.2\ R_B) \times 10^{-3} \qquad \text{(II.16)}$$

In the present study, however, (II.15) is used to determine the drag coefficient since the measurements necessary to use the Monin-Obukov procedure were not available.

C. Error Analysis

The accuracy of the exchange formulas in determining the transfer of heat depends upon the validity of the assumptions underlying the theory, the accuracy of the observational data, and the manner in which the formulas are used to calculate the heat transfer.

If we accept the theory as valid, then the effect of observational errors is shown in Table I. (Part of the table is taken from Roden (1959) as he used some of the same exchange formulas that were used in this study.)

Since the exchange formulas are non-linear in nature, using monthly mean data instead of daily or hourly values in determining the heat transfer may lead to errors. In order to determine the magnitude of these errors, daily values of

Table I

Cloud Cover C	Error Δ C	$\Delta Q_i/Q_i$ %	$\Delta Q_b/Q_b$ %	$T_s - T_a$ °C	Error (T_s-T_a)	$\Delta Q_b/Q_b$ %	$\Delta Q_s/Q_s$ %
0.0	$\pm$ 0.1	$\pm$ 4	$\pm$ 0	1.0	$\pm$ 0.1	$\pm$ 1	$\pm$ 10
0.2	$\pm$ 0.1	$\pm$ 6	$\pm$ 1	2.0	$\pm$ 0.1	$\pm$ 1	$\pm$ 5
0.4	$\pm$ 0.1	$\pm$ 9	$\pm$ 3	3.0	$\pm$ 0.1	$\pm$ 1	$\pm$ 3
0.6	$\pm$ 0.1	$\pm$ 13	$\pm$ 5	4.0	$\pm$0.1	$\pm$ 1	$\pm$ 3
0.8	$\pm$ 0.1	$\pm$ 22	$\pm$ 8	5.0	$\pm$ 0.1	$\pm$ 1	$\pm$ 2
1.0	$\pm$ 0.1	$\pm$ 48	$\pm$ 17	6.0	$\pm$ 0.1	$\pm$ 1	$\pm$ 2

Wind Velocity m/sec	Error Δ W	$\Delta Q_e/Q_e$ %	$\Delta Q_s/Q_s$ %	Humidity %	Error Δ %	$\Delta Q_b/Q_b$ %	$\Delta Q_e/Q_e$ %
2	$\pm$ 1	$\pm$ 56	$\pm$ 56	60	$\pm$ 1	$\pm$ 1	$\pm$ 2
4	$\pm$ 1	$\pm$ 30	$\pm$ 30	65	$\pm$ 1	$\pm$ 1	$\pm$ 3
6	$\pm$ 1	$\pm$ 22	$\pm$ 22	70	$\pm$ 1	$\pm$ 1	$\pm$ 3
8	$\pm$ 1	$\pm$ 17	$\pm$ 17	75	$\pm$ 1	$\pm$ 1	$\pm$ 4
10	$\pm$ 1	$\pm$ 14	$\pm$ 14	80	$\pm$ 1	$\pm$ 1	$\pm$ 5
12	$\pm$ 1	$\pm$ 12	$\pm$ 12	85	$\pm$ 1	$\pm$ 1	$\pm$ 7
14	$\pm$ 1	$\pm$ 11	$\pm$ 11	90	$\pm$ 1	$\pm$ 1	$\pm$ 10
16	$\pm$ 1	$\pm$ 9	$\pm$ 9	95	$\pm$ 1	$\pm$ 1	$\pm$ 20

sea surface temperature, air temperature, dew-point temperature, cloud cover and wind speed were obtained for weather ship stations NOVEMBER (30N - 140W) and PAPA (50N - 145W) for the period of January to December of 1962 (see Chapter III). Monthly average values of Q_i, Q_b, Q_s, Q_e and the sum of these four heat transfer terms Q_{BAL} were computed first from the daily values and averaged over the number of days in the month; in the second case, the variables were averaged over the number of days in the month and the heat transfer terms computed from these averaged values. The results are shown in Tables II and III. $\overline{Q(v)}$ denotes heat transfer averaged over the daily values, and $Q(\bar{v})$ denotes heat transfers computed from the monthly averaged variables.

For Station NOVEMBER, the yearly average per cent differences between the two methods of computing the monthly average heat transfers are 1.4 for Q_i, 1.7 for Q_b, 4.8 for Q_e, 7.8 for Q_s and 17.7 for Q_{BAL}. For Station PAPA, the per cent differences are 1.4 for Q_i, 1.9 for Q_6 9.5 for Q_e, 45.1 for Q_s and 10.4 for Q_{BAL}.

The accuracy of the exchange formulas increases as the value of the heat transfer increases since the errors resulting from both observational and averaging effects are inversely proportional to the heat transfer. The theoretical accuracy of the formulas is also higher when large heat transfers occur.

Table II

Ship Station NOVEMBER (30N - 140W)

North	$\overline{Q_i(v)}$	$Q_i(\bar{v})$	$\overline{Q_b(v)}$	$Q_b(\bar{v})$	$\overline{Q_e(v)}$	$Q_e(\bar{v})$	$\overline{Q_s(v)}$	$Q_s(\bar{v})$	$\overline{Q_{BAL}(v)}$	$Q_{BAL}(\bar{v})$
January	217	221	128	131	266	257	31	26	-208	-193
% dif	1.4		1.9		3.4		14.8		6.8	
February	307	313	141	144	313	303	40	39	-186	-173
% dif	1.8		1.9		3.0		1.6		6.9	
March	355	359	145	147	217	207	30	26	-38	-21
% dif	1.3		1.4		4.8		12.4		43.9	
April	432	440	134	137	194	184	17	16	87	103
% dif	1.7		2.5		5.0		10.6		18.0	
May	466	471	141	143	247	238	38	35	40	55
% dif	1.1		1.1		3.3		7.9		36.4	
June	456	462	125	128	198	192	16	13	117	130
% dif	1.3		1.7		3.3		16.4		10.9	
July	465	472	129	131	258	251	28	27	52	63
% dif	1.5		2.0		2.7		.4		22.4	
August	499	507	129	132	192	184	13	12	165	178
% dif	1.7		2.4		4.2		.6		8.1	
September	437	444	132	135	210	187	10	10	84	111
% dif	1.6		2.3		11.2		.0		32.9	
October	346	350	136	137	306	311	26	27	-121	-125
% dif	1.2		1.3		1.7		2.4		3.0	
November	287	289	155	156	263	250	31	30	-162	-147
% dif	.8		.7		4.9		5.9		9.8	
December	205	209	136	138	319	350	29	35	-278	-314
% dif	1.7		1.4		10.0		20.1		12.9	

Table III

Ship Station PAPA (50N - 145W)

North	$\overline{Q_i(v)}$	$Q_i(\bar{v})$	$\overline{Q_b(v)}$	$Q_b(\bar{v})$	$\overline{Q_e(v)}$	$Q_e(\bar{v})$	$\overline{Q_s(v)}$	$Q_s(\bar{v})$	$\overline{Q_{BAL}(v)}$	$Q_{BAL}(\bar{v})$
January	59	60	105	108	40	62	-29	-16	-57	-93
% dif	1.8		2.1		55.1		44.8		63.5	
February	121	124	121	125	56	45	10	10	-65	-57
% dif	2.1		3.4		18.4		8.6		12.1	
March	201	204	118	120	104	101	30	29	-52	-47
% dif	1.7		2.3		2.7		4.8		9.5	
April	334	338	136	139	114	117	44	36	40	46
% dif	1.4		2.2		2.7		17.3		15.6	
May	357	362	112	113	77	75	8	9	160	164
% dif	1.2		1.4		3.0		11.5		2.5	
June	355	357	100	101	57	55	5	5	193	197
% dif	.7		.8		3.9		.6		1.9	
July	346	348	94	95	28	28	-7	-4	231	230
% dif	.7		1.3		1.9		41.4		.6	
August	286	289	95	97	52	55	-1	2	140	135
% dif	1.1		1.7		5.5		382.2		3.0	
September	236	240	119	121	159	162	22	20	-63	-63
% dif	1.4		1.9		1.9		9.0		.1	
October	153	155	124	126	191	176	23	22	-185	-169
% dif	1.4		1.5		7.6		5.1		8.6	
November	79	80	132	134	355	330	110	99	-517	-482
% dif	1.3		1.6		7.1		9.6		6.7	
December	50	51	121	124	116	110	30	32	-217	-216
% dif	1.8		2.4		4.6		5.8		.7	

Since large transfers occur at times of strong winds, the wind shear keeps the atmospheric stratification close to neutral values, and these are the conditions for which the formulas were derived.

It is also seen from Tables II and III that the errors resulting from averaging procedures are smaller for Q_i and Q_b than for Q_e and Q_s. This result is due to the fact that there is a correlation on a daily basis between the wind speed u_a and the air-sea temperature difference $T_s - T_a$ and between the wind speed u_a and the air-sea specific humidity difference $q_s - q_a$. If the monthly average heat transfers are given by

$$\overline{Q}_e \propto (\bar{q}_s - \bar{q}_a)\,\bar{u}_a + CV\,(q_s - q_a)\,u_a \qquad \text{(II.17)}$$

and

$$\overline{Q}_s \propto (\bar{T}_s - \bar{T}_a)\,\bar{u}_a + CV\,(T_s - T_a)\,u_a \qquad \text{(II.18)}$$

where the bar denotes an average over daily values and CV denotes "covariance between" the second terms in (II.17) and (II.18) represent the contributions of the correlations between the variables and the first terms the contributions of the monthly averaged variables. If only monthly averaged variables are used, the second terms are neglected, and small errors are produced.

Since monthly averaged variables were the only ones avail-

able over a long time period (see Chapter III), they were used in this study to compute the heat transfer values. However, the investigation of the data from the two weather ships indicates that the errors involved in this procedure are, in the average, only 10% of the actual values. The work of Malkus (1962) and Kraus and Morrison (1966) also support this conclusion.

III. Data Preparation

A. Monthly Averaged Data

Monthly averaged values of sea surface temperature, air temperature, wet-bulb temperature, cloud cover and wind speed were obtained for an 84 month period, January 1951 to December 1957, from Dr. O. E. Sette of the Bureau of Commercial Fisheries at Stanford University. The data are in the form of averages for two-degree latitude and longitude squares and cover the North Pacific Ocean from 20°S to 60°N. However, in this study only those values north of 20°N were used since the coverage is excellent in this region; usually more than 500 observations per two-degree square were available for the 84 month period, and in some squares more than 5000 observations were given.

The data were first copied onto Marsden Square sheets (10-degree latitude-longitude squares with subdivisions for each 2-degree square within them) and those values obviously in error were eliminated. Overlapping averages of 9 values in each quadrant of the 10-degree square were taken, and these values were plotted in their respective positions on a map of the North Pacific. The 4 values in each of the 10-degree Marsden Squares were then averaged to obtain a value at each 5-degree latitude-longitude intersection. Finally, the 162 resulting values were punched onto cards for further use on a 7094 IBM computer.

For the computation of geostrophic winds and heat transfer terms, monthly average sea-level pressure values were taken from charts supplied by the Extended Forecast Division of the U. S. Weather Bureau and were also punched onto cards.

The 162-point network of points, extending from 20°N to 55°N and from coast to coast, gives a picture of the large-scale features of each of the variables used in the computations and each of the computed heat transfer terms. It is felt that this network is adequate for one to be able to learn something about the large-scale interaction of ocean and atmosphere on a monthly and seasonal time scale.

In his work using the same data, Wyrtki (1965, 1966) subtracted 1.2°F from all of the sea-surface temperatures. This correction was suggested by Saur (1963) to convert injection temperatures to actual ocean temperatures. This correction was not used in this study, however, since the reported air and wet-bulb temperatures are probably also biased on the high side due to radiational effects of the ships on which the measurements were made. Since no information on this effect was available and since the temperature values always appear as differences in the exchange formulas, it was decided to use the sea surface temperatures as reported.

The values of the specific humidity at the sea surface were computed from the saturation vapor pressures over water

at the reported sea surface temperatures with the following relationships:

$$q_s = \frac{\epsilon e_s}{p}, \tag{III.1}$$

and

$$e_s = .98e_o, \tag{III.2}$$

where q_s is the specific humidity, $\epsilon = .622$, e_s is the saturation vapor pressure over the sea, e_o is the saturation vapor pressure over fresh water taken from the Smithsonian Meteorological Tables (1958), and p is the sea-level pressure in millibars.

The values of the specific humidity of the air were obtained from the following relationships:

$$(T_a - T_w)\ (C_p + wC_{pw}) = (w' - w)\ L, \tag{III.3}$$

$$e_a = \frac{wp}{w + \epsilon} \tag{III.4}$$

and

$$q_a = \epsilon \frac{e_a}{p}, \tag{III.5}$$

where T_a is the temperature of the air approaching the wet-bulb, T_w is the temperature of the saturated air leaving the wet-bulb, C_p is the specific heat at constant pressure of the

dry air, C_{pw} is the specific heat of water vapor, w is the mixing ratio of the approaching unsaturated air, w' is the mixing ratio of the saturated air, L is the latent heat of vaporization, and q_a is the specific humidity of the unsaturated air.

B. Daily Averaged Data

Daily averaged values of sea surface temperature, air temperature, dew-point temperature, cloud cover, and wind speed were obtained for the 12 months of 1962 for weather ship stations PAPA (50°N - 145°W) and NOVEMBER (30°N - 140°W) from Dr. Glenn Flittner of the Bureau of Commercial Fisheries at La Jolla, California. The data were first tabulated by month and then punched onto cards for further analysis and use.

IV. Heat Exchange Calculations

A. Results Using Monthly Averaged Data

Values of Q_i, Q_b, Q_e, Q_s and the total heat transfer across the sea surface

$$Q = Q_i = Q_b - Q_e - Q_s \qquad \text{(IV.1)}$$

were computed for each of the 84 months of the period under investigation, using the formulas developed in Chapter II. The results were averaged over the 7 years for each quantity and each month and are shown along with their respective standard deviations in Figures A12 through A71. They were also averaged over all of the 84 months in the period, and these results are shown in Figures A1 through A11.

1. The values of Q_i (incoming radiation corrected for cloud cover) averaged over the 84-month period are shown in Figure A1. They range from 124 cal/cm^2/day at 55°N to 432 cal/cm^2/day at 20°N and show a strong dependence upon latitude; variations along a latitude circle represent variations in the average cloud cover. Maximum incoming radiation occurs between 20°N and 30°N from the Hawaii Islands to the Philippines due to the comparatively low cloud cover in this area as shown in Figure A8. The values of the standard deviation

at each of the 162 points reflect the fluctuations in Q_i due to the yearly cycle of incoming radiation and to the fluctuation in the cloud cover from year to year during the 7-year period.

The values of Q_b (effective back radiation) averaged over the 84 months are shown in Figure A2. They range from 87 cal/cm^2/day at 50°N to 143 cal/cm^2/day at 35°N and show little seasonal change. Effective back radiation is high in the region of the Kuroshio Current due to the large sea-air temperature difference and low in the high latitudes due to the large amount of cloud cover in this region. The standard deviations of Q_b are all comparatively low and indicate that there is little seasonal or year-to-year change in the back radiation.

The 84-month averages and standard deviations of Q_e (latent heat transfer) are presented in Figure A3. The average values range from 84 cal/cm^2/day at 55°N to 384 cal/cm^2/day at 35°N. The amount of heat lost from the sea surface due to evaporation is lowest in the high latitudes due to the low vapor pressure difference in this region and highest in the region of the Kuroshio due to the large vapor pressure differences there. The relatively large values of the standard deviations reflect the large seasonal fluctuations of Q_e, especially in the area of the Kuroshio Current. The average values of Q_e show the same distribution over the map as those

computed by Wyrtki (1965). However, the magnitudes are larger than his values due to the fact that Wyrtki subtracted 1.2°F from the sea-surface temperature values, giving him lower values of the sea-surface vapor pressure. Part of the differences may also be attributed to the use of a drag coefficient in this study that is a function of the wind speed and not a constant value as was used by Wyrtki.

The values of the 84-month averages and standard deviations for Q_s (sensible heat transfer) are shown in Figure A4. The average values range from 6 cal/cm^2/day at 40°N - 125°W to 106 cal/cm^2/day at 35°N - 145°E. The largest values occur in the region of the Kuroshio, where the air-sea temperature difference is large, while the smallest values occur along 20°N and the California coast, where the sea-air temperature difference is small or reversed. The large values of the standard deviations reflect the seasonal variation of the sensible heat transfer, especially off of the Asian coast, where large masses of cold air move out from the continent during the winter months.

The 84-month averages and standard deviations of the total heat transfer across the sea surface SLHT or Q are shown in Figure A5. The average values range from -328 cal/cm^2/day at 35°N - 145°E to 117 cal/cm^2/day at 30°N - 115°W. The preponderance of negative values indicates that during the year the North Pacific Ocean loses more heat than it gains

at the surface above 20°N. The largest amount of heat is lost in the region of the Kuroshio, where back radiation, evaporation and sensible heat loss are high. There is a small heat gain along 20°N between 145°E and 165°E due to high incoming radiation and another heat gain along the California and Mexican coasts which is caused by small values of evaporation and sensible heat loss. In comparing these values to those given by Wyrtki (1965), it is seen that his map shows much less heat loss above 20°N. This result is due to the larger values of sensible and latent loss used in this study, giving larger values of total heat lost at the surface. The extremely large values of the standard deviations in Q indicate that there are large seasonal and year-to-year variations in the total heat transfer.

The values of the total heat transfer were integrated over the North Pacific north of 20°N. The result indicates that the ocean loses 7×10^{14} cal/sec through the surface north of 20°N. Wyrtki (1965) calculated the total integral of heat transfer over the entire North Pacific from the equator poleward and found that the ocean gains 3×10^{14} cal/sec, or about 10 per cent of the incoming radiation. The difference between the two calculations shows that there is a heat gain of 10×10^{14} cal/sec between the equator and 20°N and that it is this region that accounts for the yearly heat gain of the North Pacific. The magnitude of this heat gain between the

equator and 20°N is uncertain, however, due to the different values of latent and sensible heat used by Wyrtki and this study. Since the values in the latter were larger, resulting in a larger heat loss above 20°N than Wyrtki's work would show, the magnitude of the heat gain should be smaller than calculated.

The 84-month average values and standard deviations of sea-surface temperature, air temperature, cloud cover, observed wind speed, specific humidity and Bowen Ratio are shown in Figures A6 through A11. They are given here as reference maps and will not be discussed.

2. The values of Q_i, Q_b, Q_e, Q_s, and Q averaged over 7 years for each month are shown in Figures A12 through A71. The values of the standard deviations over the 7-year period are shown in order to give some idea of the variability of each of the heat transfer terms on a year-to-year basis.

In order to facilitate the analysis of these maps, the first 2 harmonics (first harmonic has a period equal to one year or 12 months) of the Fourier Series for each transfer term were computed at each of the 162 points on the map. Along with the 2 Fourier coefficients, the percentage of the series variance accounted for by each of the harmonics was also computed. This type of analysis was found to be extremely useful in interpreting the monthly and seasonal cycles of the

data, since the 2 harmonics together usually accounted for over 95 per cent of the variance at each point; in fact, over most areas of the map the first harmonic or yearly cycle accounted for over 90 per cent of the variance. By determining the phase of each of the harmonics and printing them in map form, it was also possible to compare the relative times of maximum and minimum values of each series at each of the points.

The values of Q_i averaged over the 7-year period for each month are presented in Figures A12 through A23. The largest values of Q_i at each latitude occur in June, while the smallest values occur in December due to the motion of the earth around the sun and the tilt of the earth's axis of rotation with respect to the plane of revolution. The Fourier analysis shows that there is a regular yearly cycle as expected. The first harmonic accounts for over 90 per cent of the variance at most points, with the exception of the area from 20°N to 30°N and from 110°W to 140°W, where the percentage is reduced to 60 due to the effect of cloud cover variation without a uniform yearly cycle.

Figures A24 through A35 show the 7-year average values and standard deviations of the effective back radiation Q_b. Due to the low values of cloud cover and the large values of the sea-air temperature differences, the largest values of Q_b occur in January. The Fourier analysis again shows a regular yearly cycle with the maximum values occurring in December

and January and the minimum values in June and July. Relatively low values of the standard deviations indicate that there is little year-to-year variability of Q_b. The low values of the amplitude of the first harmonic in the Fourier analysis also show that there is only a small range between the maximum and minimum values of Q_b throughout the year.

The 7-year average values and standard deviations of Q_e for each month are given in Figures A36 through A47. The results of the Fourier analysis show that there is a pronounced yearly cycle in Q_e and that the maximum values occur in December, while the minimum values occur in June. The first harmonic accounts for more than 90 per cent of the series variance in all areas except from 20°N to 25°N and 110°W to 170°W, where the percentage falls to as low as 5. This result is due to the fact that both the specific humidity difference and the observed wind speed fail to have regular yearly cycles in this area. The amplitude of the first harmonic and the 7-year standard deviations are largest in the area from 30°N to 45°N and 180°E to 125°E, reflecting the effect of the large masses of cold, dry air that move off of the Asian continent during the winter months.

Figures A48 through A59 show the 7-year average values and standard deviations of Q_s for each month of the year. Again, the Fourier analysis shows that a regular cycle occurs with the maximum values in November and December and the

minimum values in May and June. This yearly cycle is due to the fact that both the sea-air temperature difference and the observed wind speed also have regular yearly cycles with maxima and minima in the same months. Negative values of Q_s (heat gained by sea surface) occur in the high latitudes from May through September, reflecting the fact that the air temperatures are warmer than the sea temperatures during these months. The relatively large values of the standard deviation, especially in the summer months, indicate the large year-to-year variability that occurs in Q_s.

Figures A60 through A71 show the 7-year averages and standard deviations of the total heat transfer through the surface Q. It is seen that negative values of Q, implying heat loss from the ocean surface, occur from September through April, while positive values, implying heat gain by the surface layer, occur from April through September. The results of the Fourier analysis show that there is a regular yearly cycle in Q with the maximum values occurring in June and the minimum values occurring in December. The first harmonic of the series accounts for over 95 per cent of the variance in all areas except those in which there are no regular cycles of Q_i, Q_b, Q_e, and Q_s.

In looking at the maps for the different months, it is seen that heating of the surface layer begins first in March

along the 20°N latitude from 130°E to 165°E and begins last in the region of the Kuroshio Current in the latter part of April. The heating continues in all areas from May through August except in the region between Hawaii and Baja California, where some cooling occurs due to the high evaporation in all months. Cooling of the surface layer first begins in August at 20°N and 125°E to 135°E, then in the region of the Kuroshio during September, and finally spreads to all regions by October. The cooling continues from October through March, with the largest values occurring in December and January off of the Asian coast, where over 700 cal/cm^2/day are lost due to the high latent and sensible heat transfer from ocean to atmosphere. The large values of the standard deviations reflect the large year-to-year variability in Q due to the corresponding large variability in Q_e and Q_s.

3. The values of the sea-surface temperature SST, the surface air temperature SAT, and the change in sea-surface temperature from month to month Δ SST averaged over the 7-year period for each month are shown in Figures A72 through A107.

Figures A72 through A83 show the average values and the 7-year standard deviations for SST. Fourier analysis of the data at each of the 162 grid-points shows that there is a regular yearly cycle in all areas, with the first harmonic

accounting for over 95 per cent of the variance at all points. The maximum amplitudes of the yearly cycle occur in the area of the Japan Sea and the Kuroshio Current, where the yearly range of the sea-surface temperature is 18 to 24°F. The minimum values of the amplitudes occur in the area from 120°W to 170°W and 20°N to 30°N, where the yearly range is only 4 to 7°F.

The Fourier analysis also show that the maximum values of sea-surface temperature occur in the latter part of August and the early part of September and that the minimum values occur in the latter part of February and the early part of March.

In comparing the yearly cycles of the total heat transfer across the sea surface Q and the sea-surface temperature SST, it is seen that the two are strongly related. In all areas of the maps except the southeast corner, the sea surface reaches a maximum temperature at the end of the heating cycle (positive Q) and a minimum temperature at the end of the cooling cycle (negative Q).

Figures 1 through 4 show the cycles of Q and SST at various points along the latitudes 20°N, 35°N, 40°N and 50°N. (For a more extensive presentation of this type of analysis, see Wyrtki, 1966.) Large changes in Q throughout the year produce corresponding large changes in SST, whereas small changes in Q produce small changes in SST. This relationship between

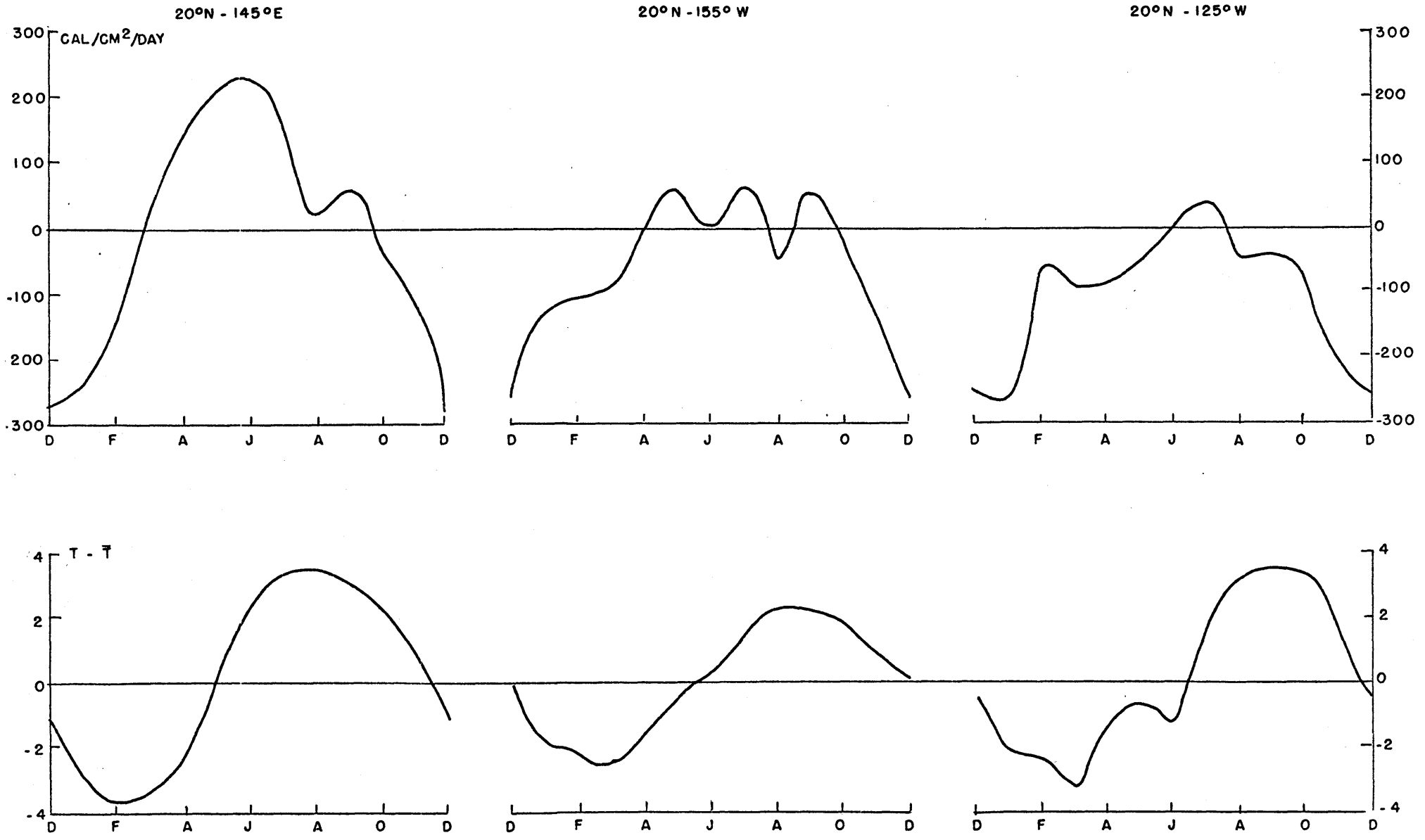
20°N - 145°E
20°N - 155° W
20°N - 125° W
CAL/CM2/DAY
300
200
100
0
-100
-200
-300
D F A J A O D
T - T̄
4
2
0
-2
-4

Figure 1

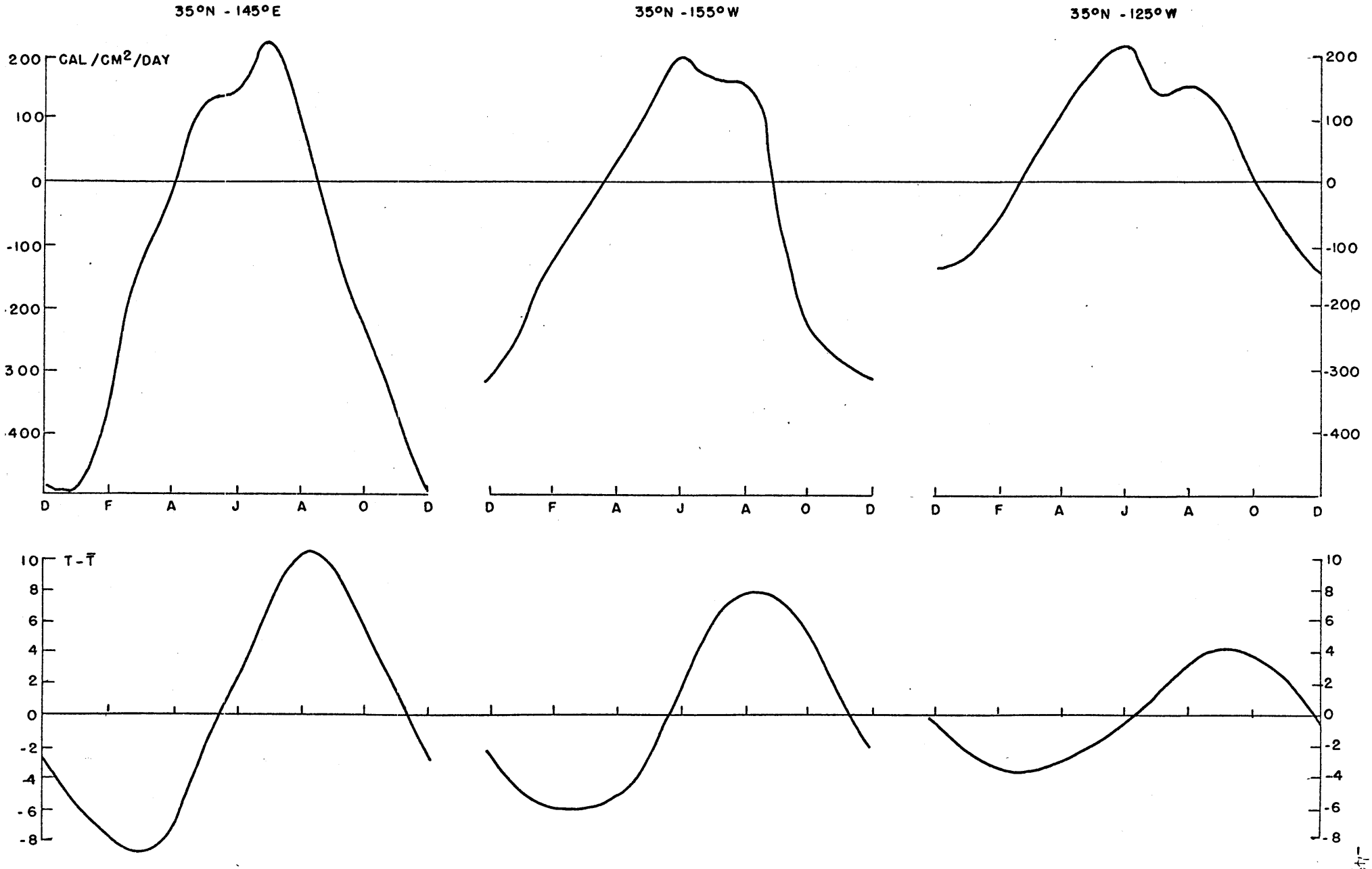
35°N - 145°E
35°N - 155°W
35°N - 125°W
CAL / CM² / DAY
200
100
0
-100
-200
300
400
D F A J A O D
T - T̄
10
8
6
4
2
0
-2
-4
-6
-8

Figure 2

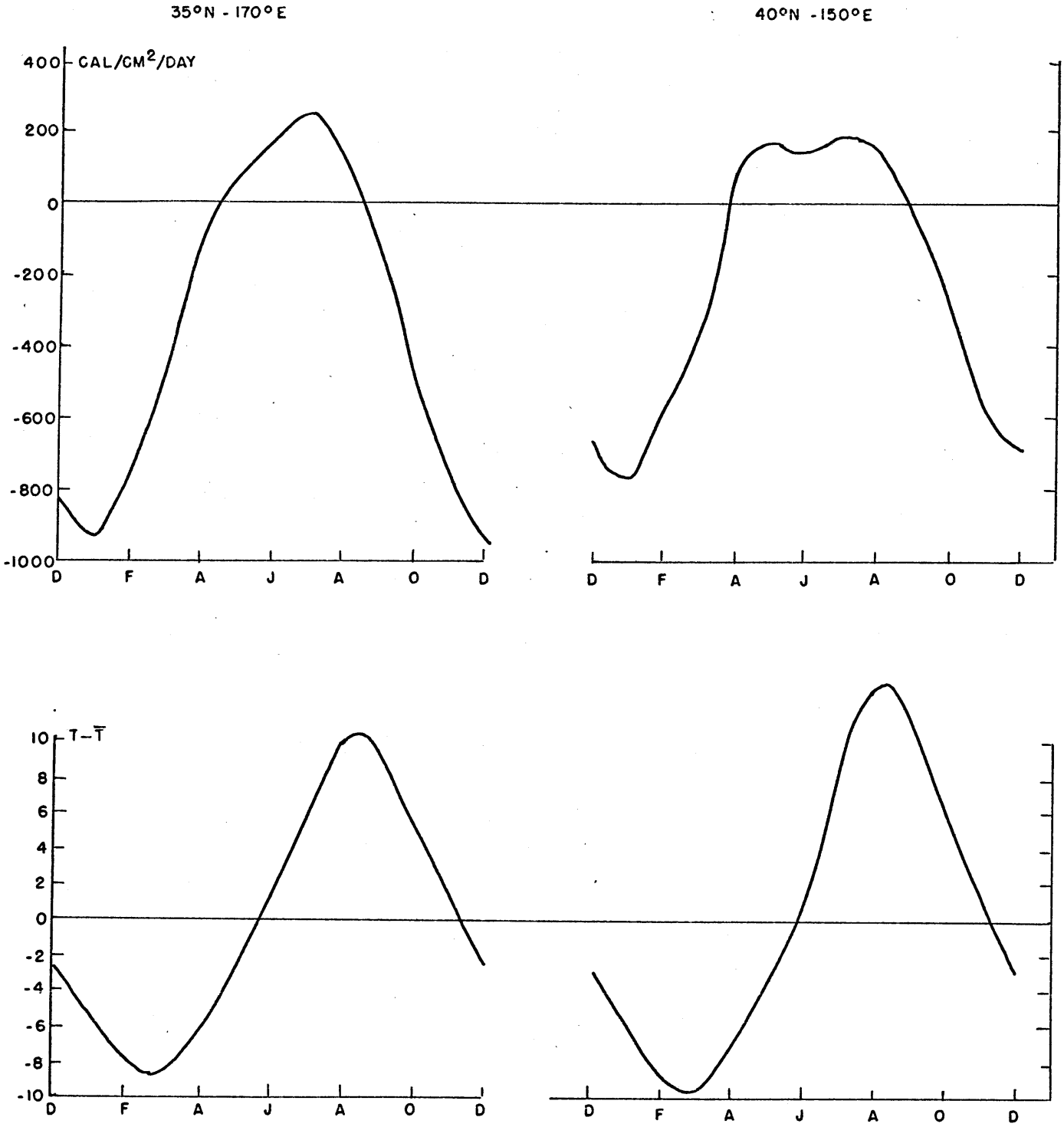
35°N - 170°E
40°N - 150°E
400
CAL/CM²/DAY
200
0
-200
-400
-600
-800
-1000
D
F
A
J
A
O
D
10
T-T̄
8
6
4
2
0
-2
-4
-6
-8
-10

Figure 3

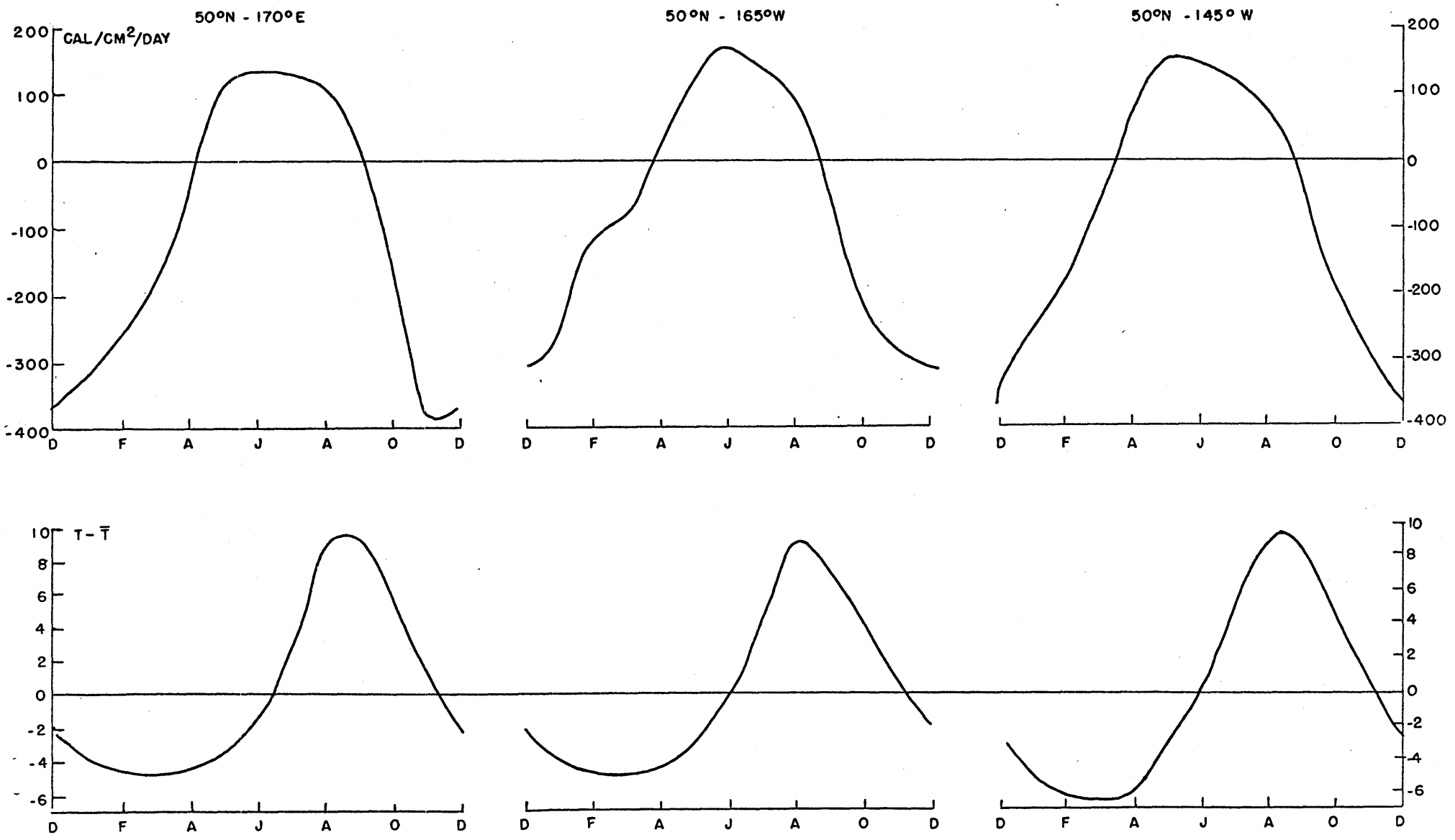
50°N - 170°E
50°N - 165°W
50°N - 145° W
CAL/CM²/DAY
200
100
0
-100
-200
-300
-400
D F A J A O D
T - T̄
10
8
6
4
2
0
-2
-4
-6

Figure 4

the average or normal values of the total heat transfer across the sea surface and the sea-surface temperature suggests that the year-to-year changes in the total heat transfer for a particular month will be accompanied by year-to-year changes or anomalies in the sea-surface temperature for the same month. This is indeed the case, as will be shown in Chapter V.

Figures A84 through A95 show the 7-year average values and standard deviations of the surface air temperature SAT. The results of the Fourier analysis show that a regular yearly cycle is also present in the air temperature, with over 95 per cent of the series variance accounted for by the first harmonic. The maximum and minimum values of SAT occur at the same times as those of the sea-surface temperature, August through early September and February through early March respectively. In both the sea and air temperatures, the maximum values tend to occur somewhat earlier (early August) in the western part of the ocean than in the eastern part (early September). This result is also reflected in the fact that the heating cycle lasts approximately 1 month longer in the eastern part of the ocean than in the western part; there is a definite shift from August to September in the time when the heating cycle ends as one moves eastward across the ocean.

The strength of the California Current and the accompanying cold advection in the months of June, July and August

may play an important role in determining the end of the heating cycle in the western part of the North Pacific. During these months, the strong advection of cold water keeps the sea-surface temperature somewhat lower than it would be if there were no advection. These lower temperatures, in turn, keep the transfer of latent and sensible heat down and let Q remain positive (heat gain by sea surface) throughout August and early September. As the advection weakens, the ocean temperature rises until the incoming radiation is balanced by the heat lost from the surface due to back radiation and latent and sensible heat transfer. At this point, the surface layer of the ocean begins to lose more heat than it gains, and the sea-surface temperature begins to fall.

The relationship between the yearly cycles of the normal values of SST and SAT indicate that year-to-year fluctuations or anomalies in SST will be accompanied by corresponding fluctuations in SAT. From correlation studies between the anomalies of the two data series, reported on in Chapter V, it was found that this is exactly what occurs.

Figures A96 through A107 show the 7-year average values and standard deviations of the month-to-month change in the sea-surface temperature ΔSST. These values were computed by taking the difference between the average value of a particular month and the following month and the average value of the same month and the preceding one. We thus have linear approximations

to the change in SST across each of the 84 months in the data series. The results of the Fourier analysis show that there is a regular yearly cycle in Δ SST, especially in the lower latitudes. Above 35°N the second harmonic becomes important and accounts for approximately 15 per cent of the variance in these areas. The maximum increase of the sea-surface temperature over a month occurs from the middle of May to the middle of June, while the maximum decrease occurs from the middle of December to the middle of January. During the times of little or no change in the sea-surface temperature (early march and early September) the heat content of the ocean surface layer changes very little, and a balance must exist between the transfer of heat across the sea surface and the advection within the surface layer.

The monthly mean values of the observed daily wind speed were averaged over the 7-year period and subjected to Fourier analysis. The results show that there is a regular yearly cycle over most of the ocean areas with the exception of the area 20°N to 30°N and from 110°W to 170°E. Over the rest of the ocean, the first harmonic accounts for over 90 per cent of the variance and, in the central and western parts, for over 95 per cent. The largest amplitudes, 250 cm/sec, occur between 35°N and 50°n and from the Asian coast eastward to longitude 175°E. Large amplitudes also appear in the Gulf of Alaska, a region of frequent cyclogenesis. As expected,

the largest values of the wind speed occur during January and the minimum values in July.

The values of the Bowen ratio (Q_s/Q_e) were also averaged over the 7-year period for each month and Fourier analyzed. The results show that a regular yearly cycle occurs only in the middle latitudes of the western part of the North Pacific. In this area the ratio has an annual range of .4 to 1.4 with the maximum values occurring in January and the minimum values in July. In the other areas, the Bowen ratio has a value of about .1 with little annual variation.

4. Using the heat balance equation in the form

$$-\rho c_p H(\vec{v}\cdot\vec{\nabla}T) = \rho c_p H\frac{\partial T}{\partial t} - Q \qquad \text{(IV.2)}$$

where H is the depth of the upper mixed layer of the ocean, $\vec{v}$ is the velocity within the mixed layer, T is the temperature of the mixed layer, and Q is the total heat transfer across the sea surface, an estimate of the total heat advection within the mixed layer, or the left-hand side of the equation (IV.2), can be obtained using the observed values of the change in heat content of the layer and the calculated total heat transfer.

Using the values of $\partial T/\partial t$, or Δ SST, and Q determined previously and values of H taken from a study of the thermal

condition of the North Pacific Ocean by Pattullo and Cochrane (1951), estimates of the heat advection within the mixed layer were determined at each of the 162 grid-points for each of the 12 months. The values are given in Figures A108 through A119.

Due to the uncertainties in the monthly distributions of the mixed layer depths H, not much confidence can be placed in these computed values of heat advection. However, several features of the monthly maps appear to be in agreement with what is known about the current patterns in the surface layer of the North Pacific, especially during the months from October through May. During these months, there is strong advection of warm water from the lower latitudes to the higher latitudes in the western part of the ocean; this is particularly true in the region of the Kuroshio Current. In the eastern part of the ocean off of the California and Mexican coasts, there is a weaker advection of cold water from the higher latitudes to the lower ones. This is also the case from June through September. However, during these 4 months the maps show that there is cold advection of water within the surface layer in the region of the Kuroshio in contrast to what is expected due to the transport of the geostrophic and wind-drift currents. The reason for this discrepancy probably lies in the fact that the monthly charts of the mixed layer depth for the region show a marked decrease from June through September, going from 250 feet in May to 50 feet in June. Looking

at the first term on the right-hand side of equation (IV.2), it is seen that for positive values of Q and $\partial T/\partial t$, small values of H can give negative values or cold advection for the left-hand side.

Another uncertainty in the method is the amount of heat that is lost from the mixed layer across the seasonal thermocline. Since this heat loss is believed to be compensated by an up-welling of cold water through the region of the thermocline, the large negative values calculated for the advection could reflect this heat loss or up-welling. In the following simple model of the surface layer, it will be shown that the heat received or lost at the surface is balanced by a change in the temperature of the surface layer, horizontal advection of heat into or out of the layer, and loss of heat across the region of the thermocline.

The equation of heat flow may be written as

$$\frac{\partial T}{\partial t} + \frac{\partial}{\partial x}(Tu) + \frac{\partial}{\partial y}(Tv) + \frac{\partial}{\partial z}(Tw) - \frac{\partial}{\partial z}\left(K\frac{\partial T}{\partial z}\right) = 0, \qquad \text{(IV.3)}$$

where T is the temperature, u, v and w are velocity components in the x,y and z directions, and K is the vertical heat exchange coefficient (only vertical mixing considered). Using the equation of continuity in the form

$$\frac{\partial u}{\partial x} + \frac{\partial v}{\partial y} + \frac{\partial w}{\partial z} = 0, \qquad \text{(IV.4)}$$

and placing the direction of flow along the y-axis (u = o), we get

$$\frac{\partial T}{\partial t} + \frac{\partial}{\partial y}(Tv) + \frac{\partial}{\partial z}\left(Tw - K\frac{\partial T}{\partial z}\right) = 0, \qquad \text{(IV.5)}$$

Integrating over the mixed layer depth H in which T is independent of z and letting $V = \int_{-H}^{o} v\,dz$, then

$$H\frac{\partial T}{\partial t} + \frac{\partial}{\partial y}(TV) - \left(Tw - K\frac{\partial T}{\partial z}\right)_{z=-H} = \frac{Q}{\rho c_p} \qquad \text{(IV.6)}$$

since w = o and $K\,\partial T/\partial z = Q/\rho\, cp$ at z = o.

In the discontinuity layer or the region of the seasonal thermocline, we assume that the downward flux of heat due to thermal conduction is balanced by water ascending with the constant velocity w. We can then write the relation

$$w\,(T - T_D) = A\frac{\partial T}{\partial z} \qquad \text{(IV.7)}$$

in which $(T - T_D)$ is the temperature gradient across the discontinuity layer.

Substituting equation (IV.7) and the vertically integrated continuity equation,

$$\int_{-H}^{o}\frac{\partial v}{\partial y}\,dz = -\int_{-H}^{o}\frac{\partial w}{\partial z}\,dz$$

or $$\frac{\partial V}{\partial y} = w_{z=-H} \,,$$

into equation (IV.6) we obtain

$$H\frac{\partial T}{\partial t} + V\frac{\partial T}{\partial y} + (T - T_D)w = \frac{Q}{\rho C_p} \,. \qquad \text{(IV.8)}$$

This equation states that the total heat transfer across the ocean surface (Q) is balanced by the change in temperature of the mixed layer, horizontal advection within the layer, and a loss of heat into the region of the thermocline. The last mechanism heats the water ascending from below, which passes into the horizontal flow within the surface layer.

Using a value of 2×10^{-5} cm/sec for the vertical velocity through the discontinuity layer (Wyrtki, 1960) and 20°C for $T - T_D$, a value of 35 cal/cm^2/day is obtained for the heat loss from the surface layer due to vertical mixing at the bottom of the layer. Although this value is not large, it would reduce the magnitude of the right-hand side of equation (IV.2) and help to give more reasonable values for the horizontal heat advection.

The values of the heat advection determined from the heat balance equation were integrated over each latitude circle at 5-degree intervals from 20°N to 55°N and also over the

entire North Pacific Ocean from 17.5°N to 57.5°n. The results of the calculations are shown in Table IV. It is seen from the table that warm advection occurs over the ocean from January through May, with the largest values occurring in March where 14.6×10^{14} cal/sec is advected into the surface layer. Cold advection occurs from June through December, with 6.6×10^{14} cal/sec being advected out of the surface layer above 17.5°N in September.

As was mentioned above, the values of cold advection during the summer months are uncertain due to the unreliable nature of the mixed layer depth values, especially in the western part of the ocean. In a study on the meridional heat transport by ocean currents, Bryan (1962) used a method combining hydrographic station data and climatological values of surface wind stress to compute the meridional transport of heat across various latitudes in the Atlantic and Pacific Oceans. Using data obtained during August of 1955 at 32°N in the North Pacific Ocean, he calculated that there was a southward transport of heat by large-scale motions of approximately 2.8×10^{14} cal/sec. From Table IV it is seen that a southward transport of heat of 2.2×10^{14} cal/sec occurs at 32°N. While the magnitudes of the two calculations differ by a factor of 1.3, the direction of heat transport is the same for both studies. Bryan concludes that more east-west sections are needed to determine whether this southward heat transport is characteristic

Table IV

LAT	JAN	FEB	MAR	APR	MAY	JUN	JUL	AUG	SEP	OCT	NOV	DEC
55°N	.2	.1	.6	.4	.3	-.1	.0	-.1	-.3	-.2	-.3	-.2
50°N	.2	.4	.8	.5	.2	-.2	.0	-.1	-.7	-.9	-1.1	-.5
45°N	.3	.7	1.2	.5	-.1	-.4	-.2	-.3	-1.1	-1.4	-1.6	-.5
40°N	1.0	1.6	2.3	1.2	.4	-.2	-.2	-.6	-.7	-.7	-.4	.1
35°N	1.0	2.1	2.9	1.6	.9	.0	-.5	-1.1	-.6	-.4	.2	-.1
30°N	-.3	1.3	2.7	1.3	.4	-.3	-.6	-1.1	-1.0	-.1	-.4	-1.4
25°N	-.4	.7	2.4	1.1	.3	-.5	-.4	-.4	-1.1	-.6	-1.1	-1.1
20°N	.2	.4	1.8	.9	.7	.2	-.3	.5	-1.1	-.8	-1.2	-.1
Total Area Integral	2.1	7.3	14.6	7.5	3.2	-1.5	-2.2	-3.3	-6.6	-5.6	-5.8	-3.8

Units: 10^{14} cal/sec

of other years and other seasons. The results of the present work indicate that this transport is not characteristic of all seasons, since a northward transport of heat occurs during the winter and spring months at all latitudes above 20°N.

B. Results Using Daily Averaged Data

In order to find out how much variability occurs during a month in the heat transfer terms and in the sea-surface temperature, daily values of certain meteorological parameters were obtained for ocean stations PAPA (50°N - 145°W) and NOVEMBER (30°N - 140°W) in the North Pacific Ocean for 1962 (see Chapter III). The data were used in the heat transfer equations developed in Chapter II to compute Q_i, Q_b, Q_e, Q_s and Q on a daily basis. These daily values of the heat transfer terms were then averaged over each of the 12 months to get monthly averaged values; in addition, the standard deviations for each of the terms were calculated for each month.

1. The monthly averaged values of Q_i, $Q_e + Q_s$, and Q are shown in Figure 5 for station NOVEMBER and Figure 6 for station PAPA; at the bottom of each of the Figures, the value of the sea-surface temperature for each month minus the

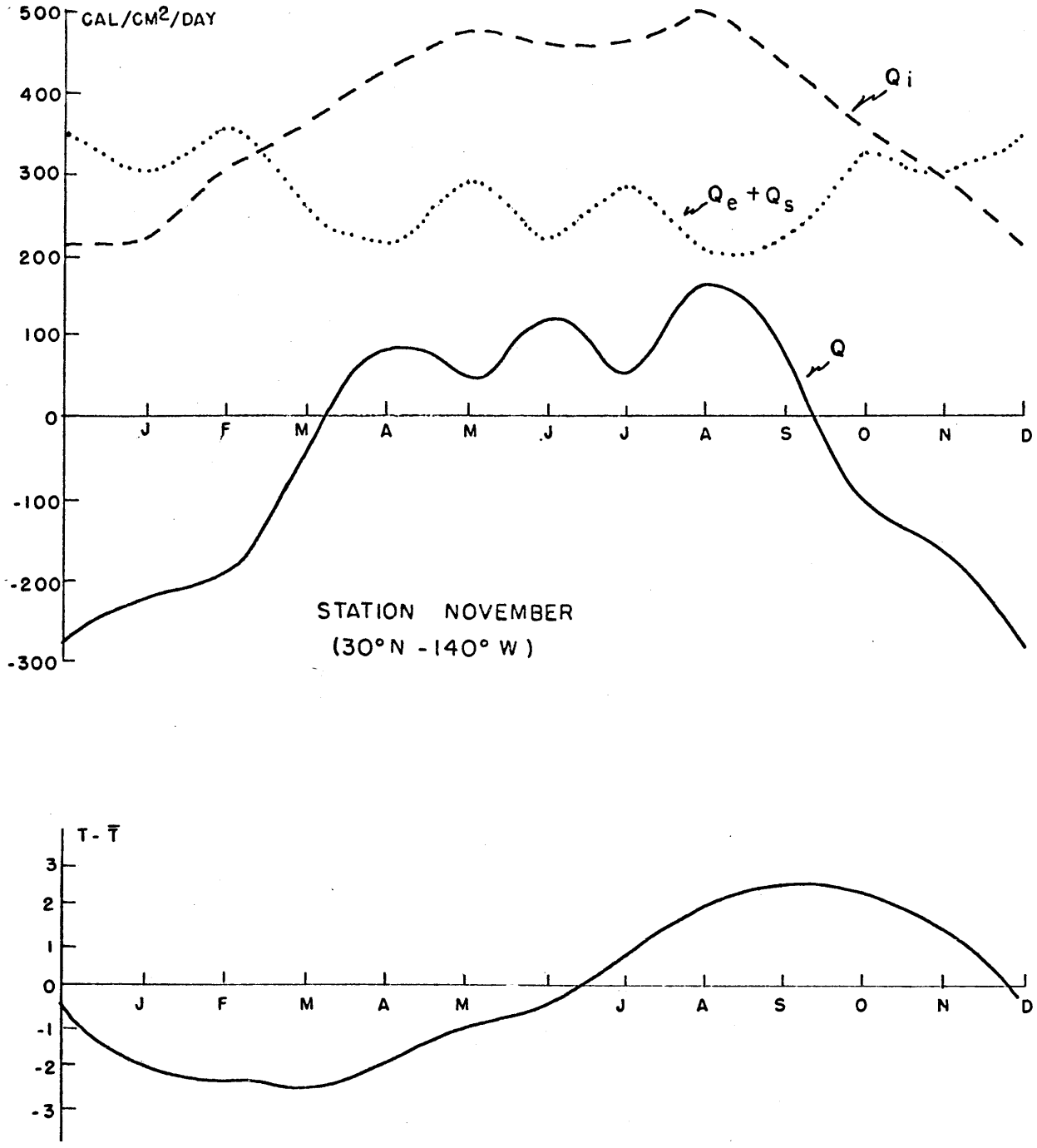
500
CAL/CM2/DAY
400
300
200
100
0
-100
-200
-300
Qi
Qe + Qs
Q
J
F
M
A
M
J
J
A
S
O
N
D
STATION NOVEMBER
(30° N - 140° W)
T - T̄
3
2
1
0
-1
-2
-3
J
F
M
A
M
J
A
S
O
N
D

Figure 5

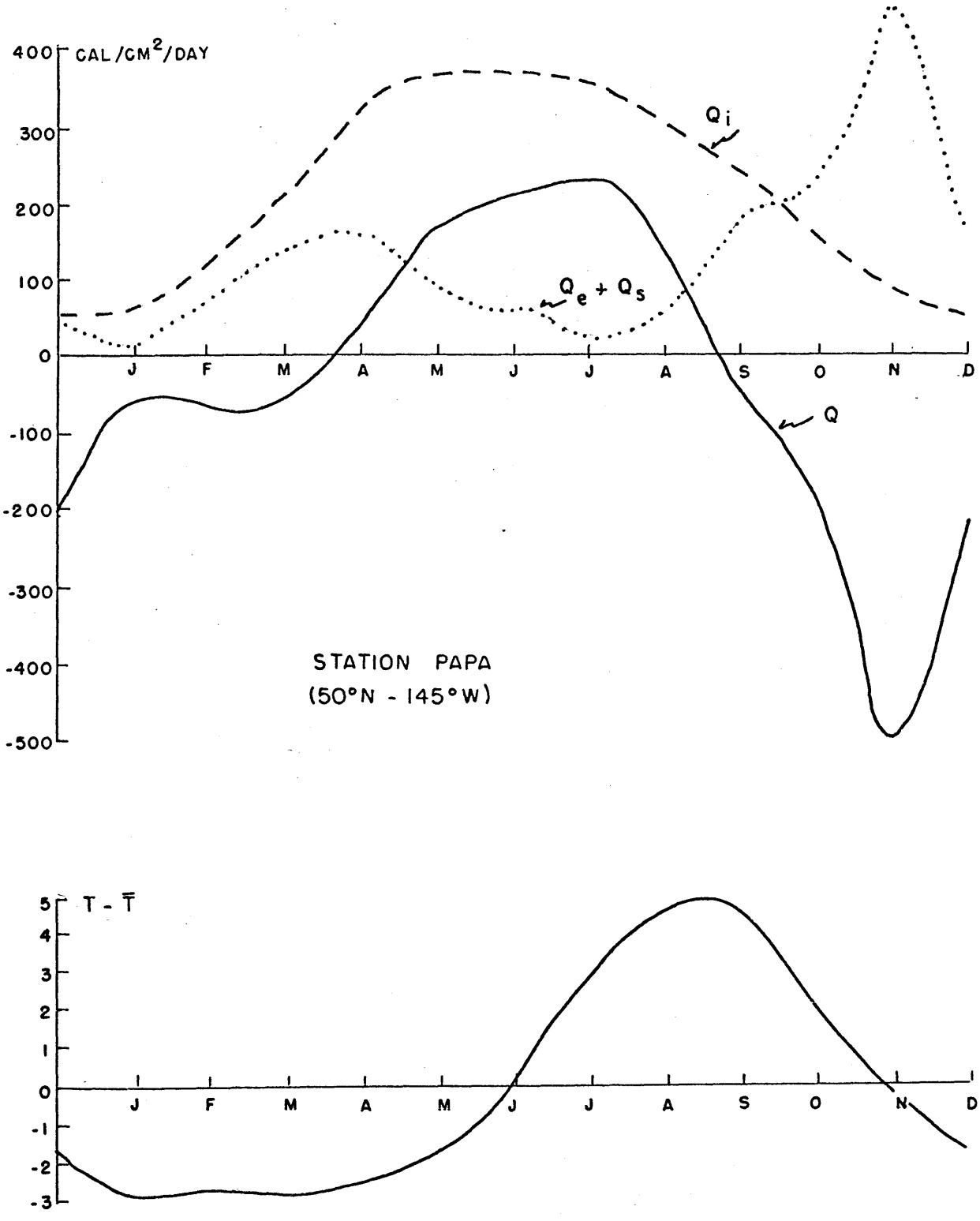
400
CAL/CM^2/DAY
300
200
100
0
-100
-200
-300
-400
-500
J
F
M
A
M
J
J
A
S
O
N
D
Q_i
$Q_e + Q_s$
Q
STATION PAPA
(50°N - 145°W)
T - $\bar{T}$
5
4
3
2
1
0
-1
-2
-3

Figure 6

yearly mean is also given. At each of the stations the heating cycle begins in March and ends in September. The variations in the total heat transfer Q during the summer months at station NOVEMBER reflect the variations in the latent and sensible heat flux $Q_e + Q_s$ throughout these months. At station PAPA the large negative value of Q in November is a consequence of the large value of $Q_e + Q_s$ during this month. The values of the effective back radiation show little monthly variation and have values of about 120 cal/cm^2/day for station PAPA and 135 cal/cm^2/day for station NOVEMBER.

2. Tables V and VI show the monthly averaged values and standard deviations over the daily values of Q_i, Q_b, Q_e, Q_s, Q and SST for stations NOVEMBER and PAPA respectively. The values of the standard deviations for Q_i are comparatively low and reflect the fluctuations in the cloud cover during the individual months. The standard deviations for Q_b are also low (approximately 20 per cent of the average values) and again reflect the fluctuations in the daily cloud cover values. However, the standard deviation values for Q_e and Q_s are extremely large, at times exceeding the magnitudes of the average values themselves. These large fluctuations throughout each of the months are due to the combined effects of fluctuations in the vapor pressure or temperature differences between sea and air and the daily values of the surface

Table V

	JAN	FEB	MAR	APR	MAY	JUN	JUL	AUG	SEP	OCT	NOV	DEC
Q_i	217	307	355	432	466	456	465	499	437	346	287	205
s	41	61	64	84	76	81	90	84	72	51	33	42
Q_b	128	141	145	134	141	125	129	129	132	136	155	136
s	21	31	24	23	27	16	17	16	17	20	22	32
Q_e	266	313	217	194	247	198	258	192	210	306	263	319
s	169	235	134	103	115	103	116	105	192	138	147	199
Q_s	31	40	30	17	38	16	28	13	10	26	31	29
s	34	39	27	20	27	17	12	10	15	13	24	37
Q	-208	-186	-38	87	40	117	52	165	84	-121	-162	-278
s	221	296	170	157	152	147	167	157	233	178	184	233
SST	18.7	18.5	18.1	18.8	19.8	20.2	21.5	22.6	23.3	23.0	22.0	20.2
s	.5	.0	.2	.0	.3	.7	.3	.9	.4	.5	.7	1.0

Monthly averaged values and standard deviations of Q_i, Q_b, Q_e, Q_s, Q and SST for station (NOVEMBER) 30°N - 140°W).

Units: cal/cm^2/day for Q's and °0 for SST.

Table VI

	JAN	FEB	MAR	APR	MAY	JUN	JUL	AUG	SEP	OCT	NOV	DEC
Q_i	59	121	201	334	357	355	346	286	236	153	79	50
s	15	30	47	68	77	61	59	60	50	32	17	12
Q_b	105	121	118	136	112	100	94	95	119	124	132	121
s	36	29	29	25	28	20	15	20	27	32	33	37
Q_e	40	56	104	114	77	57	28	52	159	191	355	116
s	98	84	94	71	75	69	37	52	153	177	240	158
Q_s	-29	10	30	44	8	5	-7	-1	22	23	110	30
s	58	36	58	65	36	23	12	15	51	45	117	97
Q	-57	-65	-52	40	160	193	231	140	-63	-185	-517	-217
s	173	125	160	129	99	94	59	73	202	218	367	271
SST	5.9	5.9	5.9	6.2	7.2	9.0	11.6	13.1	13.5	10.3	8.6	6.9
s	.2	.4	.3	.5	.5	1.0	1.0	.6	.8	.6	.6	.3

Monthly averaged values and standard deviations of Q_i, Q_b, Q_e, Q_s, Q and SST for station PAPA (50°N - 145°W).

Units: cal/cm^2/day for Q's and °C for SST.

wind speed. However, since the transfer equations are non-linear in nature, it is not possible to determine which of the terms is primarily responsible for the large daily variations in Q_e and Q_s.

The large standard deviation values for Q are a result of the combined effects of daily fluctuations in Q_i, Q_b, Q_e and Q_s. However, since Q_e and Q_s have such large standard deviation values with respect to their average values, it is these 2 terms that are primarily responsible for the large daily variation of the total heat transfer Q.

Compared to the heating terms, the standard deviations of the sea-surface temperature are quite low. This result suggests that the large variability of the total heat transfer on a daily basis is compensated by fluctuations in the depth of the mixed layer and by fluctuations in the strength of the horizontal advection within the mixed layer caused by the wind stress on the ocean surface. A study of the mixed layer depth values for station PAPA during 1962 by the Pacific Oceanographic Group of the Fisheries Research Board of Canada shows that the standard deviations of the daily layer depth values over a month can be as large as 40 per cent of the monthly averaged values; the yearly average of the standard deviation values is 17 per cent of the monthly mean layer depths. A study of the daily values of the total heat transfer across the

surface and the daily change in sea-surface temperature at stations NOVEMBER and PAPA showed that there was very little correlation between the two terms.

V. Discussion of Sea-Surface Temperature and Heat Transfer Anomalies

A. Spatial and Temporal Scales of Anomalies

1. In addition to the 7-year average values of SST and SAT for each month, the departures of each yearly value for a given month from the average or normal value also were computed. These departures or anomalies were printed out in map form for each month and each quantity and also punched onto cards for further analysis. Figures 7 and 8 show typical maps for the sea-surface and air temperature anomaly patterns.

(Many of the results reported below first appeared in a report written in 1966 by Dr. Hurd C. Willett and myself for the National Science Foundation. This report will be quoted extensively, especially when discussing the magnitude and duration of the SST and SAT anomalies.)

In looking at the anomaly maps of both SST and SAT for the 7-year period, it is seen that values of the same sign and magnitude occur in fairly extensive geographical areas. The magnitudes of the SST anomalies have values of 2°F to 4°F except in the coastal areas and particularly off of the Asian coast in winter, where larger values occur. The SAT anomalies are slightly higher than those of SST; however, this difference is usually not greater than 50 per cent. Ex-

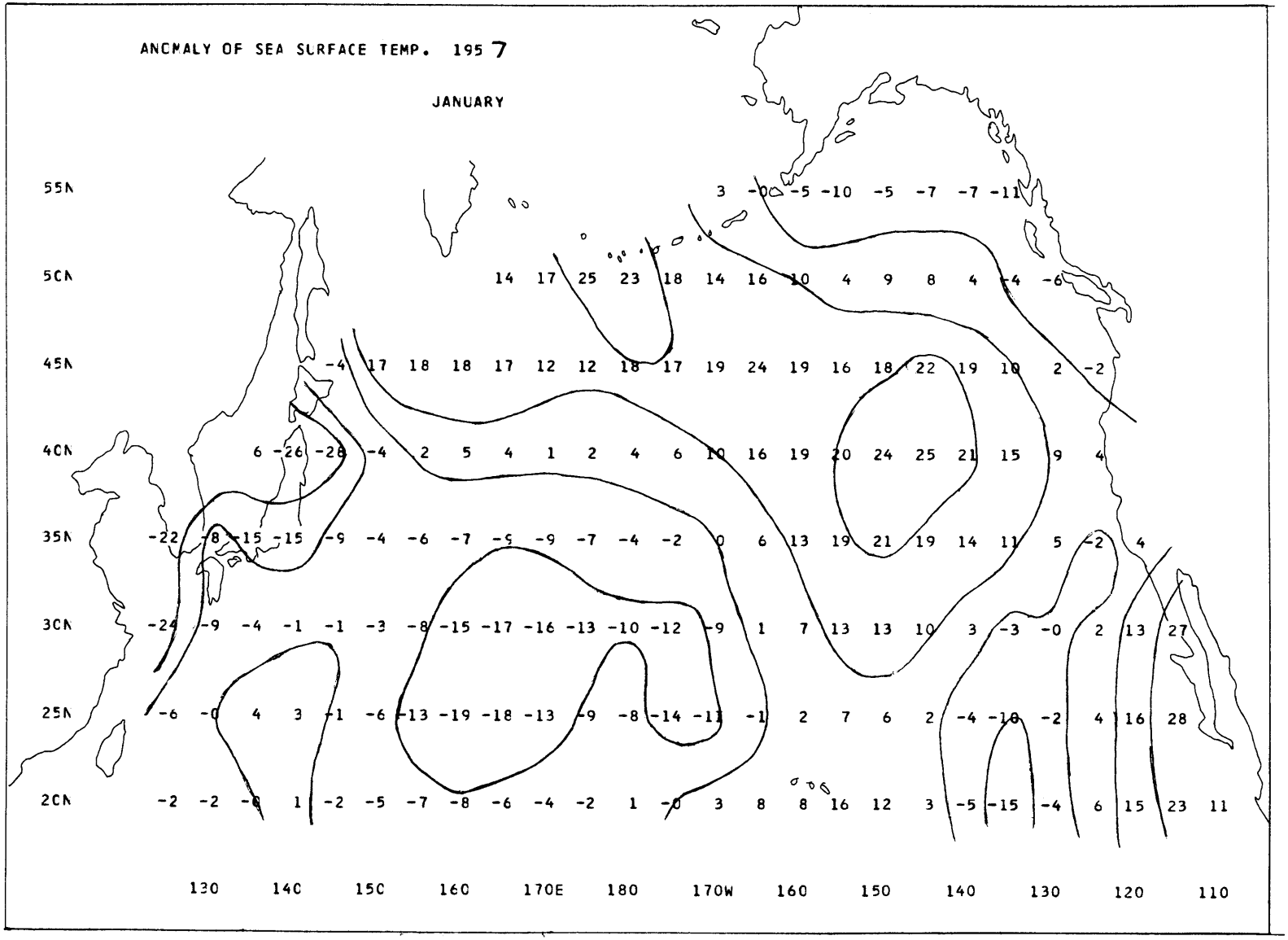

Figure 7. Anomaly pattern of sea-surface temperature. December 1957. (^{o}F x 10)

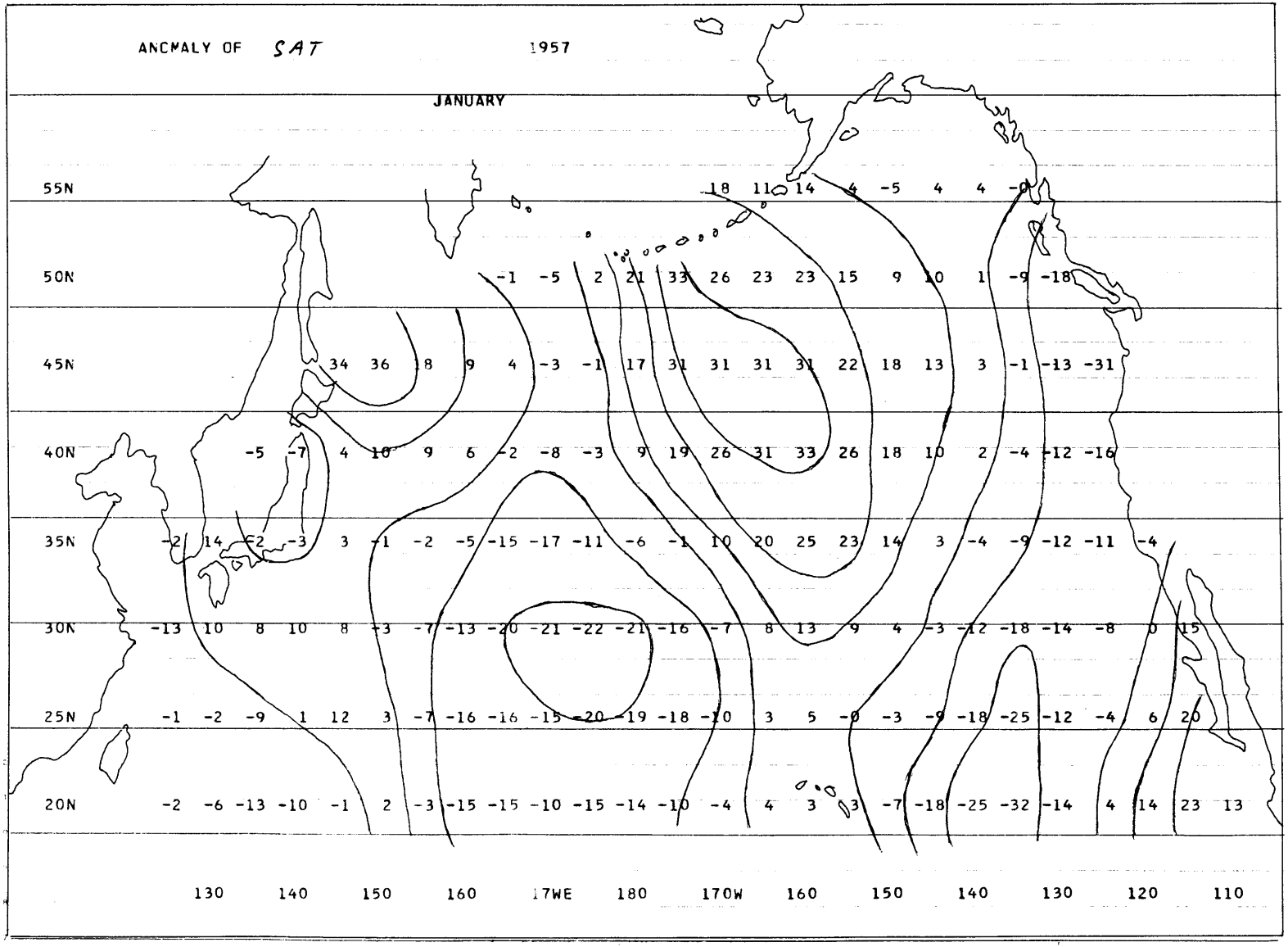

Figure 8. Anomaly pattern of surface air temperature. December 1957. (^{o}F x 10)

cept for these coastal regions, there is no outstanding difference between anomaly magnitudes for the different months and seasons.

Although there is a large degree of month-to-month persistence in the SST anomaly patterns, in many cases geographically extensive areas of large anomalies are eliminated or even reversed in sign in a single month's time. It is apparent that the effect of even a strong anomaly pattern in SST is not sufficient in some cases to prevent a change in the large-scale wind pattern and other meteorological parameters from completely destroying the anomalies.

In contrast to the month-to-month persistence, year-to-year persistence of the large-scale features of the anomaly patterns is not at all apparent. There appear to be no more cases of notable year-to-year persistence of a strong anomaly pattern than there are of complete elimination or even reversal of such a pattern. This conclusion applies to both sea-surface and air temperatures. For weak anomaly patterns, the year-to-year comparison generally suggests that a random relationship exists.

For a more objective analysis of the persistence of the monthly mean SST and SAT anomalies, a selection was made of 15 points, the intersections of the 25th, 35th and 45th parallels with the five meridians 150°E, 170°E, 170°W,

150°W and 130°W. This group of points covers most of the central North Pacific and permits a reasonable north-south and east-west comparison of conditions to be made.

For each of the 15 grid-points, a count was made of the total number of changes of sign of the anomalies that occurred during the 84-month period and also of the longest unbroken period of months for which the sign of the anomaly remained unchanged.

The average number of changes of sign of the SST anomalies over the period is 25, indicating that the average duration of an anomaly of the same sign is 3 and 1/3 months. The corresponding figures for the monthly mean anomalies of SAT are 28 and 3 months, respectively. For the SST anomalies, the average maximum period of consecutive months without change of sign is 14, with the maximum number of months at a point being 20. The same numbers for the SAT values are 13 and 19 months, respectively, and indicate that there is no significant difference between the stability of the sea and air temperature anomalies on a monthly mean basis.

There is no latitudinal variation in the stability of the anomaly values of SAT. SST anomalies, however, show a tendency toward maximum stability at 35°N and toward minimum stability at 25°N.

In addition to the "count study", auto-correlations of SST and SAT anomalies were made at 1, 2 and 3 months lag for

all 162 points on the map over the 84-month period. For the SST anomalies, the average value of the correlation coefficients over the 162 points is .53 at 1 month lag, .35 at 2 months lag, and .28 at 3 months lag; the maximum values of the individual coefficients occurred at 35°N for all 3 lags. For the SAT anomalies, the corresponding values are .40, .28 and .25, respectively; the latitudinal averages were approximately the same at all latitudes. These results tend to support the conclusions obtained from the "count study".

Lag correlations at 1 and 2 years also were computed for the SST and SAT anomalies on a seasonal basis, i.e. the 3 individual months of a season were correlated with the corresponding 3 months of the same season 1 and 2 years later. There is a consistent negative auto-correlation at all of the 15 selected points mentioned above at both the 1 and 2 years lag for both the sea and air temperature anomalies. This negative correlation again supports the conclusion of the "count study" that there is no year-to-year persisitence of these anomalies.

In order to determine how the sea and air temperatures are related to one another, contemporary correlation coefficients between the SST and SAT anomalies were computed for the entire 162-point network on a monthly, seasonal, yearly, and 84-month basis. The following discussion of the results will concern the 15 selected grid-points for the monthly, yearly and 84-month period basis and the entire 162 grid-points for the seasonal

basis.

The average value of the correlation between SST and SAT anomalies over the 12 months and the 15 points is .75, with only 4 of the 180 coefficients slightly negative. By month the coefficients ranged from .53 for January to .88 for May and September. The only significant variation of the correlation by latitude or longitude is that the average value of the 36 coefficients on the 150°E meridian is .67, while the average value of the other 4 meridians is .77. This difference reflects the effect of the Asian continent on the air masses that move over the ocean during the winter months.

For the correlations computed on a seasonal basis, the 162-point average values are .51 for winter, (December, January and February) .69 for spring, (March, April and May) .83 for summer (June, July and August) and .78 for fall (September, October and November). For all seasons except winter, the largest values occurred along 35°N.

When the correlation between the anomalies is computed by the 12 months of each of the 7 years separately, the average value of the 15 points is largest in 1957 (.76) and smallest in 1953 (.55). Again the largest values tend to occur along the 35th parallel.

The combination of all 84 months of the period raises the overall average correlation to .77 and reduces the geographical range of the coefficients. The latitudinal averages go from

.73 on the 25th parallel to .80 on the 35th, and the meridional values from .69 on the 150°W meridian to .79 on the others.

The principal facts learned from the above studies are that there is very little long-term persistence of both the sea and air temperature anomalies and that the anomaly patterns of both aea and air temperature are strongly related to each other. As Dr. Willett points out, "If feedback from ocean to atmosphere is to be accepted as a primary factor in the maintenance of long-term persistently anomalous patterns of the general circulation, then the water temperature anomalies must be markedly more stable (persistent) from month-to-month and year-to-year than are those of the atmospheric circulation. We know that the large-scale anomalies of the atmospheric circulation fluctuate in large amplitude in relatively short periods of time. To maintain a long-term persistent anomaly of the general circulation, we require some factor of control that is stable over correspondingly long periods, to the extent that it can pull the general circulation back into line when it goes off on a tangent." From the investigation of the persistence of the sea-surface temperature anomalies in the North Pacific Ocean, it does not seem that these anomalies provide the required control factor.

2. Monthly departures from the 7-year average values of the heat transfer terms Q_i, Q_b, Q_e, Q_s and Q also were

computed, printed out in map form, and punched onto cards.

The monthly departures or anomalies of the incoming radiation Q_i reflect the year-to-year variability in the cloud cover over the ocean. Their spatial scales are not as extensive as those of the sea-surface and air temperatures and are not as geographically coherent, i.e. high and low values as well as those of opposite sign occur close together at times. The magnitudes of the anomalies range from 5 to 20 per cent of the monthly average values and show very little month-to-month persistence.

Auto-correlations of the Q_i anomalies at 1, 2 and 3 months lag were computed over the 84-month period. The average value of the 162 correlation coefficients on the map is .04 at 1 month lag with very little latitudinal variation; a maximum value of .12 occurred at 20°N, 25°N, and 30°N and a minimum value of -.08 occurred at 55°N. The average values at 2 and 3 months lag were both negative, indicating that there is very little persistence in the Q_i anomalies due to the lack of persistence in the cloud cover anomalies.

The anomaly patterns of the effective back radiation Q_b also show very little geographical size or coherence, although they are more extensive than those of Q_i. As was shown by the size of the standard deviation values of Q_b discussed in Chapter IV, the magnitude of the anomalies are comparatively small, ranging from less than 1 per cent to 10 per cent of the

monthly average values. The average value of the correlation coefficients is .02 at 1 month lag and negative at both 2 and 3 months lag. These results show that there is very little persistence in the Q_b anomalies, as is the case for those of Q_i.

The anomaly patterns of the latent heat transfer Q_e are much larger in geographical size and magnitude than those of Q_i and Q_b and also tend to have more geographical coherence. At times, 25 per cent of the entire map is covered by an anomaly pattern of the same sign and magnitude. The magnitudes of the anomalies vary widely over areas of the map and from month to month, ranging from less than 1 per cent to over 75 per cent of the monthly average values. There is surprisingly little persistence in the latent heat anomaly patterns, with the average value of the auto-correlation coefficient at 1 month lag being -.15; the coefficients at 2 and 3 month lags are also negative.

It would be interesting to know which factor in the transfer equation is primarily responsible for the month-to-month and year-to-year fluctuations in the latent heat transfer. However, due to the non-linear nature of the equation, it is not possible to separate the effects of fluctuations in the vapor pressure difference and in the surface wind speed. A perturbation analysis of the transfer equation was tried in which the equation was written as

$$Q_e \propto \overline{q}\,\overline{u} + \overline{u}\;\; q' + \overline{q}\,u' + \;\; q'u' \quad , \qquad (V.1)$$

where Q_e is a monthly value of the latent heat transfer, $\overline{q}$ and $\overline{u}$ are the 7-year averages of the specific humidity and wind speed for a particular month, and q' and u' are the departures of particular monthly values from the average values. If the 4th term and either the 2nd or 3rd terms on the right-hand side of equation (V.1) were small compared to the other 2 terms, we could say that the remaining 2nd or 3rd term was responsible for the fluctuations in Q_e since $\overline{q}\,\overline{u}$ is a constant. However, it turns out that the last 3 terms are about the same order of magnitude and no information is gained.

One can find out something about the relative importance of the ocean and atmosphere in fluctuations of the vapor pressure or specific humidity, since the variance of the difference can be written as

$$V\,(q_s - q_a) = CV\; q_s.(q_s - q_a) \quad + CV\; q_a.(q_a - q_s) \quad , \qquad (V.2)$$

where V denotes "variance of", CV denotes "covariance between", and q_s and q_a are the specific humidities of the sea and air, respectively.

The two covariance terms were computed over the 7-year period for the mid-season months of January and July. For the month of January, it was found that fluctuations in the specific humidity of the air account for 2/3 or more of the variance in $(q_s - q_a)$ at 135 of the 162 points on the map, that fluctuations in the specific humidity of the sea surface account for 2/3 or more of the variance of $(q_s - q_a)$ at 14 of the 162 points, and that the fluctuations of both quantities are of approximately equal importance at 13 of the 162 points. For the month of July, fluctuations in q_s account for 2/3 or more of the variance in $(q_s - q_a)$ at 69 points, fluctuations in q_a account for 2/3 or more of the variance at 67 points, and the fluctuations of q_s and q_a are of equal importance at 26 points. From this it is concluded that fluctuations in the specific humidity of the air are more predominant than those of the sea surface during the winter months, and that the two fluctuations are of equal importance during the summer months.

The anomaly patterns of the sensible heat transfer Q_s are similar to those of Q_e in that they are geographically coherent and can cover a large portion of the entire map during some months. Their magnitude also varies widely from month to month, ranging from less than 1 per cent of the monthly average values to over 100 per cent during the summer months when the sensible heat transfer is small. The

anomalies also have very little month-to-month persistence; the average auto-correlation coefficient at 1 month lag is -.15, and the values at 2 and 3 months lag are also negative.

The same type of perturbation analysis of the transfer equation for sensible heat was attempted as was done for the latent heat equation. Again, the 4 terms of the expansion were of approximately equal magnitude, and nothing was learned about the relative importance of fluctuations in the sea-air temperature difference and the wind speed in determining fluctuations in the sensible heat transfer. However, a covariance analysis of the sea-air temperature difference was done with the following results: for January, fluctuations in the air temperature T_a account for 2/3 or more of the variance in the sea-air temperature difference $(T_s - T_a)$ at 132 points, fluctuations in T_s account for the same amount of variance in $(T_s - T_a)$ at 20 points, and the fluctuations of T_s and T_a are of equal importance at 10 points; for the month of July, the corresponding numbers are 99, 45 and 18, respectively; as for the specific humidity, air temperature fluctuations are more predominant during the winter months while both air and sea temperature fluctuations are of approximately equal importance during the summer months.

The anomaly patterns of the total heat transfer Q vary widely over the map for a particular month and from month-to-month during the 84-month period. Since the anomalies of

Q_i and Q_b are comparatively small, these fluctuations are primarily due to the fluctuations in Q_e and Q_s. The magnitudes of the Q anomalies range from less than 1 per cent of the monthly average values to over 200 per cent, with the largest values occurring in the summer months. Although there is some geographical coherence in the anomalies, it is not as great as that for Q_e and Q_s. From the values of the auto-correlation coefficients computed at 1, 2 and 3 months lag over the 84-month period (-.14, -.14 and -.09), there appears to be very little persistence in the anomaly patterns. This result is not surprising, since there was also very little persistence found in the 4 quanitities that make up the total heat transfer.

B. Relationships Between Sea-Surface Temperature Fluctuations and Heat Transfer Anomalies

In Section A we saw that sea-surface temperature anomalies of fairly extensive geographical size occurred in all of the 84 months under investigation. The magnitudes of the anomalies varied widely from area to area and from month to month. It was also noted that the anomaly patterns exhibited some persistence in that the auto-correlations at the individual points remained positive on the average to about 3 months lag. Two questions arise from these observations: (1) What causes the anomaly patterns of sea-surface temperature to be so different from year to year during the same month and in the same area; and (2) What accounts for the month-to-month persistence of the anomaly patterns. The first question will be dealt with below in sub-sections 1, 2, 3, 4 and 5, in which the results of correlation studies between anomalies in the heat transfer between ocean and atmosphere and anomalies in the sea-surface temperature will be discussed. The second question is not easily answered, but will be discussed in sub-section 6.

1. In an attempt to account for the large-scale anomaly patterns that occur in the sea-surface temperature, a series of correlation studies was made in which the 7-year average values of Q_i, Q_b, Q_e, Q_s, Q and ΔSST for each month were subtracted from the individual monthly values and the results

correlated against each other over the 7-year period. The correlation coefficients were computed in 3 ways: (1) using the 7 pairs of anomaly values for each of the 12 months; (2) using the 21 pairs of values for each season of the 7 years; and (3) using all 84 pairs of values for the 7-year period. The anomalies of the change in sea-surface temperature over a month ΔSST were used instead of the SST anomalies since it is the change in temperature over a time period that is affected by heat transfer during a particular month; using the SST anomalies themselves would not be correct since part of the anomaly could have been caused by heat transfer during a preceding month.

The results of correlating the anomalies of the individual heat transfer terms Q_i, Q_b, Q_e and Q_s with the anomalies of ΔSST show that no one term is primarily responsible for producing fluctuations in the sea-surface temperature. However, when the anomaly patterns of the total heat transfer across the ocean surface Q were correlated with the anomaly patterns of ΔSST, significant results were obtained.

On a seasonal basis, i.e. using 21 pairs of values in each correlation coefficient, the average values of the 162 coefficients on the map are .36 for winter (December, January, and February), .21 for spring (March, April and May), .27 for summer (June, July and August) and .27 for fall (September, October and November). The largest individual

values occur in winter, in which there are 67 points at which the coefficients are larger than the 5 per cent confidence limit. The corresponding numbers for the other seasons are 49 for spring, 41 for summer, and 40 for fall. The latitudinal averages of the correlations for winter are shown in Table VII along with those for the other three seasons. Although the magnitudes of the coefficients are not very large, the fact that they are positive over the entire map in each of the seasons indicates that the sea-surface temperature anomalies are related to anomalies in the total heat transfer across the sea surface.

In addition to the seasonal correlations, all 84 months were combined and a correlation was computed at each of the 162 grid-points over this period. The results are shown in Figure 9. Of the 162 coefficients on the map, 102 reach the 5 per cent confidence level of .22 and 86 reach the 1 per cent level of .28.

In order to get some idea of the variability of the relation between anomalies of Q and those of Δ SST, pattern correlation coefficients between the two quantities for each of the 84 months of the period were computed. They range from -.27 in March of 1953 to .73 in December of 1953. Over the 7-year period, the month of December has the largest average value of .43, while the month of March has the lowest average value of .10.

Table VII

	Winter	Spring	Summer	Fall	Year
55°N	.20	-.18	.29	.16	.12
50°N	.34	.18	.31	.31	.28
45°N	.38	.24	.26	.36	.31
40°N	.40	.24	.40	.42	.36
35°N	.45	.35	.31	.34	.36
30°N	.45	.27	.21	.25	.30
25°N	.27	.32	.20	.20	.25
20°N	.35	.26	.18	.09	.22

Average latitudinal correlation coefficient between anomalies of total heat transfer Q and anomalies of change in sea-surface temperature Δ SST.

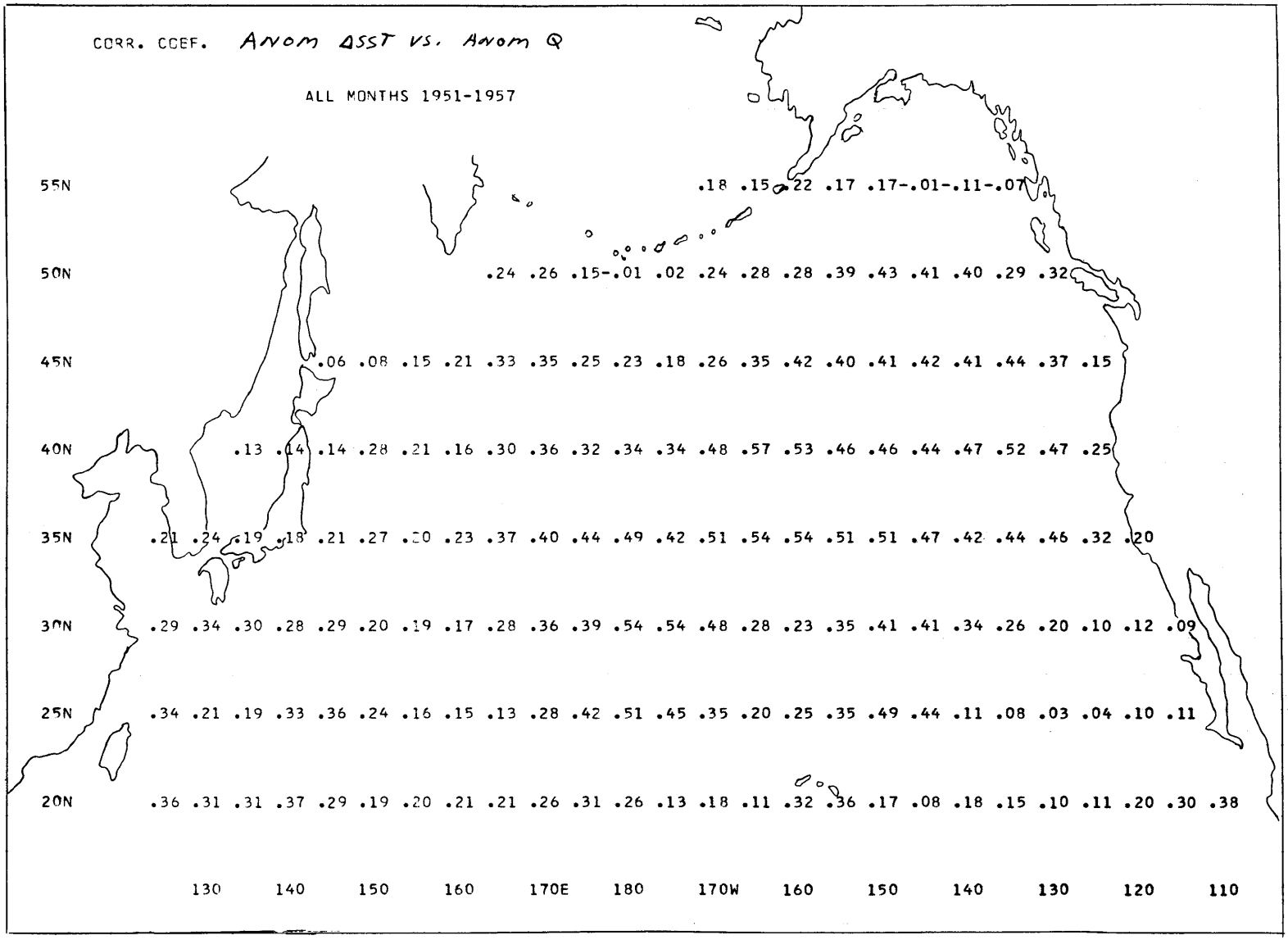

Figure 9. Correlations between the anomalies of total heat transfer across the sea-surface Q and anomalies of Δ SST based on 84 months of data from 1951 through 1957.

There is very little variability between years in the 12-month average value of the pattern correlation coefficients; they range from .21 in 1951 to .28 in 1953, 1955 and 1957. Whether averaged over the 7-year period for each month or over the 12 months of each of the 7 years, the pattern correlation coefficients are all significant at the 5 per cent confidence level and many are significant at the 1 per cent level.

2. Another method of changing the temperature of the sea surface is by the horizontal advection of surface water across sea-surface temperature iso-therms. Adopting a method first proposed by Namias (1959, 1965), in which he considers that the advection of surface water is about 45° to the right of the surface geostrophic flow, the change in sea-surface temperature was computed at each grid-point for each month using the north-south and east-west gradients of sea-surface temperature and the north-south and east-west components of the surface geostrophic flow. The present method differs from that of Namias in that contemporary values of the sea-surface temperature gradient were used instead of previously determined "normal" values.

Using the empirical expression for the transport of water 45° to the right of the surface wind stress proposed by Ekman,

$$v/w = 0.0127/(\sin\phi)^{1/2} \qquad \text{(V.3)}$$

where v is the velocity of the surface water, w is the velocity of the geostrophic wind, and ϕ is the latitude, the advection of temperature can be determined from the relation

$$- \vec{v} \cdot \vec{\nabla} T \tag{V.4}$$

where $\vec{v}$ is the water velocity and $\vec{\nabla} T$ is the gradient of sea-surface temperature at a grid-point.

In computing the values of the east-west and north-south components of the geostrophic wind, u_g and v_g, monthly averaged values of the sea-level pressure were used. The components were computed at each of the 162 grid-points using finite difference approximations to the geostrophic wind equations in spherical coordinates. The horizontal gradients of the sea-surface temperature $(T_s)_\lambda$ and $(T_s)_\phi$ were computed by applying finite difference approximations to the gradient relationships in spherical coordinates,

$$(T_s)_\lambda = \frac{1}{R \cos\phi} \frac{\partial T_s}{\partial \lambda} \approx \frac{1}{R \cos\phi} \frac{\Delta T_s}{\Delta \lambda}$$

and (V.5)

$$(T_s)_\phi = \frac{1}{R} \frac{\partial T_s}{\partial \phi} \approx \frac{1}{R} \frac{\Delta T_s}{\Delta \phi} \quad ,$$

where R is the radius of the earth and λ and ϕ denote longitude and latitude in radians. The grid spacing was 5°

and $\Delta\lambda$ and $\Delta\phi$ were 10° or π /18 radians.

Once the components of the geostrophic wind were known, the surface water velocity components, u_s and v_s, were then determined from

$$u_s = \frac{0.0127}{\sqrt{2}(\sin\phi)^{1/2}} \quad (u_g + v_g) \tag{V.6}$$

and

$$v_s = \frac{0.0127}{\sqrt{2}(\sin\phi)^{1/2}} \quad (v_g - u_g).$$

The surface temperature advection was then computed from

$$-\vec{v} \cdot \vec{\nabla} T \approx - \left[u_s(T)_\lambda + v_s(T)_\phi \right] \quad . \tag{V.7}$$

Anomalies of the surface temperature advection were computed for each of the 84 months in the same manner as for the heat transfer and temperature terms, and the results correlated with the anomalies of Δ SST on a seasonal and an 84-month basis.

On the seasonal basis, the average values of the 162 coefficients on the map are .22 for winter, .19 for spring, .10 for summer, and .21 for fall. As in the case of the surface heat transfer correlations, the largest values occur in winter, where there are 35 values reaching the 5 per cent confidence

level. The corresponding numbers of the other seasons are 25 for spring, 17 for summer, and 27 for fall. The latitudinal averages of the correlations for each season are shown in Table VIII. The correlations are consistently highest at 45°N and lowest at 20°N during all of the seasons.

The correlation coefficients based on the 84-month data series are shown in Figure 10. Of the 162 values on the map, 74 reach the 5 per cent confidence level and 44 reach the 1 per cent level. By and large, the best results were obtained between latitudes 30°N and 50°N and in the central part of the ocean away from coastal boundaries. The poor results at the latitudes 20°N and 25°N agree with those found by Namias (1965) and may be due to the low variability of temperature in this region, in which observational errors could be as large as the anomalies themselves. The area of low correlation in the western part of the map is probably due to the effect of the variability in the Kuroshio Current. This current's large northward transport of water and its meanders could easily overshadow the effect of temperature advection due to surface wind-drift in this area.

Pattern correlations between each of the two sets of anomalies were also computed for each of the 84 months in the period. The values range from -.18 in January of 1955 and July of 1953 to .55 in January of 1956. If the correlation values are averaged over the 7-year period for each month,

Table VIII

	Winter	Spring	Summer	Fall	Year
55°N	.11	.12	.20	.22	.16
50°N	.29	.32	.12	.34	.27
45°N	.33	.40	.18	.41	.33
40°N	.34	.23	.16	.31	.26
35°N	.39	.25	.05	.20	.22
30°N	.32	.26	.06	.01	.16
25°N	.09	.04	.08	.08	.07
20°N	-.12	-.07	-.04	.12	-.02

Average latitudinal correlation coefficients between anomalies of horizontal temperature advection and anomalies of change in sea-surface temperature Δ SST.

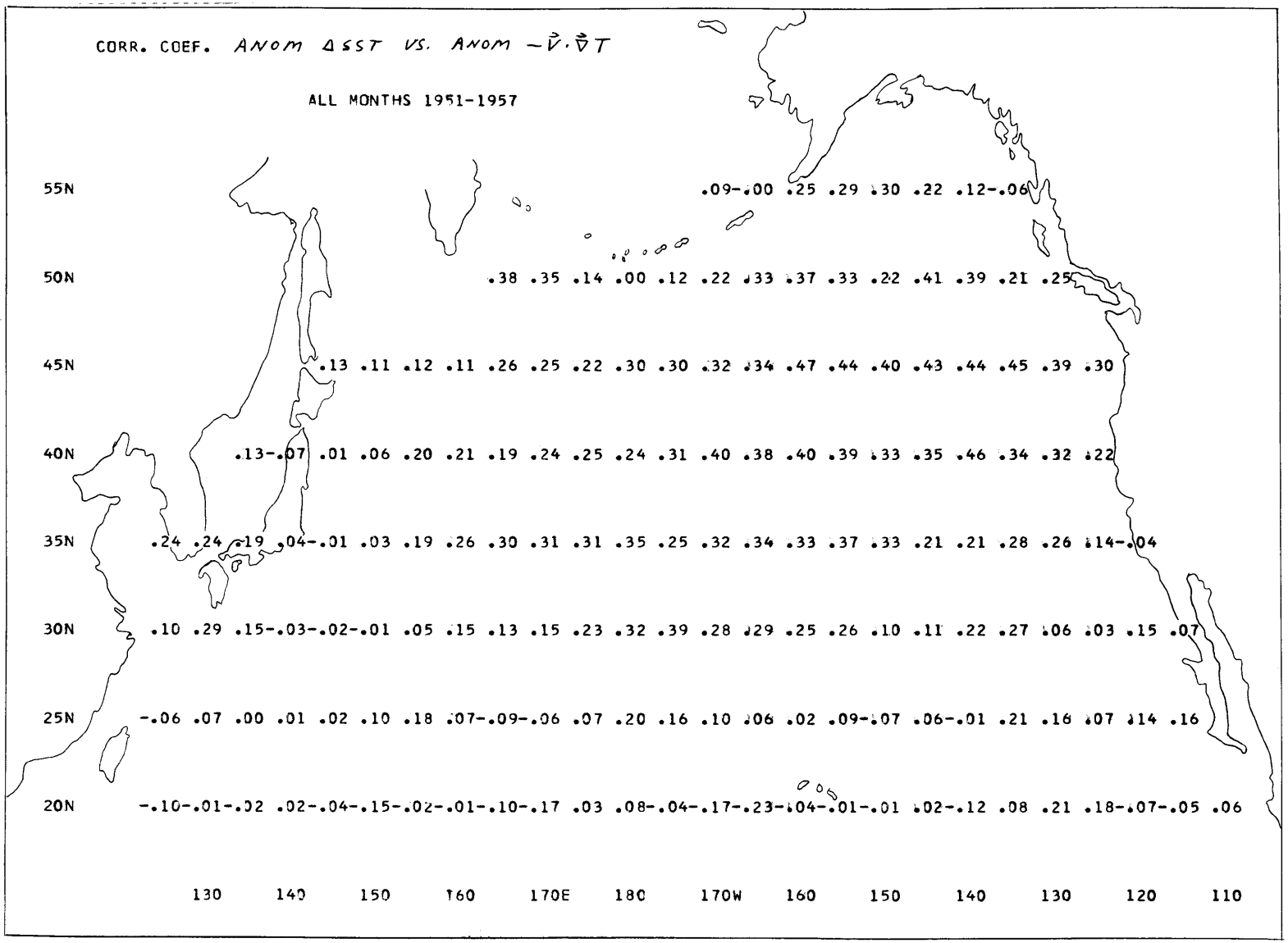

Figure 10. Correlations between the anomalies of horizontal temperature advection and the anomalies of Δ SST based on 84 months of data from 1951 through 1957.

September has the largest value of .32, while June has the lowest value of .04. There is a great deal of variability between years in the 12 month average values of the pattern correlations, with the results ranging from .08 in 1954 and 1955 to .28 in 1951. About half of the average values are significant at the 5 per cent confidence level.

Several other methods of computing horizontal temperature advection were also tried. The empirical formula of Witting (1909),

$$\vec{v}_s = K \sqrt{\vec{v}_g} \quad , \tag{V.8}$$

where $\vec{v}_s$ is the velocity of the surface water, $\vec{v}_g$ is the geostrophic wind averaged over some time period, and K is a constant equal to 4.8 was used to compute the u and v components of the surface drift. However, when the results of the sea-surface temperature advection anomalies computed from these components were correlated with the anomalies of Δ SST, no significant correlation patterns were obtained for any season. This method is the same one that is used by the U.S. Fleet Numerical Weather Facility (FNWF) at Monterey, California, to compute temperature advection due to wind drift. They base their calculations on daily rather than monthly averaged data, however, and this may account for the difference between their success in using the method and our failure.

An attempt was also made to compute the vertically integrated horizontal heat advection in the upper mixed layer of the ocean due to Ekman transport and to correlate the results with the observed changes in the temperature of the layer ΔSST. In order to determine this advection,

$$-c_p \int_{-D}^{0} (\rho \vec{v}_e \cdot \vec{\nabla} T)\, dz \quad , \tag{V.9}$$

where v_e is the horizontal velocity vector, T is the temperature at depth -z, and -D is the depth of the mixed layer, the assumption was made that T is independent of z and equal to the surface temperature T_s. Then (V.9) can be reduced to

$$-c_p \left[\int_{-D}^{0} \rho v_e dz \right] \cdot \vec{\nabla} T_s \quad . \tag{V.10}$$

Using the relationships

$$\int_{-D}^{0} \rho u \, dz = U_e = \tau_\phi / f$$

and

$$\int_{-D}^{0} \rho v \, dz = V_e = -\tau_\lambda / f, \tag{V.11}$$

where U_e and V_e are the vertically integrated east-west and north-south components of the Ekman transport, τ_λ and τ_ϕ are the east-west and north-south components of the surface wind stress, and f is the Coriolis parameter, the vertically

integrated horizontal heat advection was then computed from

$$-c_p \int_{-D}^{0} \rho \vec{v}_e dz \cdot \vec{\nabla} T_s = -c_p \left[U_e (T_s)_\lambda + V_e (T_s)_\phi \right] , \qquad (V.12)$$

where $(T_s)_\lambda$ and $(T_s)_\phi$ are the east-west and north-south components of the sea-surface temperature gradient. The components of the wind stress τ_λ and τ_ϕ were determined from

$$\tau_\lambda = \rho_a C_D (u_s^2 + v_s^2)^{1/2} \cdot u_s , \qquad (V.13)$$

and

$$\tau_\phi = \rho_a C_D (u_s^2 + v_s^2)^{1/2} \cdot v_s ,$$

where ρ_a is the density of air, u_s and v_s are the components of the surface wind velocity, and C_D is the drag coefficient and a function of the surface wind strength.

The results of correlating the anomalies of the horizontal heat advection due to Ekman transport and the anomalies of Δ SST also showed no significant correlation patterns in any of the seasons or over the entire 84-month period.

From the above studies on the effect of surface current advection on changes in the sea-surface temperature, it seems as if surface winds are capable of driving a shallow surface layer of the ocean at 45° to the right of the wind direction quite freely back and forth over the sea surface, at least in the central parts of the ocean. Although the results of this

study are based on monthly averaged data, it seems reasonable to assume that the same type of movement can occur on a daily basis due to the passage of storm systems. The work of the FNWF at Monterey supports this idea, since their temperature analyses and forecasts are made on a daily basis, and their results have been verified to some degree by actual observations.

3. In an attempt to improve the correlations between the large-scale anomaly patterns of the sea-surface temperature and the possible physical mechanisms responsible for these anomalies, the changes in sea-surface temperature during a month due to heat transfer across the sea surface were added to the changes in sea-surface temperature due to horizontal wind-drift temperature advection.

The change in temperature of the upper mixed layer (assumed equal to the change in the sea-surface temperature) can be computed from the relation

$$\frac{Q}{\rho C_p H} \quad , \tag{V.14}$$

where Q is the total heat trnasfer across the sea surface, ρ is the density of sea water, C_p is the specific heat of sea water, and H is the depth of the mixed layer. The change in temperature ΔT over a period of time Δt can then be

written as

$$\frac{\Delta T}{\Delta t} = \frac{Q}{\rho C_p H} - \vec{v} \cdot \vec{\nabla} T \ , \qquad (V.15)$$

where $- \vec{v} \cdot \vec{\nabla} T$ is the contribution due to horizontal advection.

Since the year-to-year variations in the monthly values of the mixed layer depth H are not known over large areas of the North Pacific, the "normal" values of H given by Pattullo and Cochrane (1951) were used in all of the computations. This procedure could lead to considerable errors in determining the monthly values of $Q/\rho C_p H$, since the results of data taken at weathership stations in the North Pacific (see Chapter IV) have shown that large variations in H can occur between years for the same month. As was also mentioned in Chapter IV, there is some doubt as to the validity of the mixed layer depth values for some months in the eastern part of the ocean. (This uncertainty may be cleared up in the near future, however, since Mrs. Margaret Robinson at the Scripps Institution of Oceanography is presently preparing maps of the seasonal thermocline depth for all areas of the North Pacific based on all available bathythermograph observations.)

Again, monthly anomalies of the computed temperature change were calculated and the results correlated on both a seasonal and an 84-month basis. On the seasonal basis, the average values of the 162 correlation coefficients on the map

are .38 for winter, .22 for spring, .28 for summer and .28 for fall. For the winter season, 78 values reach the 5 per cent confidence level and 44 reach the 1 per cent confidence level. For the other 3 seasons, the corresponding numbers are 51 and 24 for spring, 43 and 19 for summer, and 45 and 18 for fall. The latitudinal averages of the correlations are shown in Table IX.

The correlation coefficients based on the 84-month data series are shown in Figure 11. Of the 162 values on the map, 112 reach the 5 per cent confidence level and 91 reach the 1 per cent level. Again, the best results were obtained between the latitudes 30°N and 50°N and in the central part of the ocean away from the coastal boundaries. The results near the coasts and along the 20th and 25th parallels are better, however, than those obtained using only the horizontal temperature advection equation, indicating that anomalies in the total heat transfer across the sea surface play an important role in determining sea-surface temperature fluctuations in these areas.

The pattern correlations computed between the anomalies of the computed change in temperature and Δ SST range from -.27 in March of 1953 to .75 in December of 1953. When the pattern correlations are averaged over the 7-year period for each month, December has the largest value of .41 and March has the lowest value of .07. As in the previous two correla-

Table IX

	Winter	Spring	Summer	Fall	Year
55°N	.21	-.09	.30	.20	.16
50°N	.38	.14	.32	.36	.30
45°N	.43	.23	.27	.41	.34
40°N	.44	.28	.40	.42	.38
35°N	.49	.41	.33	.32	.39
30°N	.48	.27	.22	.26	.31
25°N	.28	.31	.21	.20	.25
20°N	.35	.25	.18	.09	.22

Average latitudinal correlation coefficients between anomalies of Δ SST and anomalies of the sum of sea-surface temperature change due to heat transfer through the sea surface and that due to horizontal wind-drift advection.

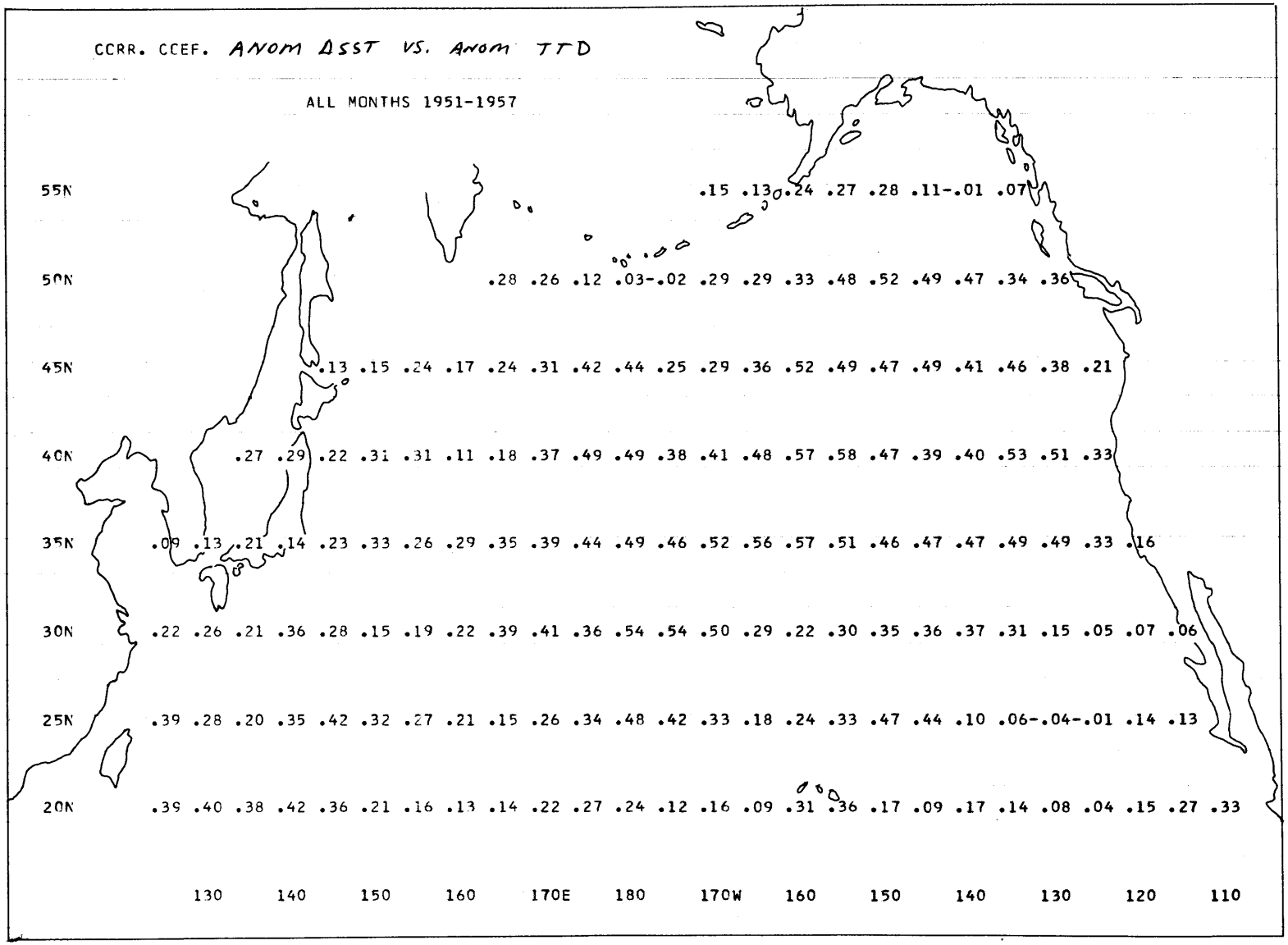

Figure 11. Correlations between the anomalies of the sum of the change in SST due to heat transfer across the sea surface and to horizontal temperature advection and the anomalies of Δ SST based on 84 months of data from 1951 through 1957.

tion studies, there is little variability between years in the 12-month average values of the pattern correlations; the results range from .24 in 1951 to .29 in 1955.

The results obtained by combining the effects of heat transfer across the sea surface and those of horizontal temperature advection are somewhat better than using either of the terms by itself. The main problem in this method is that the temperature differences computed from the surface heat transfer term are much larger in magnitude than those determined from the advection term. When the two are added together, the former term greatly overshadows the effect of the latter and not much information is gained. The temperature differences or anomalies computed from the surface heat transfer term are, in fact, larger by an order of magnitude than any of those observed in the 84-month period under investigation. The reasons for this discrepancy probably lie in using unreliable values for the depth of the mixed layer H and in the fact that there is a loss of heat through the bottom of the mixed layer due to vertical eddy diffusion, which is unaccounted for in this study. Before more reliable values of temperature anomalies in the mixed layer can be obtained, much will have to be learned about the causes of fluctuations in the mixed layer depth and about the nature of heat loss across the thermocline region.

4. An attempt was made to see if vertical velocities induced at the bottom of the Ekman surfac layer had any effect upon the sea-surface temperature anomalies. These velocities were computed from the relation

$$w_e = \frac{\beta}{\rho f}(V - V_e), \qquad (V.17)$$

where w_e is the vertical velocity beneath the layer, f is the Coriolis parameter, β is the latitudinal variation of the Coriolis paramater, V is the vertically integrated total meridional transport, and V_e is the vertically integrated Ekman meridional transport. (A derivation of this equation is given on pages 43 through 45 in the report prepared by Willett and Clark for the National Science Foundation in 1966.)

The monthly averaged values of V and V_e were taken from the work done by Fofonoff (1960-1963) on transport computations for the North Pacific Ocean for the Fisheries Research Board of Canada.

The vertical velocities were computed at each of the 162 grid-points for all 84 months, and the monthly anomalies were obtained by subtracting the 7-year average value for each month from the 7 individual monthly values. These results were then correlated with the anomalies of Δ SST on a seasonal basis.

The results of the correlation study show that anomalies

in the vertical velocity beneath the Ekman layer, alone, have little effect on the sea-surface temperature anomalies. The average values of the 162 grid-point correlation coefficients are -.06 for winter, .00 for spring, -.11 for summer and -.15 for fall. The slight negative correlation between the two anomaly patterns for three of the seasons indicates that an anomalous upward transport of water from beneath the Ekman layer tends to lower the temperature of the surface layer. The relationship is not very strong, however, since the average correlation coefficients are very small for each of the four seasons.

In order to test the combined effects of heat transfer across the surface layer, horizontal temperature advection, and vertical transport of water beneath the Ekman layer, a multiple linear correlation analysis was computed for the three terms, Δ SST, the sum of temperature change caused by heat transfer across the ocean surface and of temperature change caused by horizontal advection (TTD), and the vertical velocity induced at the bottom of the Ekman layer (VV). The computations were done at each of the 162 grid-points and for each of the seasons using the relationship

$$R_{3.21}^2 = \frac{r_{31}^2 + r_{32}^2 - 2r_{31}\, r_{32}\, r_{12}}{1 - r_{12}^2} \quad , \qquad (V.18)$$

where $R_{3.21}^2$ is the percentage of the variance of ΔSST accounted for by relation to TTD and VV, r_{31} is the linear correlation coefficient between ΔSST and TTD, r_{32} is the linear correlation coefficient between ΔSST and VV, and r_{12} is the linear correlation coefficient between TTD and VV.

The results of the analysis are shown in Table X. It is seen from the table that the percentage of the variance of ΔSST accounted for by relation to the other variables is increased from 20 to 25 per cent in winter, 13 to 18 per cent in spring, 12 to 18 per cent in summer, and 13 to 14 per cent in fall by including the effects of the vertical velocities beneath the Ekman layer. The magnitudes of the increase are the largest in the higher latitudes, indicating that upwelling associated with Ekman layer divergence may be an important factor in determining the temperature of the surface layer in this region.

As for the statistical significance of the results of the multiple correlation analysis, 58 of the 162 values on the map reach the 5 per cent confidence level and 36 reach the 1 per cent level for winter, 45 of the 162 values reach the 5 per cent level and 15 reach the 1 per cent level for spring, 34 of the 162 values reach the 5 per cent level and 10 reach the 1 per cent level for summer, and 36 of the 162 values reach the 5 per cent level and 13 reach the 1 per cent level for fall. By chance alone, it is expected that 8 of the 162

Table X

	Winter		Spring		Summer		Fall	
	TTD	TTD and VV	TTD	TTD and VV	TTD	TTD and VV	TTD	TTD and VV
55°N	12	19	4	6	11	17	7	19
50°N	19	25	12	21	14	20	15	22
45°N	22	30	16	21	11	16	20	24
40°N	23	27	15	19	20	25	22	27
35°N	28	31	18	21	17	23	15	19
30°N	25	30	14	22	10	14	10	12
25°N	16	21	16	21	7	12	10	15
20°N	14	18	9	17	8	14	7	12
Average	20	25	13	18	12	18	13	19

Percentage of variance of Δ SST accounted for by relation to TTD and to TTD plus VV.

values on the map would reach the 5 per cent level and 2 of the 162 values would reach the 1 per cent level.

5. In order to see how large the errors are in computing the temperature of the mixed layer, the observed values of ΔSST (Δ SSTO) were subtracted from the computed values of Δ SST (Δ SSTC) for all grid-points and all months. These results were averaged over the 7-year period for each of the 12 months and 162 points; the departures from these mean or normal values were then computed and punched onto cards for further analysis.

From the maps of the normal values of (Δ SSTC-ΔSSTO), it is seen that the errors are all an order of magnitude larger than the observed values and have the largest values in all 12 months in the western part of the ocean. This last fact is probably due to having neglected the transport of heat by the Kuroshio in calculating the SSTC values. In fall and winter, the (ΔSSTC-ΔSSTO) values are negative for all points, indicating that the temperature decreases due to heat loss were over computed. During the summer months, the (Δ SSTC-Δ SSTO) values were positive at all points, indicating that the temperature increases due to heat gain were also over computed. During the spring months, the (Δ SSTC-Δ SSTO) values were of smaller magnitude and mixed in sign; this indicates that the computed changes in temperature are closer to the observed values and that over computation occurred for both heat loss and heat gain.

If the computed heat transfers and the observed tempera-

ture changes are the correct order of magnitude, then there must be heat advection occurring in both horizontal and vertical directions. In his 1965 paper, Wyrtki, using the same data as in this report, calculated that the heat gain of 3×10^{14} cal/sec of the surface layer of the North Pacific Ocean must be compensated by deep water ascending with an average velocity of 1.25×10^{-5} cm/sec. This upward transport of cold water and an outflow of warm deep water of 8×10^{6} m^3/sec, partly through the Indonesian waters and partly in the eastern tropical Pacific from the counter current to the south of the equational current, maintains the thermal structure of the ocean in the presence of a net heat gain.

In order to maintain the temperature distribution of the ocean in the presence of horizontal inequalities of heat exchange, there must be a horizontal advection of heat in the surface layer of about 10×10^{6} m^3/sec. Wyrtki comments that this is a weak circulation in comparison to the Kuroshio transport of 65×10^{6} m^3/sec and is, therefore, relatively sensitive to transient changes in the strength of the heat sources and sinks. From Wyrtki's study and the present one, it has been shown that pronounced changes in these sources and sinks do occur on a seasonal and monthly basis and could help to account for the anomalies of sea-surface temperature by influencing the horizontal surface currents.

In spite of the deficiencies of the methods described above, it appears that heat transfer across the sea surface, horizontal temperature advection due to wind drift, and vertical velocities induced beneath the Ekman layer profoundly affect the temperature of the ocean's surface, at least on a monthly and seasonal basis. In order to improve our knowledge of sea-surface temperature fluctuations, more and better observations of oceanographic and meteorological parameters are needed, especially at shorter time scales; we need to develop better equations to express the transfer of heat between ocean and atmosphere and also between the surface layer of the ocean and its lower regions; more information is needed concerning the variations of the surface wind stress at all time scales and the response of ocean surface currents to these variations; and, finally, a theory is needed that treats the ocean and atmosphere as two interacting media, from which the transfer of various properties across their common boundary can be computed.

6. In section A of this chapter, we found that there was a fair degree of persistence in the sea-surface temperature anomaly patterns at 1, 2 and 3 months lag. We did not, however, find any significant persistence in the anomalies of the total heat transfer across the sea surface or in the anomalies of the horizontal temperature advection. This persistence in the sea-surface temperature anomalies must then be

related in some way to the dynamics of forced and free convection that occur in the upper mixed layer of the ocean.

Following the reasoning of Kraus and Rooth (1961), we consider that the sea is cooled at the surface by evaporation, conduction and infra-red radiation. However, heating by the absorption of solar radiation extends to an appreciable depth, and, therefore, there must be a layer in which heat is transported upwards. This turbulent upward flux of heat is associated with free convection and tends to produce a layer of nearly constant potential temperature. In addition to this free convection, the surface layer is stirred by the action of the wind, which also tends to produce a layer of constant potential temperature through forced convection. Thus, changes in the heat transfer across the ocean surface and the accompanying changes in the surface wind stress should have a profound influence on the temperature and depth of the ocean's upper mixed layer.

Using data obtained from weathership station Echo (35°N-48°W) for July, August and September of 1958 and 1959, Kraus and Rooth computed 10-day means of the heat loss B across the surface layer and the heat added to the surface layer through solar radiation S. The difference between S and B is the heat balance of the quasi-isothermal of mixed surface layer. Comparing the values of (S-B) with the values of the mixed layer depth, they found that there is a direct relation between the

two quantities. In other words, when (S-B) is small, indicating large cooling of the surface, the depth of the mixed layer increases; when (S-B) is large, indicating small cooling or heating of the surface, the depth of the mixed layer decreases. In periods of large cooling, the increased effects of free and forced convection combine to increase mixing in the surface layer and to deepen the effects of this mixing. In periods of small cooling, when the winds are usually reduced in magnitude, free and forced convection are weakened, and their effects are confinced to a shallower surface layer.

This relation between the heat transfer balance at the ocean surface and the depth of the mixed layer may offer a clue to the persistence of sea-surface temperature anomalies. An increase in the cooling rate of the ocean surface, due primarily to increases in sensible and latent heat transfer, causes an increase in the intensity of mixing in the surface layer and also in the depth of the mixed layer. Even though the temperature of the mixed layer does decrease due to the increased loss of heat, this decrease is not as large as it would be if there were no change in the layer depth. The increased mixing and the associated increase in layer depth allow the heat loss to be tapped from a greater volume of water, thus reducing the change in temperature of the surface layer. This process would tend to keep both positive and negative temperature anomalies more stable than would be

expected if no fluctations in mixed layer depth occurred.

On the other hand, a decrease in the cooling rate or an increase in the heating of the ocean surface causes a decrease in the intensity of mixing and in the depth of the mixed layer. The corresponding change in temperature of the mixed layer is therefore larger than it would be if there were no change in the layer depth, since a smaller volume of water is affected by the heat transfer. This process would tend to stabilize negative temperature anomalies and unstabilize positive anomalies when (S-B) is negative, When (S-B) is positive, it would tend to stabilize positive temperature anomalies and unstabilize negative anomalies.

From the remarks made in the above two paragraphs, it is concluded that fluctuation in the mixed layer depth may play an important part in the persistence of sea-surface temperature anomalies on a month-to-month basis. These fluctuations may also help to explain the pronounced changes in anomaly patterns that were observed at times during the 84-month period, since some changes in the total heat transfer across the sea surface can render the sea-surface temperature anomaly patterns more unstable than would be expected if no fluctuations in the mixed layer depth occurred.

The effects of horizontal heat advection due to wind drift may also be an important factor in the persistence of sea-surface temperature anomalies. However, the auto-correlations of

the temperature advection anomalies for the 84 month period show no persistence at 1, 2 and 3 months lag (the average values of the 162 grid points on the map were negative for all 3 months).

VI. Additional Results

A. Comparison of observed sea-surface temperature and total surface heat transfer cycles with theoretical results.

After this thesis had been completed, two papers were found in the January, 1967, issue of Tellus by Kraus and Turner in which a general theory of the seasonal thermocline is presented. The results of the theory give the depth of the mixed layer or seasonal thermocline and the temperature of the layer as a function of time and quite general external energy inputs. The backbone of the theory is two equations, a thermal energy balance equation for the mixed layer and a mechanical energy balance equation for the layer, which are as follows:

$$h \frac{dT_s}{dt} + \Lambda (T_s - T_h) \frac{dh}{dt} = S + B - S_e^{-\beta h} \approx S + B \quad \text{(VI.1)}$$

where h is the depth of the layer, T_s is the temperature of the layer, T_h is the temperature below the layer, S is the penetrating component of the solar radiation, β is the extinction coefficient, B is the heat exchange between ocean and atmosphere due to back radiation and latent and sensible heat transfer, and Λ is the Heaviside unit function, defined as

$$\Lambda \equiv \Lambda\left(\frac{dh}{dt}\right) = \begin{matrix} 1 \\ 0 \end{matrix} \text{ for } \begin{matrix} \frac{dh}{dt} > 0 \\ \frac{dh}{dt} < 0 \end{matrix} \quad ;$$

and

$$\frac{1}{2}\frac{dT_s}{dt} h^2 + \Lambda (T_s - T_h)\frac{dh}{dt} = G - D + \frac{S}{\beta} , \qquad \text{(VI.2)}$$

where the first term on the left-hand side represents the potential energy change associated with the change in temperature of the layer, the second term on the left-hand side represents the potential energy change due to the entrainment of water as the depth of the thermocline increases ($dh/dt > 0$), and the terms on the right-hand side represent the energy change due to mechanical stirring by the wind, dissipation of energy within the layer, and convection due to internal heating.

Equations (VI.1) and (VI.2) can be transformed into

$$\frac{dT_s}{dt} = \frac{2}{h^2}\left[(S + B)h - (G - D + \frac{S}{\beta})\right] \qquad \text{(VI.3)}$$

and

$$\Lambda \frac{dh}{dt} = \frac{1}{(T_s - T_h)h}\left[\Lambda(G - D + \frac{S}{\beta}) - (S + B)h\right] . \qquad \text{(VI.4)}$$

When the thermocline is rising, $\Delta 1 = 0$ ($dh/st < 0$) and

$$h = \frac{2\,G - D + S/\beta}{S + B} \quad . \tag{VI.5}$$

Substituting (VI.5) into (VI.3), we get

$$\frac{dT_s}{dt} = \frac{2\,G - D + S/\beta}{h^2} = \frac{1}{2}\,\frac{(S + B)^2}{G - D + S/\beta} \quad . \tag{VI.6}$$

Differentiating (VI.5) with the assumption that seasonal variations of the solar radiation S are larger than the corresponding changes of G and D, we get

$$\frac{dh}{dt} \approx \frac{1}{(S + B)} \quad (\frac{2}{\beta} - h)\,\frac{dS}{dt} \quad . \tag{VI.7}$$

Since $h > 2/\beta$, we find that h and -S are in phase and that the layer depth h has a minimum at the time of the summer solstice when $dS/dt = 0$. Equation (VI.6) shows that the temperature T_s is still increasing when $dS/dt = 0$ and that, in fact, the warming is most rapid (dTS/dt has maximum values) when h is close to its minimum. The temperature T_s reaches its maximum value later in the season.

When the thermocline is falling, the depth h is large, and the product $(S + B)h$ will always exceed the stirring terms in equations (VI.3) and (VI.4). Since $(S + B)$ is negative at this time, this product will account for most of the rates

of increase of layer depth and decrease in temperature.

Using a symmetrical saw tooth heating function for (S + B) and letting D = 0 and $\beta = \infty$, Kraus and Turner calculated the variation of T_s and h with respect to time throughout one complete heating and cooling cycle. The results obtained look just like the curves for the heating and sea-surface temperature cycles presented in Figures 1 through 6 of this thesis (see Chapter IV). In fact, the observed results, (1) that the heating cycle reaches a maximum in June, (2) that the maximum change in temperature occurs between May and June, (3) that the sea-surface temperature reaches a maximum somewhat before the end of the heating cycle (August vs. September), and (4) that the minimum of sea-surface temperature occurs at the end of the cooling cycle, agree almost exactly with the theoretical results. We thus conclude that during the heating part of the cycle, the depth of the mixed layer and its temperature are controlled by a combination of wind stirring and penetrative radiation; during the cooling part of the cycle, they are controlled primarily by surface cooling. In other words, during the heating cycle both terms inside the square brackets of equations (VI.3) and (VI.4) are important; during the cooling cycle, the first term in the square brackets of equation (VI.3) and the second term of equation (VI.4) are predominant.

B. Relationship between anomalies of the sea-surface temperature and anomalies of the specific humidity of the air.

Since the values of the specific humidity of the air q_a had been computed for each of the 84 months in order to obtain the values of the latent heat transfer, the anomalies of q_a were computed and the results correlated on a contemporary basis with the anomalies of SST. The results of the correlation analysis on a seasonal basis are shown in Table XI.

It is seen from the table that a strong relationship exists between the two anomaly series; the average values of the 162 coefficients on the map are .36 for winter, .46 for spring, .61 for summer and .58 for fall. Of the 162 coefficients on each of the maps, 86 reach the 5 per cent confidence level and 60 reach the 1 per cent confidence level for winter, 112 reach the 5 per cent level and 71 reach the 1 per cent level for spring, 122 reach the 5 per cent level and 102 reach the 1 per cent level for summer, and 130 reach the 5 per cent level and 107 reach the 1 per cent level for fall. In all of the seasons, these numbers are significantly larger that those expected by chance alone (8 for the 5 per cent level and 2 for the 1 per cent level).

Pattern correlations also were computed between each of the anomaly series for all of the 84 months. The monthly values of the coefficients averaged over the 7 years range from .37 in February and March to .60 in june. If the pattern

Table XI

	Winter	Spring	Summer	Fall	Year
55°N	-.16	.24	.54	.52	.28
50°N	.35	.41	.77	.58	.53
45°N	.59	.45	.79	.64	.62
40°N	.39	.51	.73	.68	.58
35°N	.36	.52	.72	.63	.56
30°N	.38	.59	.59	.65	.55
25°N	.48	.54	.35	.54	.48
20°N	.47	.45	.40	.38	.42

Average latitudinal correlation coefficients between the anomalies of SST and those of the specific humidity of the air.

correlations are averaged over the 12 months of each year, these average values range from .38 in 1951 to .62 in 1957.

The above results suggest that there is a direct relationship between the temperature of the sea surface and the amount of moisture in the air directly above it, especially during the summer and fall months. This result is not surprising since the vapor pressure of the sea surface also increases as the temperature increases and this, in turn, causes an increase in the amount of evaporation that occurs between the ocean and atmosphere. The fact that the correlations are highest during the summer months probably reflects the fact that, during the winter months, the water vapor is carried away by relatively strong winds. During the summer and fall months, the winds are weaker (see Chapter IV, Section A.3) and the moisture is allowed to build up over the area of the sea surface from which it evaporated.

C. Relationship between the anomalies of the latent heat flux computed from the transfer equations and the anomalies of atmospheric water vapor divergence.

Following the derivations given by Barnes (1965), for a column of air one square centimeter in cross-sectional area and extending from the surface of the earth to the top of the atmosphere, we have

$$\frac{dW}{dt} + \vec{\nabla} \cdot \vec{Q} = E - P \ , \qquad \text{(VI.8)}$$

where $W = \frac{1}{g} \int_0^{p_o} q_a \, dp$ = total water vapor in column,

$Q = \frac{1}{g} \int_0^{p_o} q_a \, V \, dp$ = integrated vector transport of water vapor,

q_a = specific humidity,

p = pressure

p_o = surface pressure,

E = evaporation,

P = precipitation, and

g = acceleration due to gravity.

Exapnding equation (VI.8) in geographical coordinates (λ, ϕ, p, t), we get

$$\frac{\partial W}{\partial t} + \frac{1}{a \cos \phi} \frac{\partial Q}{\partial \lambda} + \frac{1}{a} \frac{\partial Q}{\partial \phi} - \frac{Q \phi \tan \phi}{a} + \frac{\partial Q_p}{\partial p} \qquad \text{(VI.9)}$$

where λ and ϕ are longitude and latitude, respectively, and a is the radius of the earth.

If $\partial W/\partial t$ is small compared to the other terms (total water content of the column remains nearly constant during a period of time Δt), and since

$$\frac{\partial Q_p}{\partial p} = \frac{\partial}{\partial p}\int_0^{p_o} q_a \omega \, d_p = 0 \ , \qquad \text{(VI.10)}$$

where $\omega = \partial p/\partial t$, then

$$\vec{\nabla} \cdot \vec{Q} = \frac{1}{a \cos\phi}\left[\frac{\partial Q}{\partial \lambda} + \frac{\partial (Q_\phi \cos \phi)}{\partial \phi}\right] = E - P \ . \qquad \text{(VI.11)}$$

Equation (VI.11) states that the divergence of the vertically integrated vector transport of water vapor is equal to the difference between the amount of evaporation and precipitation occurring at the earth's surface.

Since the values of the latent heat flux or evaporation (Q_e) computed from the transfer equations developed in Chapter II were available, it was decided to compute the values of $\vec{\nabla} \cdot \vec{Q}$ for the 84 months of the period from 1951 through 1957 and compare the anomaly patterns of the two quantities. However, an extremely crude method had to be used in computing the values of $\vec{\nabla} \cdot \vec{Q}$, since the data were available on only a monthly average basis and only for the surface layer of the atmosphere. Other investigators have found that daily and hourly values have a large effect on the monthly average values of $\vec{\nabla} \cdot \vec{Q}$.

Using the u and v components of the surface geostrophic wind found previously and the monthly averaged values of q_a, the values of $\vec{\nabla} \cdot \vec{Q}$ were computed at each of the 162 grid-points by the following method: we let

$$Q_\lambda = q_a u_g \quad \text{and} \quad Q_\phi = q_a v_g ,$$

then

$$\vec{\nabla} \cdot \vec{Q} \approx \frac{1}{a \cos\phi} \left[\frac{\Delta Q_\lambda}{\Delta \lambda} + \frac{\Delta (Q_\phi \cos\phi)}{\Delta \phi} \right], \qquad \text{(VI.12)}$$

where $\Delta\lambda$ and $\Delta\phi$ are 10° or $\pi/18$ radians.

The average vlaues of the 162 correlation coefficients on the map between the anomalies of Q_e and those of $\vec{\nabla} \cdot \vec{Q}$ are .36 for winter, .25 for spring, .10 for summer and .22 for fall. For winter 78 of the 162 coefficients reach the 5 per cent confidence level and 58 reach the 1 per cent level; the corresponding numbers for the other three seasons are 56 and 27 for spring, 22 and 6 for summer, and 37 and 20 for fall. The latitudinal averages of the correlations are given in Table XII.

From the table it is seen that the largest correlations occur during the winter months and between the latitudes 25°N and 50°N. The relatively high correlations during the winter and fall months are probably due to the fact that the transfer formula used to determine the latent heat flux most accurately represents the actual heat flux when the magnitudes of this quantity are large. When the heat flux is small, as it is during the spring and summer months, the conditions under

Table XII

	Winter	Spring	Summer	Fall	Year
55°N	.15	-.02	-.03	.11	.05
50°N	.46	.23	.20	.26	.29
45°N	.57	.26	.22	.31	.34
40°N	.50	.38	.28	.39	.39
35°N	.50	.40	.23	.31	.36
30°N	.35	.37	-.02	.19	.22
25°N	.24	.29	-.02	.14	.16
20°N	.07	.07	-.04	.02	.03

Latitudinal averages of the correlation coefficients of the anomalies of Q_e and those of $\vec{\nabla} \cdot \vec{Q}$.

which the transfer formula was developed are not fulfilled, and the values computed become less reliable.

The poor results obtained at the latitudes 20°N and 55°N in all of the seasons probably reflect the fact that there were no values of Q_ϕ given at the latitudes 15°N and 60°N, and a linear approximation had to be introduced in order to get these quantities. (The values of $\Delta Q_\phi / \Delta \phi$ in the divergence equation at 20°N and 55°N were computed by taking the difference between the values of Q_ϕ at 25°N and 15°N and between the values of Q_ϕ at 60°N and 50°n and dividing the results by $\pi/18$ radians.)

Another source of error is the fact that $\vec{\nabla} \cdot \vec{Q}$ is the difference between the amount of evaporation and the amount of precipitation that occur in a given area. In correlating the anomalies of Q_e with those of $\vec{\nabla} \cdot \vec{Q}$, this fact was not taken into account, since the values of the precipitation were not available.

In spite of the deficiencies of the method in determining $\vec{\nabla} \cdot \vec{Q}$, the results of the correlation study between the anomalies of Q_e and $\vec{\nabla} \cdot \vec{Q}$ show that there is a statistically significant relation between the two series, i.e. when there is a stronger or weaker than average value of the latent heat flux between ocean and atmosphere, there is also a stronger or weaker than average value of the atmospheric water vapor divergence field. It is felt that this type of

analysis would be a valuable tool in helping to develop a better transfer formula for the latent heat flux between ocean and atmosphere, especially if it were applied to a smaller area over which daily and hourly values of the necessary meteorological and oceanographic paramters could be obtained.

VII. Conclusions

A. Summary of Results

1. Evaluation of the Transfer Formulas

a. In Chapter II, the effect of observational errors and the effect of using monthly averaged data rather than daily or hourly data on the accuracy of the exchange formulas for determining Q_i, Q_b, Q_e and Q_s were investigated. It was found that the accuracy of these formulas increases as the values of the heat transfers increase, since the errors resulting from both observational and averaging effects decrease with increased heat transfer. The theoretical accuracy of the formulas for determining Q_e and Q_s is also higher when large transfers occur; since large transfers occur at times of strong winds, the wind shear keeps the atmospheric stratification close to neutral values, and these are the conditions for which the formulas were derived.

b. A comparison was made of monthly average heat transfers determined by using the monthly averages of daily heat transfers and by using monthly average variables in the exchange formulas. It was found

that the errors involved in using the latter method are, on the average, about 10 per cent of the actual values due to correlations on a daily basis between the wind speed and air-sea property differences.

2. Heat Exchange Calculations

The study concerning the 7-year means of the monthly averaged heat transfers produced the following results:

a. The values of Q_i, Q_b, Q_e, Q_s and Q show large seasonal and year-to-year variability, especially those of Q_e, Q_s and Q.

b. The 84-month averages of the total heat transfer across the sea surface (Q) were integrated over the North Pacific from 20°N to 55°n. The result shows that the ocean loses 7×10^{14} cal/sec through the surface north of 20°N. Wyrtki (1965) calculated the total integral of heat transfer over the North Pacific from the equator poleward and found that the ocean gains 3×10^{14} cal/sec. The difference between the two calculations shows that there is a heat gain of 10×10^{14} cal/sec between the equator and 20°N and that it is this region that accounts for the yearly heat gain of the North Pacific.

c. Fourier analysis of the 12 mean monthly values of each of the heat transfer terms showed that there are regular yearly cycles in each of the terms over most of the North Pacific Ocean from 20°N to 55°N. The maximum values of Q_i occur in June, those of Q_b in January, those of Q_e in December, and those of Q_s in November, and December. There is also a regular yearly cycle in Q, with cooling of the ocean surface layer occurring from September through April and warming of the surface layer occurring from April through September.

d. Fourier analysis of the 12 mean monthly values of the sea-surface temperature (SST) showed that there is also a regular yearly cycle in this term, with the maximum values occurring in August and September and the minimum values occurring in February and March.

e. By comparing the yearly cycles of SST and Q, it was found that the maximum values of SST occur near the end of the heating cycle (positive Q) and that the minimum values occur at the end of the cooling cycle (negative Q).

f. There is a regular yearly cycle in the surface

air temperature (SAT), and the maximum and minimum values occur at the same times as those of SST. The maximum values of SST and SAT both occur earlier in the western part of the North Pacific than in the eastern part; this difference may be due to the effect of the cold advection towards the equator by the California current.

g. Fourier analysis of the change in SST from month to month (Δ SST), showed that there is a regular yearly cycle in this quantity. The maximum increase of SST occurs from the middle of May to the middle of June and the maximum decrease of SST occurs from the middle of December to the middle of January. During March and September, when the ocean surface layer temperature does not change very much, there must be a balance between the heat transfer across the sea surface and the advection that occurs within the surface layer.

h. Fourier analysis of the mean monthly values of the observed wind speeds showed that a regular yearly cycle is present, with the maximum values occurring in January and the minimum values occurring in June. The same type of analysis showed that there

is also a regular yearly cycle in the Bowen ratio (Q_s/Q_e) in only the middle latttudes and only then in the western part of the ocean, where the annual range of values is from .4 to 1.4; in the other areas the Bowen ratio has values of around .1 with very little annual variation.

i. Using the values of Q and Δ SST, the mean monthly values of the total heat advection within the mixed layer were computed. The results obtained agree with what is known about the current patterns of the North Pacific during the winter and spring months. During the summer and fall months, the values show that there is cold advection of water in the region of the Kuroshio current, in contrast to what is expected. This discrepancy may be due to the fact that the heat lost from the surface layer across the thermocline region is neglected.

j. The integrated values of the heat advection from 17.5°N to 57.5°N show that warm advection occurs over the ocean from January through May and that cold advection occurs in the remaining seven months. Compared to a study done by Bryan (1960), the cold advection of about 2.2×10^{14} cal/sec at 32°N.

agrees with the direction of heat transport calculated by him using other methods.

k. The monthly mean values of Q_i, Q_b, Q_e, Q_s and Q were determined from daily data taken at stations NOVEMBER (30°N - 140°W) and PAPA(50°N - 145°W) in 1962. The yearly cycles of these quantities were found to show the same type of variation as the results using the monthly average data. The large daily fluctuations in Q are not accompanied by large fluctuations in SST, which indicates that large fluctuations in the depth of the mixed layer may occur. Very little correlation was found between the daily fluctuations of Q and those of SST on a contemporary or lag basis.

3. Discussion of Sea-Surface Temperature and Heat Transfer Anomalies

The results of studying the anomaly patterns of the heat transfer terms and of SST and SAT are as follows:

a. The anomaly patterns of both SST and SAT can occur in fairly extensive geographical areas. The magnitudes of the SST anomalies are about 2°F to 4°F, while those of the SAT anomalies are slightly larger.

b. Although some month-to-month persistence is found in the SST anomalies, patterns can be eliminated or reversed in a month's time. The average of all autocorrelations of the SST anomalies is down to .28 at 3 months lag; for the SAT anomalies, the autocorrelations are down to .25 at 3 months lag.

c. There is a high degree of correlation between the anomalies of SST and SAT: the average maximum correlation (.83) occurs in the summer months and at the 35th parallel.

d. It is concluded from the above results that there is very little long-term persistence of both air and sea temperatures (negative autocorrelations occur at 1 and 2 years lag) and that the anomaly patterns of both air and sea temperatures are strongly related. To maintain a long-term persistent anomaly of the general atmospheric circulation, a control factor is required that is stable over long time periods so that it can pull the general circulation back into line when it goes off on a tangent. It does not seem that sea-surface temperature anomalies can provide this control factor.

e. There is very little persistence in the anomaly patterns of the heating terms Q_i, Q_b, Q_e, Q_s and Q. (Autocorrelations are negative for all terms at 1, 2 and 3 months lag.) The anomaly patterns can be large geographically, especially those of Q_e and Q_s.

f. The magnitudes of the Q anomalies vary widely over the map for a particular month and from month to month during the 84-month period under investigation. Their values range from less than 1 per cent of the mean monthly average values to over 200 per cent in the summer months.

4. Relationships Between Sea-Surface Temperature Fluctuations and Heat Transfer Anomalies

The results obtained from studying the relationships between the anomaly patterns of SST and those of the heat transfer terms are as follows:

a. By correlating the anomalies of the total heat transfer across the sea surface (Q) with the anomalies of the change in SST from month to month (Δ SST), it was found that the two series have a significant positive correlation for all seasons, the largest of which occurs in the winter months. This fact indicates

that sea-surface temperature anomalies are related to anomalies of the total heat transfer across the sea surface.

b. The anomaly series of the horizontal temperature advection due to wind drift currents are also significantly positively correlated to the anomaly series of Δ SST in all seasons. The largest average seasonal correlation coefficient occurs in winter; the coefficients for all seasons are lower than the respective values for the surface heat transfer anomaly series.

c. From the study on the effect of surface current advection on changes in the sea-surface temperature, it seems as if surface winds are capable of driving a shallow surface layer of the ocean quite freely back and forth over the sea surface in a direction of around 45° to the right of the wind stress.

d. By adding the changes in SST due to heat transfer across the sea surface to the changes in SST due to horizontal wind-drift advection and correlating the anomalies of the results with the anomalies of Δ SST, the average seasonal correlations were imporved somewhat over those obtained by using either of the two

anomaly series alone. The main difficulty in this method is that the temperature changes computed from the surface heat transfer term are much larger in magnitude than those determined from the advection term. In fact, the temperature changes computed from the surface heat transfer term are larger by an order of magnitude than any of those changes observed in the 84-month period under investigation. The reasons for this discrepancy probably lie in using unreliable values for the depth of the mixed layer and in the fact that there is a loss of heat through the bottom of the mixed layer due to vertical eddy diffusion, which is unaccounted for in this study.

e. An attempt was made to see if vertical velocities induced at the bottom of the Ekman surface layer had any effect on the SST anomalies. The results of the correlation study showed that these velocities, alone, have little effect on the SST anomalies. There is a small negative correlation between the two anomaly series for all seasons except winter, indicating that an anomalous upward transport tends to lower the temperature of the surface layer.

f. In order to test the combined effects of heat

transfer across the surface layer (Q), horizontal temperature advection (HTA), and vertical transport of water beneath the Ekman layer (VV), a multiple linear correlation analysis was computed for the three terms, Δ SST, the sum of the temperature change caused by Q and HTA, and VV. The analysis showed that, by including the effects of VV, the average percentage of the variance in Δ SST accounted for by relation to other variables is increased from 20 to 25 per cent in winter, 13 to 18 per cent in spring, 12 to 18 per cent in summer and 13 to 19 per cent in fall.

g. The differences between the computed and observed changes in SST are all an order of magnitude larger than any of the observed values and have the largest values in the western part of the ocean in all 12 months of the year. The computed values of Δ SST are closer to the observed values of Δ SST during the spring months and farthest from during the summer months.

h. The small month-to-month persistence of the SST anomalies must, in some manner, be related to the dynamics of forced and free convection in the mixed layer. Fluctuations in the strength of mixing within the layer and the associated fluctuations in the depth

of the layer can stabilize some anomaly patterns and unstabilize others. There is very little persistence in the anomaly patterns of the surface heat transfer and in those of the horizontal heat advection, and it is concluded that these have little effect on the persistence of the SST anomalies.

5. Additional Results

a. It was found that the observed results concerning the cycles of the total surface heat transfer and of the sea-surface temperature [(1) that the heating cycle reaches a maximum in June, (2) that the maximum change in temperature occurs between May and June, (3) that the sea-surface temperature reaches a maximum somewhat before the end of the heating cycle (August vs. September), and (4) that the minimum of sea-surface temperature occurs at the end of the cooling cycle] agree almost exactly with the theoretical results of a one-dimensional model of the seasonal thermocline.

b. It was found that there is a strong relation between the anomaly patterns of SST and those of the specific humidity of the air over the ocean surface;

this relation is particularly strong during the summer and fall months. From this, it is concluded that the amount of moisture in the air increases with the temperature of the sea surface below it and decreases as the ocean surface temperature decreases.

c. A statistically significant correlation was found between the anomalies of the latent heat flux from ocean to atmosphere and those of the atmospheric water vapor divergence in the surface layer of the atmosphere. When there is a stronger or weaker than average value of the latent heat flux, there is also a stronger or weaker than average value of the atmospheric water vapor divergence field. It is felt that this type of analysis would be a valuable tool in helping to develop a better transfer formula for the latent heat flux between ocean and atmosphere.

B. Suggestions for Further Study

The suggestions for further study can be divided into the following three categories:

1. Use of available data and theory. It is felt that further information about the interaction of ocean and atmosphere could be obtained by using the data and transfer formulas that are presently available. Studies of

the type presented in this paper could give a better insight into the heat exchange processes and their effects if applied to other areas of the world oceans, especially in the tropics. (At present, it is planned to continue this study in the tropical areas of the North and South Pacific Oceans during the next year.) The studies could concentrate their efforts on large or small-scale processes, since the data to do this are available. Probably the hardest part of any endeavor of this type would be to organize the data into a workable form, since their present form,as it stands, is almost useless for any statistical analysis.

2. Develop new transfer formulas to be used with old or new data. In order to develop new transfer formulas, experimental work will have to be done on the nature of turbulent transfer between the ocean and atmosphere. Since most experimental work is done on small-scale processes, it is felt that new data on oceanic and atmospheric parameters should be obtained in order to test the new theories. A good example of this type of analysis is the work done by Garstang (1965) concerning the effects of small-scale sensible heat transfer on synoptic scale weather systems. He found that diurnal variations in the sensible heat flux influence the energy flux of synop-

tic scale systems; integrated over the entire disturbance, the energy flux is found to be double the undisturbed values. The inclusion of this synoptic scale energy flux profoundly affects the large scale energy flux patterns, and casts some doubt on the validity of the present relative magnitudes of the various terms in the heat budget of the ocean and atmosphere. This type of result suggests that new studies should be made with new formulas and new data in order to eliminate these uncertainties.

3. Develop a theory that treats the ocean and atmosphere as two interacting media. At present, there is a need to develop a theory that treats the ocean and atmosphere as two interacting media, from which the transfer of various properties across their common boundary can be computed. A good example of this type of analysis is the work of Kagan and Utina (1963) in which they develop equations for describing the ocean and atmosphere and solve them numerically by using the same boundary conditions for both systems at their interface. In this way, they are able to calculate the relative parameters of ocean and atmosphere when different driving conditions are applied. Admittedly, this is a difficult problem, but it is one which must be solved before long-range predictions can be made for both atmospheric and oceanic properties.

Acknowledgements

The author would like to thank Professor Hurd C. Willett for his encouragement and advice, without which this work would not have been possible.

He would also like to thank Dr. O. E. Sette and Dr. Glenn A. Flittner of the Bureau of Commercial Fisheries for making available the data that was used in this thesis. The Bureau of Commercial Fisheries also provided financial support in the form of a fellowship grant for the 1965-66 and 1966-67 academic years.

The staff of Dr. Willett's research group, Helen Aronovitz, Wanda Burak, Madeleine Heyman, Marilyn Keegan, and Dena Varelas did an excellent job of putting the original data in a form useful for statistical analysis.

Miss Isabelle Kole did the drafting of the many figures in this report and Miss Betty Goldman and Mrs. Jane McNabb typed the final copy.

All computations were done on an IBM 7094 computer at the M.I.T. Computation Center.

Finally, the author would like to thank his wife for her constant support and encouragement throughout his entire graduate career and also for typing and editing the original manuscript.

BIBLIOGRAPHY

Arthur, R. S., 1966, Estimation of Mean Monthly Anomalies of Sea-Surface Temperature, J. Geophys. Res., 71(10), 2689-2690.

Barnes, A. A., 1965, Atmospheric Water Vapor Divergence: Measurements and Applications, AFCRL Special Reports, No. 28.

Berliand, M. E. and Berliand, T. G., 1952, Determination of effective radiation of the earth as influenced by cloud cover, Izvestia of the Academy of Sciences USSR, Series Geophizicheskaia, No. 1.

Berliand, T. G., 1960, Climatological method of total radiation, Meteorologiya i Gidrologia, No. 6, 9-12.

Berson, F. A., 1962, On the influence of variable large-scale wind systems on the heat balance in the active layer of the ocean, Tech. Mem. 25, 75 pp., National Meteorological Center, U. S. Weather Bureau.

Bjerknes, J., 1962, Synoptic survey of the interaction of sea and atmosphere in the North Atlantic, Geofysike Publikasjoner, Geophysica Norvegica, 24(3), 115-145.

Bryan, K., 1962, Measurements of meridional heat transport by ocean currents, J. Geophys. Res., 67(9), 3403-3414.

Budyko, M. I., 1956, The heat balance of the earth's surface, U. S. Dept. of Commerce Translation by N. Stepanova 1958, 259 pp.

Budyko, M. I. and Kondratiev, K. Y., 1964, The heat balance of the earth, Research in Geophysics, Vol. 2, M. I. T. Press, 529-554.

Deacon, E. L. and Webb, E. K., 1962, Small-scale interactions, Chapter 3 of Vol. 1 of The Sea, Interscience Publishers, New York and London.

Fofonoff, N. P., 1960-1963, Transport computations for the North Pacific Ocean 1951-1960, Manuscript Report Series, Fisheries Res. Board of Canada, Pacific Oceanographic Group, Nanaimo, B. C.

Garstang, M., 1965, Distribution and mechanism of energy exchange between the tropical ocean and atmosphere, Report to U. S. Army Electronics Research and Development Laboratory, Grant No. DA-AMC-28-043-64-G5.

Helland-Hansen, B. and Nansen, F., 1917, Videnskapsselskapeta Skrifter. I. Mat.-Naturn. Klasse 1916, No. 9, Kristiania 1917.

Jacobs, W. C., 1951, The energy exchange between sea and atmosphere and some of its consequences, Bulletin of the Scripps Institution of Oceanography of the University of California, 6(2), 27-122.

Johnson, J. H., Flittner, G. A., and Cline, M. W., 1965, Automatic data processing program for marine synoptic radio weather reports, U. S. Fish and Wildlife Service Special Scientific Report No. 503.

Kagan, B. A. and Utina, Z. M., 1963, On the thermodynamic interaction between sea and atmosphere, Okeanologiya, 3(2), 250-259.

Kraus, E. B. and Morrison, R. E., 1966, Local interactions between the sea and the air at monthly and annual time scales, Quart. J. R. Met. Soc., 92(391), 114-127.

Kraus, E. B. and Rooth, C., 1961, Temperature and steady state vertical heat flux in the ocean surface layers, Tellus, 13(2), 231-237.

Kraus, E. B. and Turner, J. S., 1967, A one-dimensional model of the seasonal thermocline, Part II. The general theory and its consequents, Tellus, 19(1), 98-105.

Laevastu, T., 1960, Factors affecting the temperature of the surface layer of the sea, Soc. Sci. Fennica Comm. Phys. Math.

Laevastu, T., 1966, Short-period changes and anomalies of temperature in the ocean and their effects on sound propagation, FNWF Tech. Mem. No. 18.

Namias, J., 1959, Recent seasonal interactions between North Pacific waters and the overlying atmospheric circulation, J. Geophys. Res., 64, 631-646.

Namias, J., 1963, Large-scale air-sea interactions over the North Pacific from summer 1962 through the subsequent winter, J. Geophys. Res., 68(22), 6171-6186.

Namias, J., 1965, Macroscopic association between mean monthly sea-surface temperature and the overlying winds, J. Geophys. Res., 70(10), 2307-2318.

Neuman, G., Fisher, E. and Pandolfo, J., 1958, Studies on the interaction between ocean and atmosphere with application to long range weather forecasting, Final Report Under U. S. Air Force Contract No. AF 19(604)-1284.

Pacific Oceanographic Group, Oceanographic Atlas of Ocean Weather Station "PAPA" 1956-1963, 1965, Manuscript Report Series No. 187, Fisheries Res. Board of Cancda.

Pattullo, J. G. and Cochrane, J. D., 1951, Monthly thermal condition charts for the North Pacific Ocean, MS Report No. 3, Bathythermograph Section, Scripps, Inst. Oceanog., 30 pp.

Roden, G. I., 1959, On the heat and salt balance of the California Current region, J. Mar. Res., 18(1), 36-61.

Roden, G. I., 1962, On sea-surface temperature, cloudiness and wind variations in the tropical Atlantic, J. Atm. Sci., 19(1), 66-80.

Roden, G. I., 1963, On sea level, temperature, and salinity variations in the central tropical Pacific and on Pacific Ocean islands, J. Geophys. Res., 68(2), 455-472.

Rossby, C. G. and Montgomery, R. B., 1935, The layer of frictional influence in wind and ocean currents, Pap. in Phys. Ocean. and Met., M. I. T. and W. H. O. I., Vol. III, No. 3.

Willett, H. C. and Clark, N. E., 1966, Interaction of atmosphere and ocean during climatic fluctuations, Report for NSF Grant No. 24832.

Witting, R., 1909, Zur Kenntrio den vom Winde erzengten Oberflachenstromes, Ann. Hydrogr. Marit. Met. 73, 193.

Wyrtki, K., 1961, The thermohaline circulation in relation to the general circulation in the oceans, Deep-Sea Res.,

8(1), 39-64.

Wyrtki, K., 1965, The average annual heat balance of the North Pacific Ocean and its relation to ocean circulation, J. Geophys. Res., 70(18), 4547-4560.

Wyrtki, K., 1966, Seasonal variation of heat exchange and surface temperature in the North Pacific Ocean, Report for NSF Grant No. GP-5534 at the Hawaii Institute of Geophysics, Univ. of Hawaii.

Biographical Note

The author was born on February 26, 1940, in Milford, Connecticut, and attended Milford public schools through high school.

He entered Brown University in 1958 and was graduated in 1962 with a Bachelor of Science degree in physics.

During the summers of 1962 and 1963, he was employed as a research assistant by the Woods Hole Oceanographic Institute in Woods Hole, Massachusetts.

He entered the M.I.T. Graduate School in 1962 and has been supported since the academic year of 1965-66 by a research fellowship given by the U.S. Bureau of Commercial Fisheries.

He is married to the former Joanna Bunker Rohrbaugh and they, as yet, have no children.

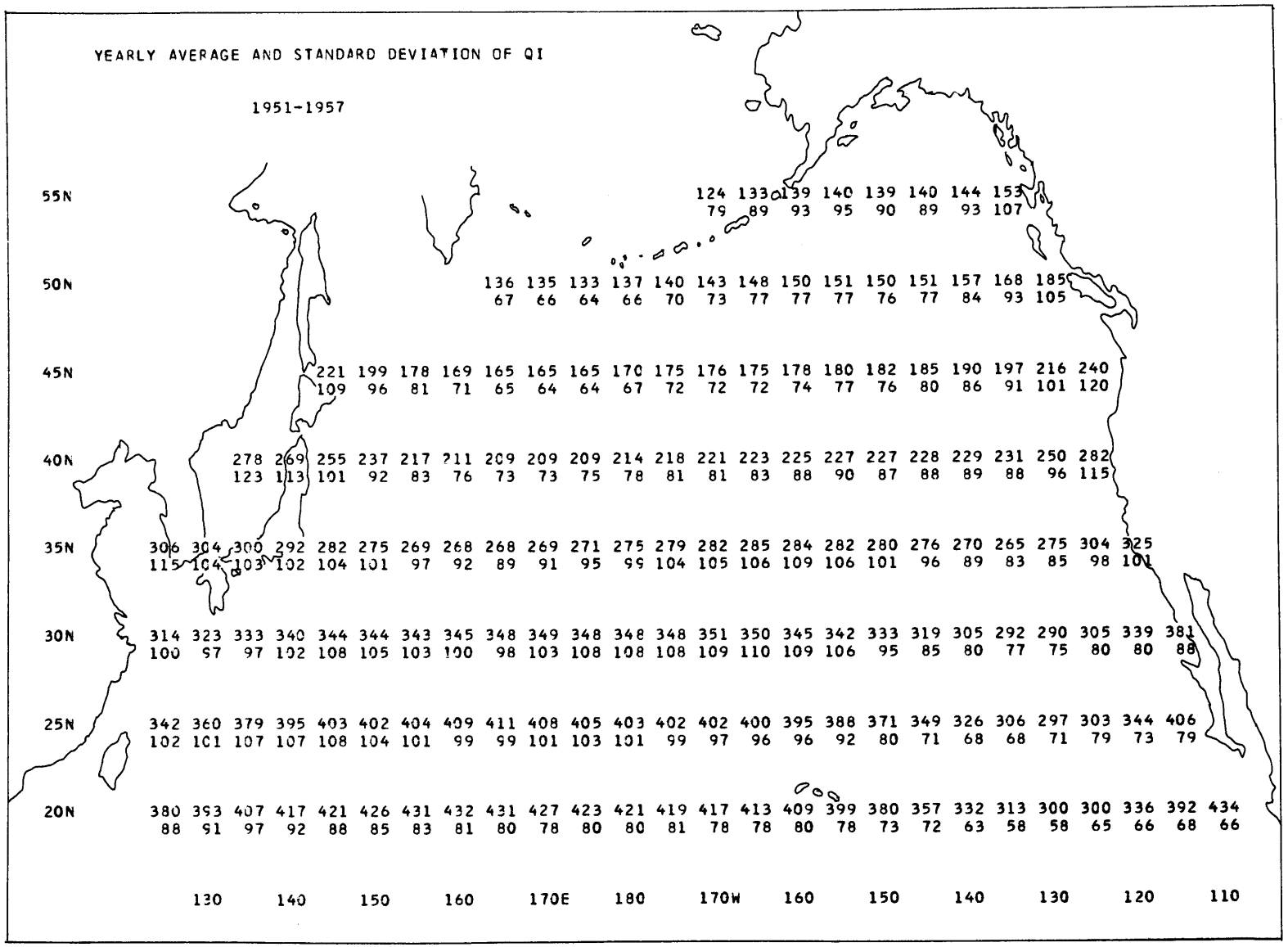

Figure A1. 84-month average values and standard deviations of the incoming radiation corrected for reflection and cloud cover. (cal/cm^2/day)

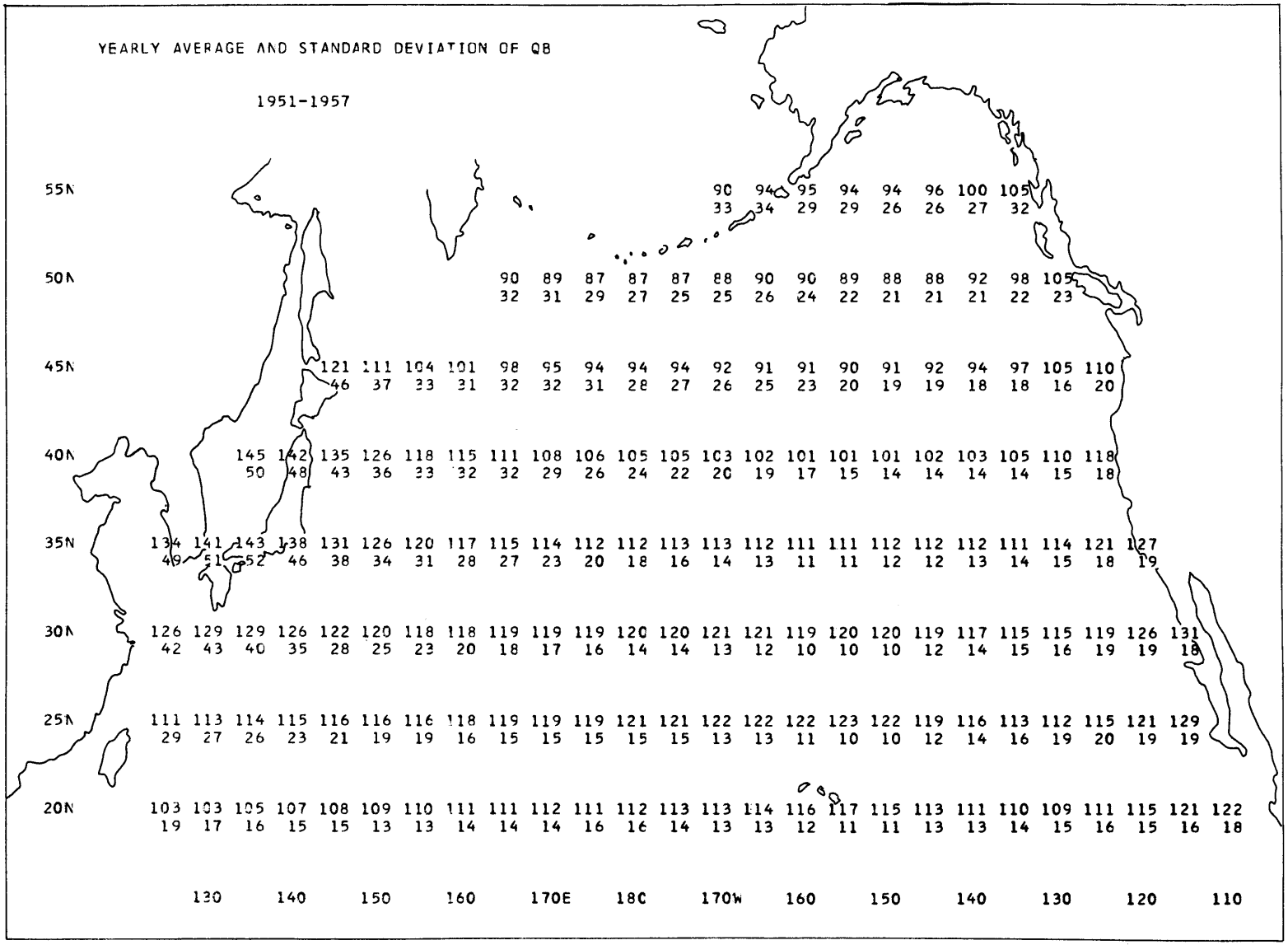

Figure A2. 84-month average values and standard deviations of the effective back radiation from the sea surface. (cal/cm^2/day)

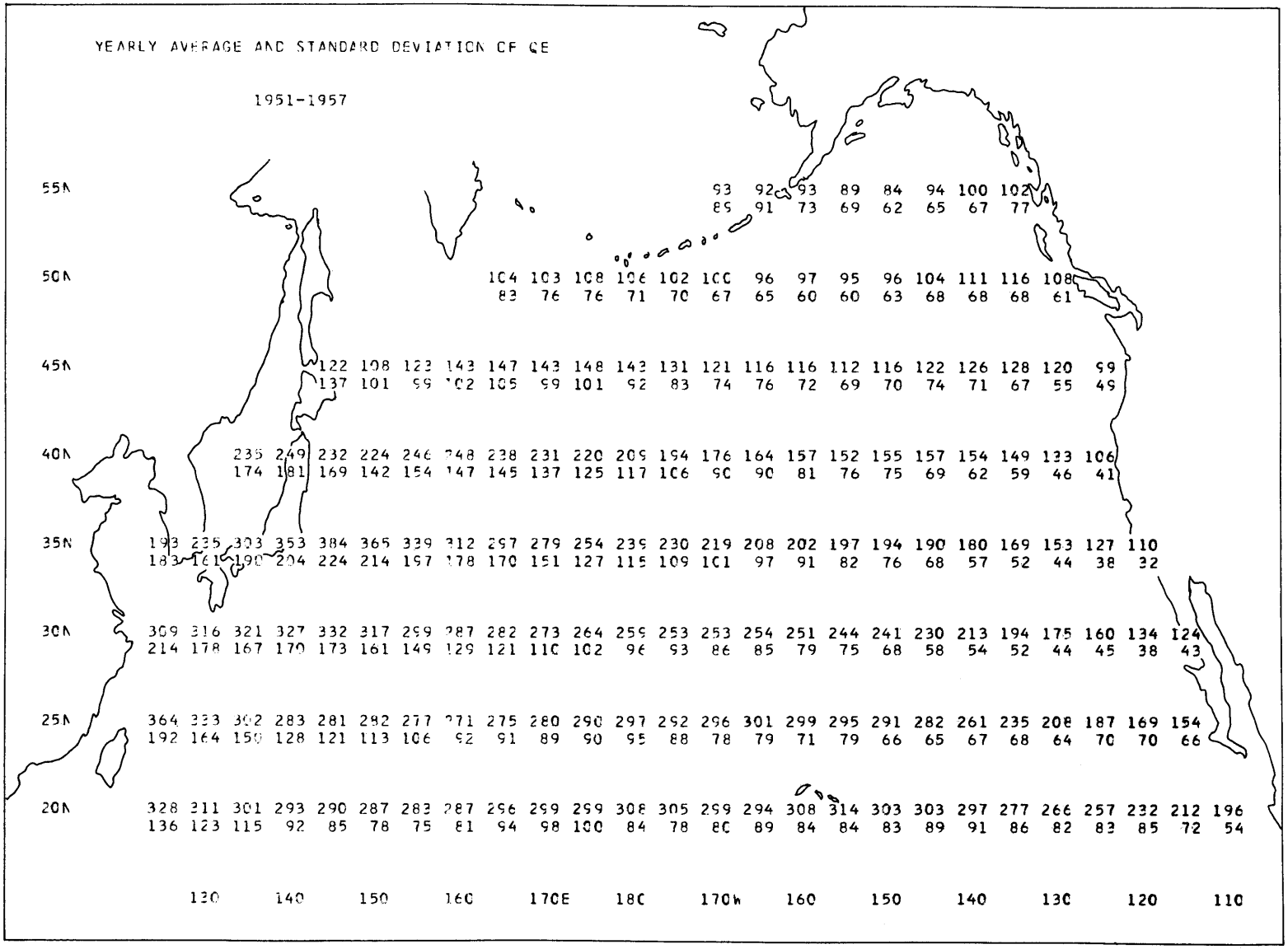

Figure A3. 84-month average values and standard deviations of the latent heat transfer between ocean and atmosphere. (cal/cm^2/day)

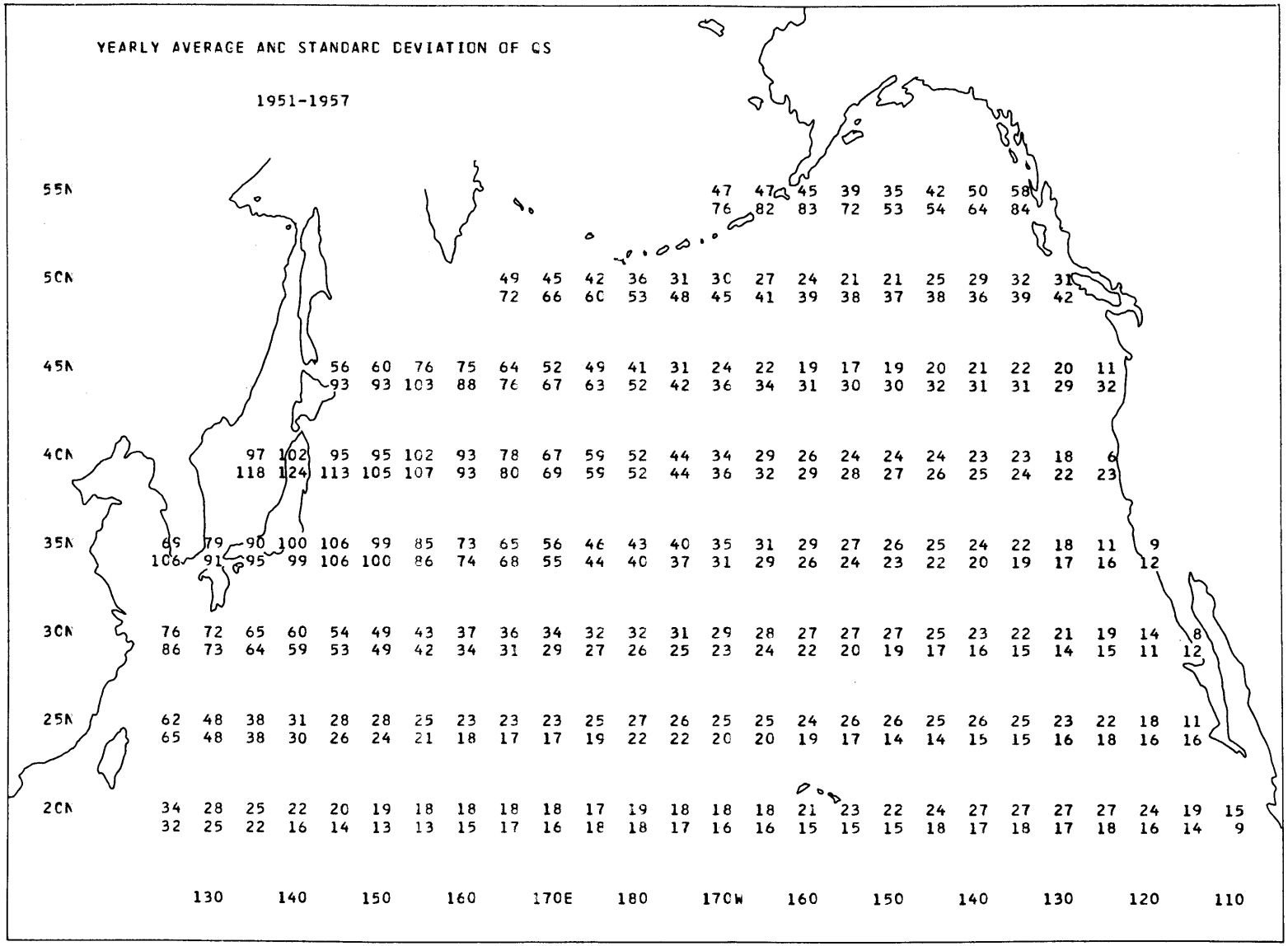

Figure A4. 84-month average values and standard deviations of the sensible heat transfer between ocean and atmosphere. (cal/cm^2 (cal/cm^2/day)

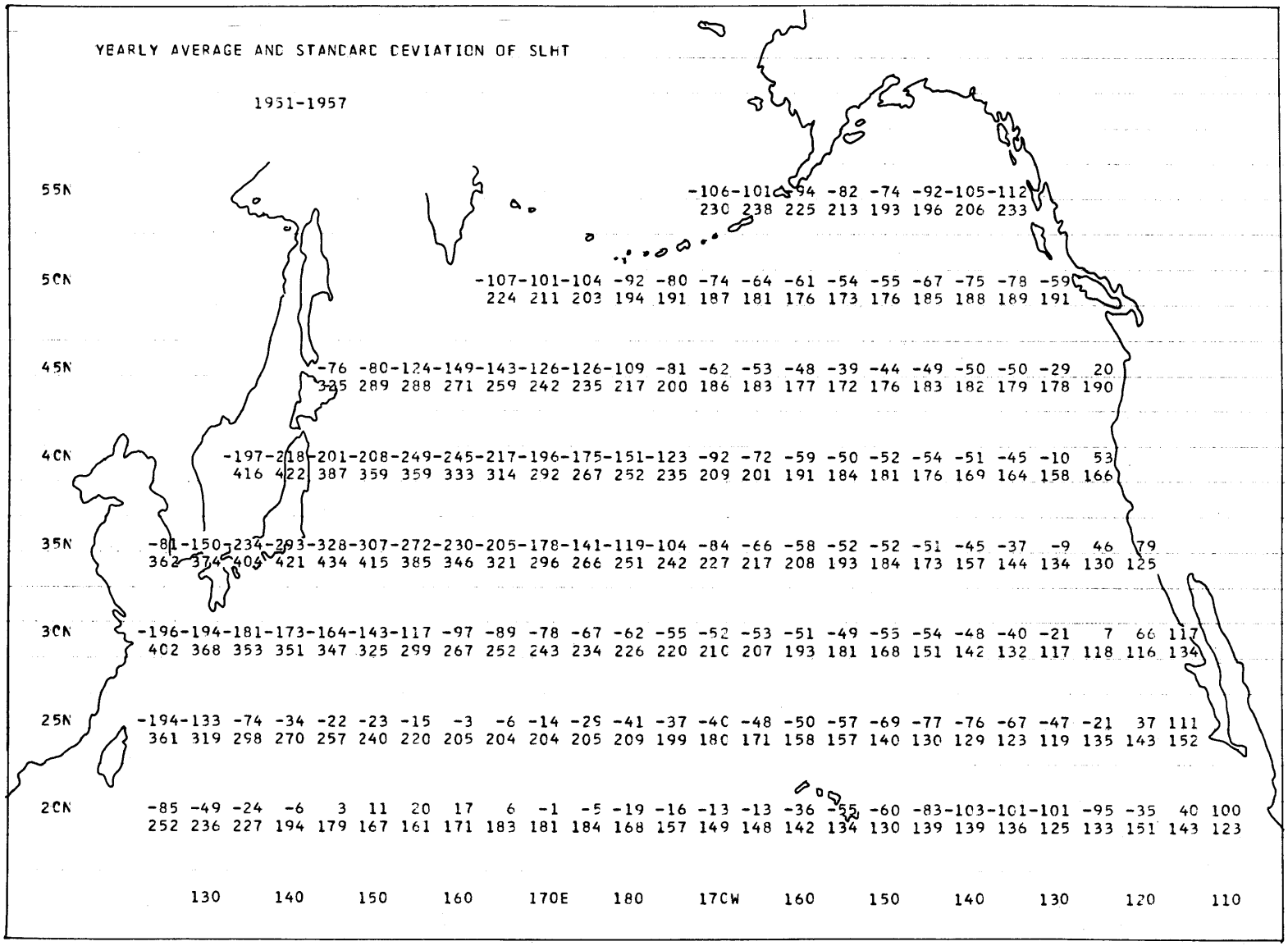

Figure A5. 84-month average values and standard deviations of the total transfer of heat between ocean and atmosphere. (cal/cm^2/day)

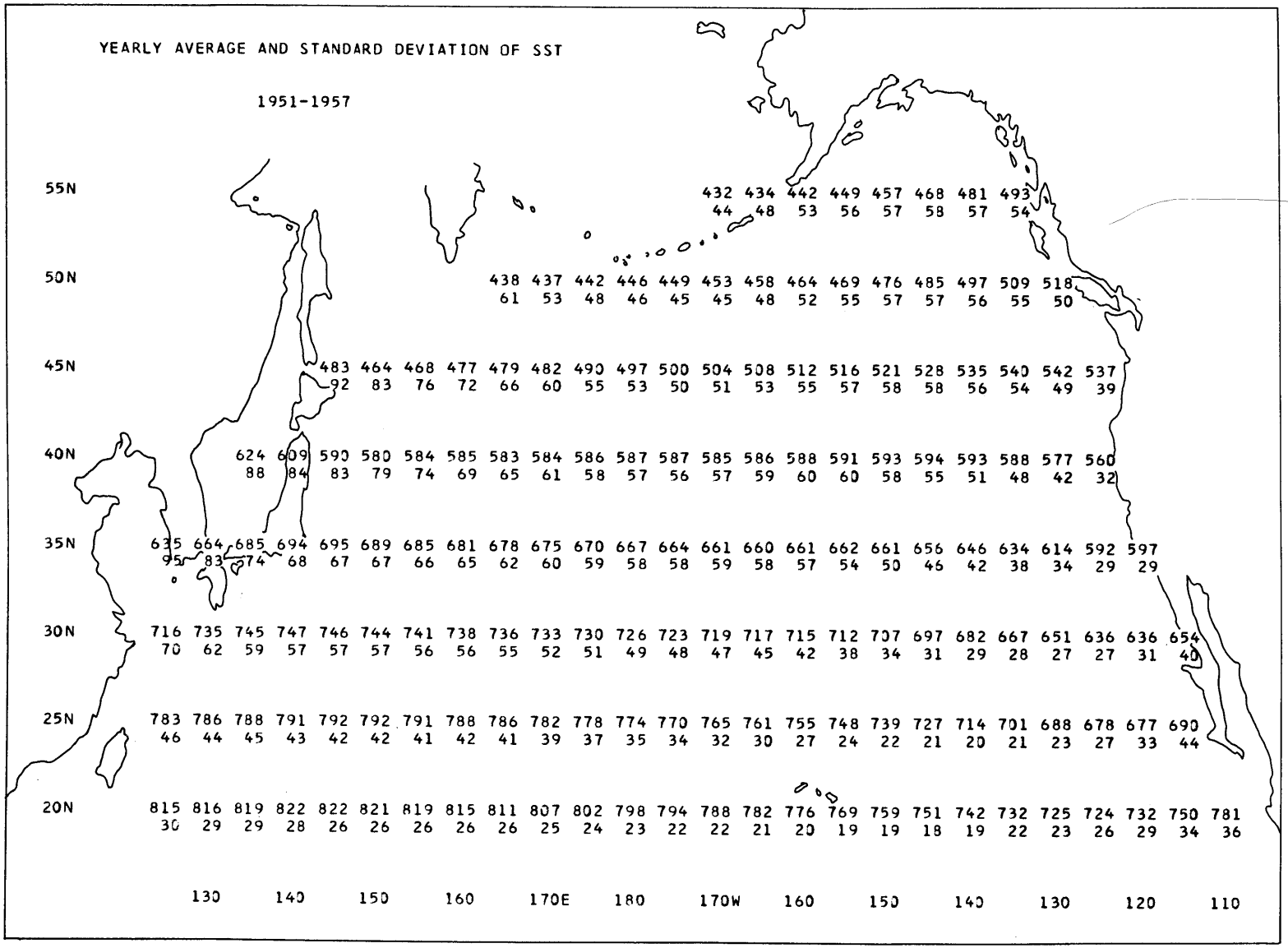

Figure A6. 84-month average values and standard deviations of the sea-surface temperature. (^{o}F x 10)

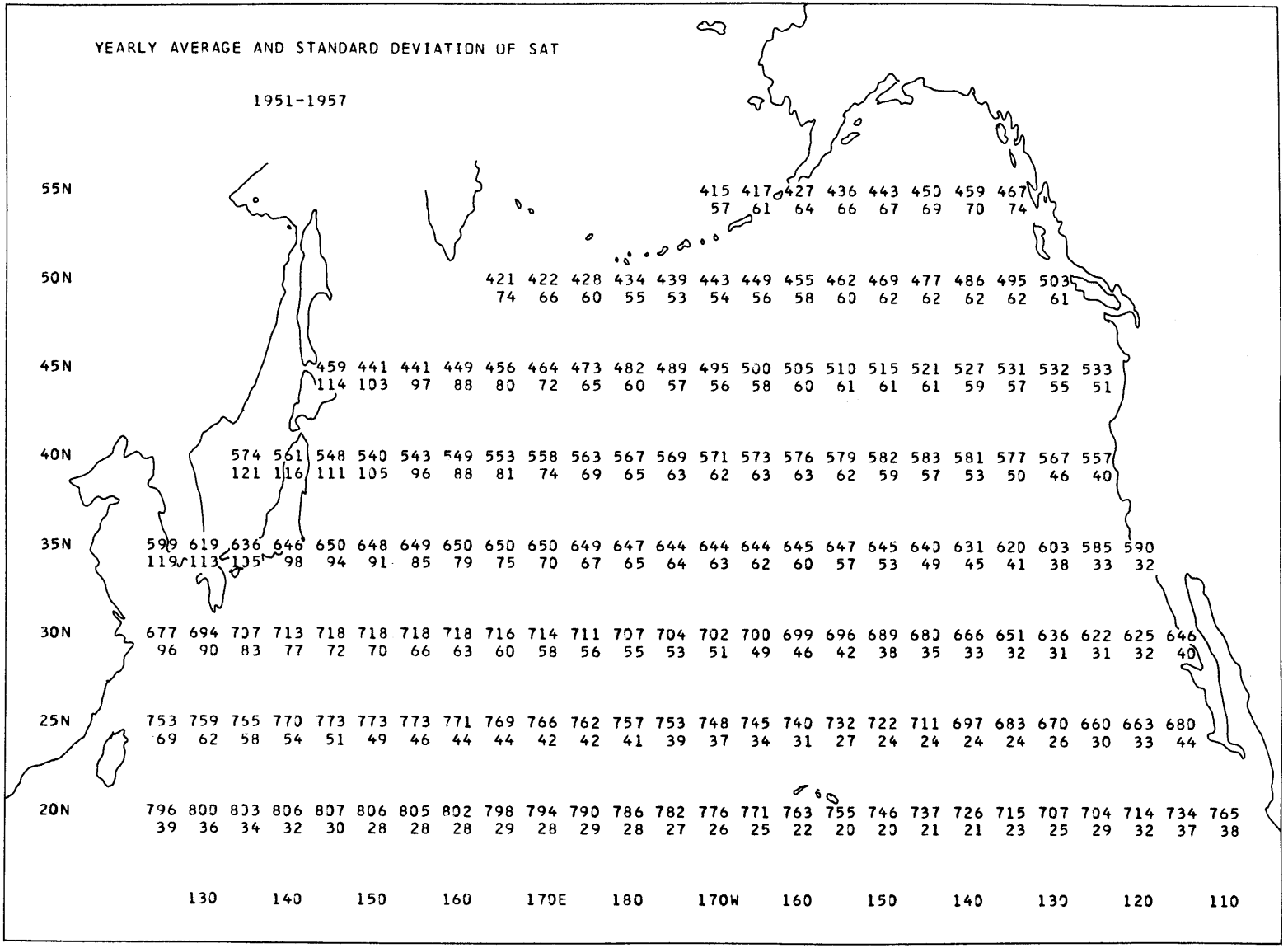

Figure A7. 84-month average values and standard deviations of the surface air temperature. (^{o}F x 10)

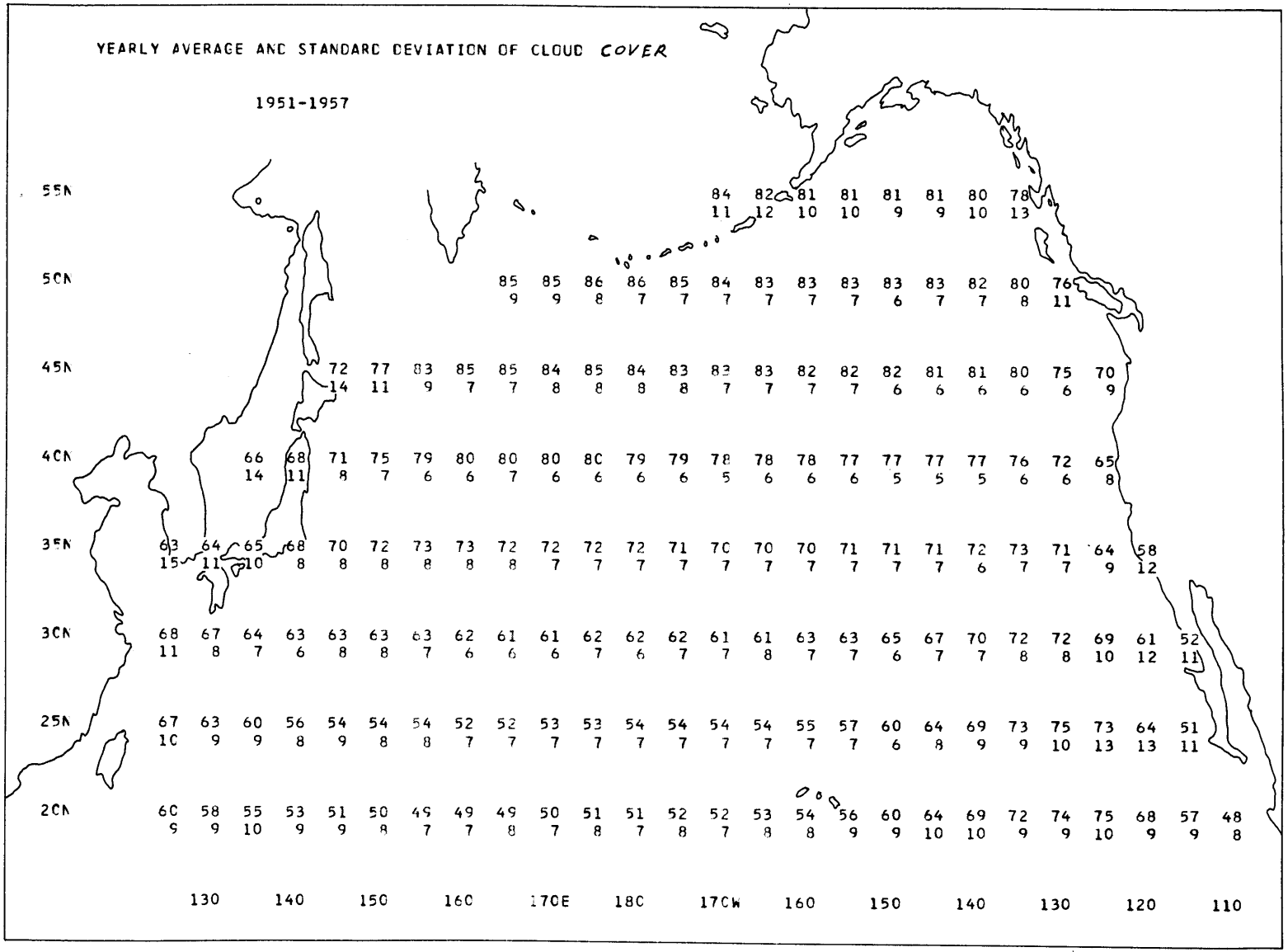

Figure A8. 84-month average values and standard deviations of the cloud cover. (% of sky covered)

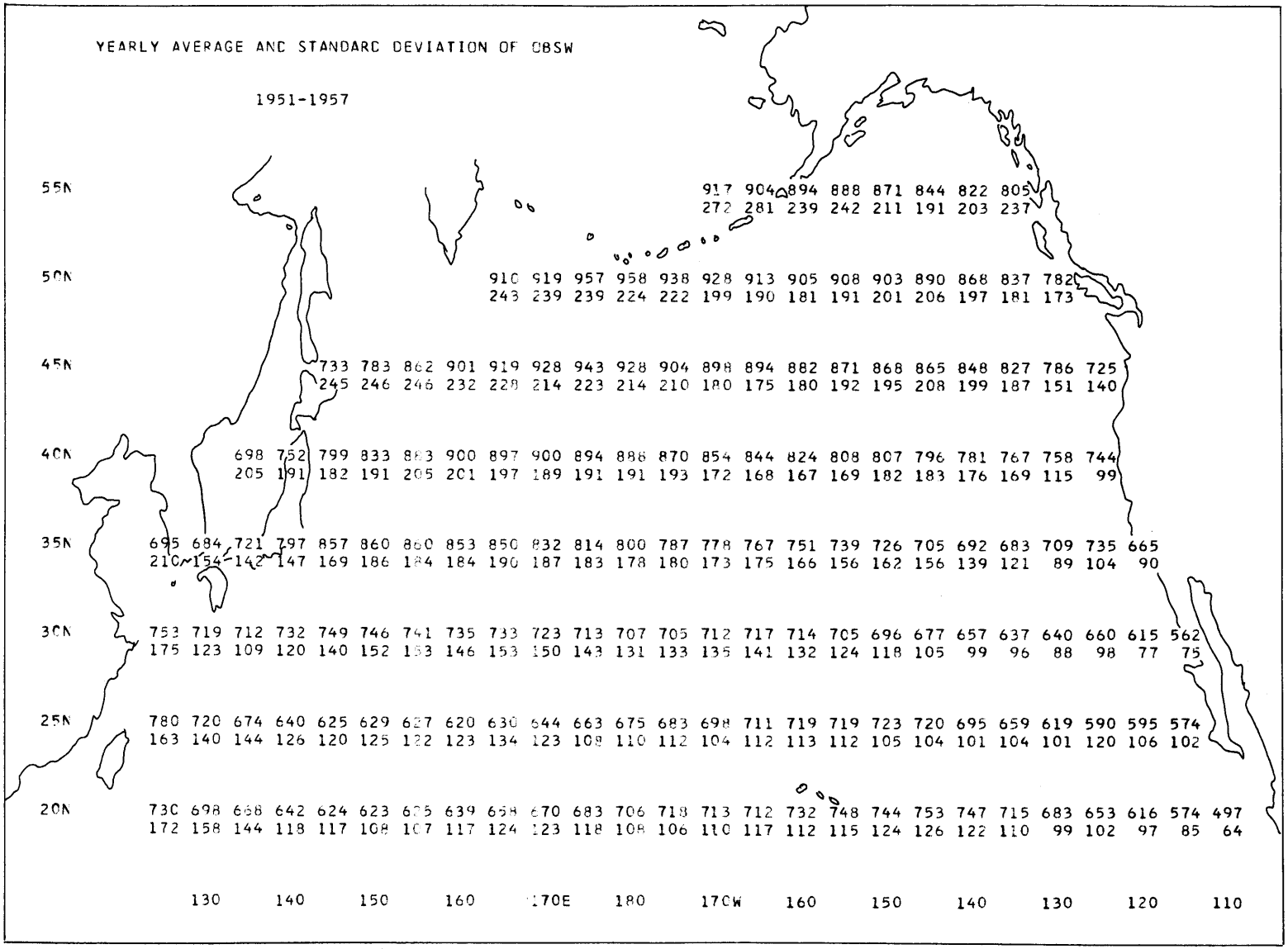

Figure A9. 84-month average values and standard deviations of the observed wind speed. (cm/sec)

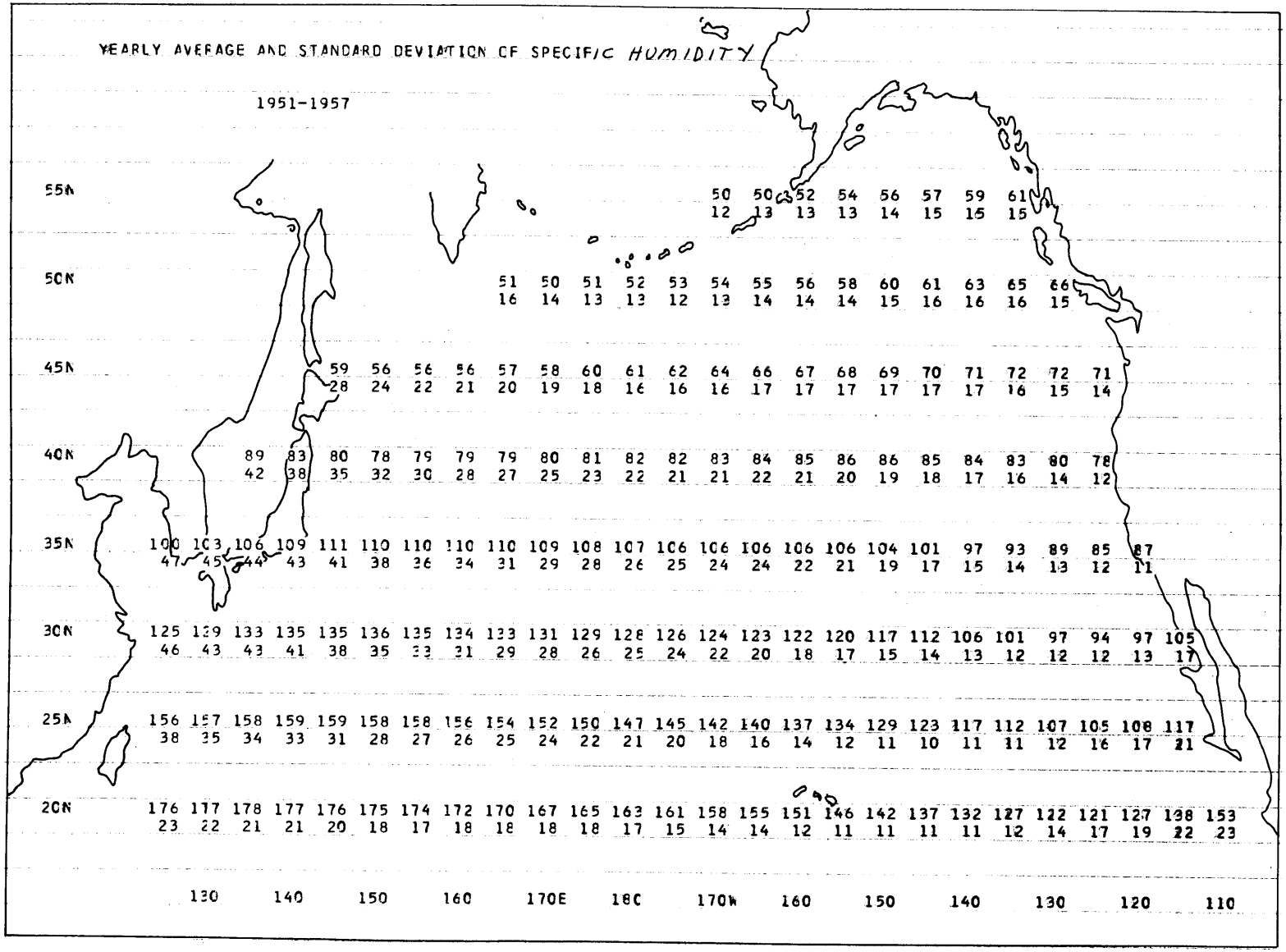

Figure A10. 84-month average values and standard deviations of the specific humidity of the air. (g/kg x 10)

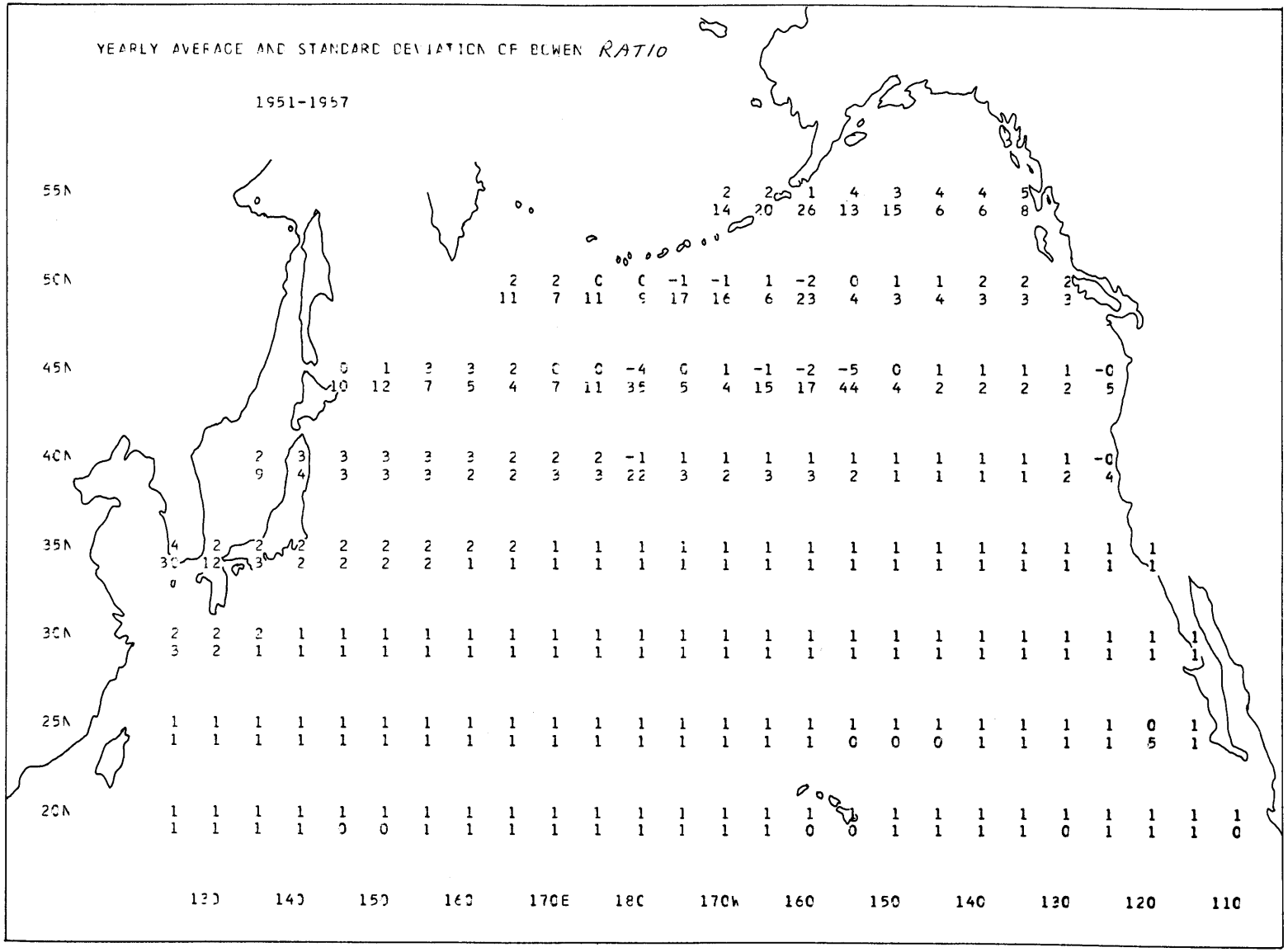

Figure A11. 84-month average values and standard deviations of the Bowen Ratio. (ratio x 10)

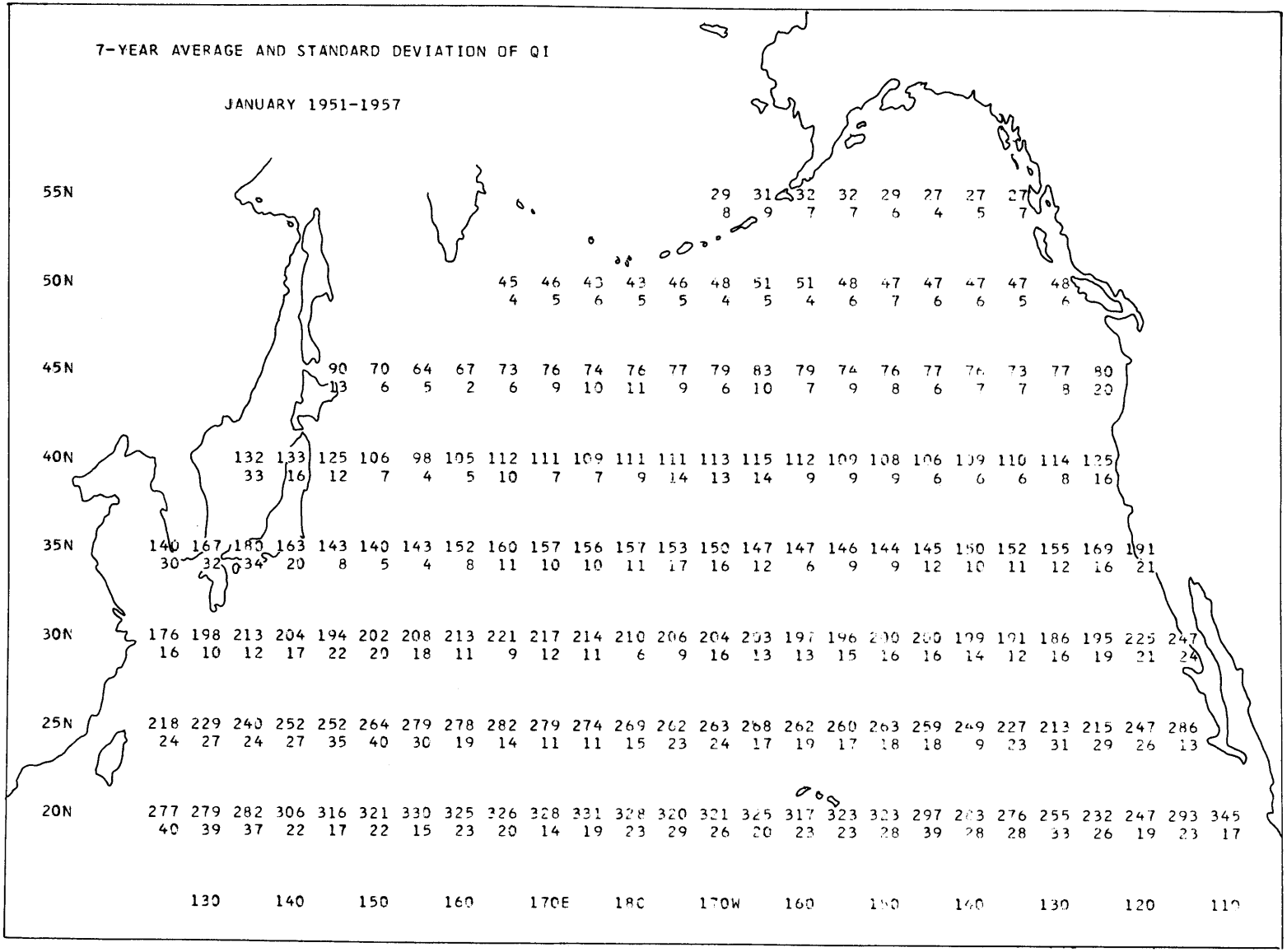

Figure A12. 7-year average values and standard deviations of the incoming radiation. January 1951-1957. (cal/cm^2/day)

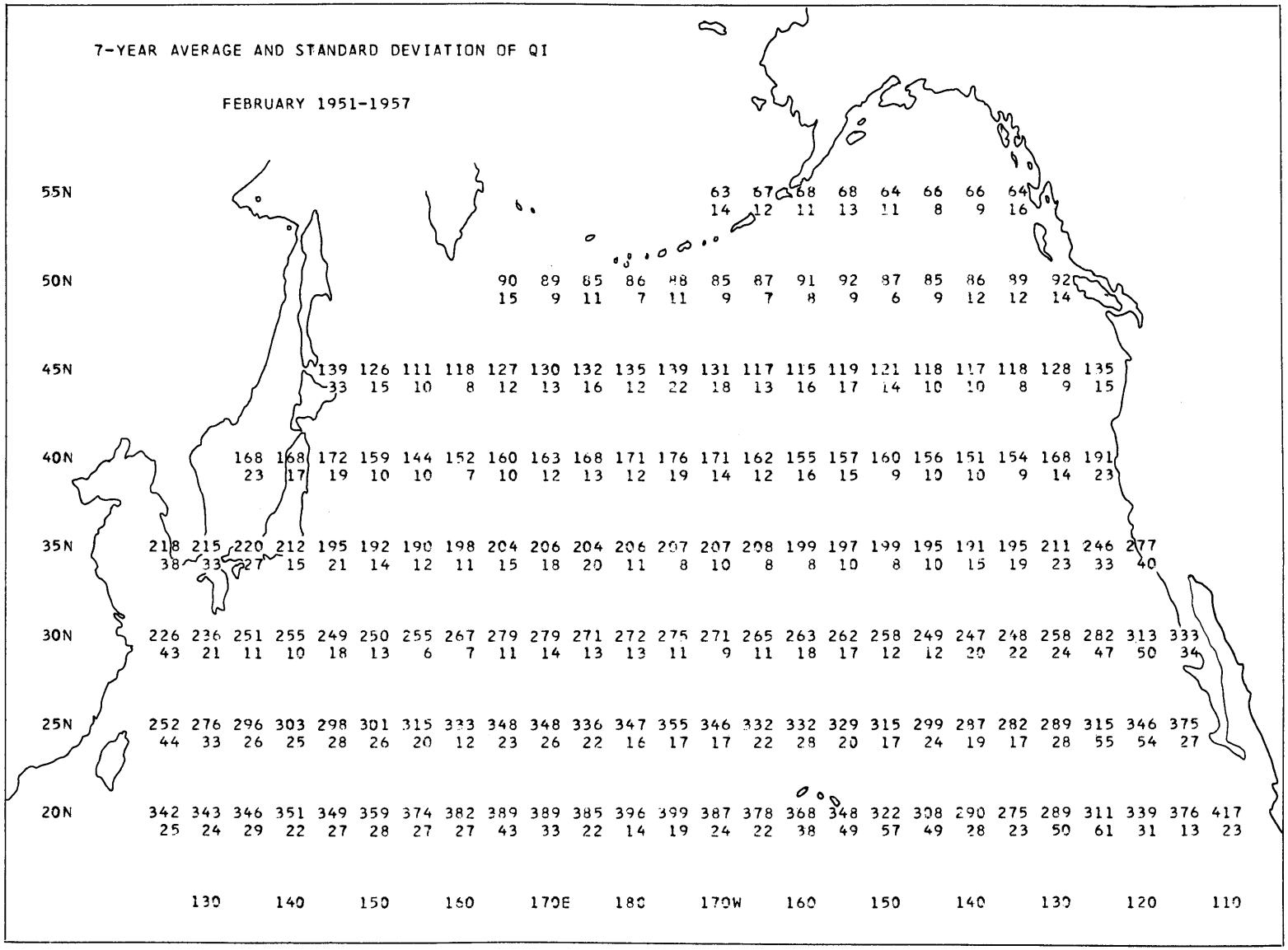

Figure A13. 7-year average values and standard deviations of the incoming radiation. February 1951-1957. (cal/cm^2/day)

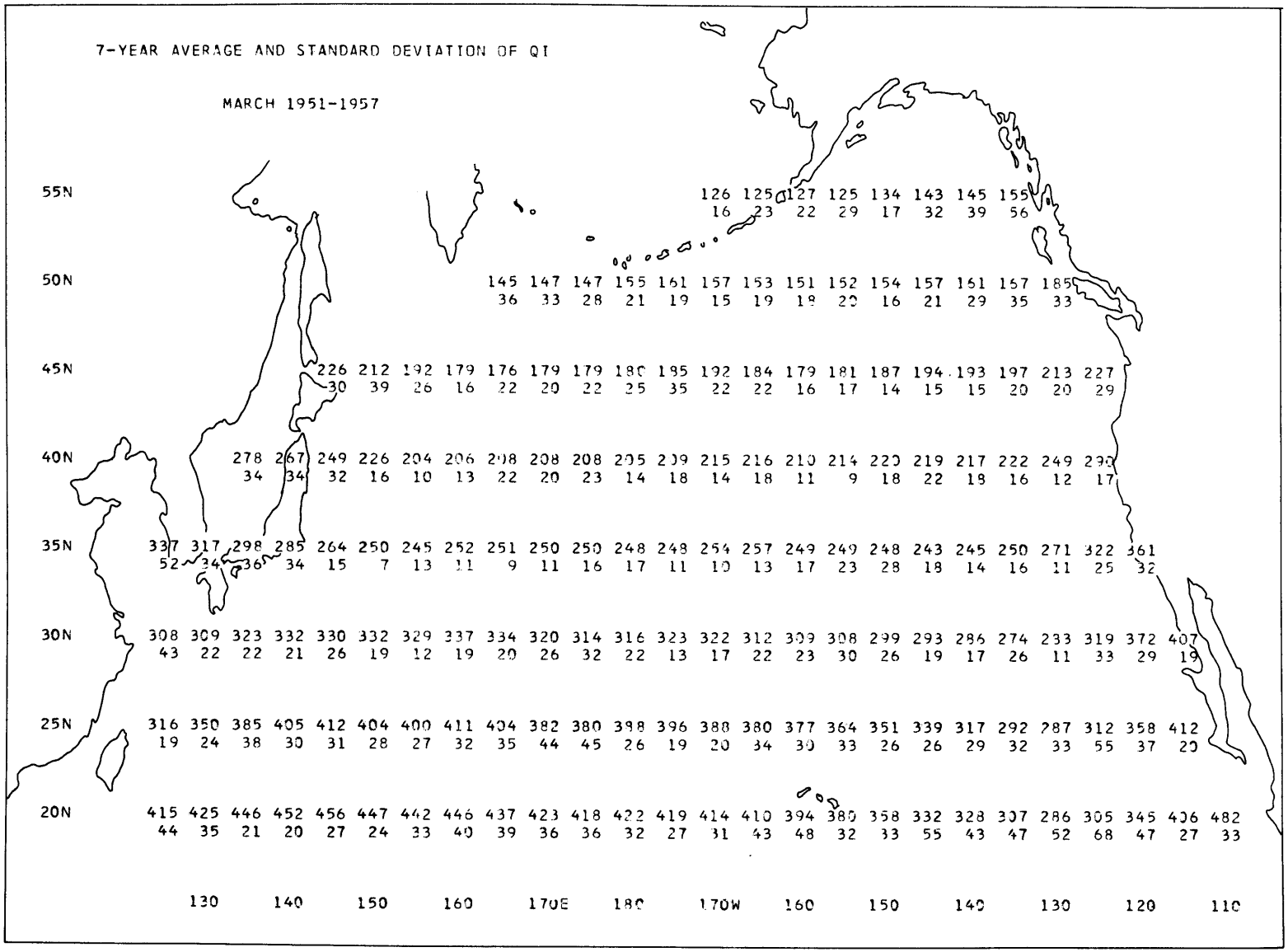

Figure A14. 7-year average values and standard deviations of the incoming radiation. March 1951-1957. (cal/cm^2/day)

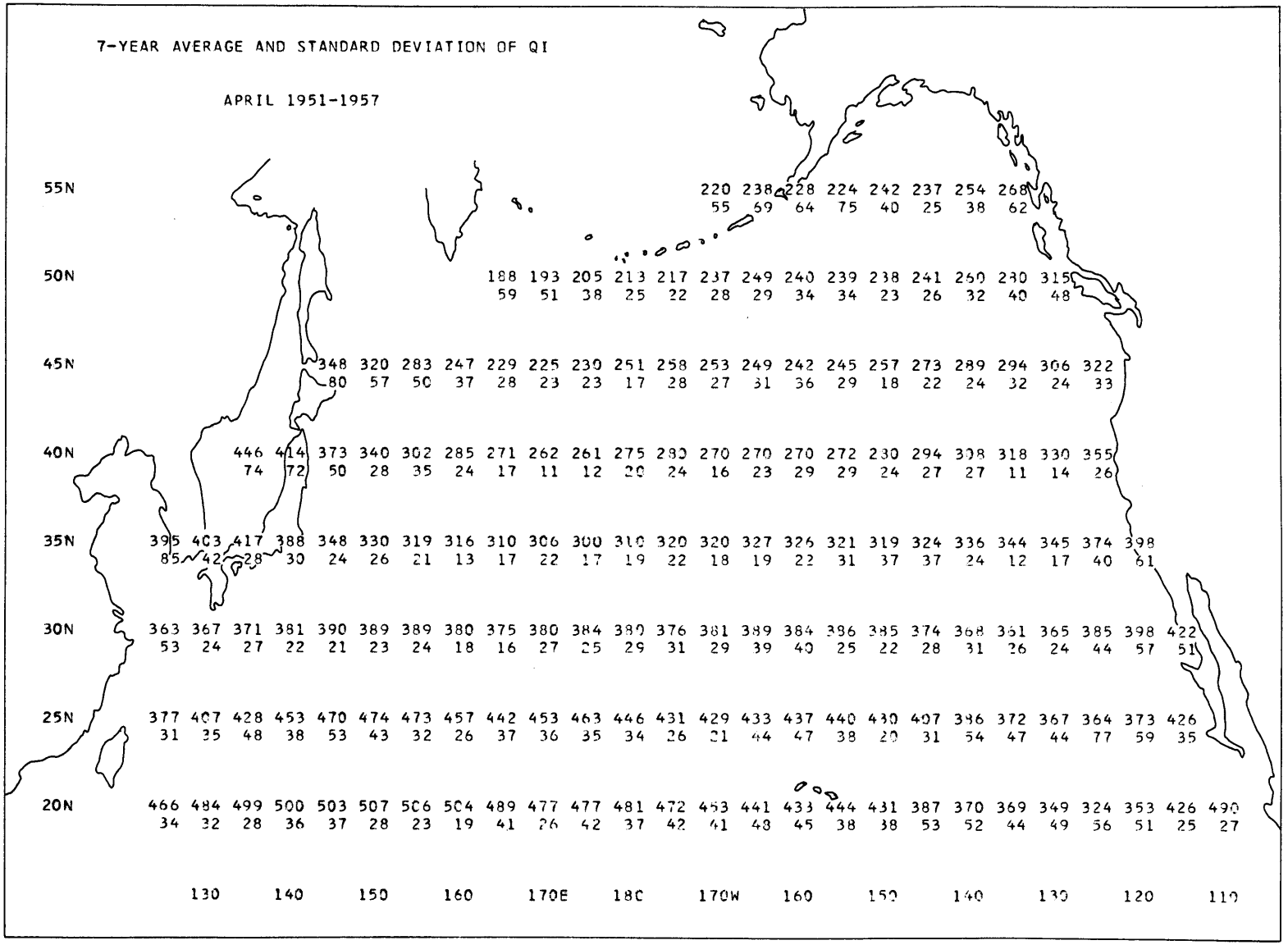

Figure A15. 7-year average values and standard deviations of the incoming radiation. April 1951-1957. (cal/cm^2/day)

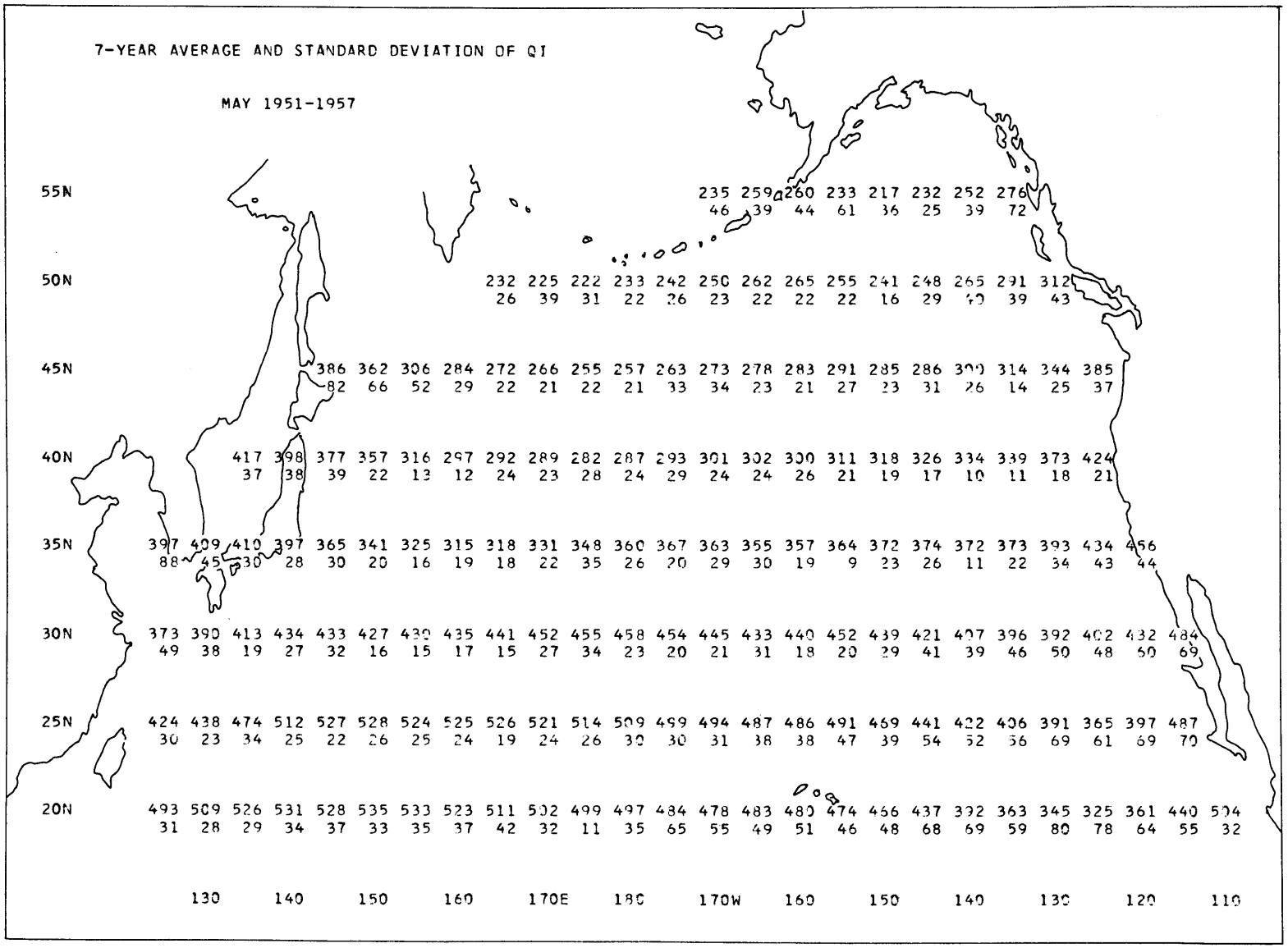

Figure A16. 7-year average values and standard deviations of the incoming radiation. May 1951-1957. (cal/cm^2/day)

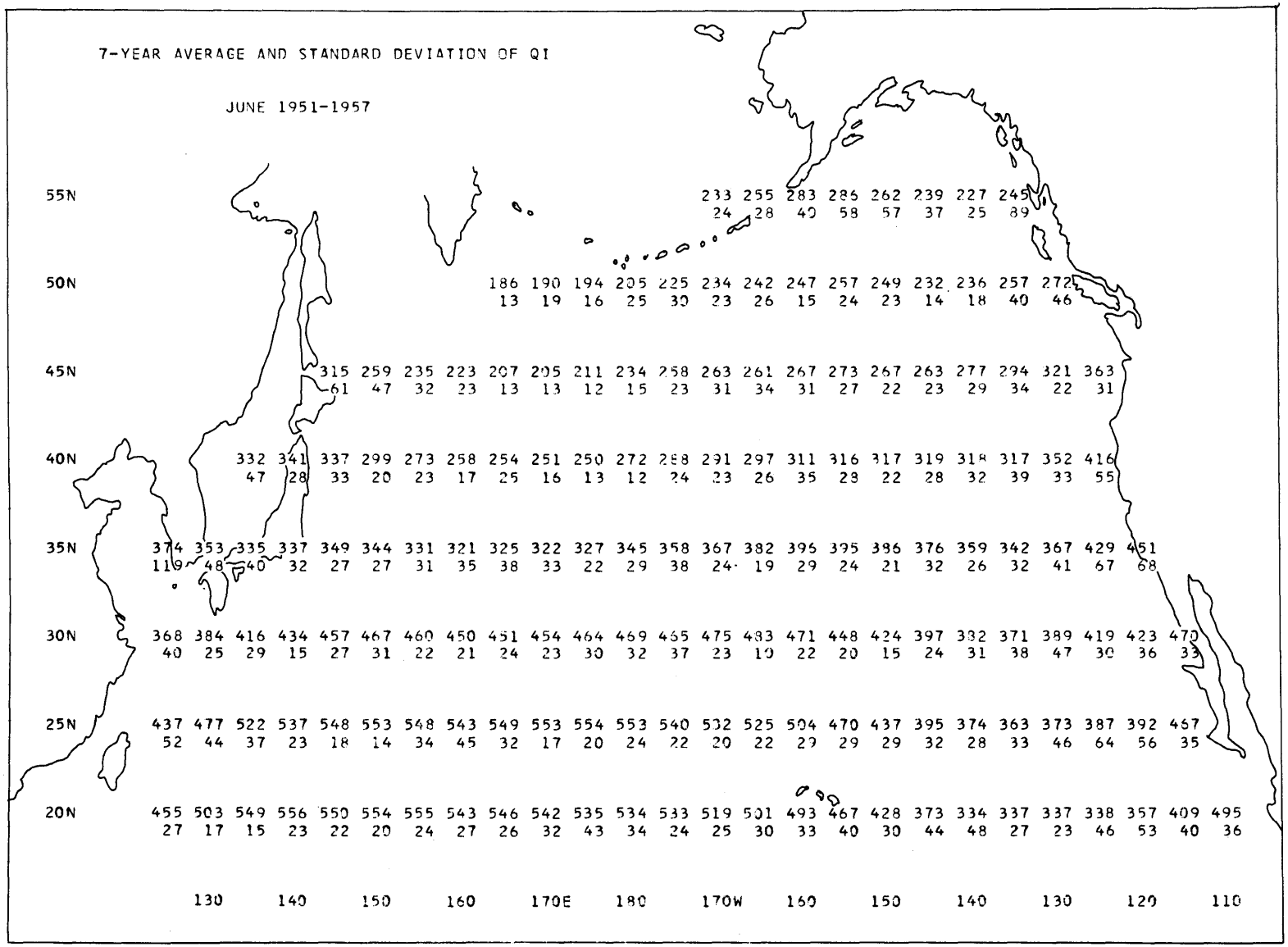

Figure A17. 7-year average values and standard deviations of the incoming radiation. June 1951-1957. (cal/cm^2/day)

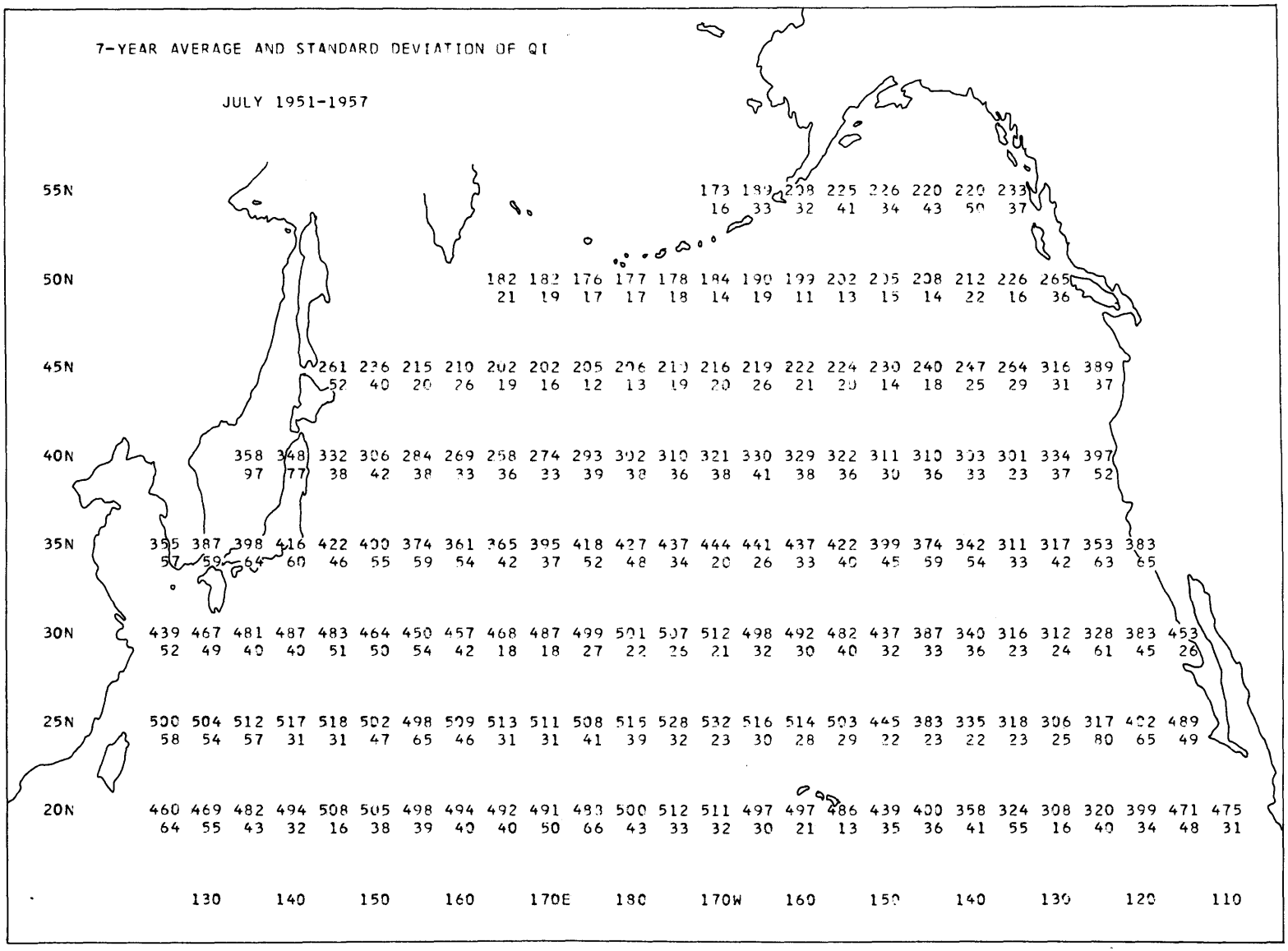

Figure A18. 7-year average values and standard deviations of the incoming radiation. July 1951-1957. (cal/cm^2/day)

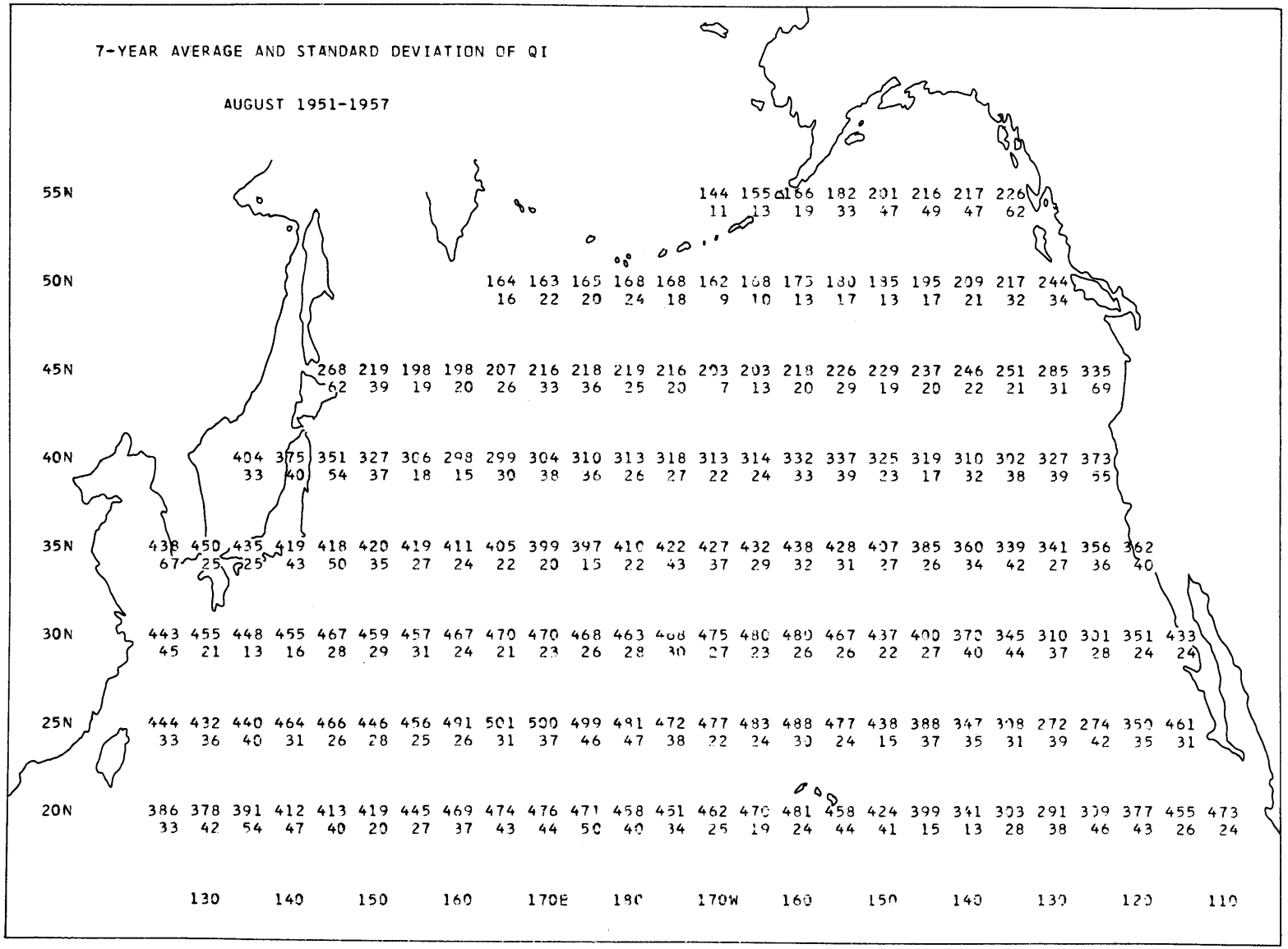

Figure A19. 7-year average values and standard deviations of the incoming radiation. August 1951-1957. (cal/cm^2/day)

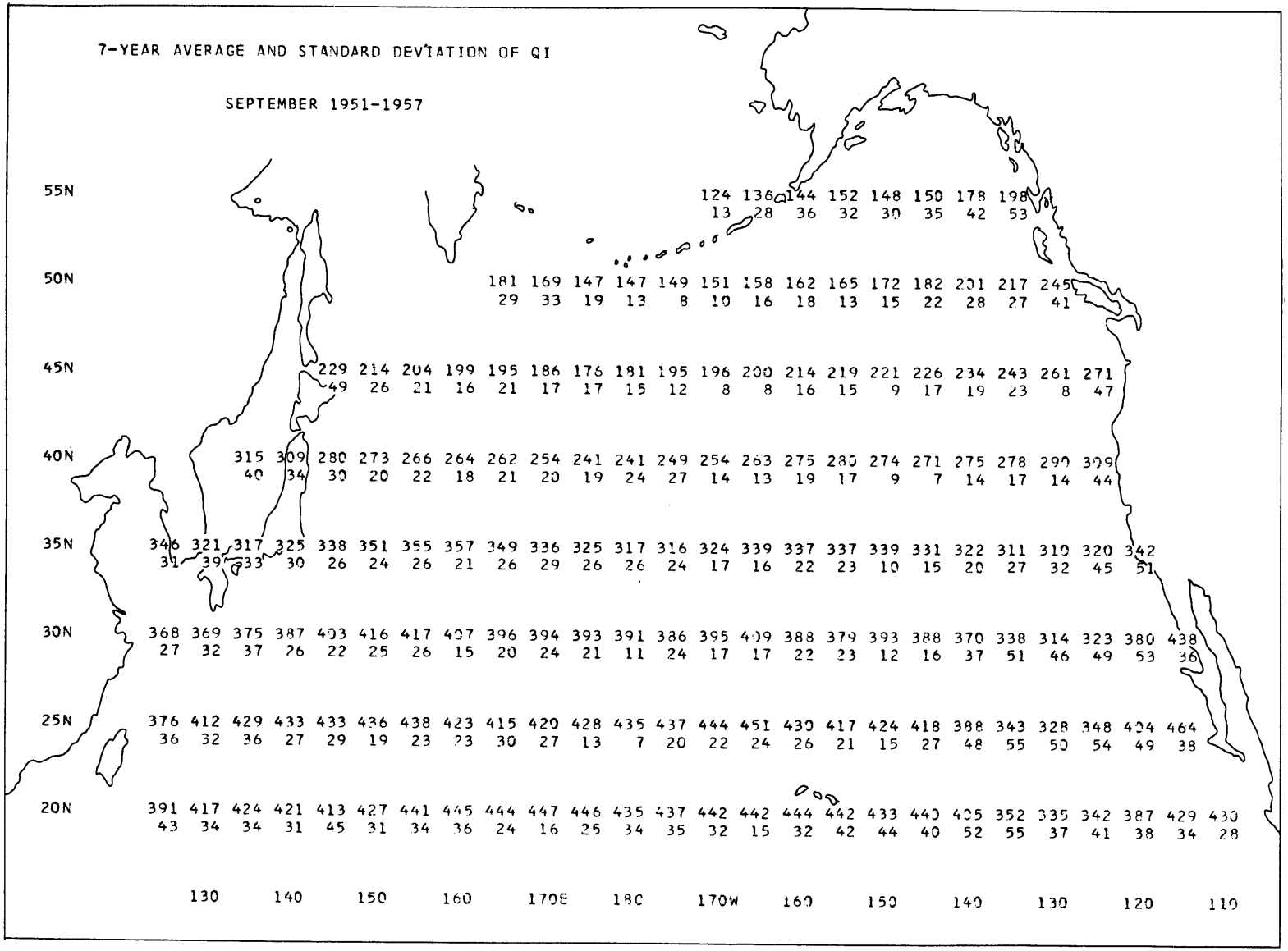

Figure A20. 7-year average values and standard deviations of the incoming radiation. September 1951-1957. (cal/cm^2/day)

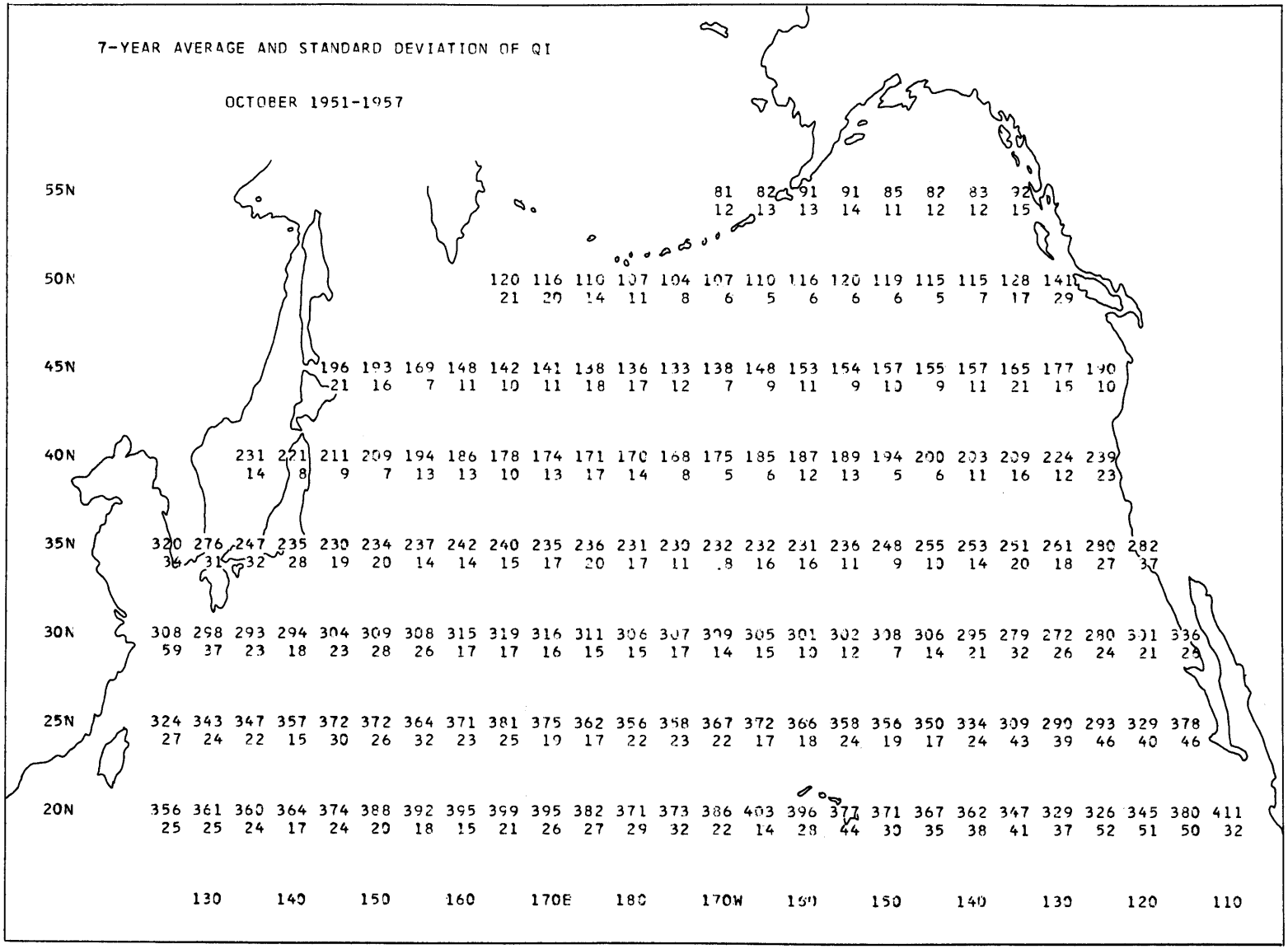

Figure A21. 7-year average values and standard deviations of the incoming radiation. October 1951-1957. (cal/cm^2/day)

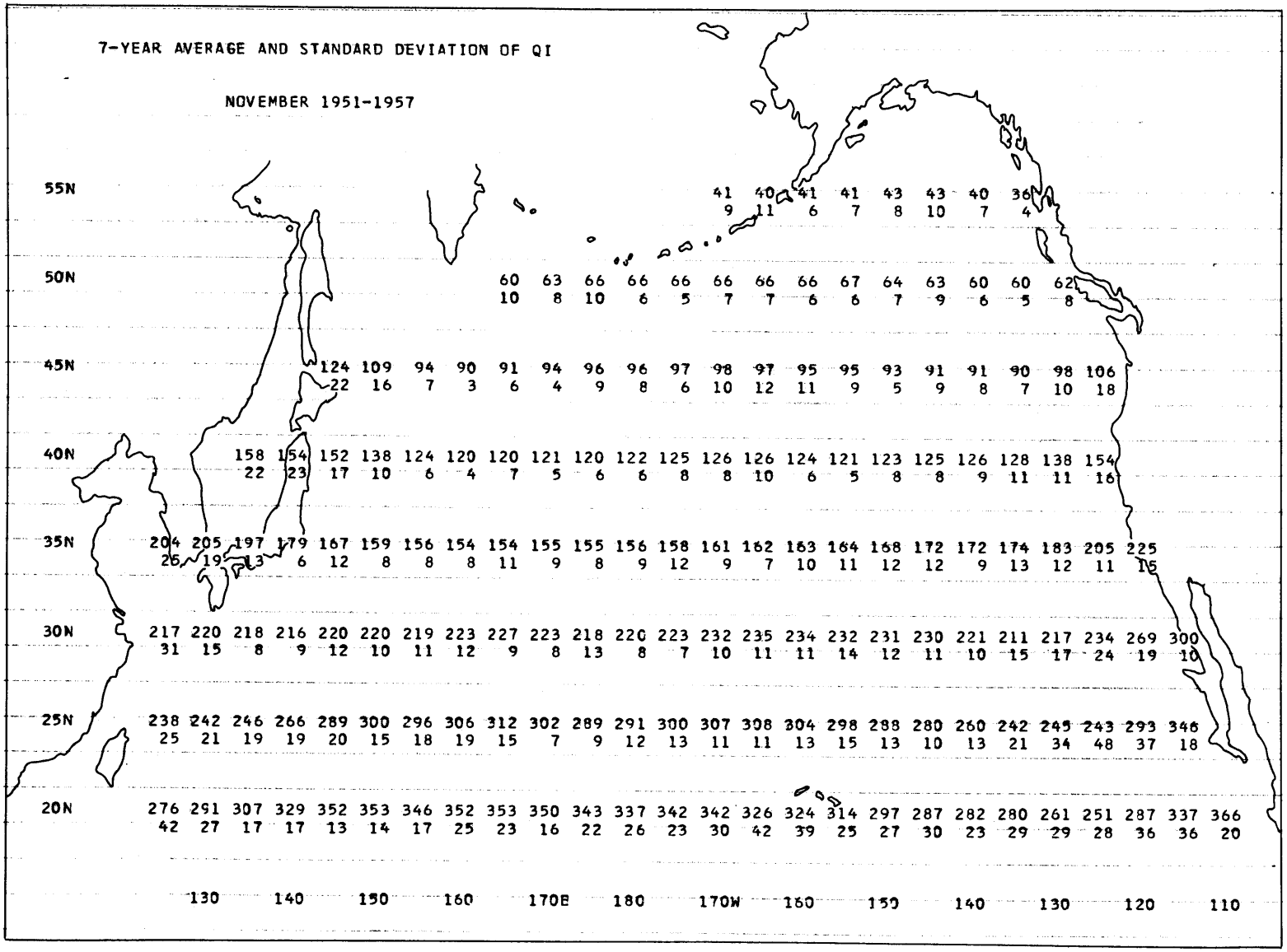

Figure A22. 7-year average values and standard deviations of the incoming radiation. November 1951-1957. (cal/cm^2/day)

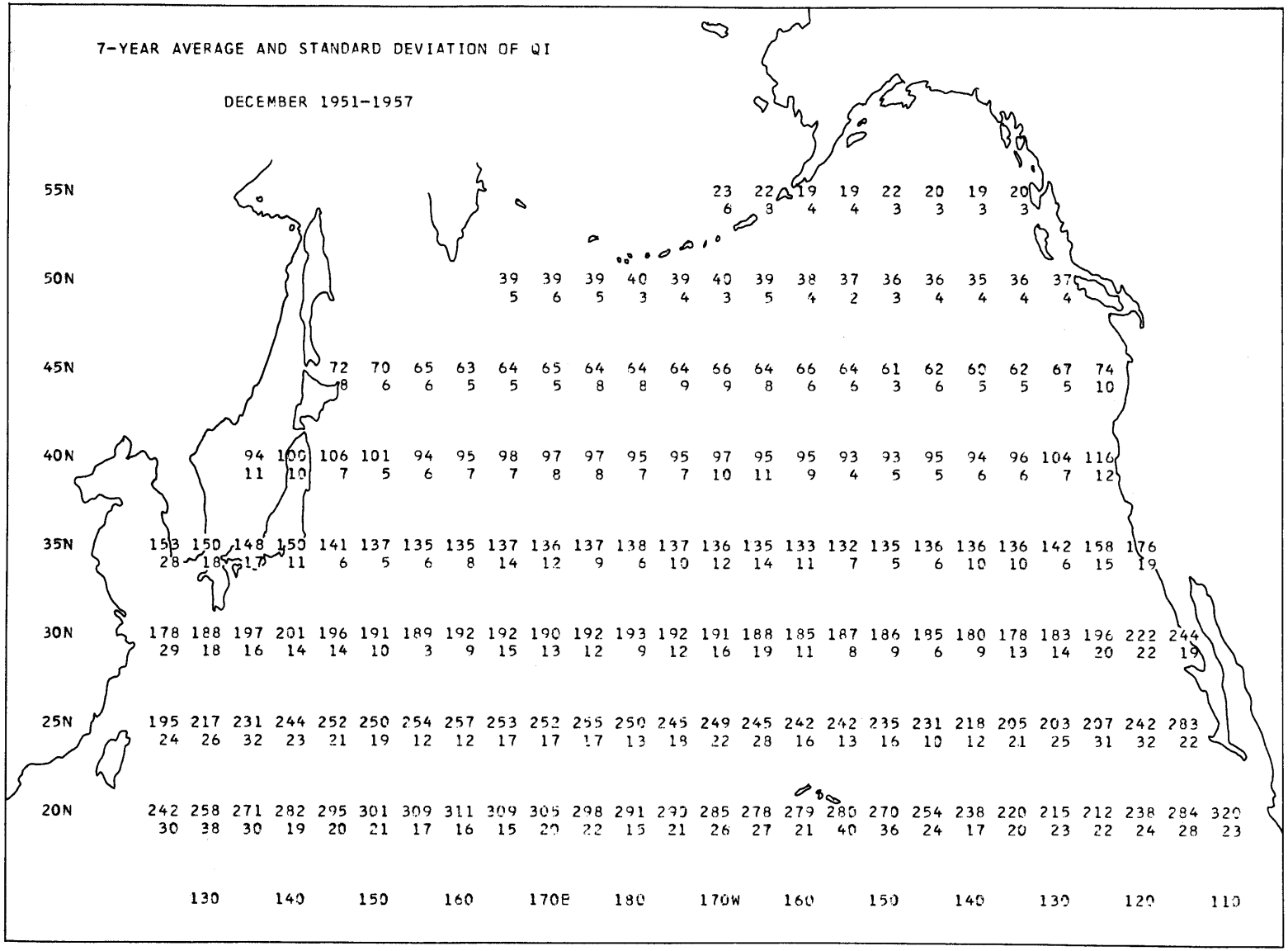

Figure A23. 7-year average values and standard deviations of the incoming radiation. December 1951-1957. (cal/cm^2/day)

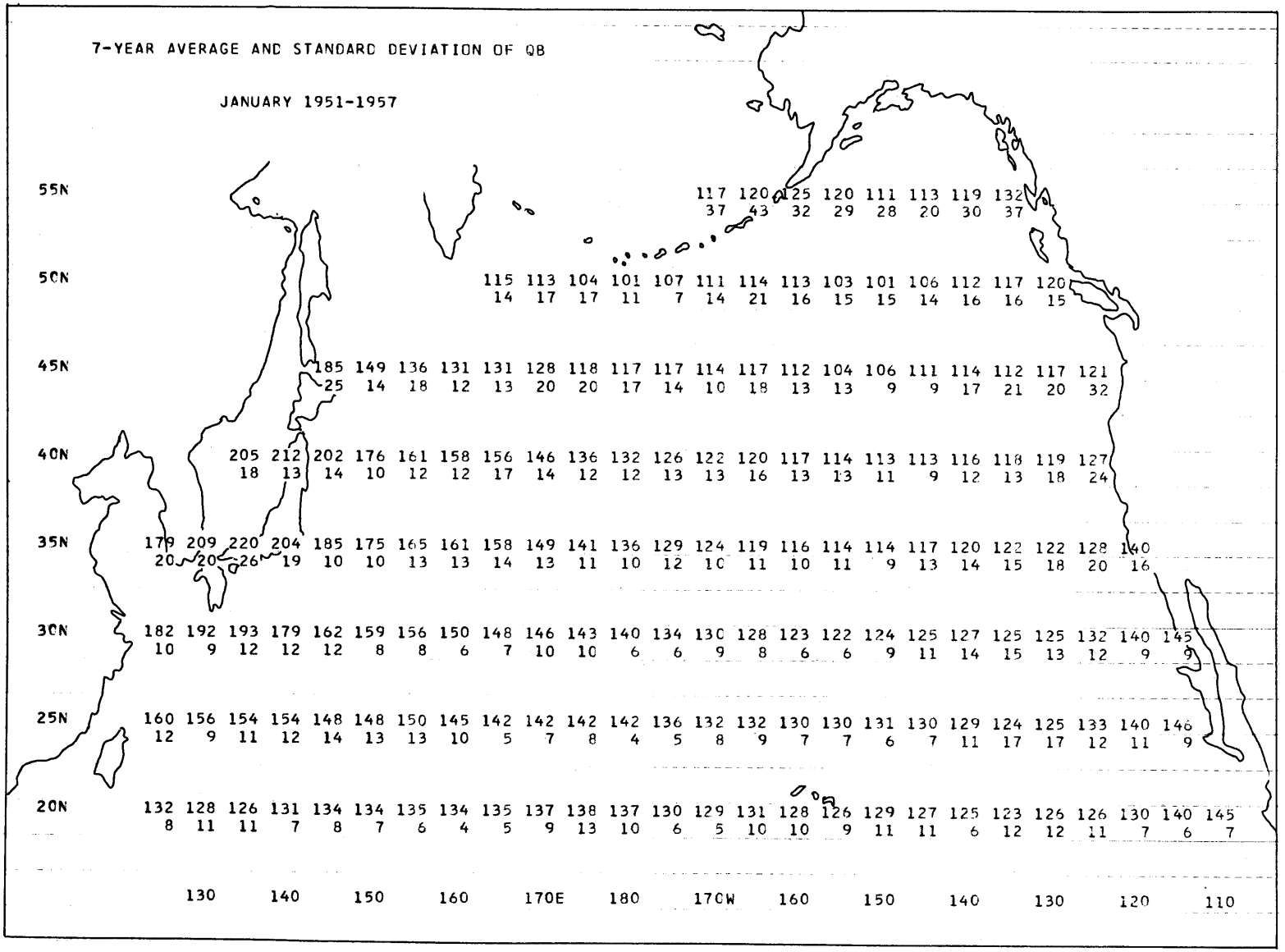

Figure A24. 7-year average values and standard deviations of the effective back radiation. January 1951-1957. (cal/cm^2/day)

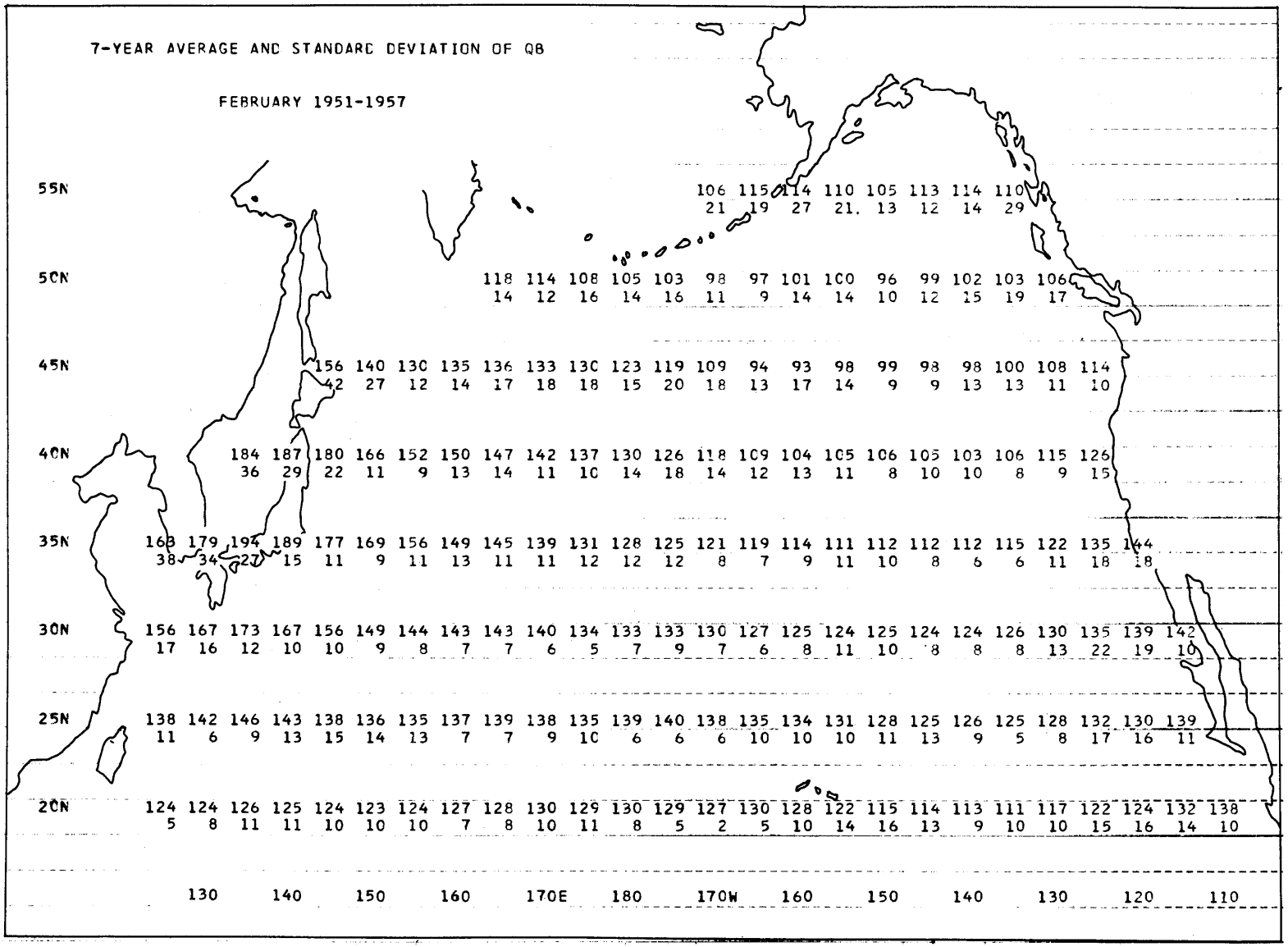

Figure A25. 7-year average values and standard deviations of the effective back radiation. February 1951-1957. (cal/cm^2/day)

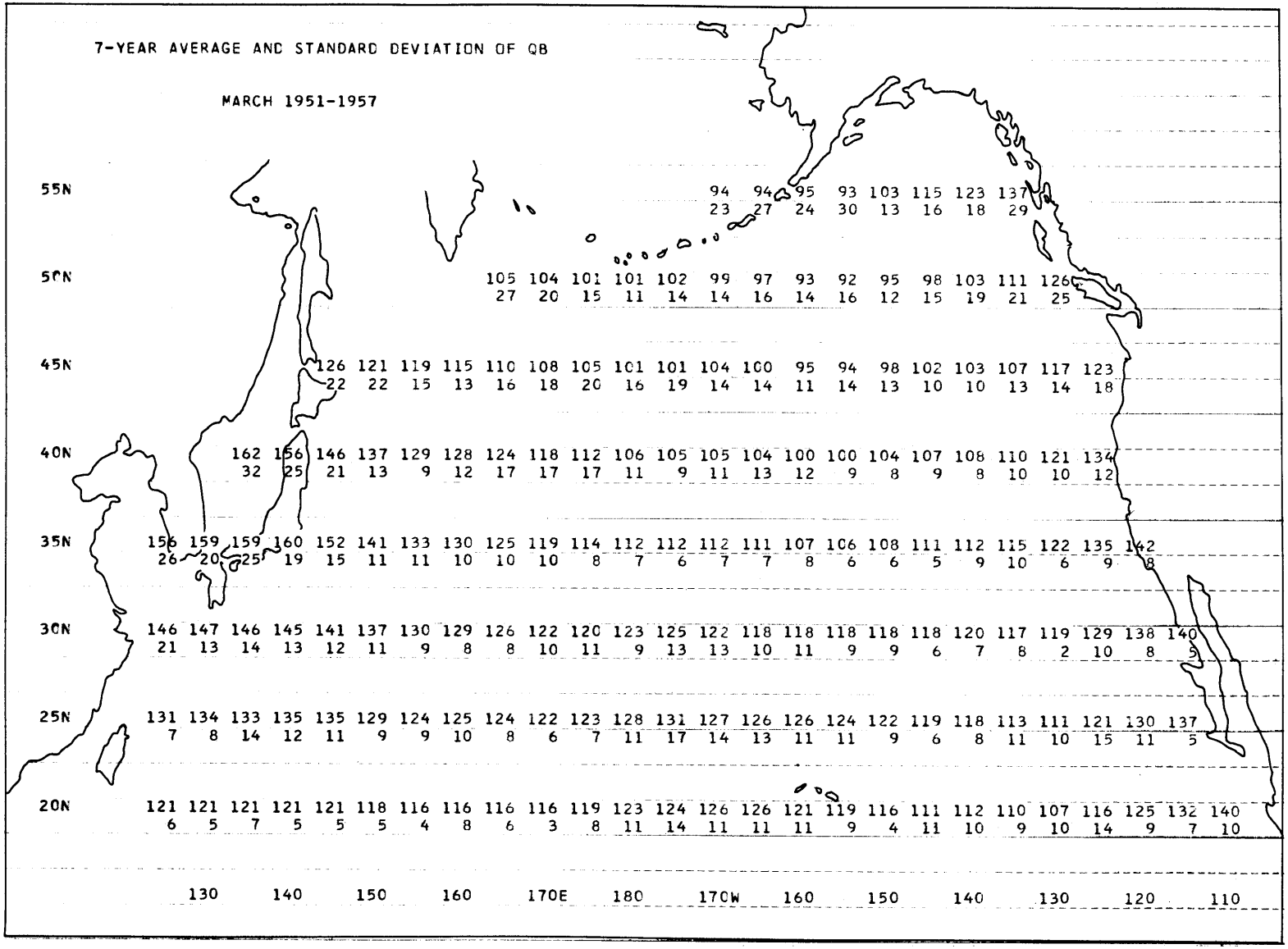

Figure A26. 7-year average values and standard deviations of the effective back radiation. March 1951-1957. (cal/cm^2/day)

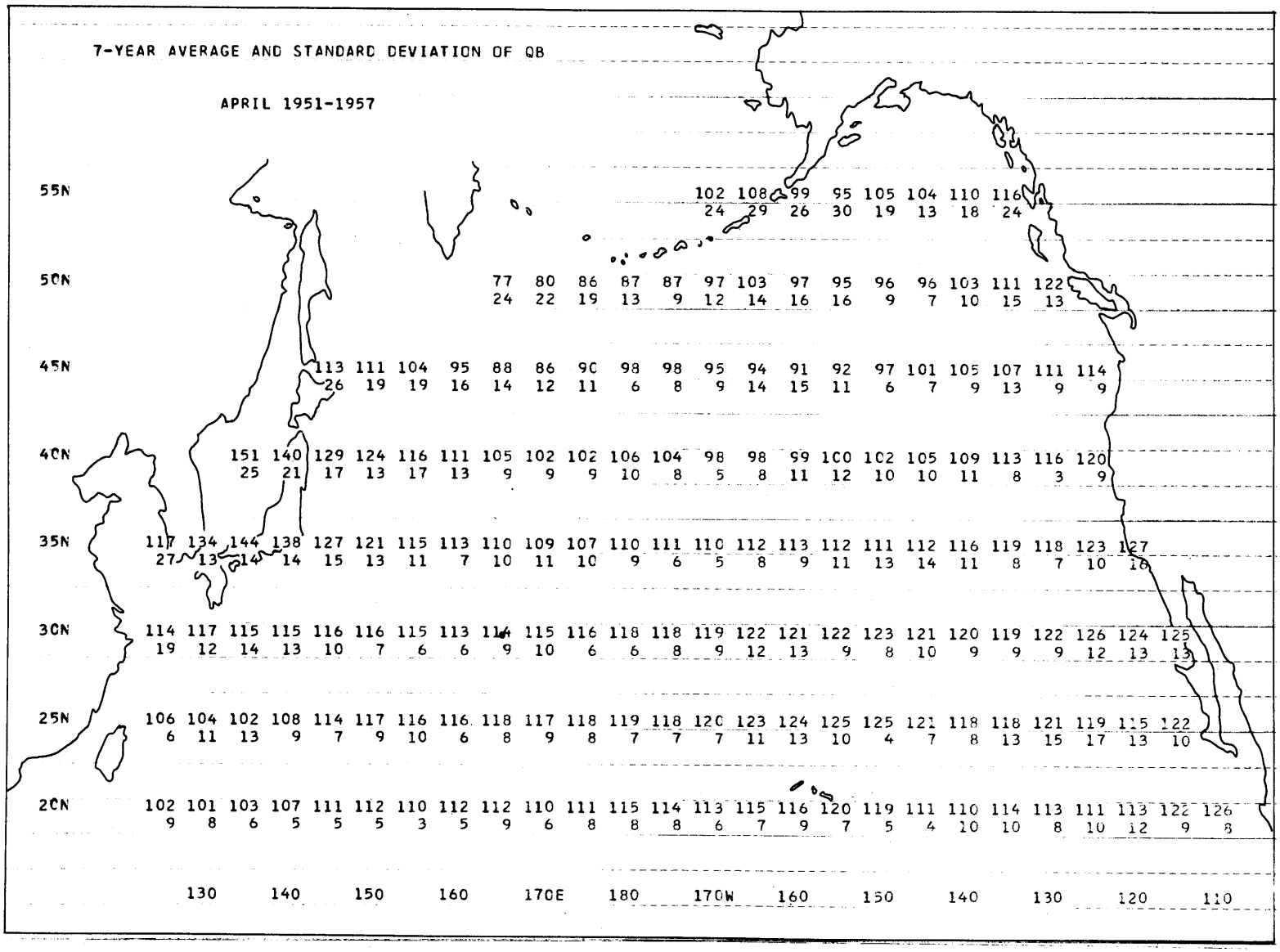

Figure A27. 7-year average values and standard deviations of the effective back radiation. April 1951-1957. (cal/cm^2/day)

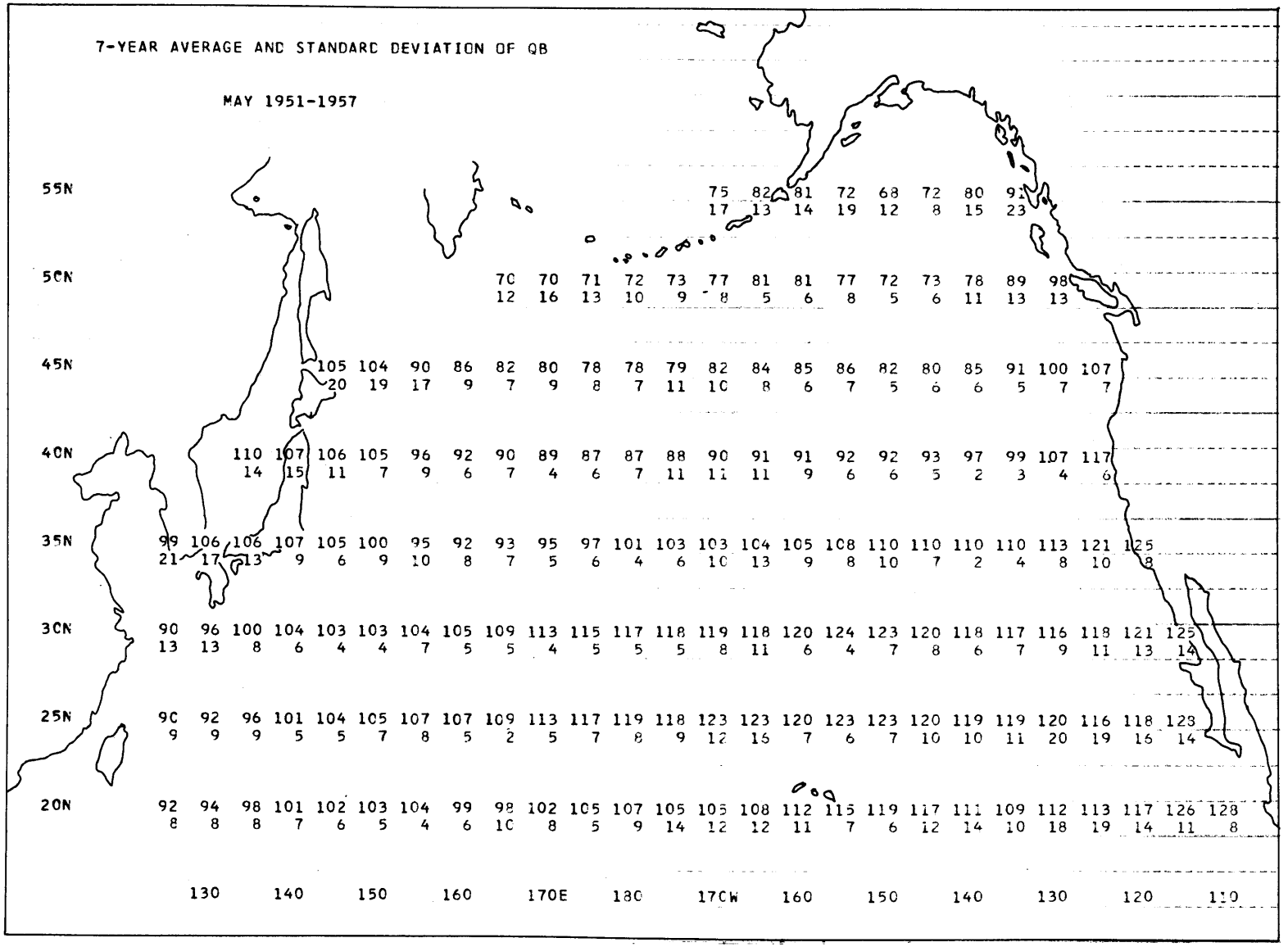

Figure A28. 7-year average values and standard deviations of the effective back radiation. May 1951-1957. (cal/cm^2/day)

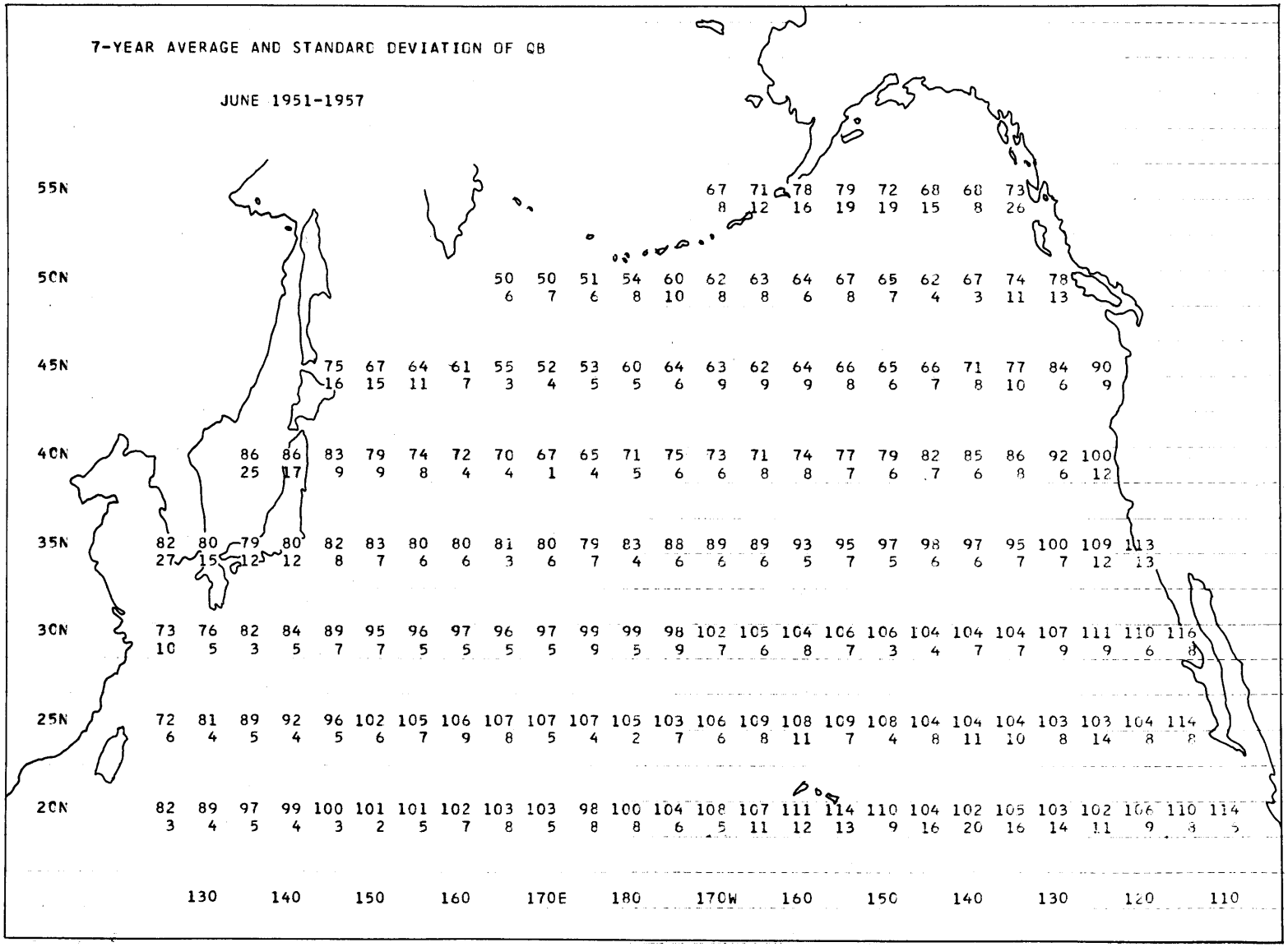

Figure A29. 7-year average values and standard deviations of the effective back radiation. June 1951-1957. (cal/cm^2/day)

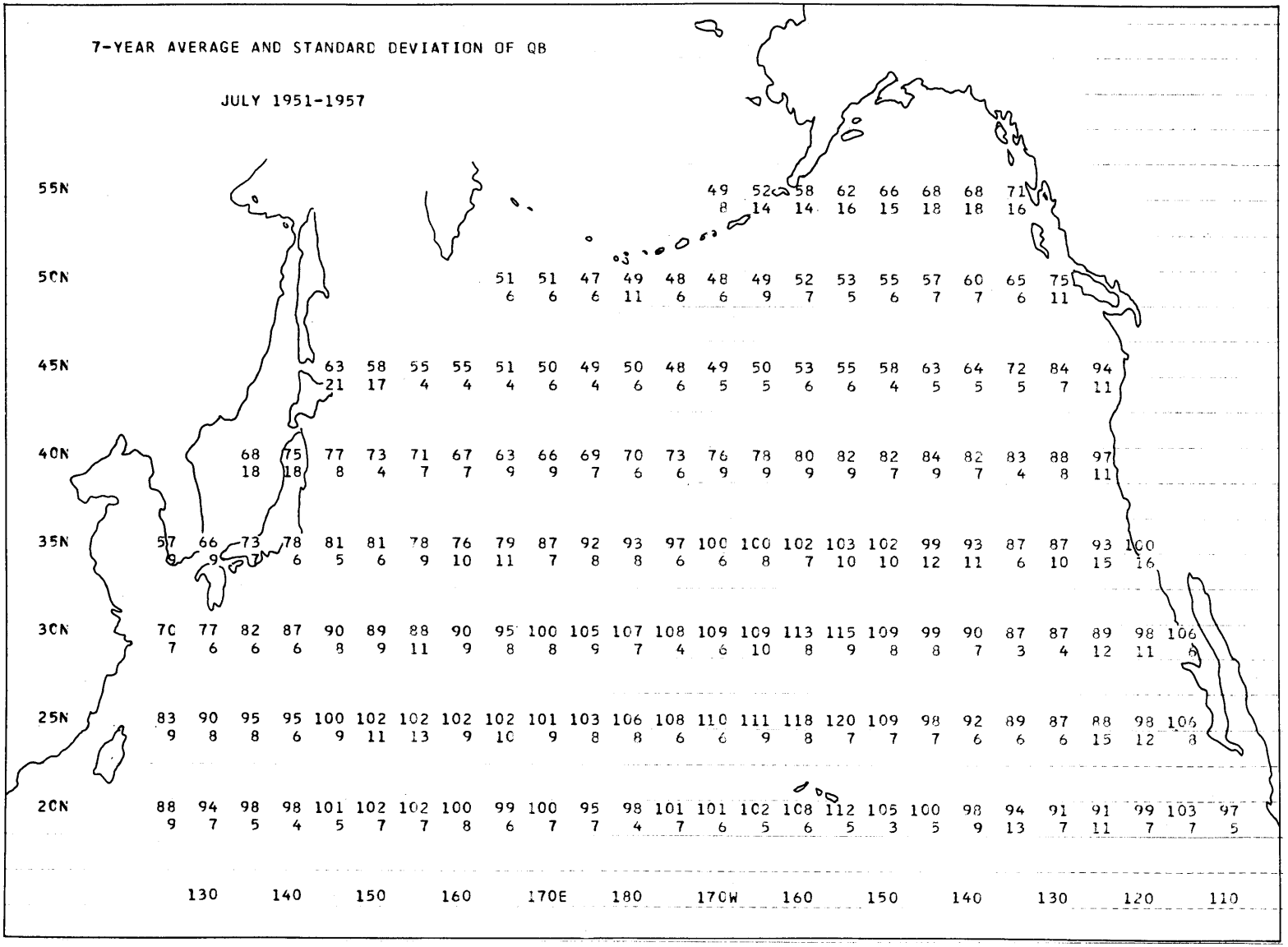

Figure A30. 7-year average values and standard deviations of the effective back radiation. July 1951-1957. (cal/cm^2/day)

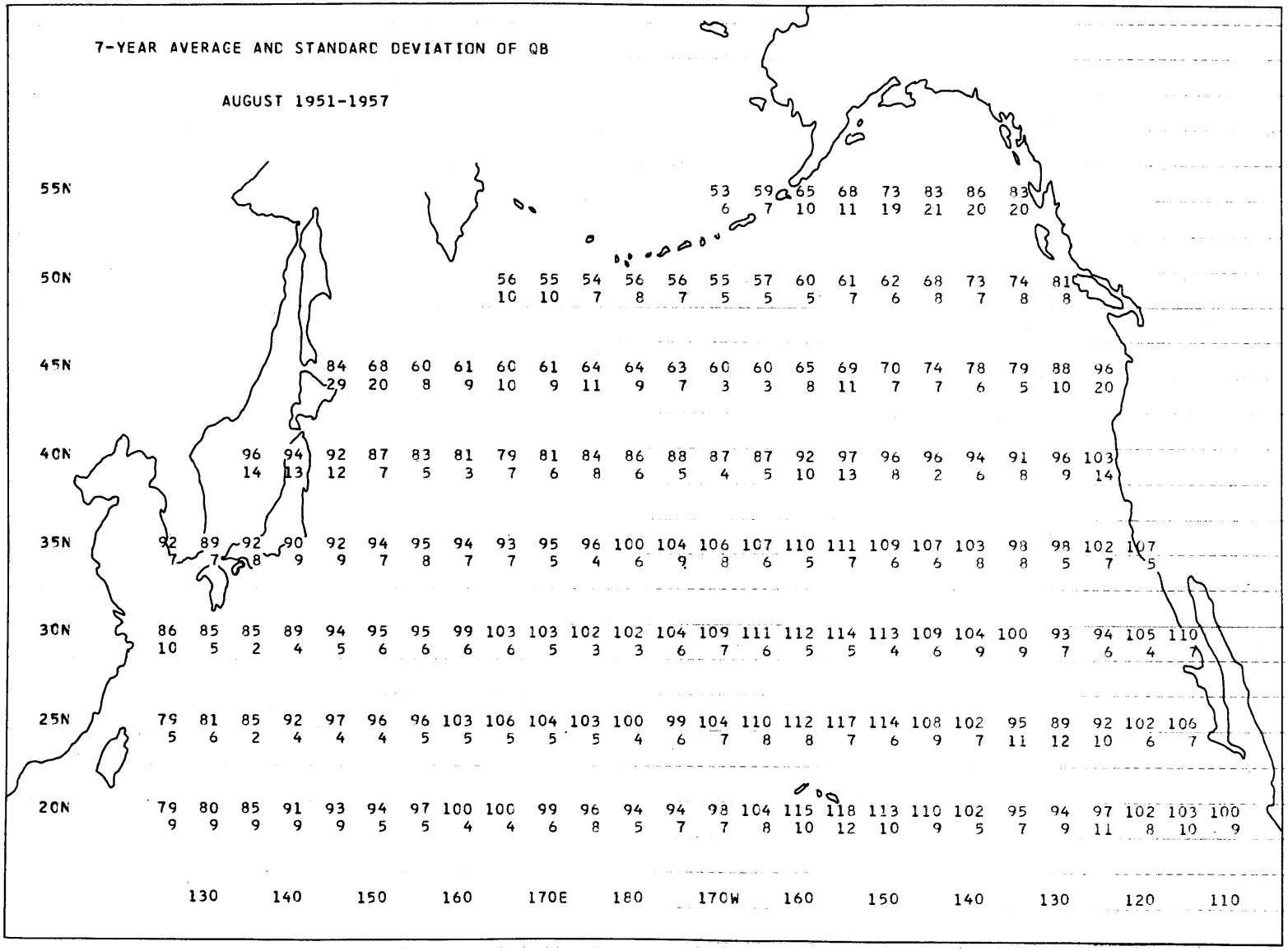

Figure A31. 7-year average values and standard deviations of the effective back radiation. August 1951-1957. (cal/cm^2/day)

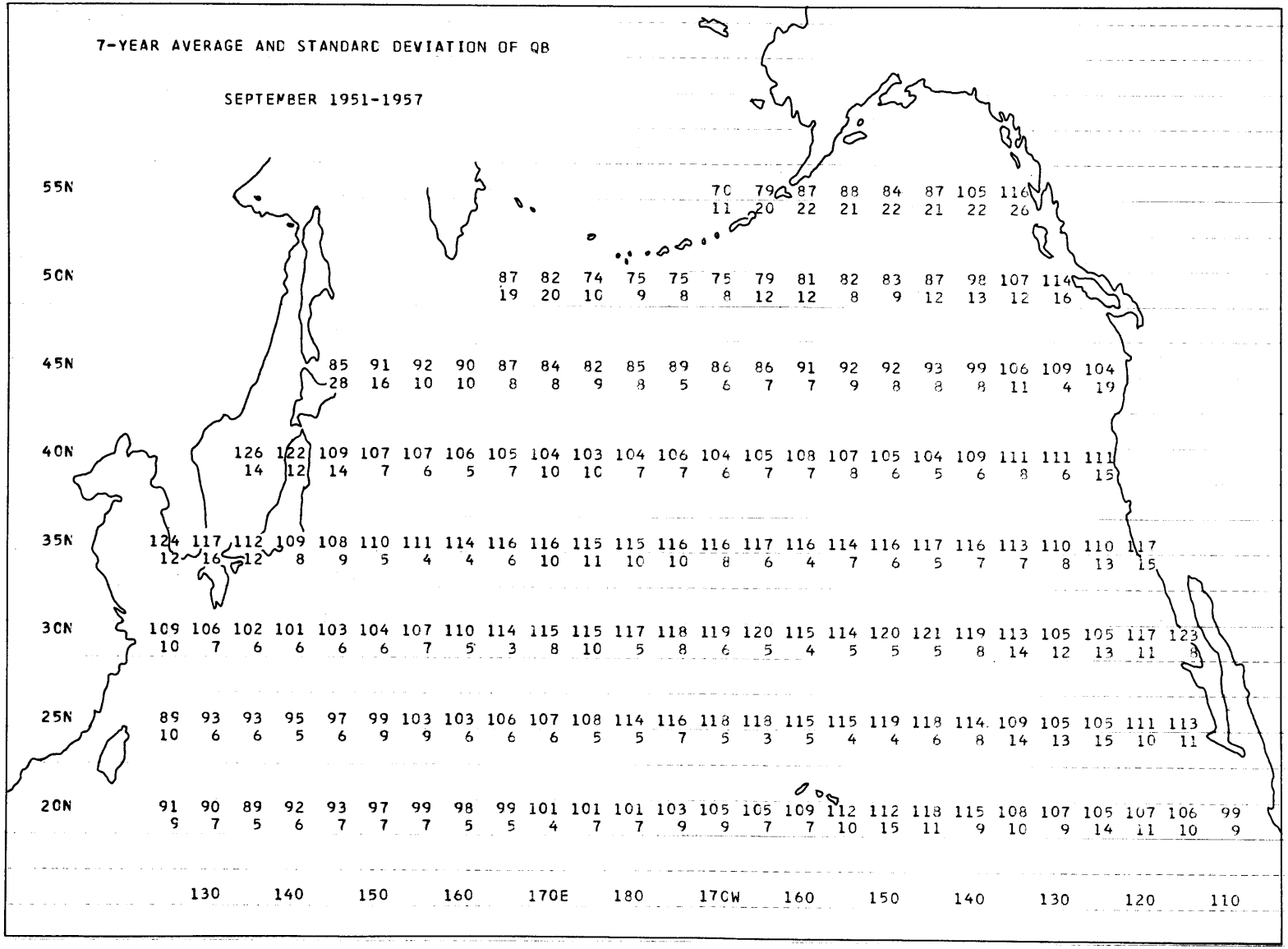

Figure A32. 7-year average values and standard deviations of the effective back radiation. September 1951-1957. (cal/cm^2/day)

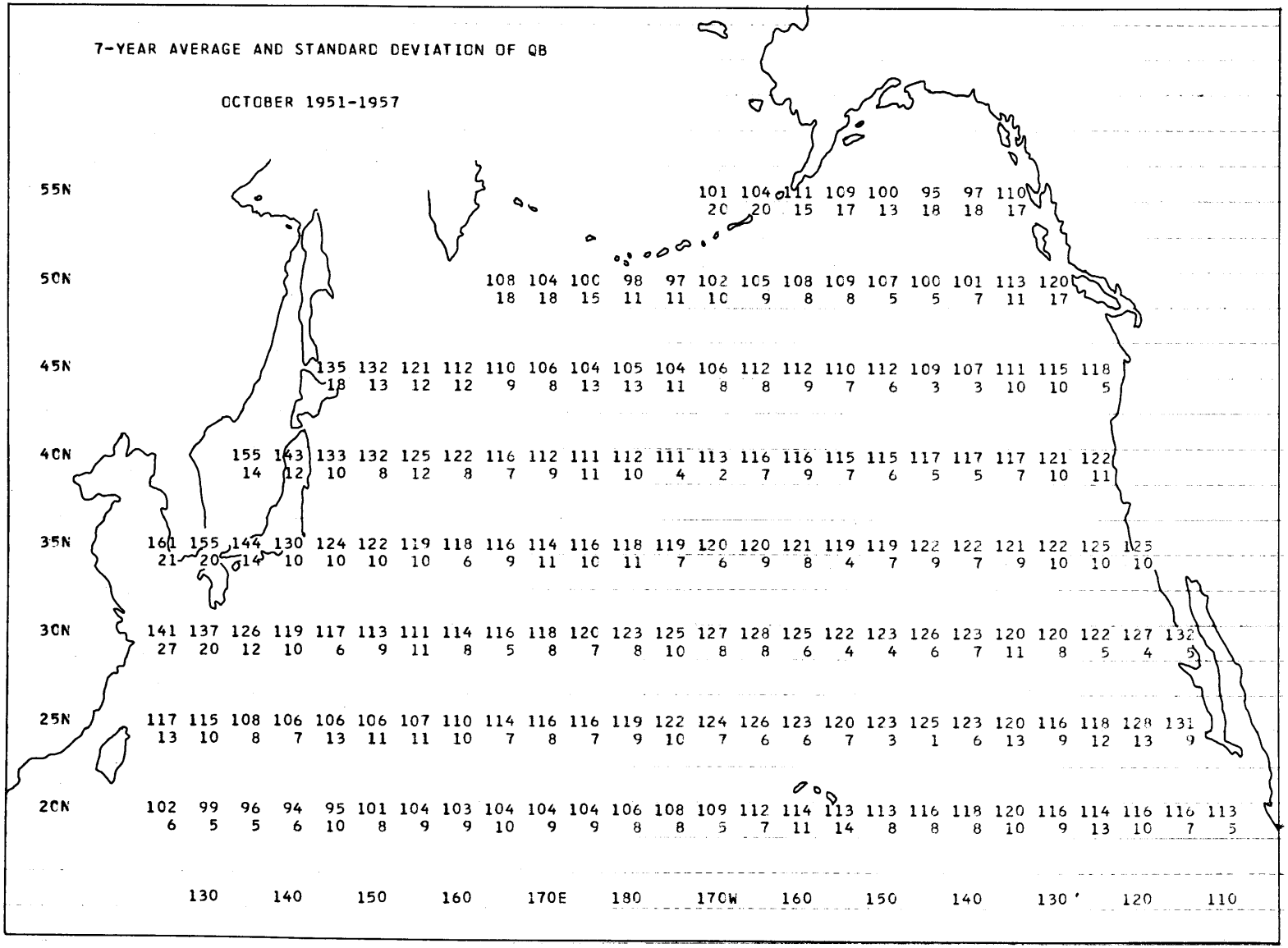

Figure A33. 7-year average values and standard deviations of the effective back radiation. October 1951-1957. (cal/cm^2/day)

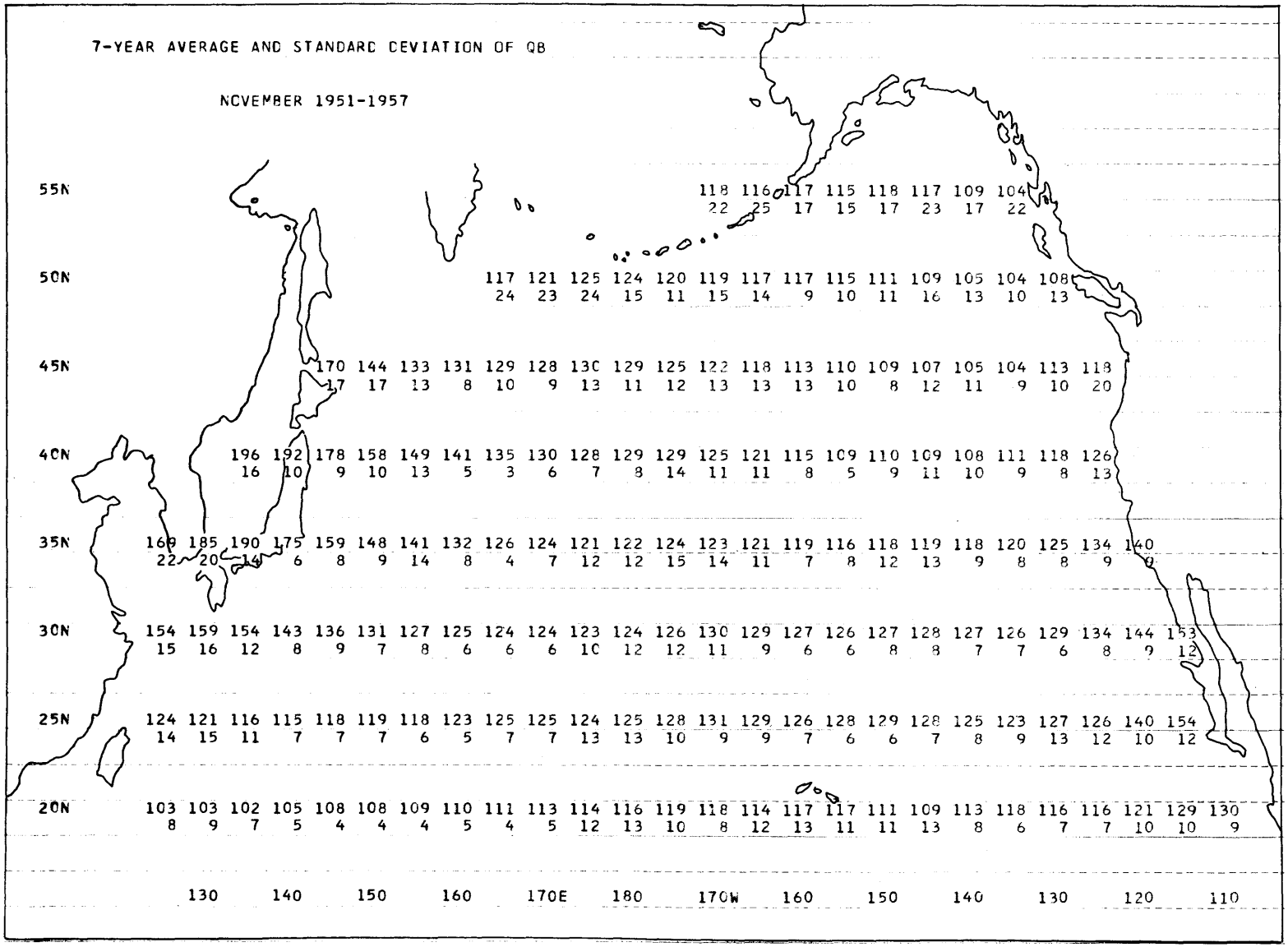

Figure A34. 7-year average values and standard deviations of the effective back radiation. November 1951-1957. (cal/cm^2/day)

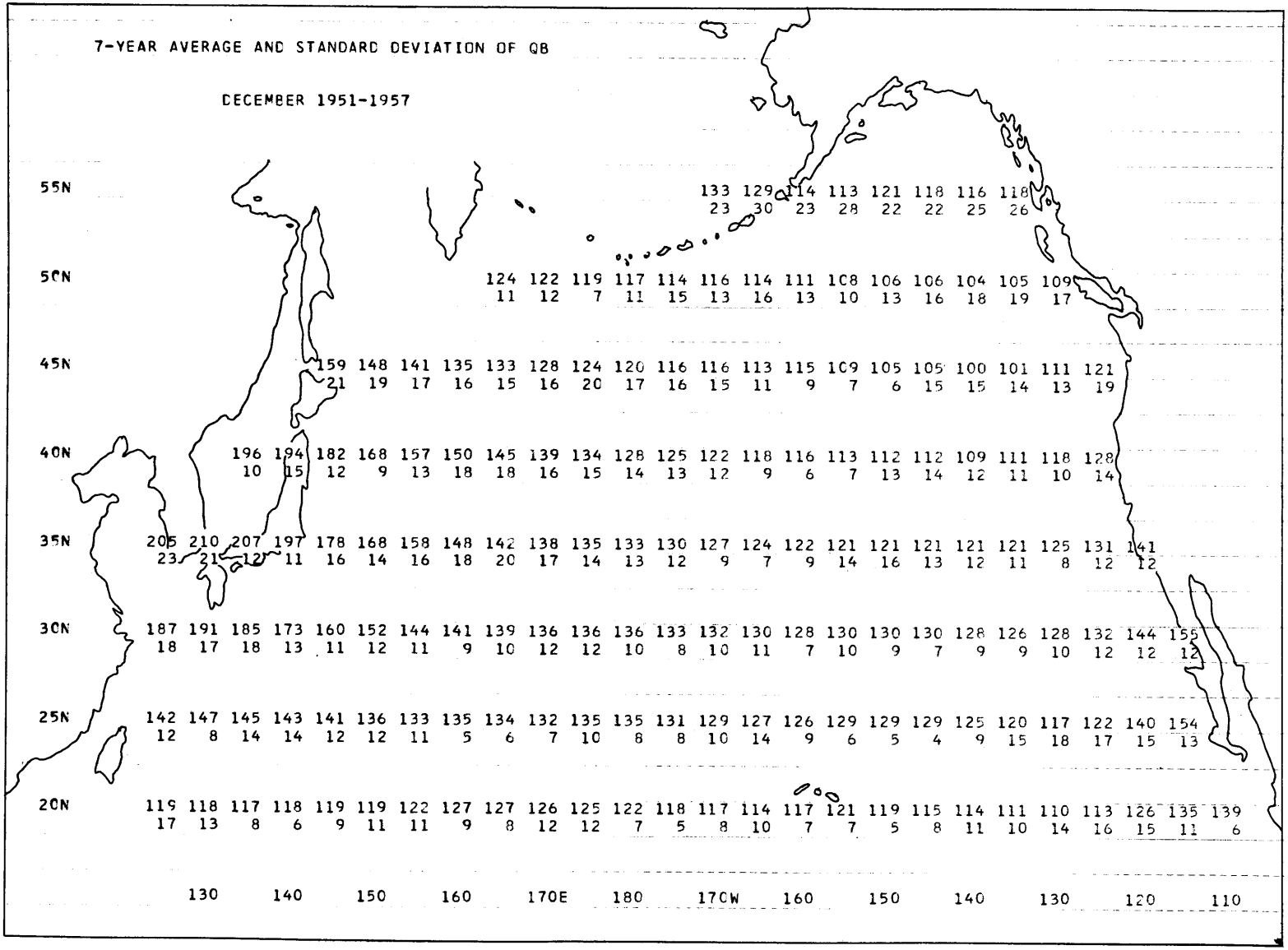

Figure A35. 7-year average values and standard deviations of the effective back radiation. December 1951-1957. (cal/cm^2/day)

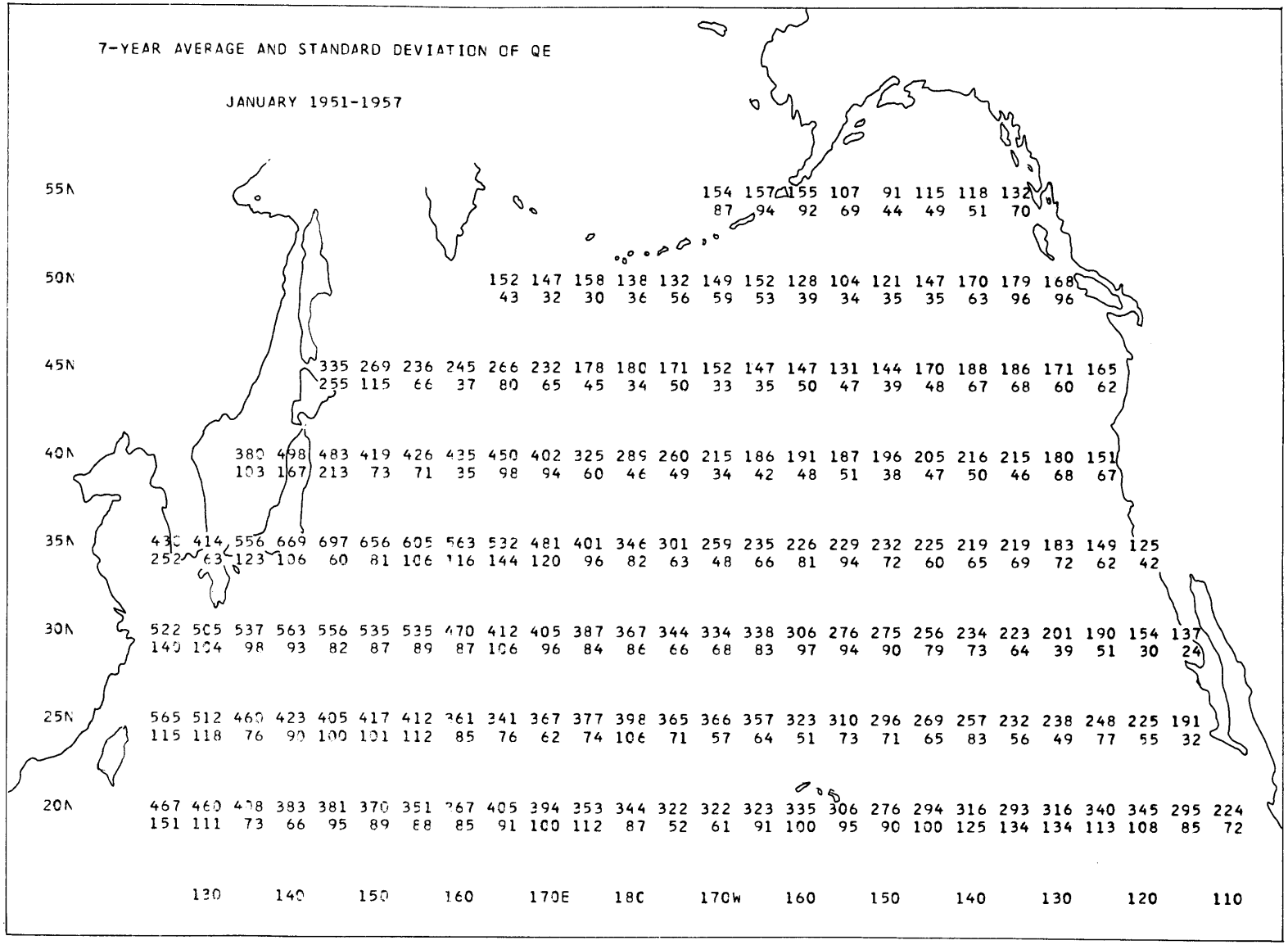

Figure A36. 7-year average values and standard deviations of the latent heat transfer. January 1951-1957. (cal/cm^2/day)

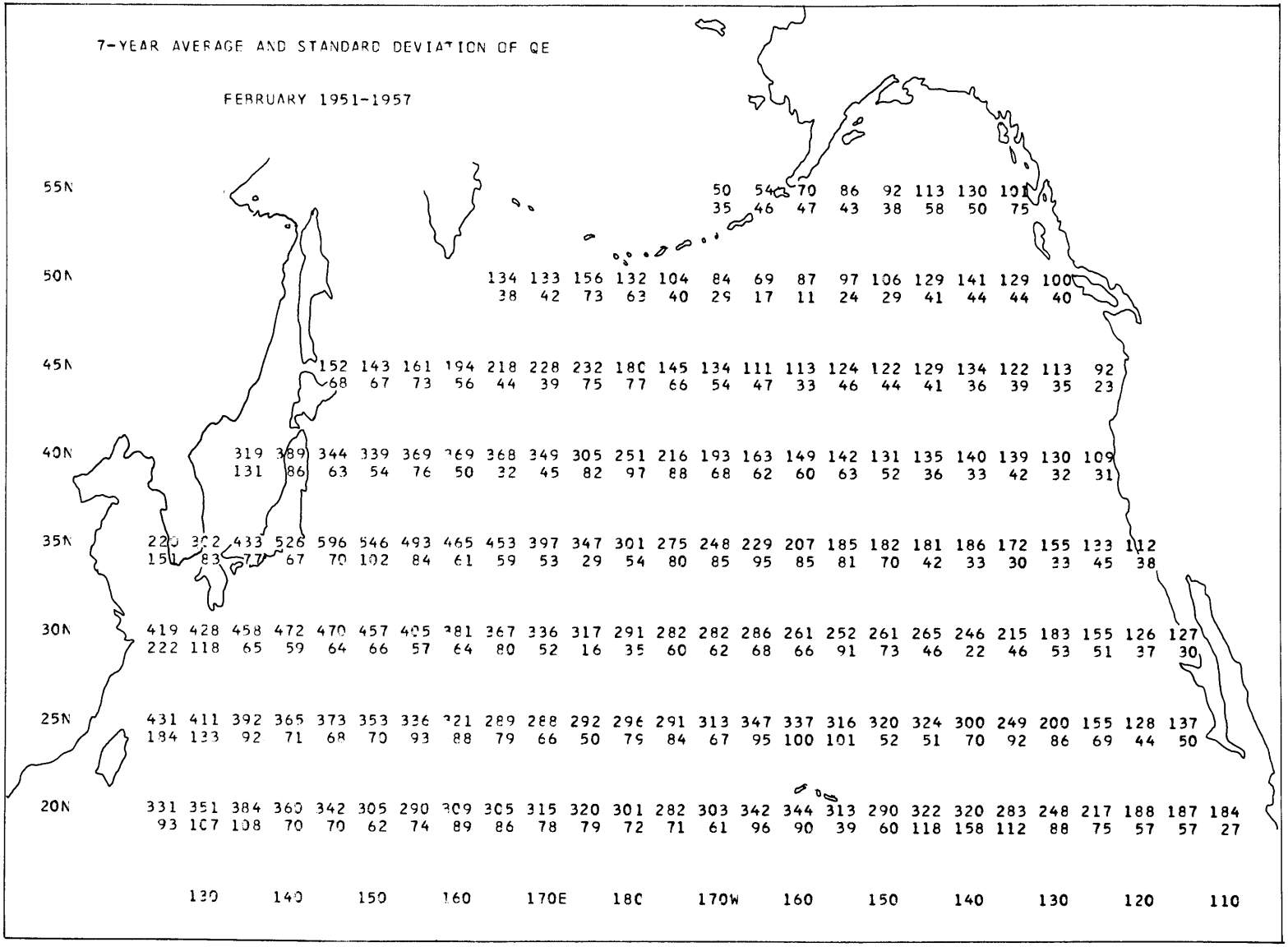

Figure A37. 7-year average values and standard deviations of the latent heat transfer. February 1951-1957. (cal/cm^2/day)

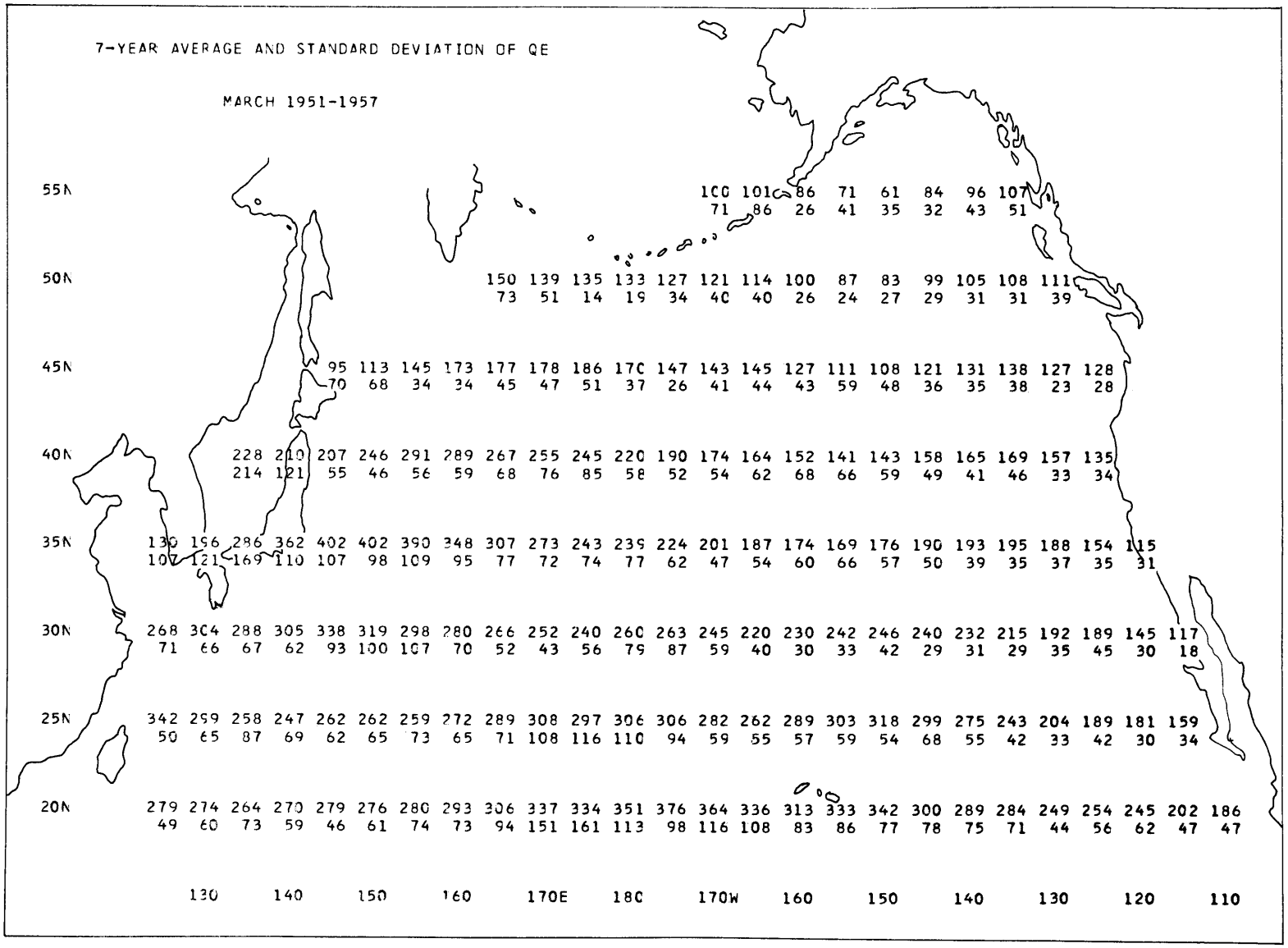

Figure A38. 7-year average values and standard deviations of the latent heat transfer. March 1951-1957. (cal/cm^2/day)

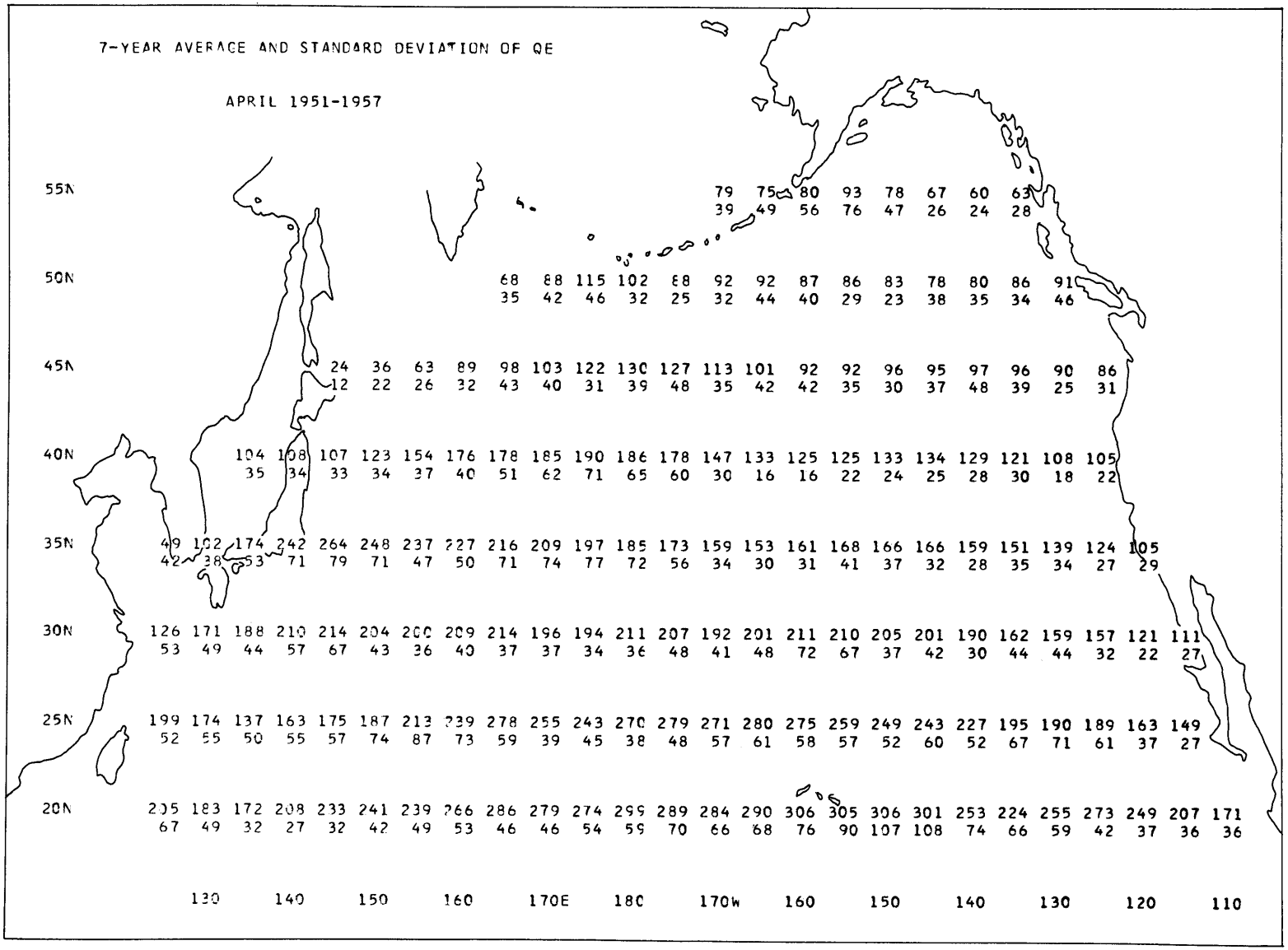

Figure A39. 7-year average values and standard deviations of the latent heat transfer. April 1951-1957. (cal/cm^2/day)

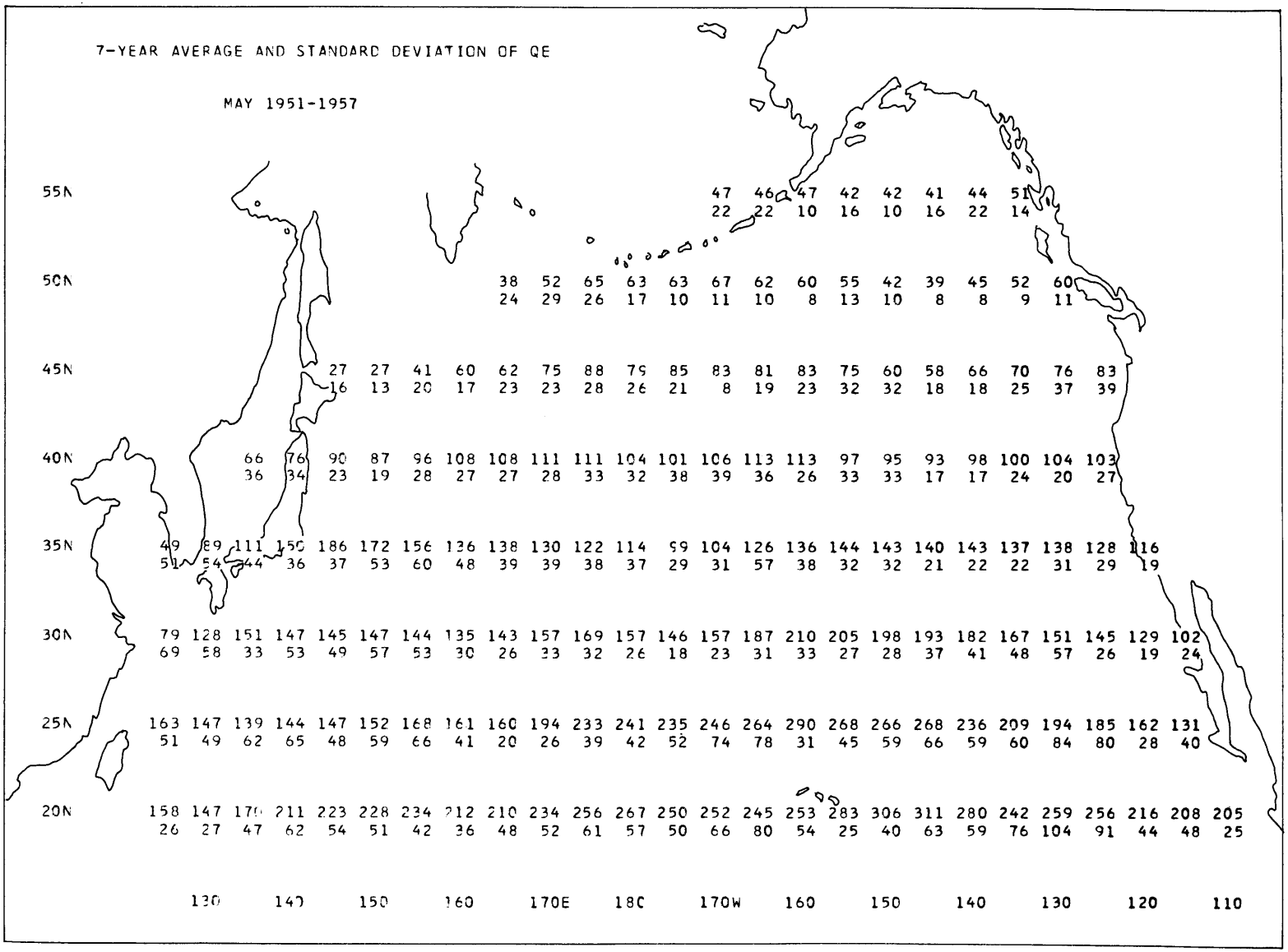

Figure A40. 7-year average values and standard deviations of the latent heat transfer. May 1951-1957. (cal/cm^2/day)

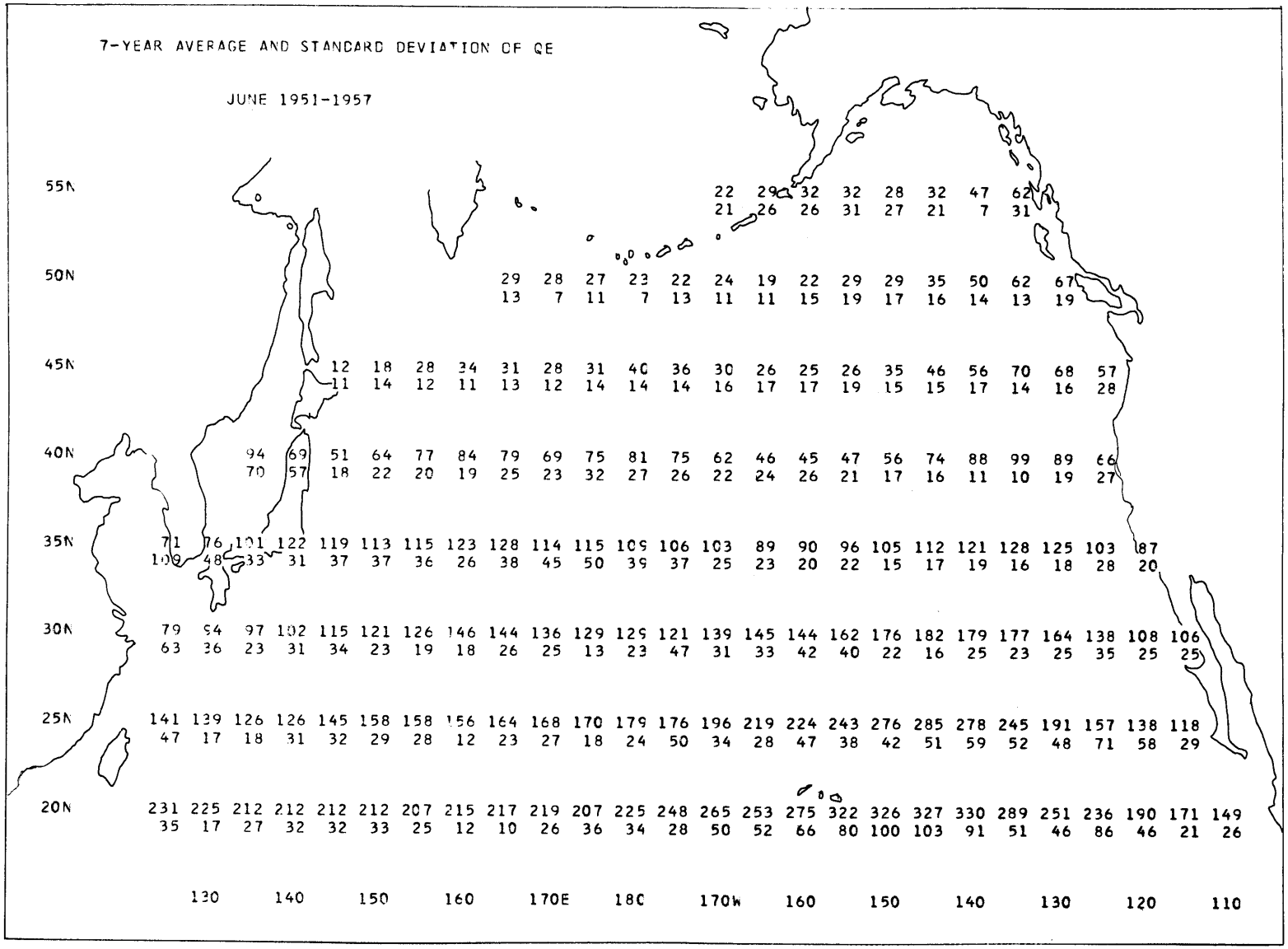

Figure A41. 7-year average values and standard deviations of the latent heat transfer. June 1951-1957. (cal/cm^2/day)

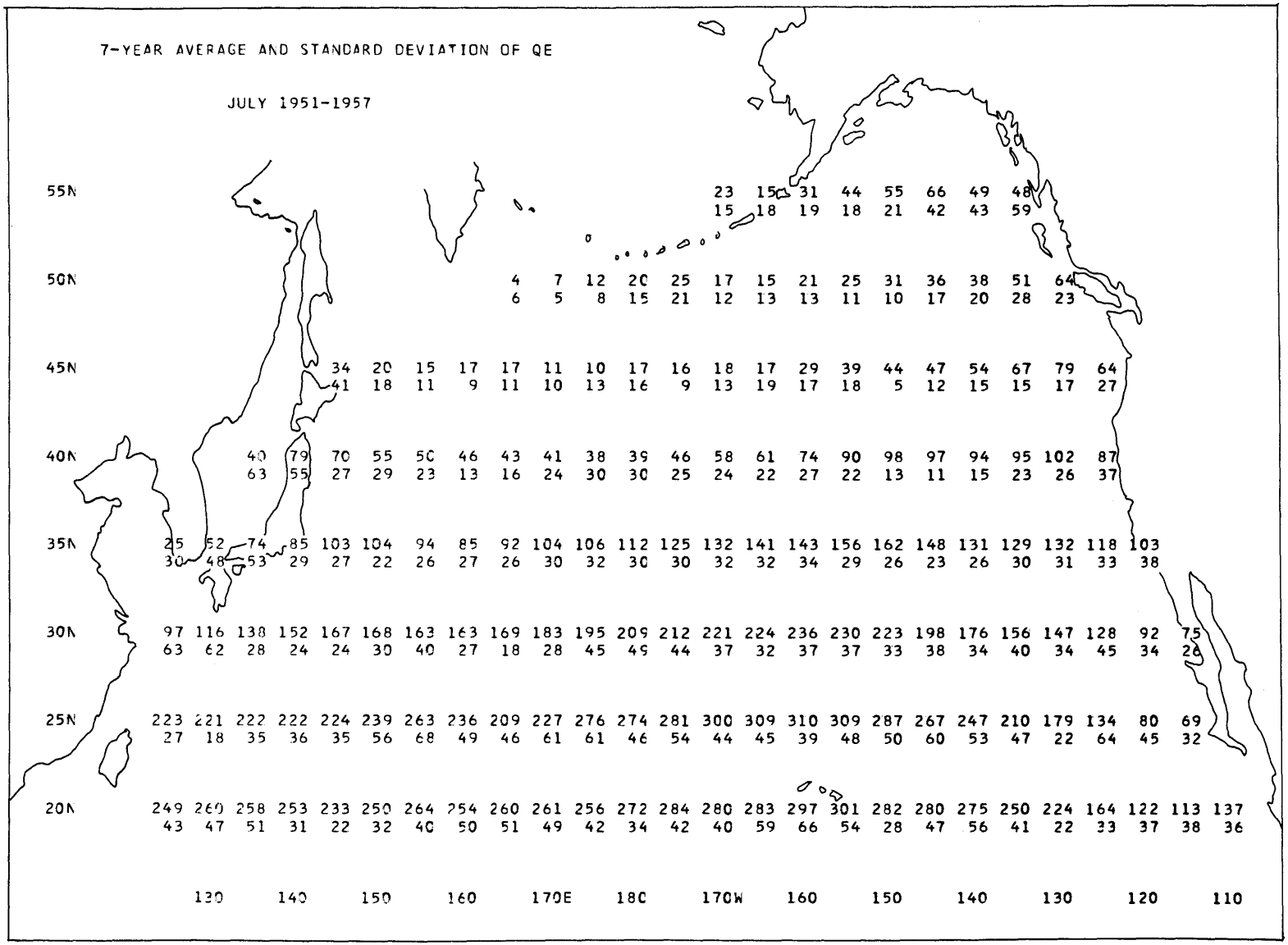

Figure A42. 7-year average values and standard deviations of the latent heat transfer. July 1951-1957. (cal/cm^2/day)

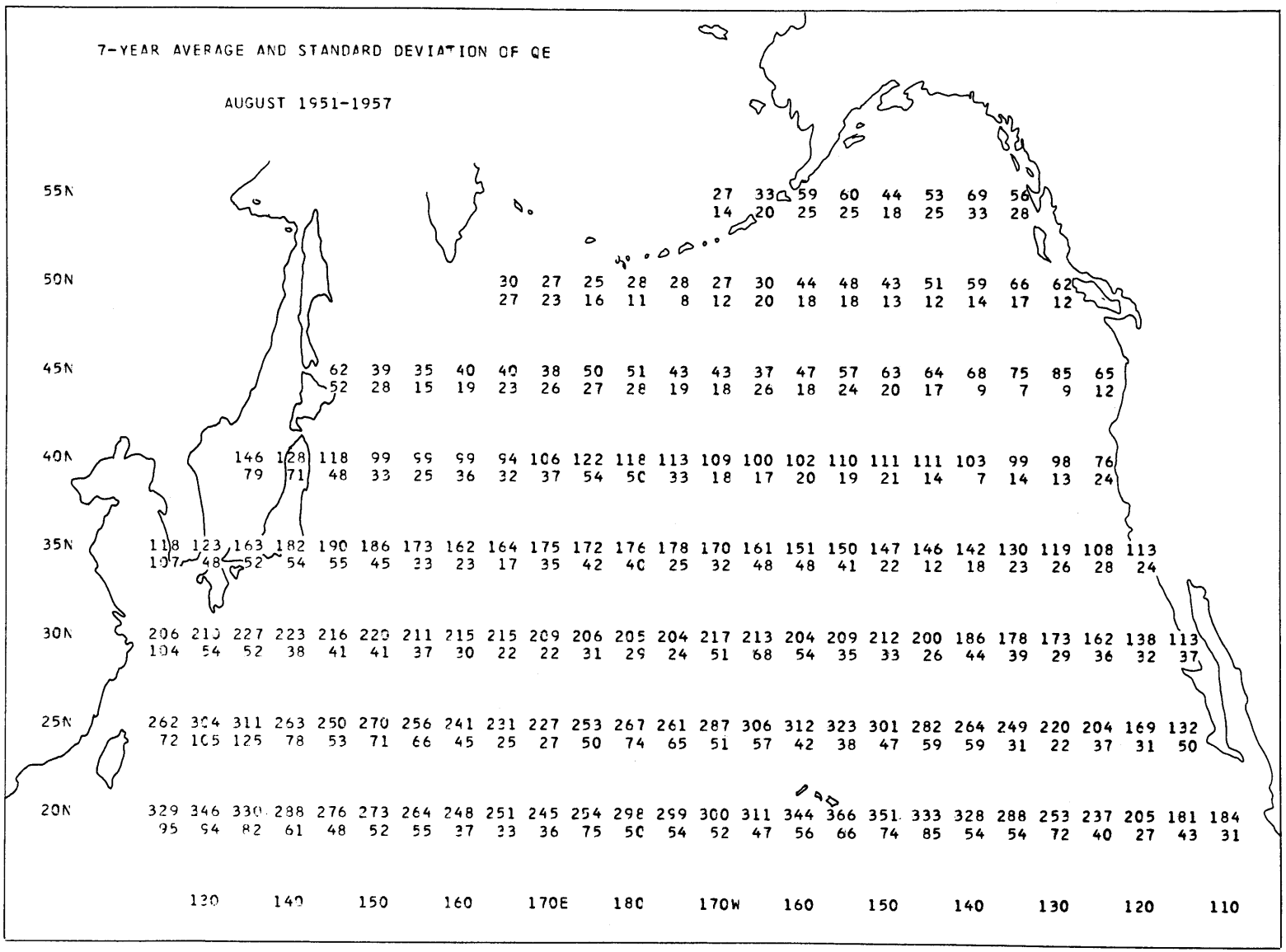

Figure A43. 7-year average values and standard deviations of the latent heat transfer. August 1951-1957. (cal/cm^2/day)

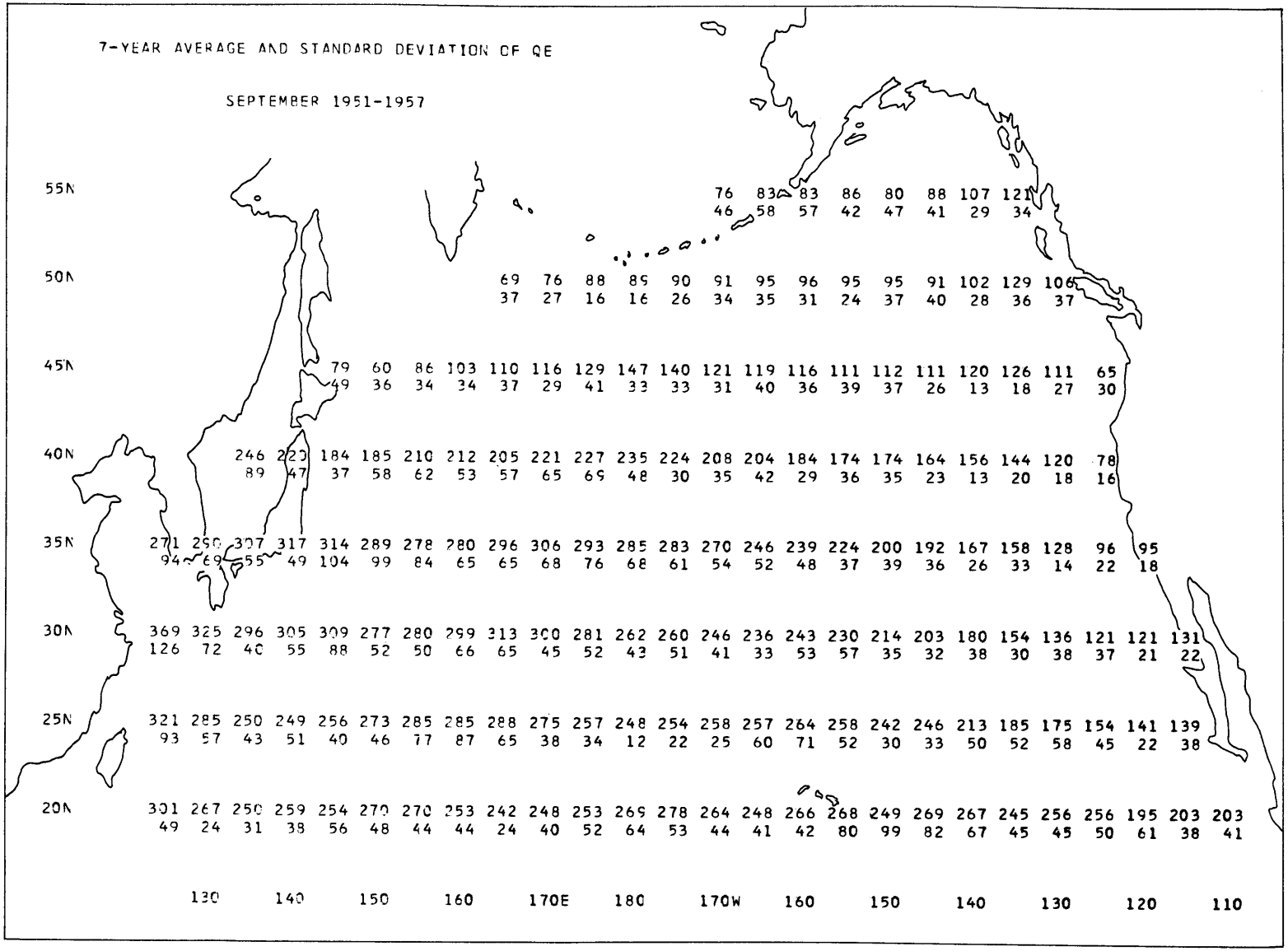

Figure A44. 7-year average values and standard deviations of the latent heat transfer. September 1951-1957. (cal/cm^2/day)

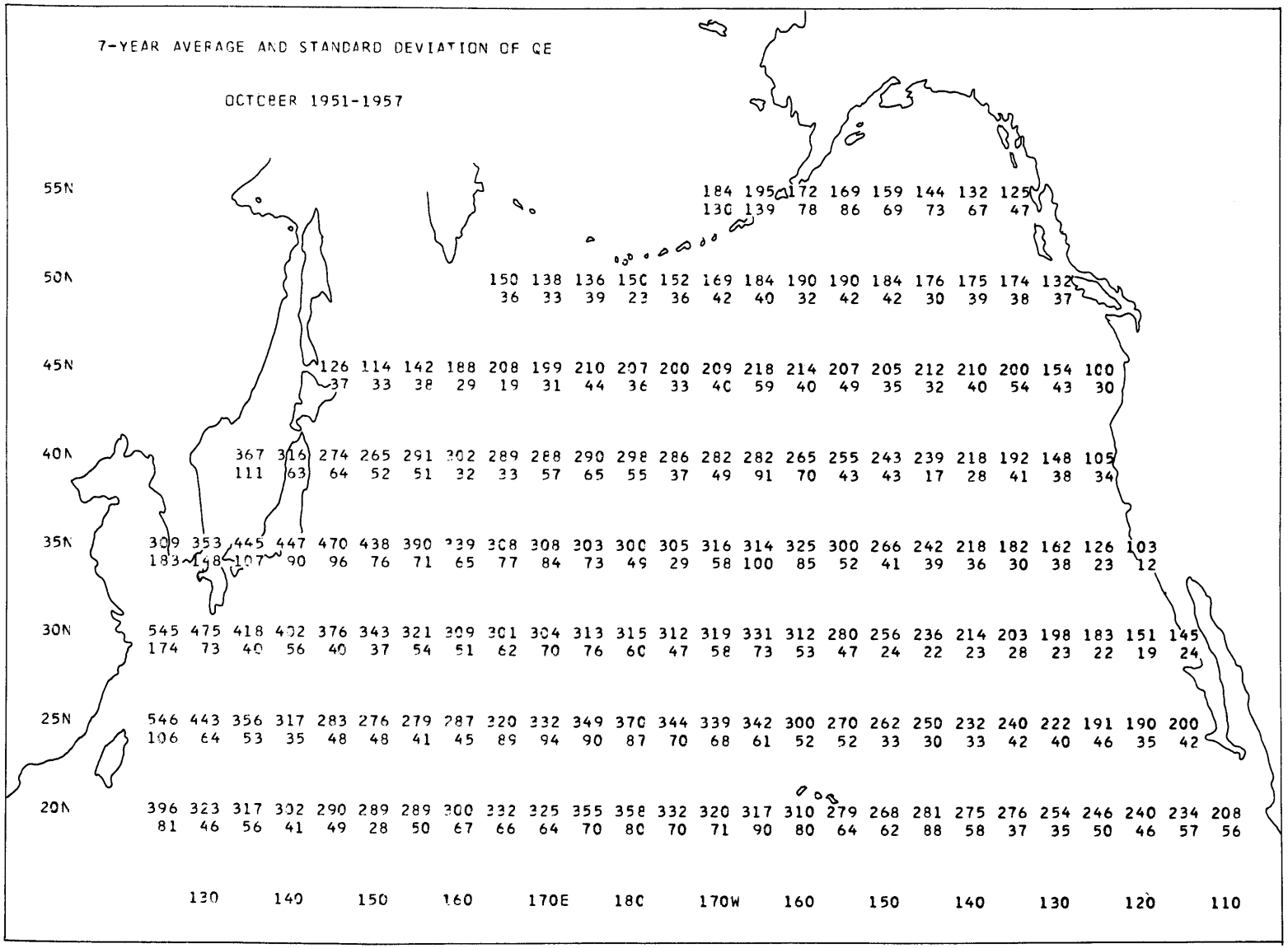

Figure A45. 7-year average values and standard deviations of the latent heat transfer. October 1951-1957. (cal/cm^2/day)

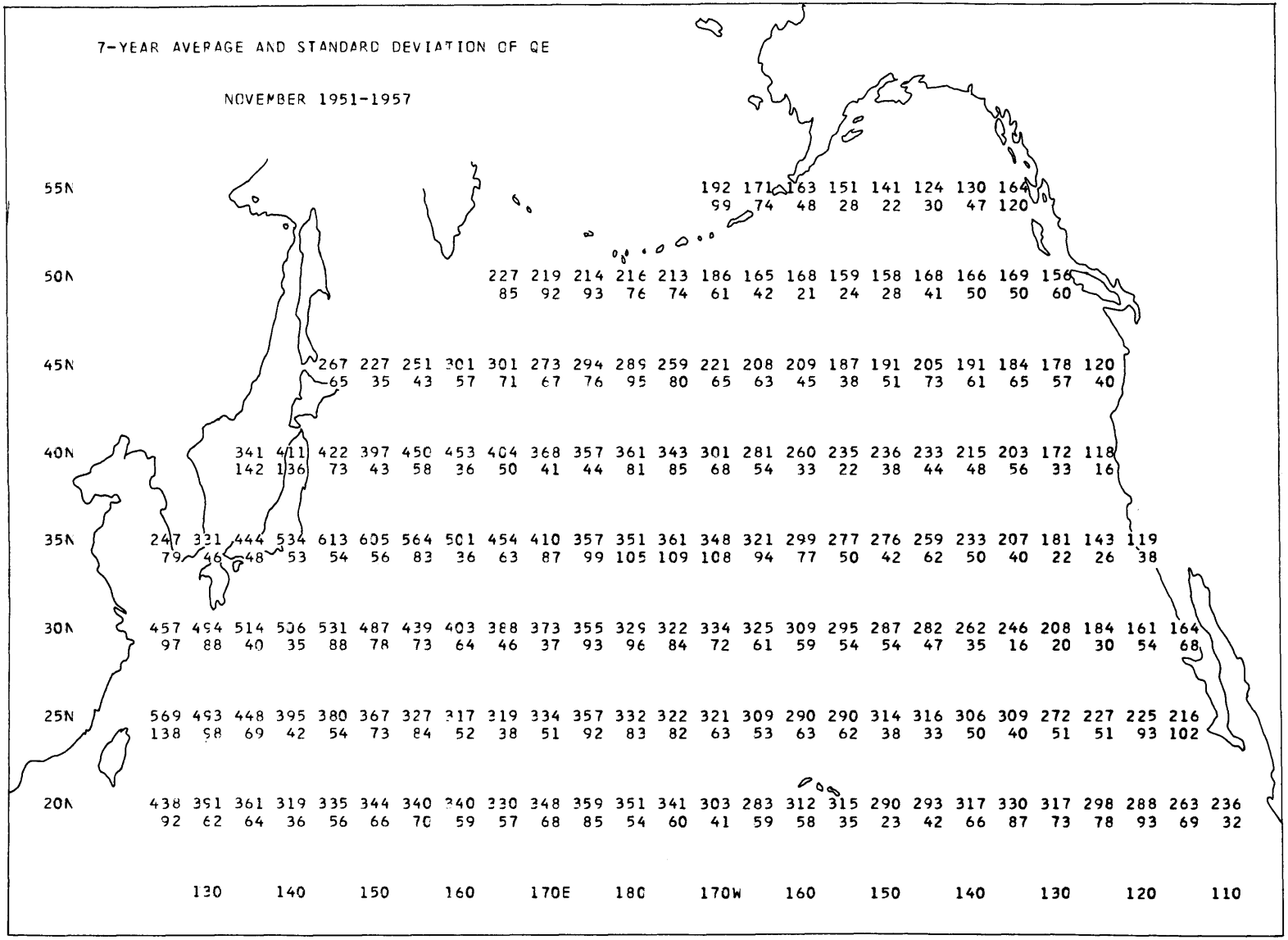

Figure A46. 7-year average values and standard deviations of the latent heat transfer. November 1951-1957. (cal/cm^2/day)

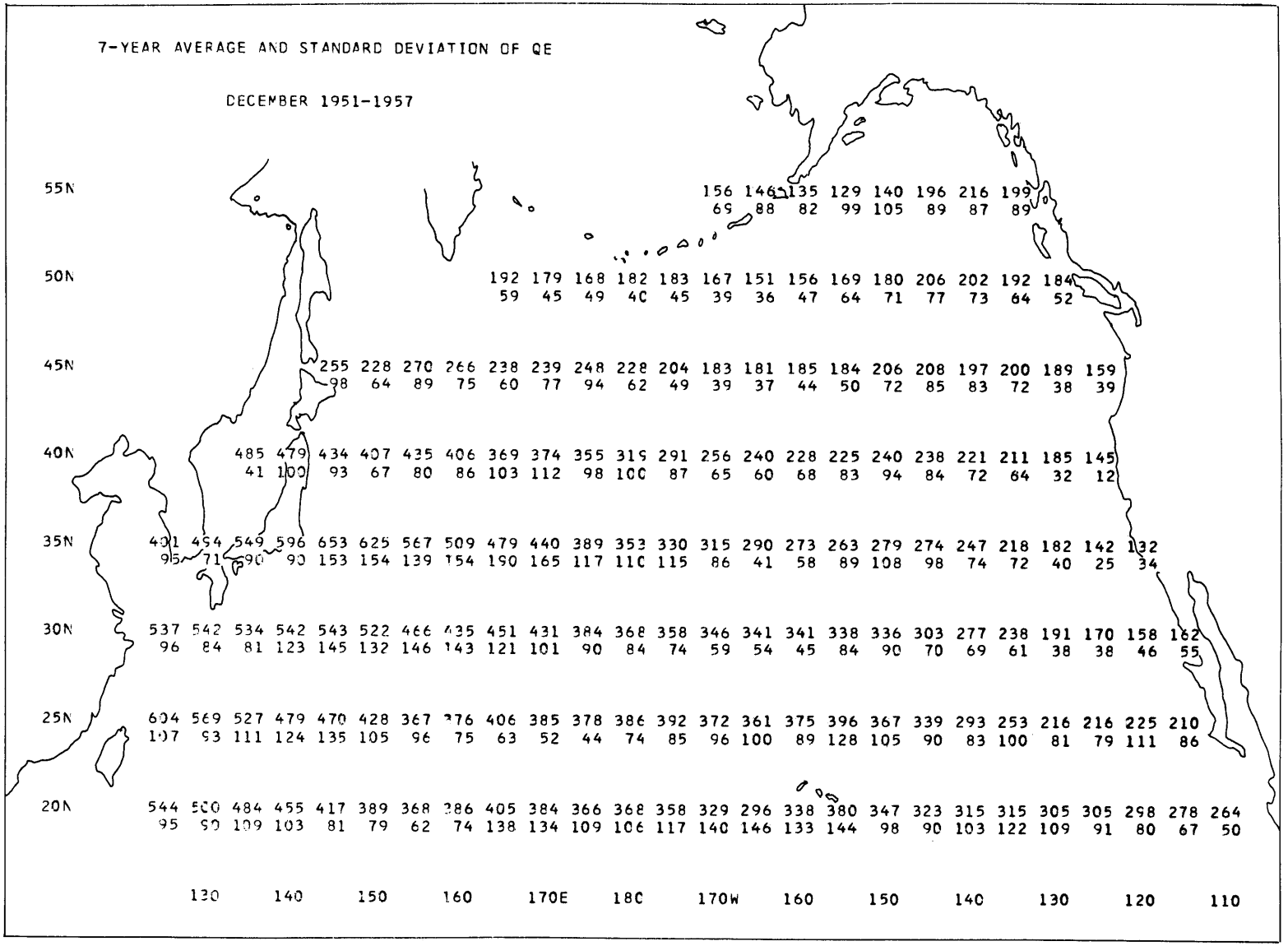

Figure A47. 7-year average values and standard deviations of the latent heat transfer. December 1951-1957. (cal/cm^2/day)

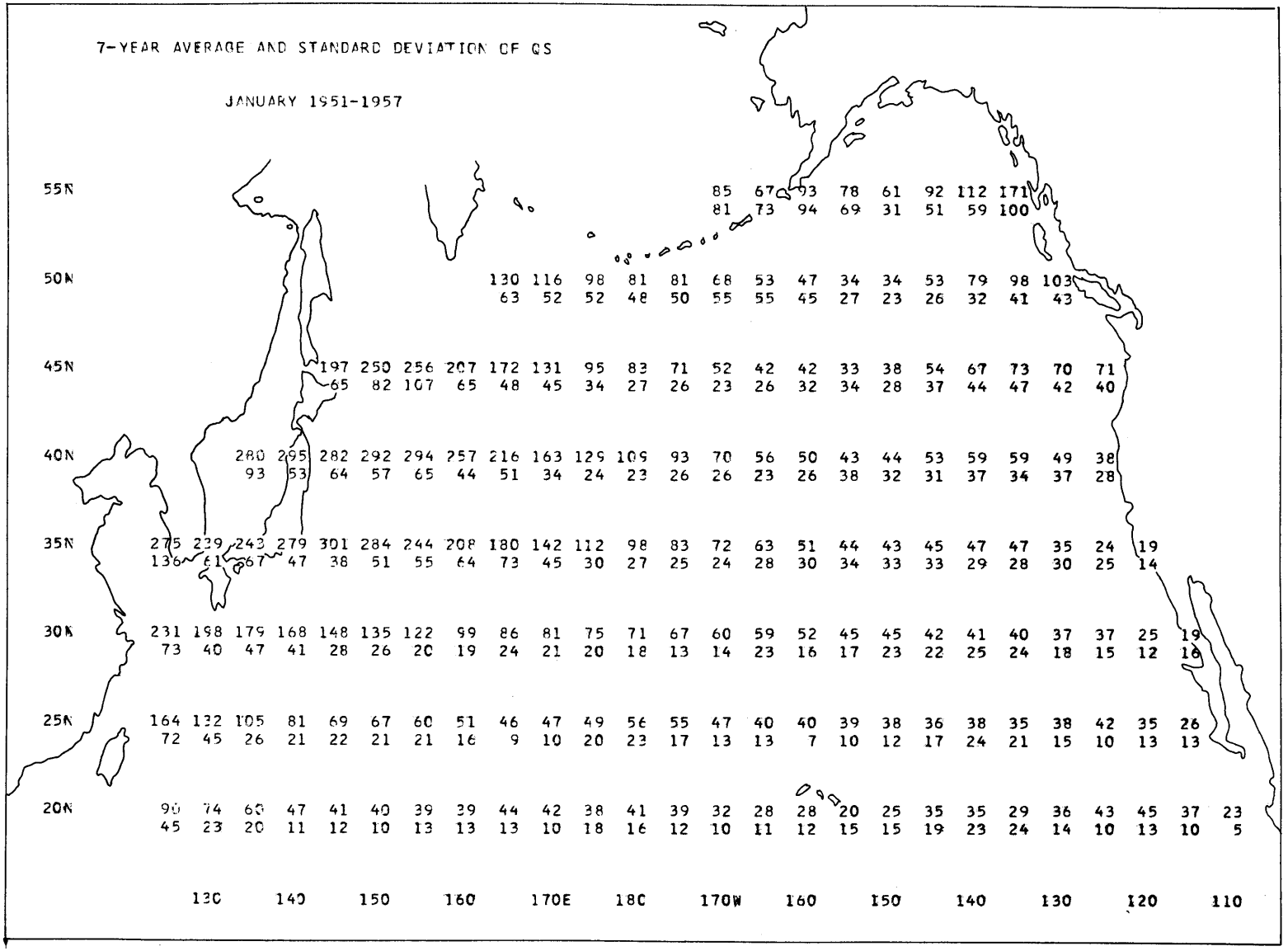

Figure A48. 7-year average values and standard deviations of the sensible heat transfer. January 1951-1957. (cal/cm^2/day)

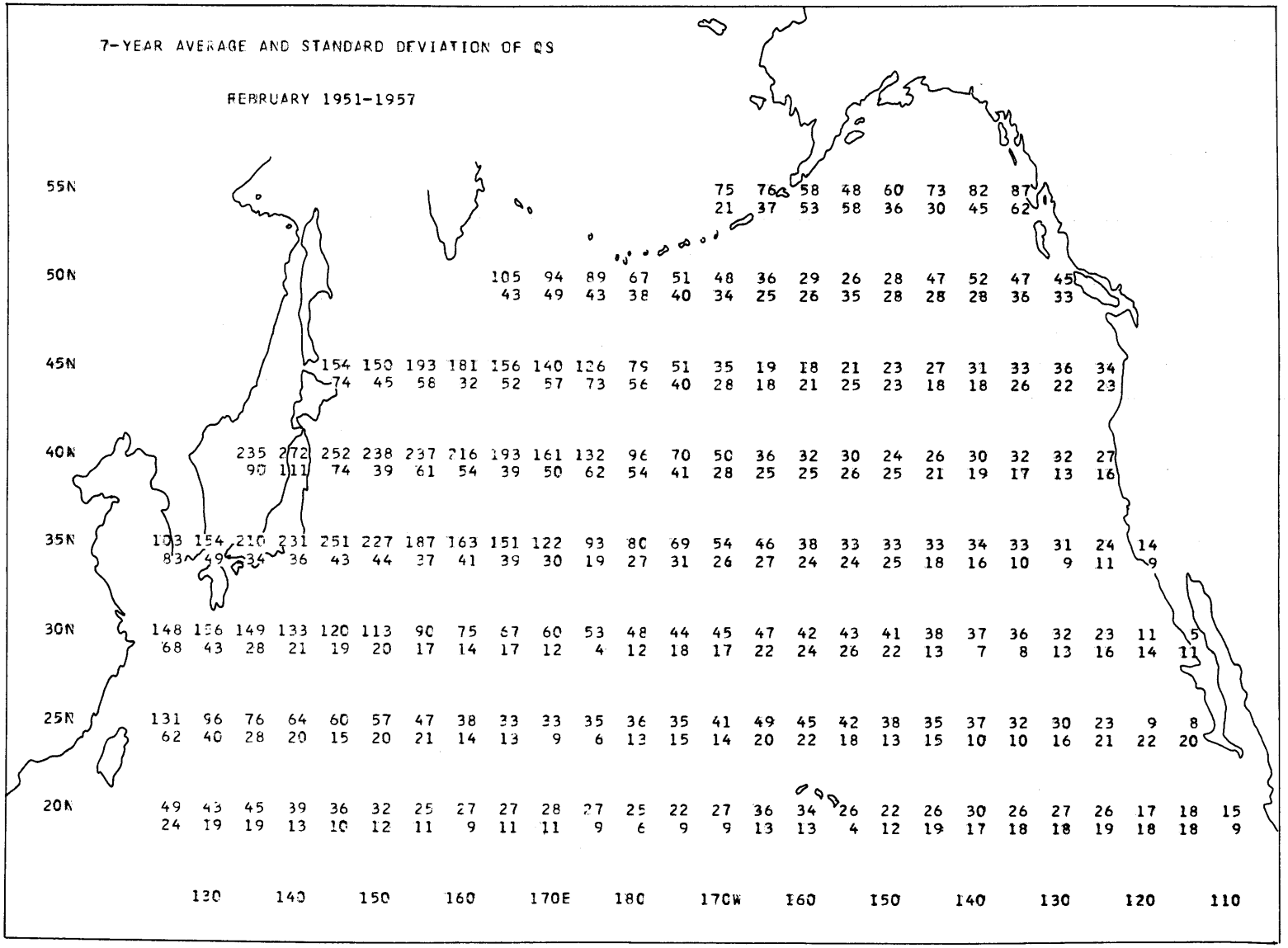

Figure A49. 7-year average values and standard deviations of the sensible heat transfer. February 1951-1957. (cal/cm^2/day)

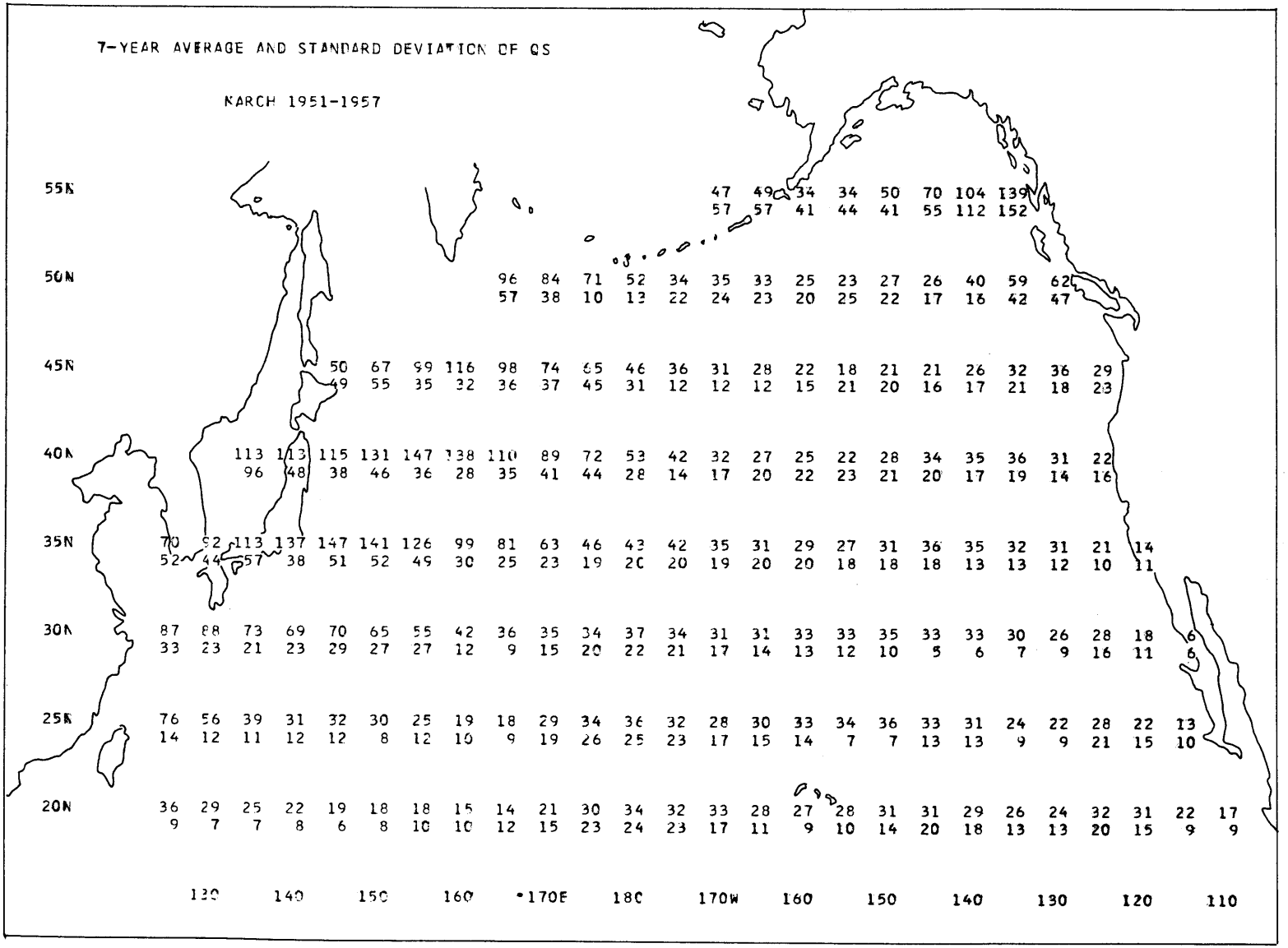

Figure A50. 7-year average values and standard deviations of the sensible heat transfer. March 1951-1957. (cal/cm^2/day)

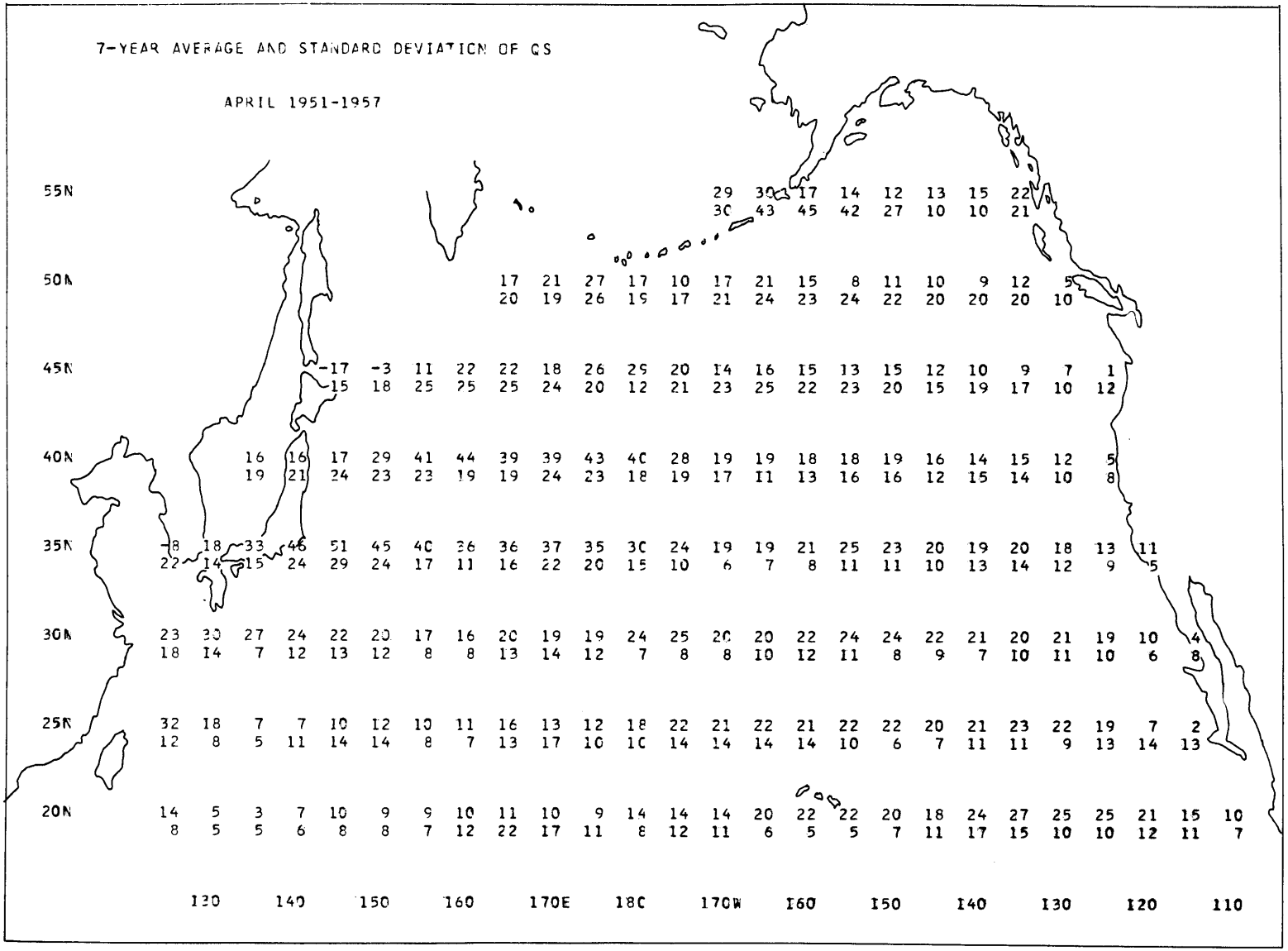

Figure A51. 7-year average values and standard deviations of the sensible heat transfer. April 1951-1957. (cal/cm^2/day)

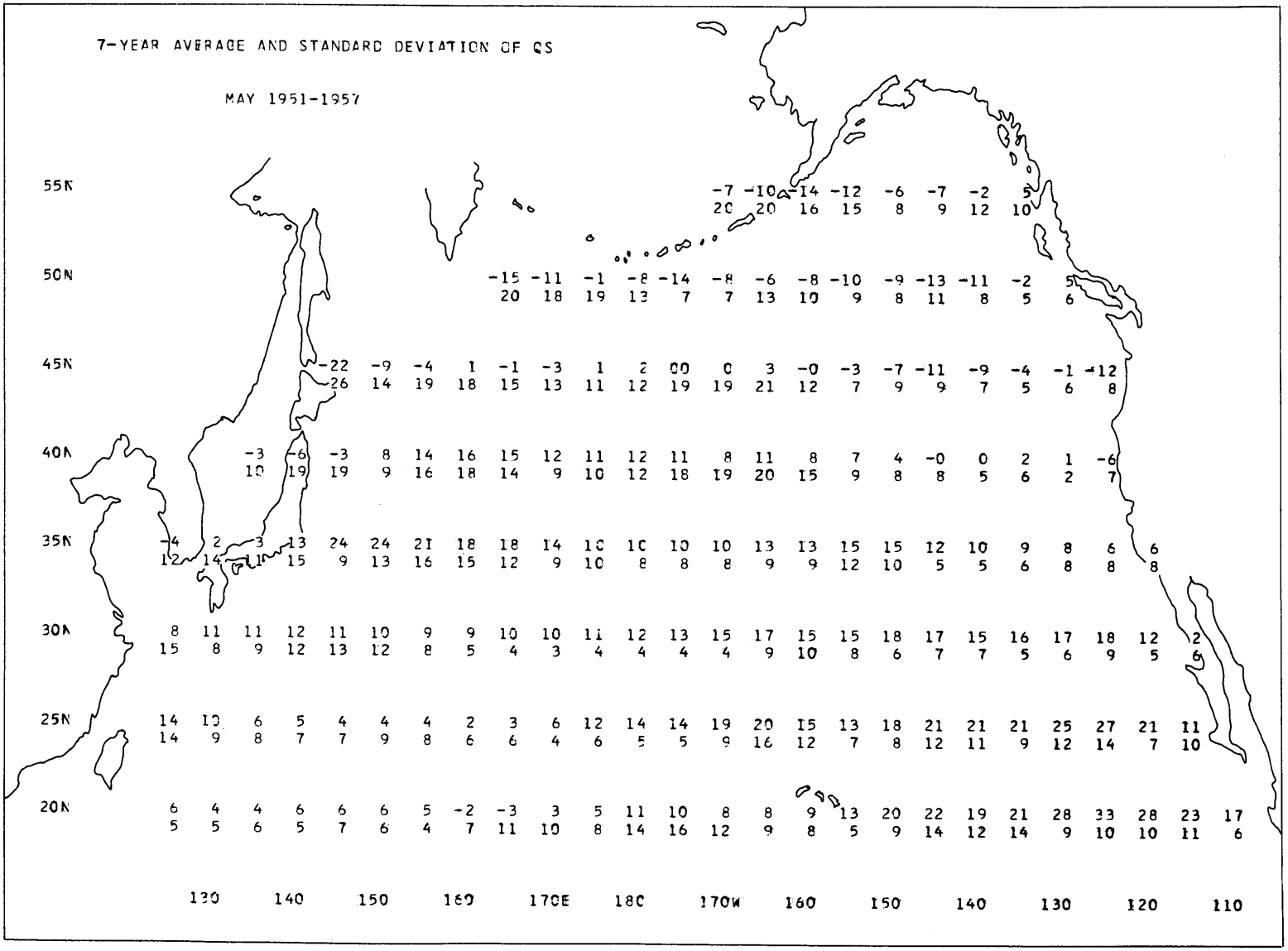

Figure A52. 7-year average values and standard deviations of the sensible heat transfer. May 1951-1957. (cal/cm^2/day)

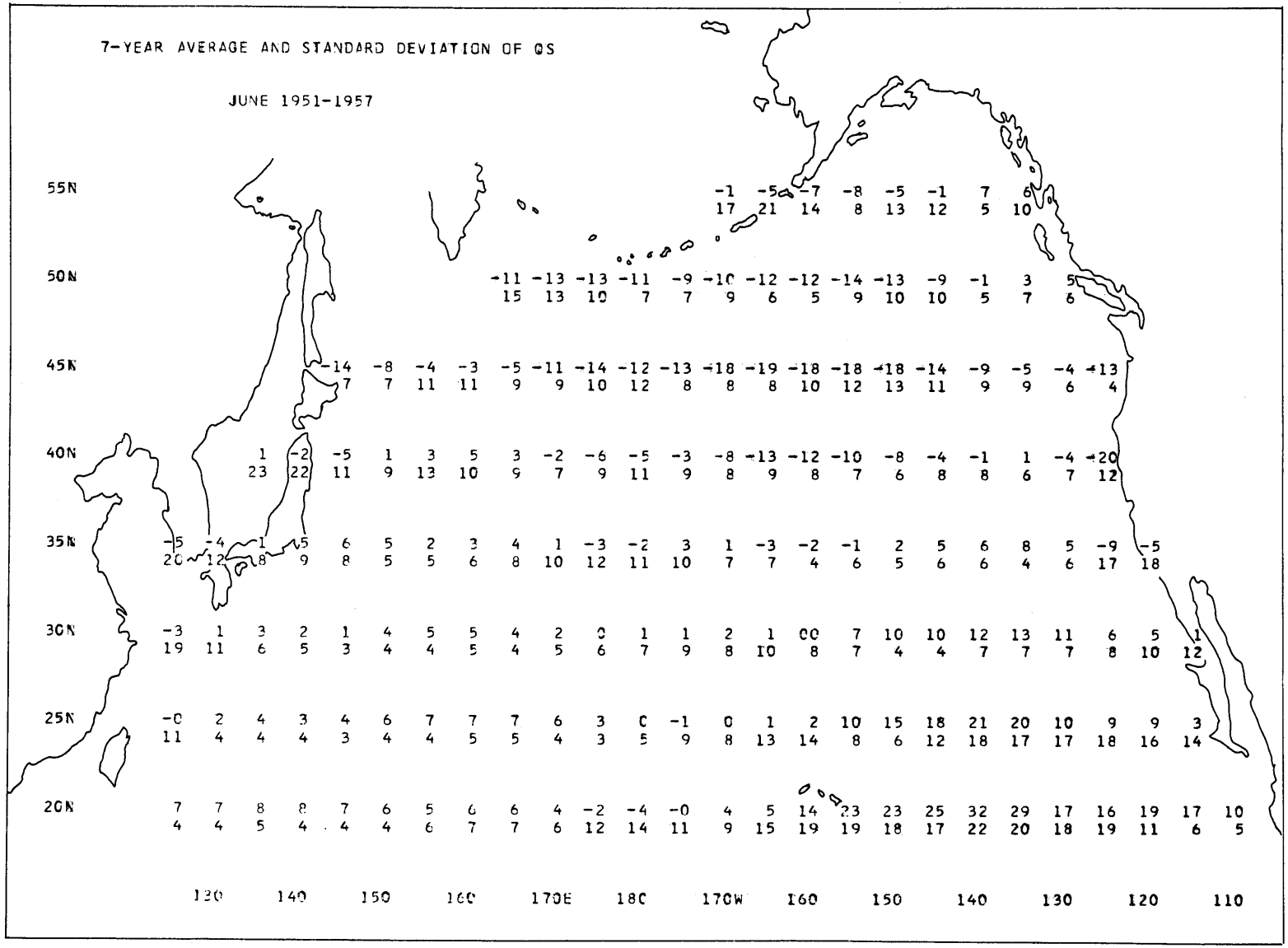

Figure A53. 7-year average values and standard deviations of the sensible heat transfer. June 1951-1957. (cal/cm^2/day)

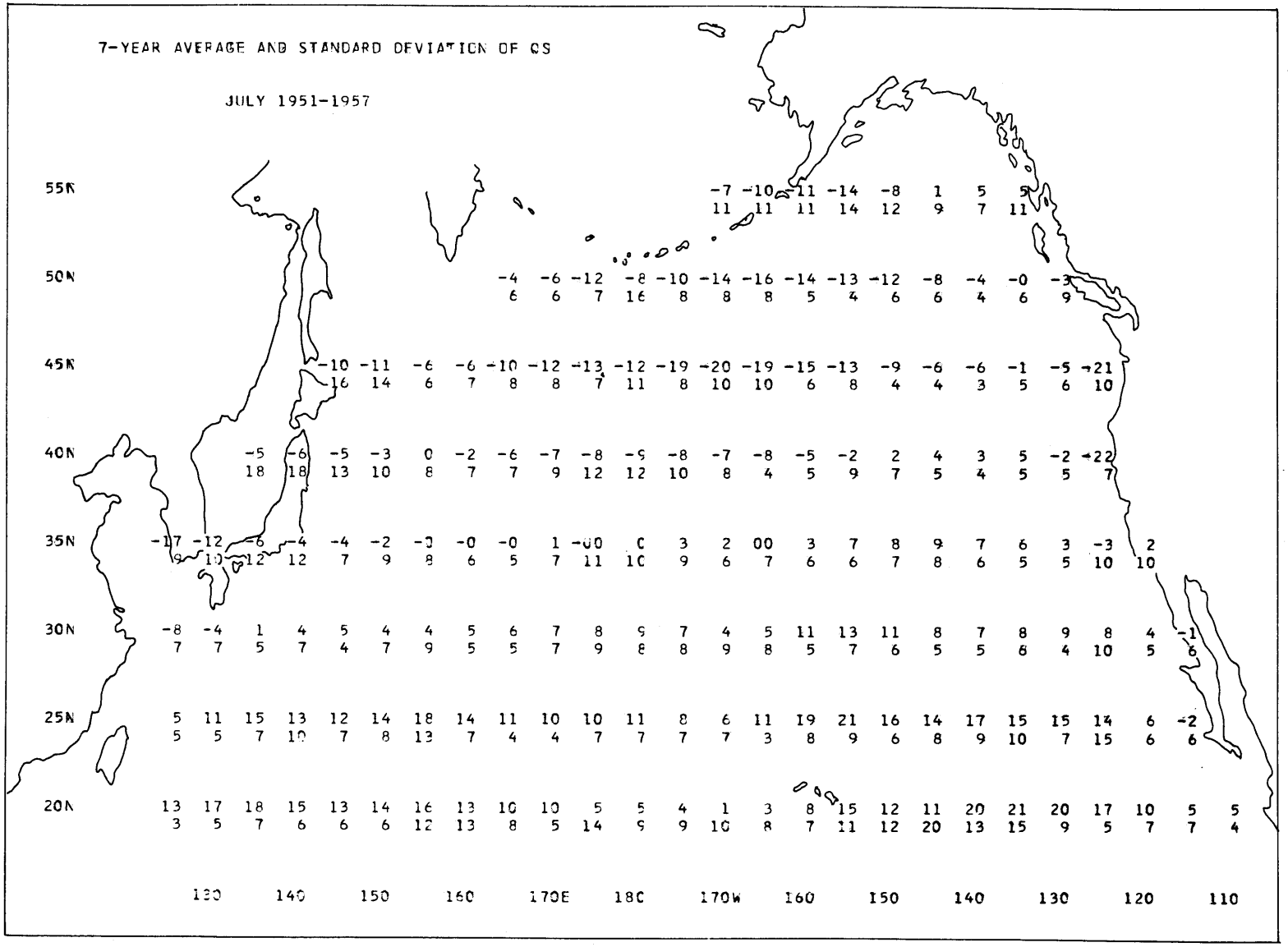

Figure A54. 7-year average values and standard deviations of the sensible heat transfer. July 1951-1957. (cal/cm^2/day)

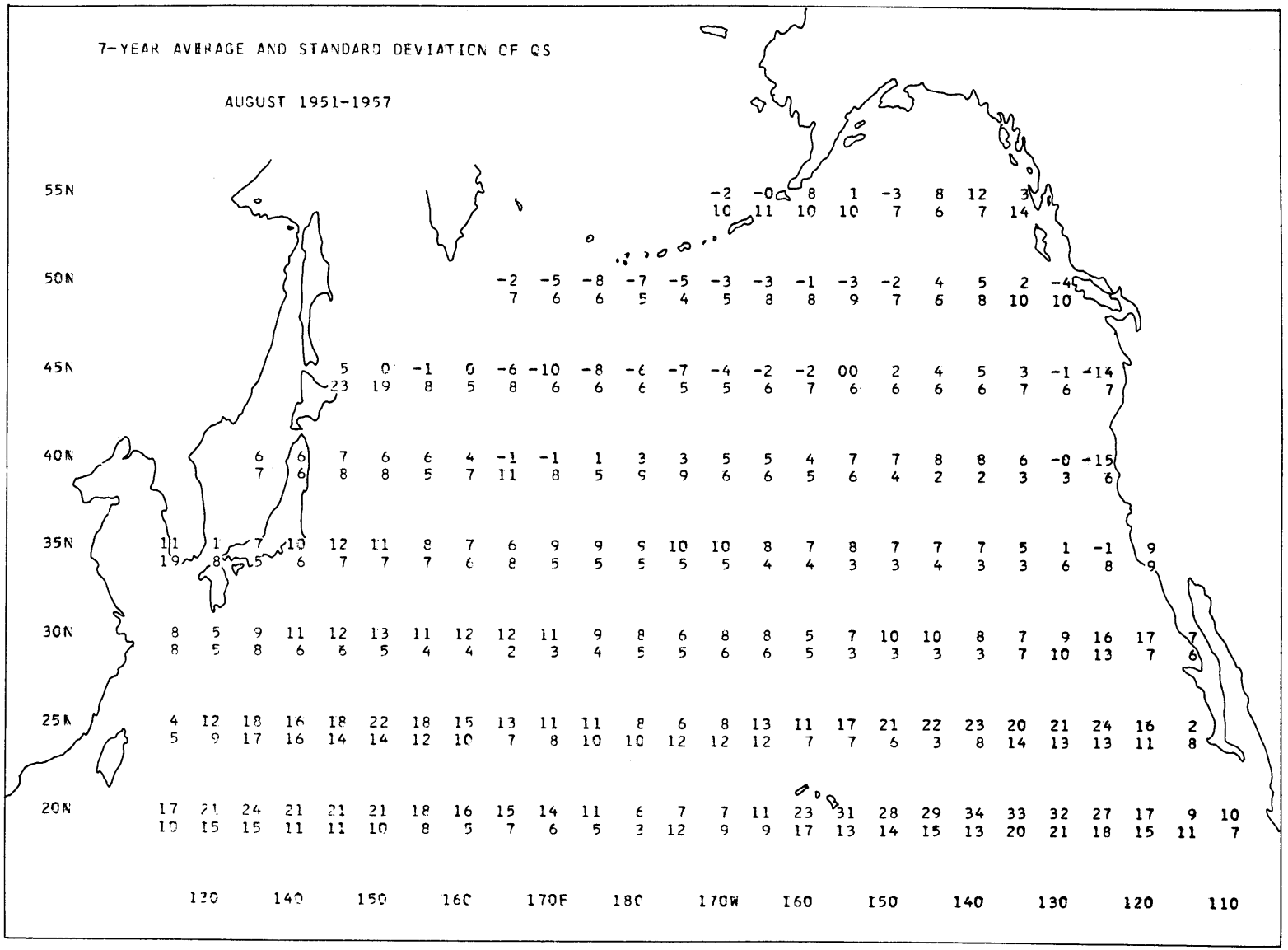

Figure A55. 7-year average values and standard deviations of the sensible heat transfer. August 1951-1957. (cal/cm^2/day)

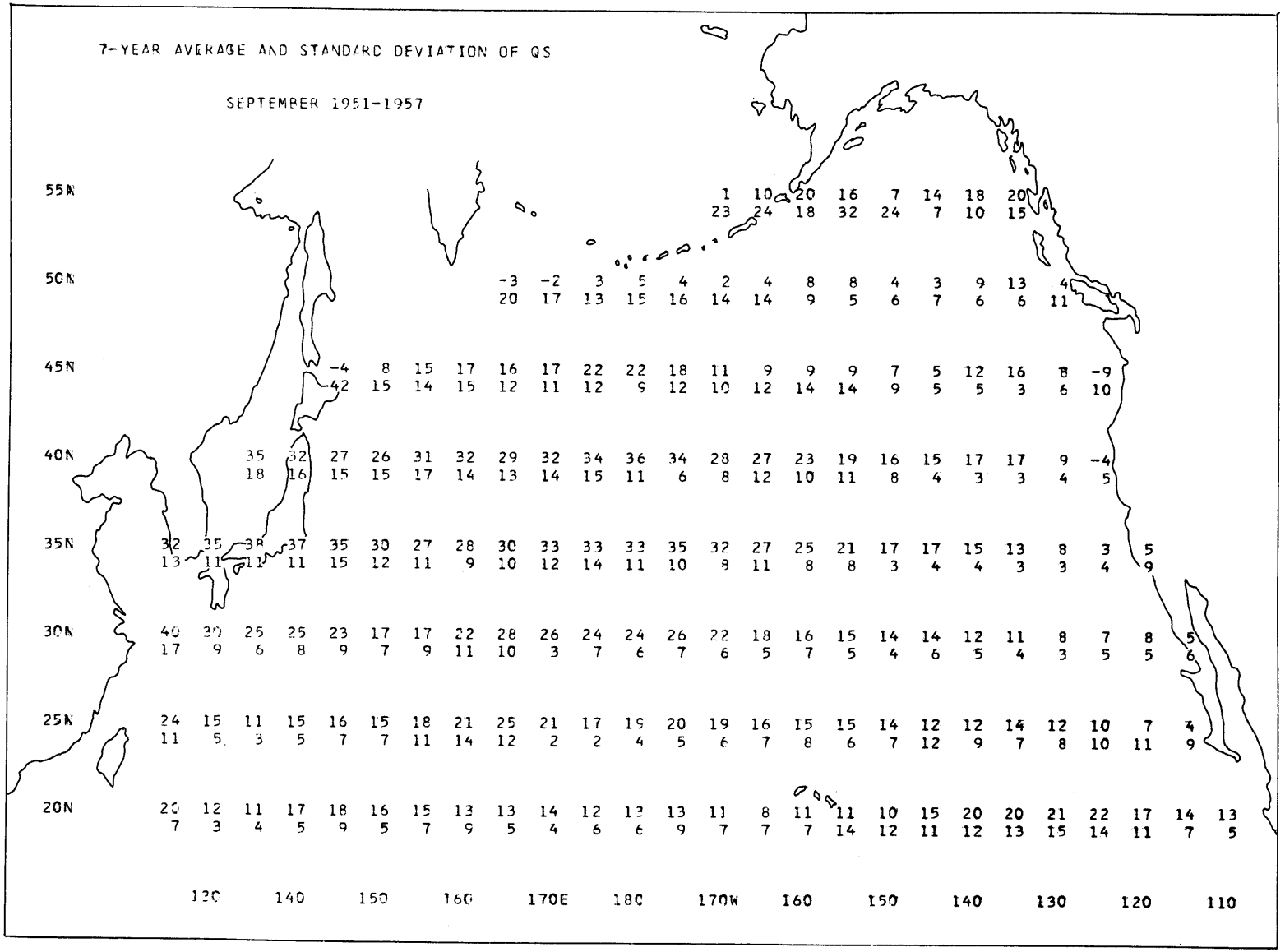

Figure A56. 7-year average values and standard deviations of the sensible heat transfer. September 1951-1957. (cal/cm^2/day)

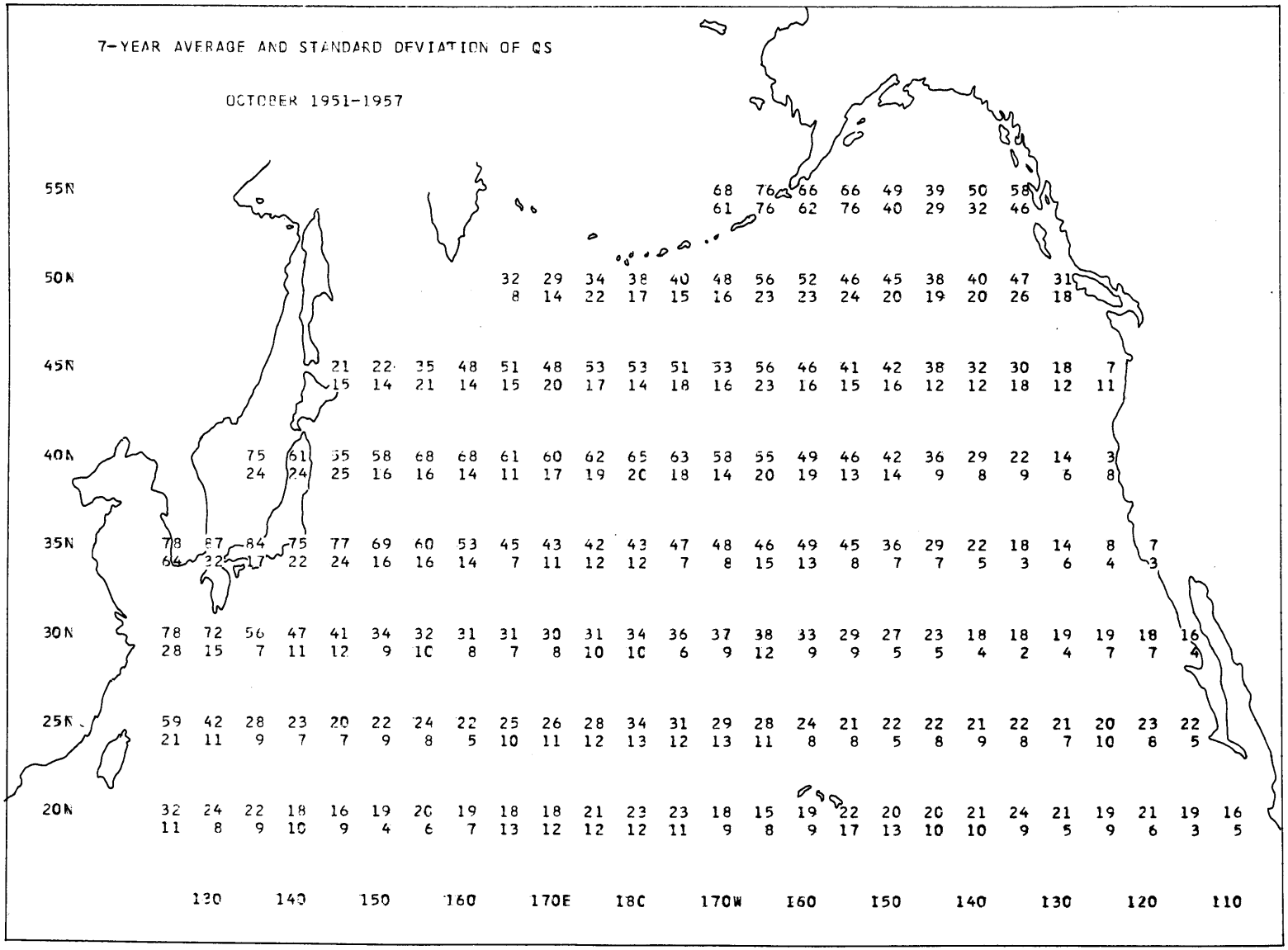

Figure A57. 7-year average values and standard deviations of the sensible heat transfer. October 1951-1957. (cal/cm^2/day)

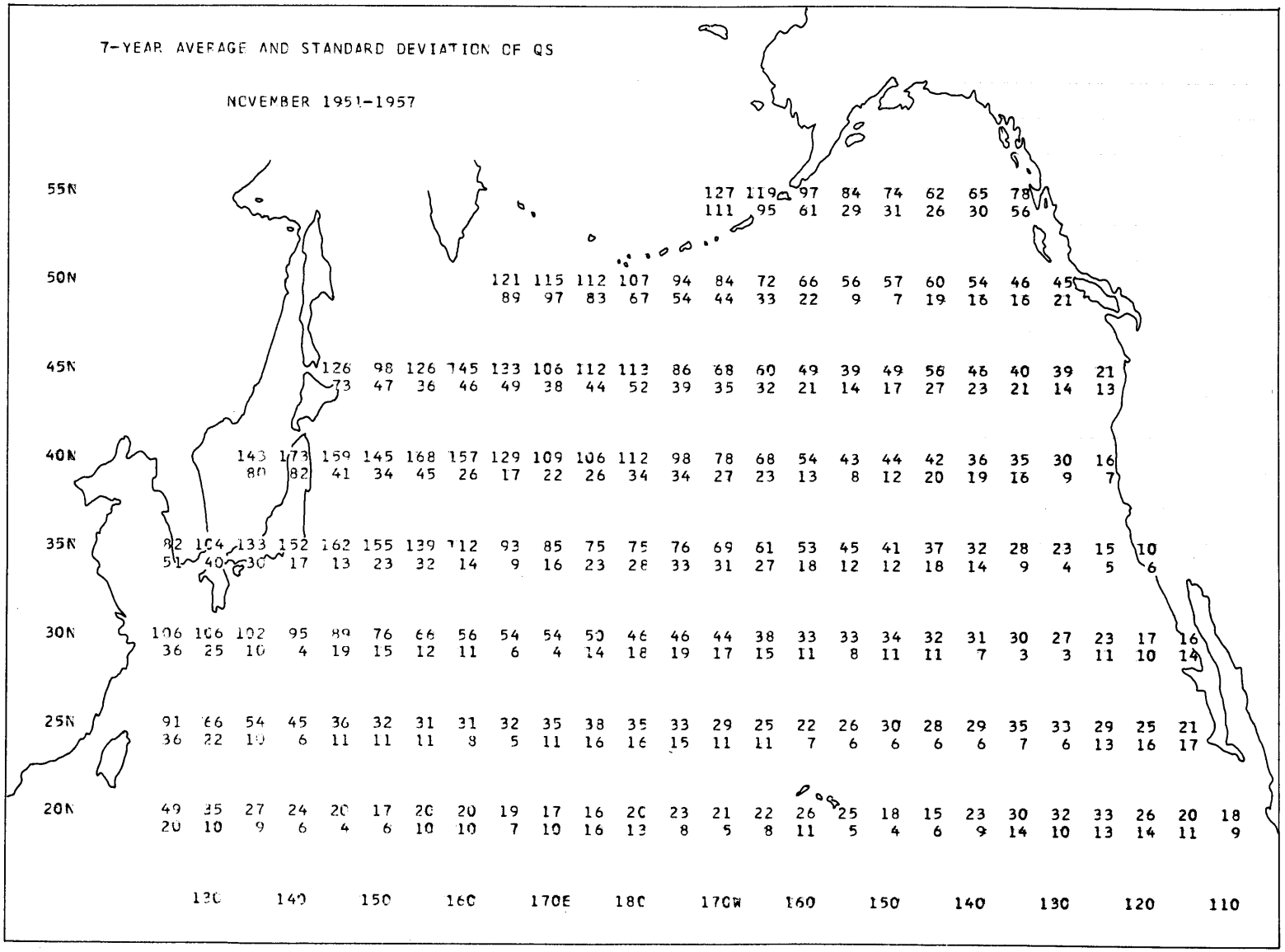

Figure A58. 7-year average values and standard deviations of the sensible heat transfer. November 1951-1957. (cal/cm^2/day)

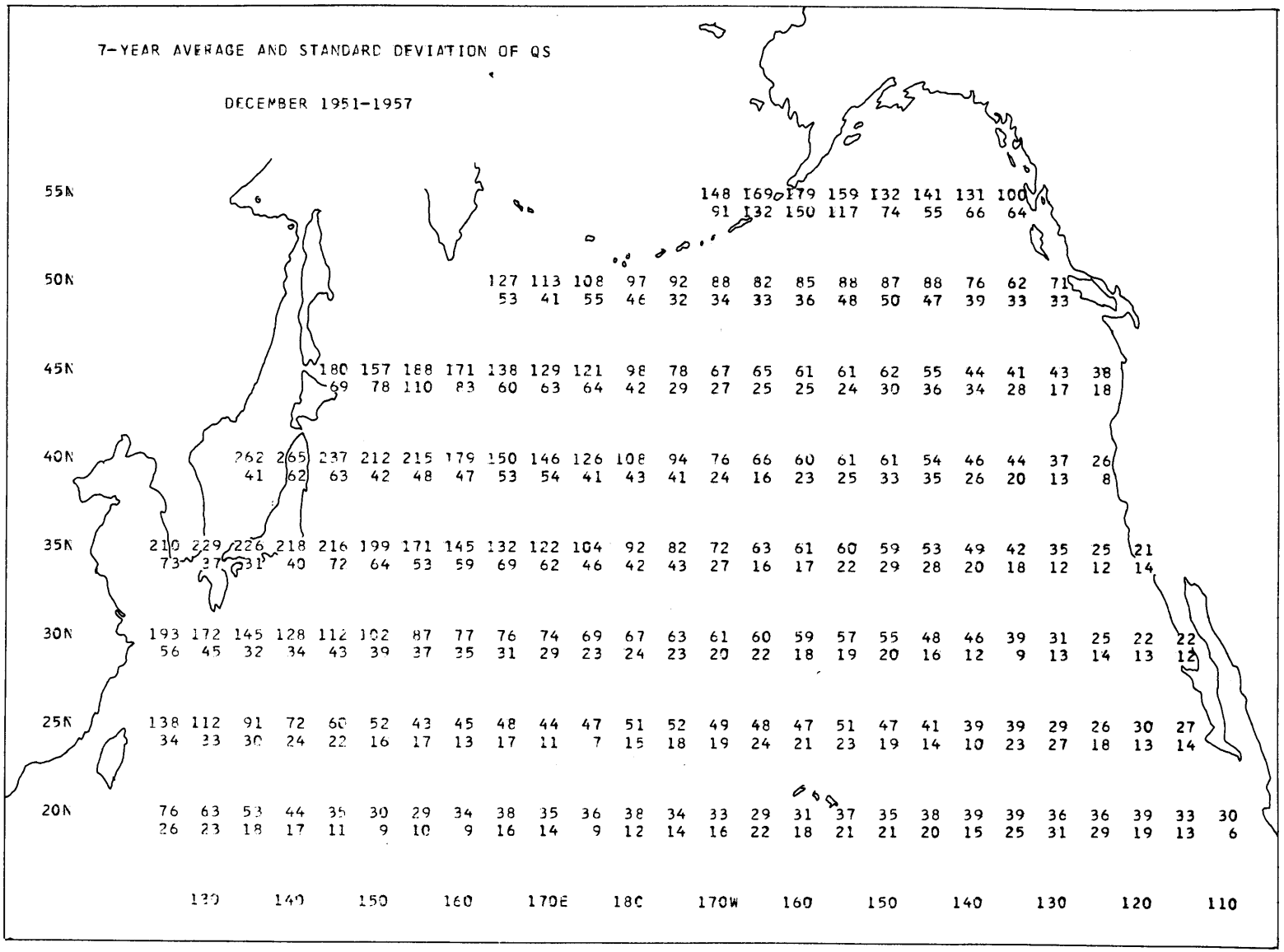

Figure A59. 7-year average values and standard deviations of the sensible heat transfer. December 1951-1957. (cal/cm^2/day)

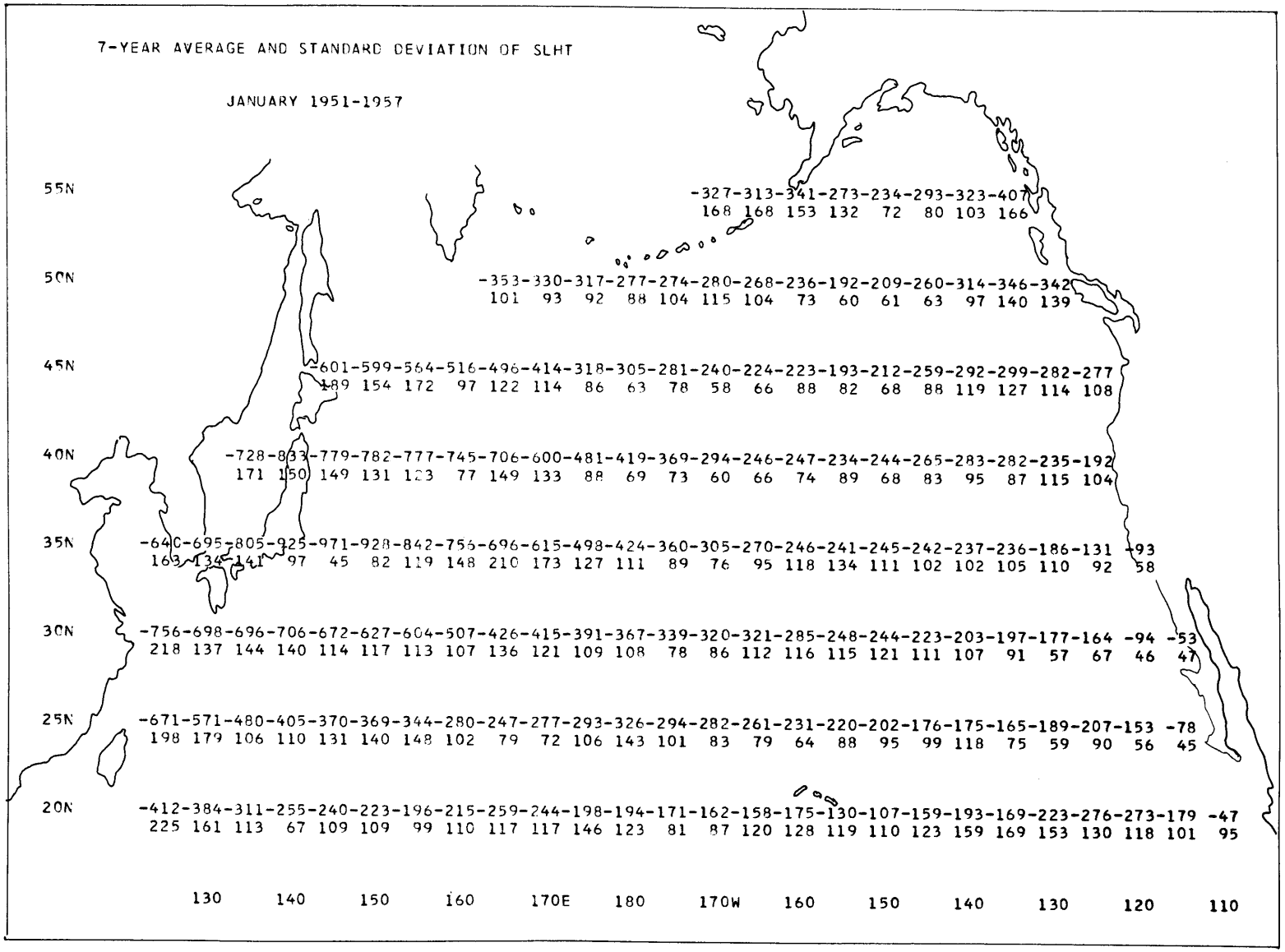

Figure A60. 7-year average values and standard deviations of the total heat transfer. January 1951-1957. (cal/cm^2/day)

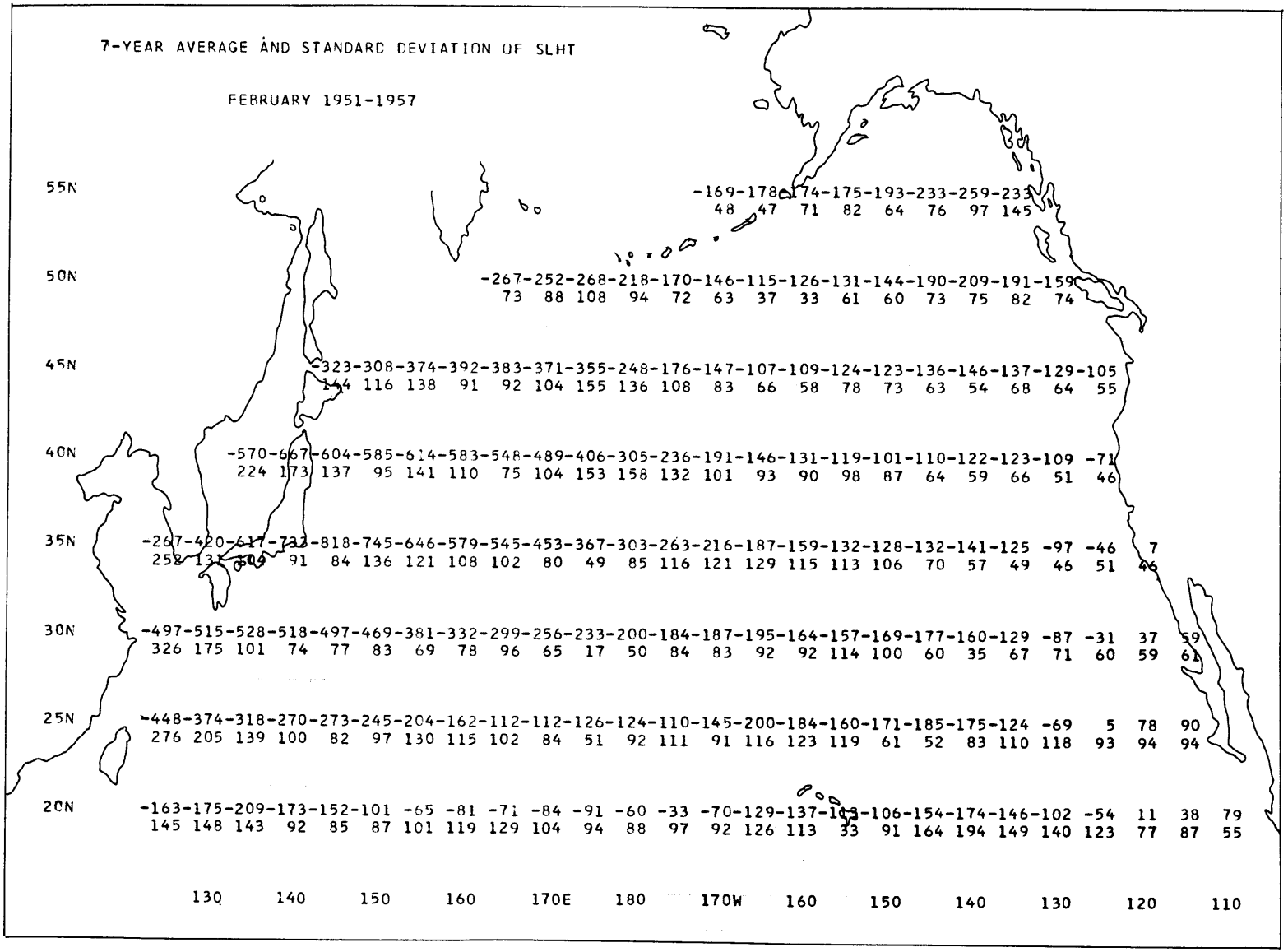

Figure A61. 7-year average values and standard deviations of the total heat transfer. February 1951-1957. (cal/cm^2/day)

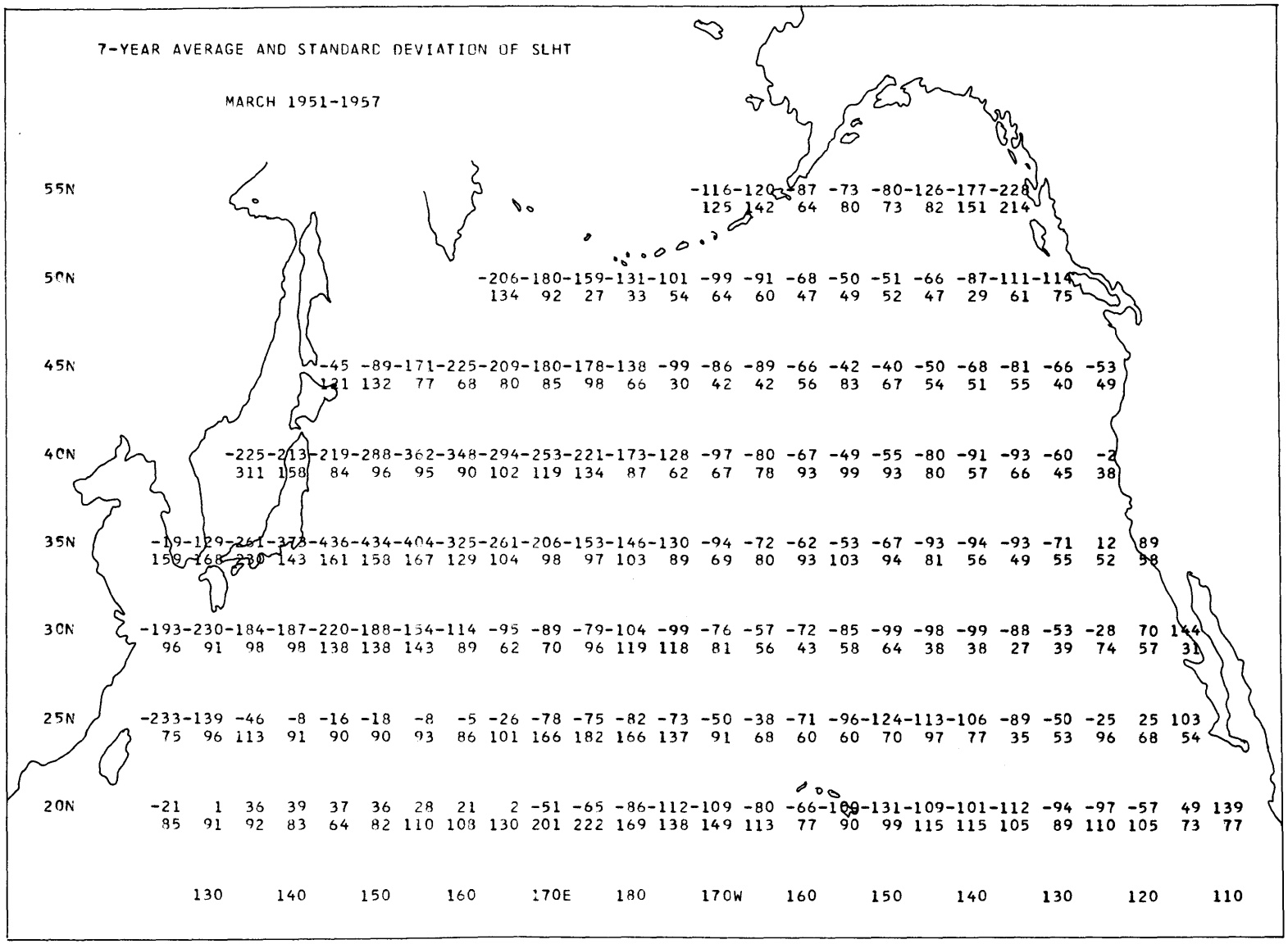

Figure A62. 7-year average values and standard deviations of the total heat transfer. March 1951-1957. (cal/cm^2/day)

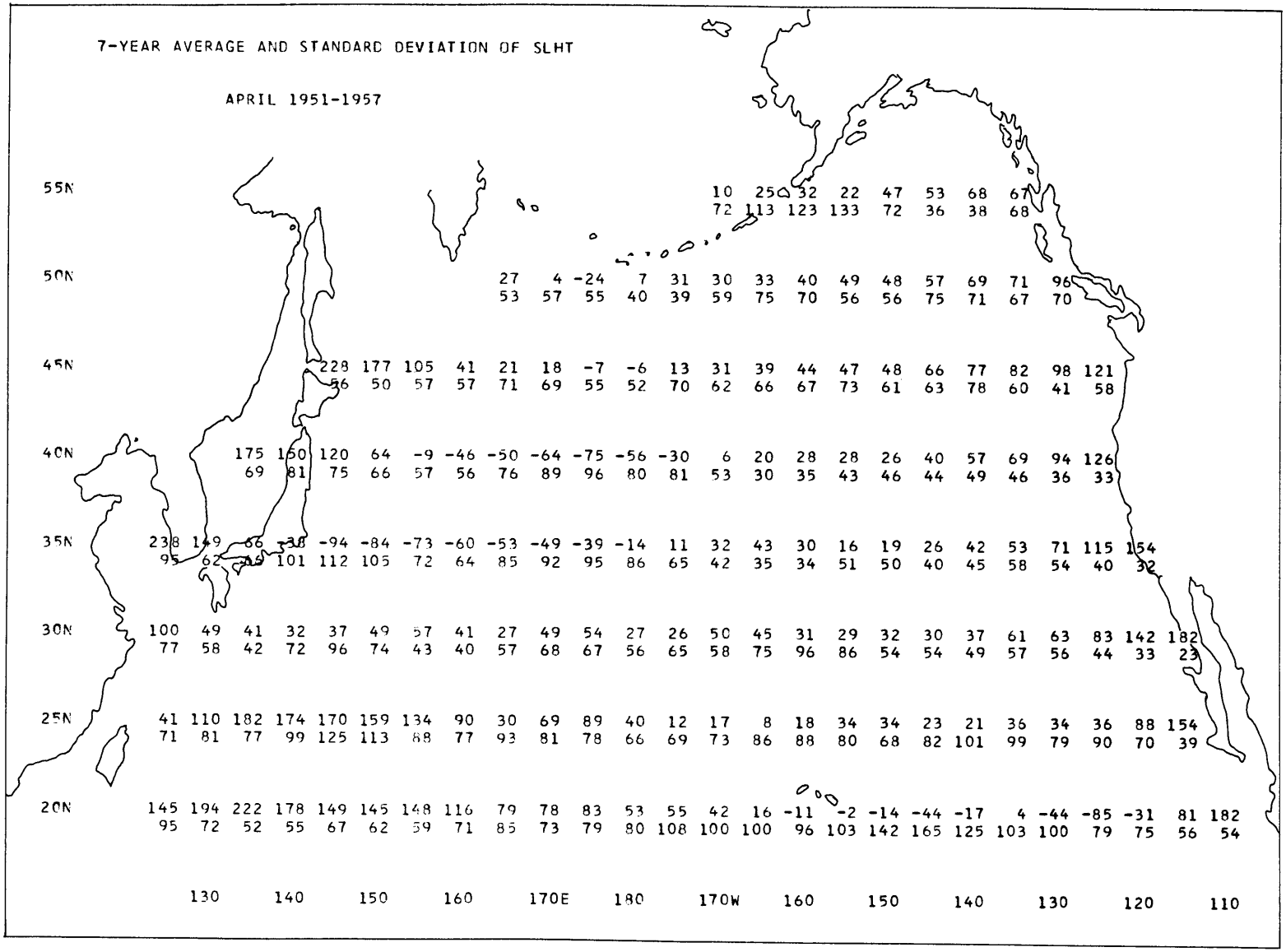

Figure A63. 7-year average values and standard deviations of the total heat transfer. April 1951-1957. (cal/cm^2/day)

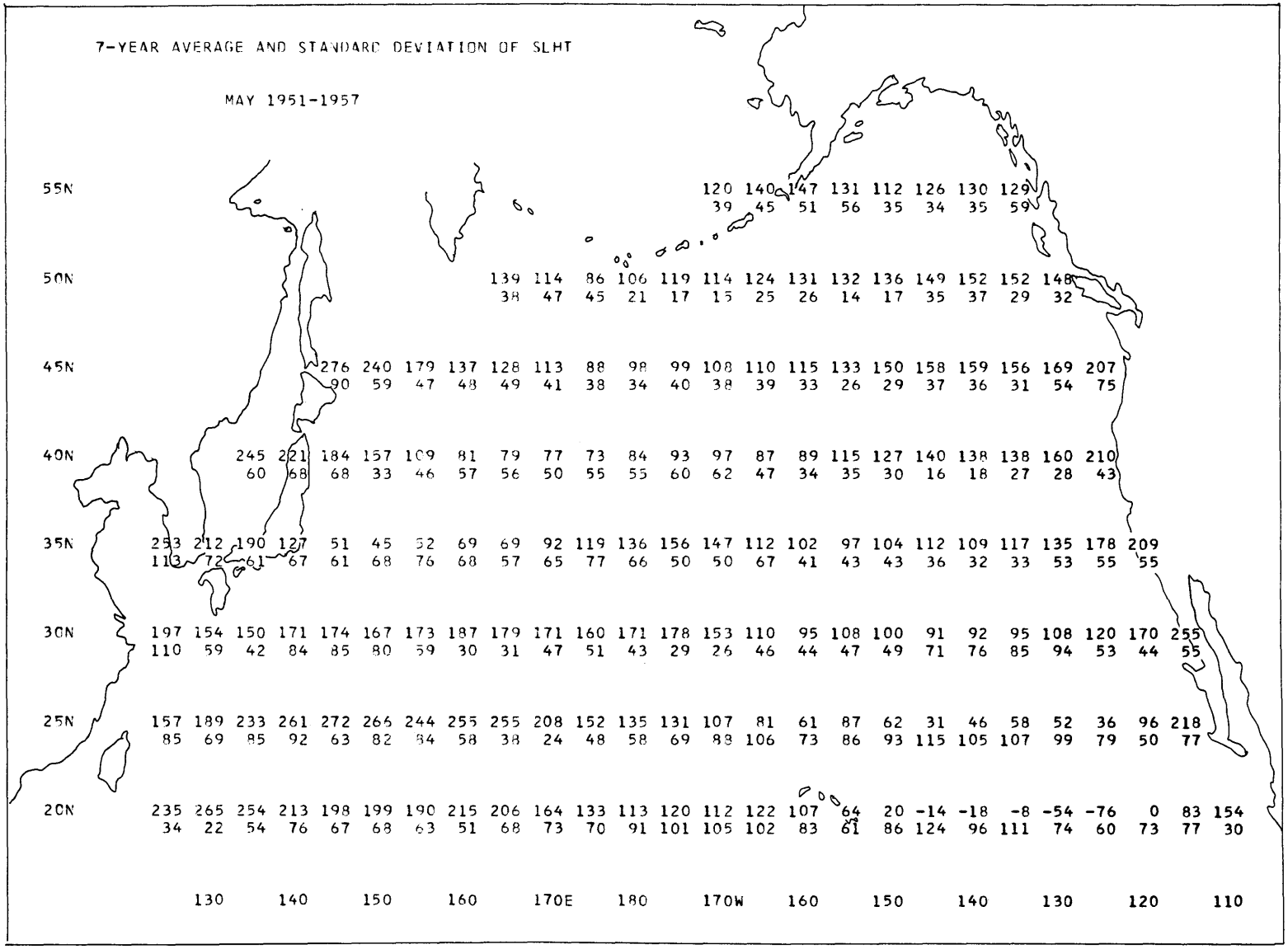

Figure A64. 7-year average values and standard deviations of the total heat transfer. May 1951-1957. (cal/cm^2/day)

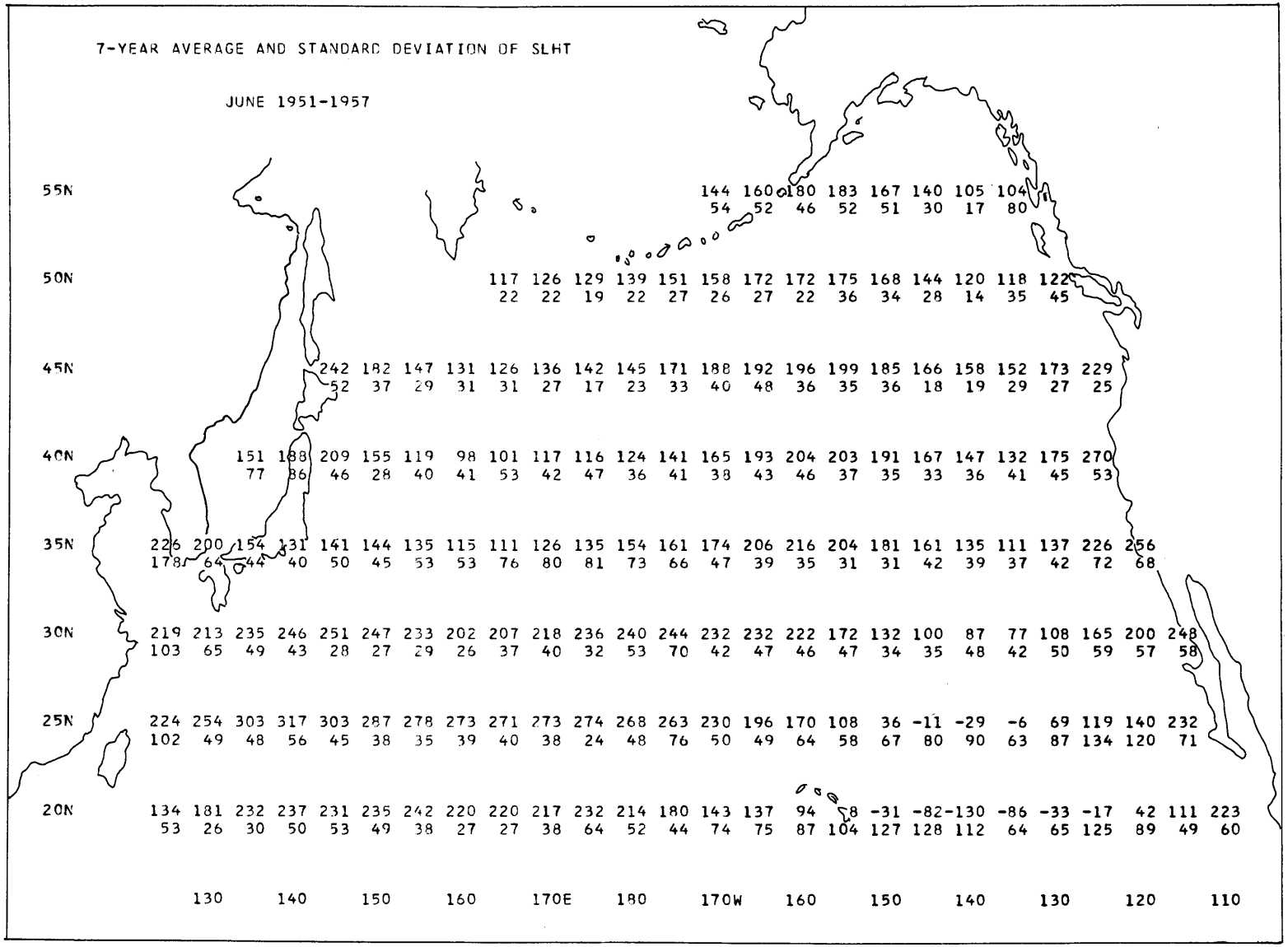

Figure A65. 7-year average values and standard deviations of the total heat transfer. June 1951-1957. (cal/cm^2/day)

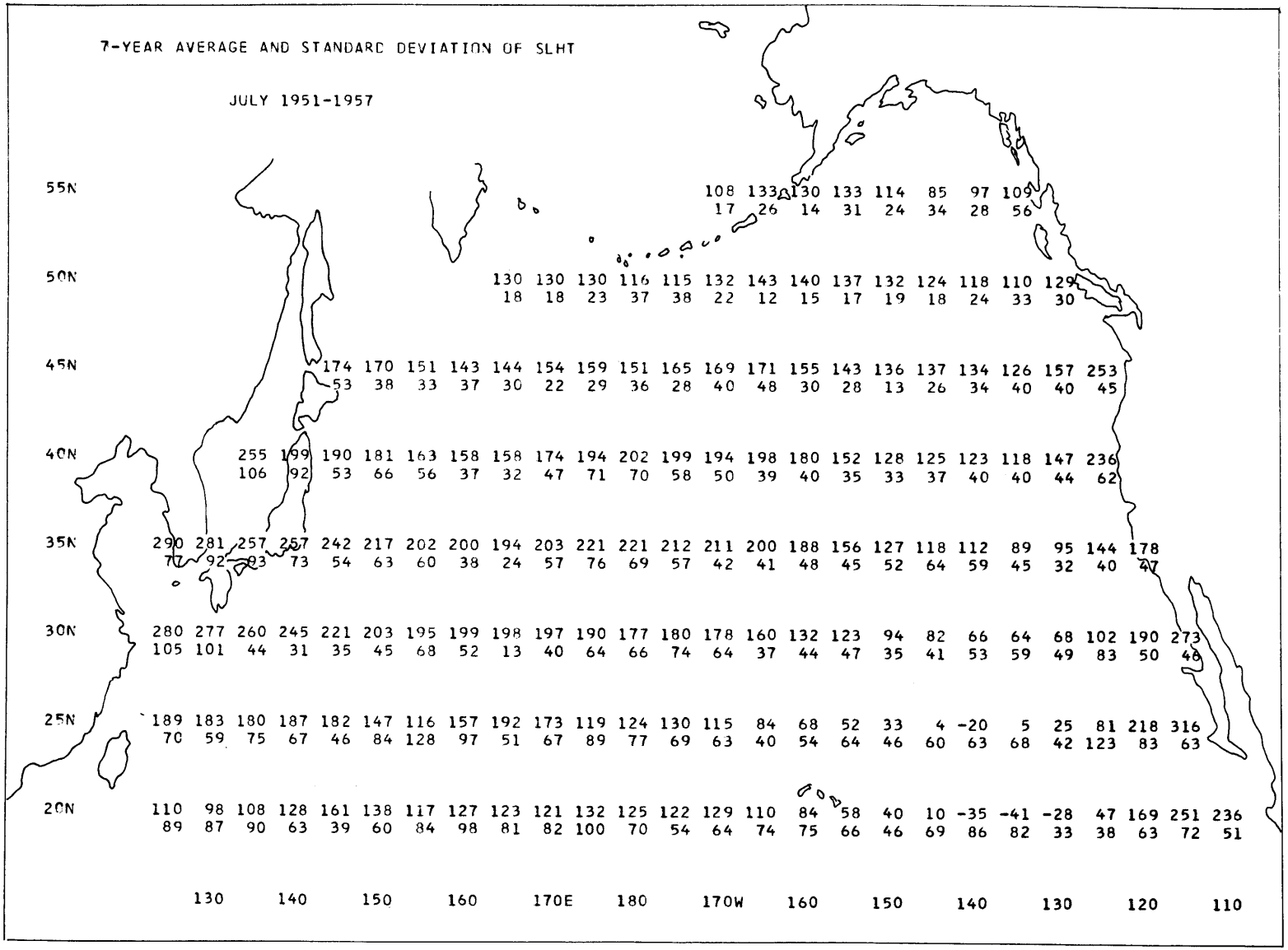

Figure A66. 7-year average values and standard deviations of the total heat transfer. July 1951-1957. (cal/cm^2/day)

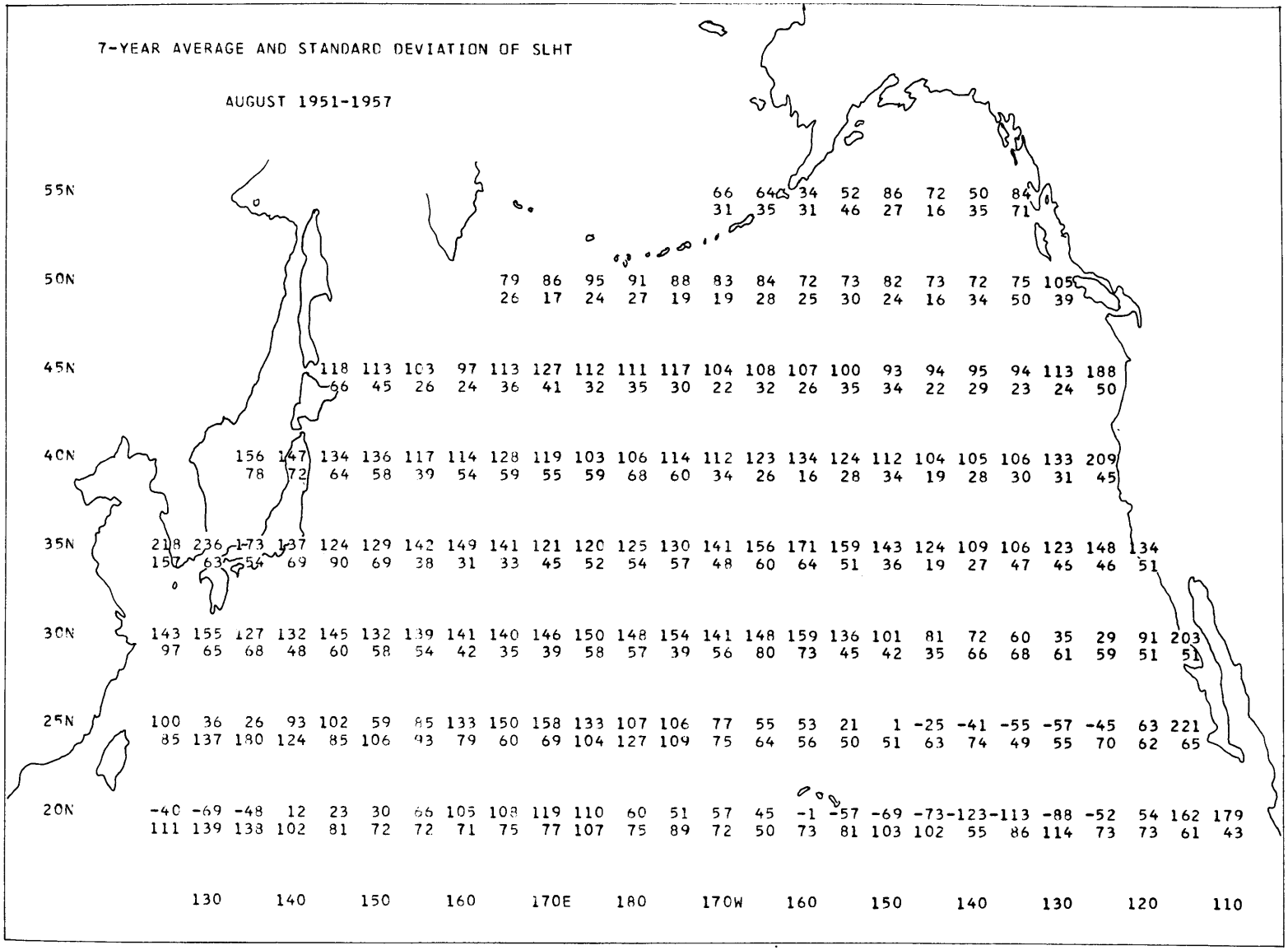

Figure A67. 7-year average values and standard deviations of the total heat transfer. August 1951-1957. (cal/cm^2/day)

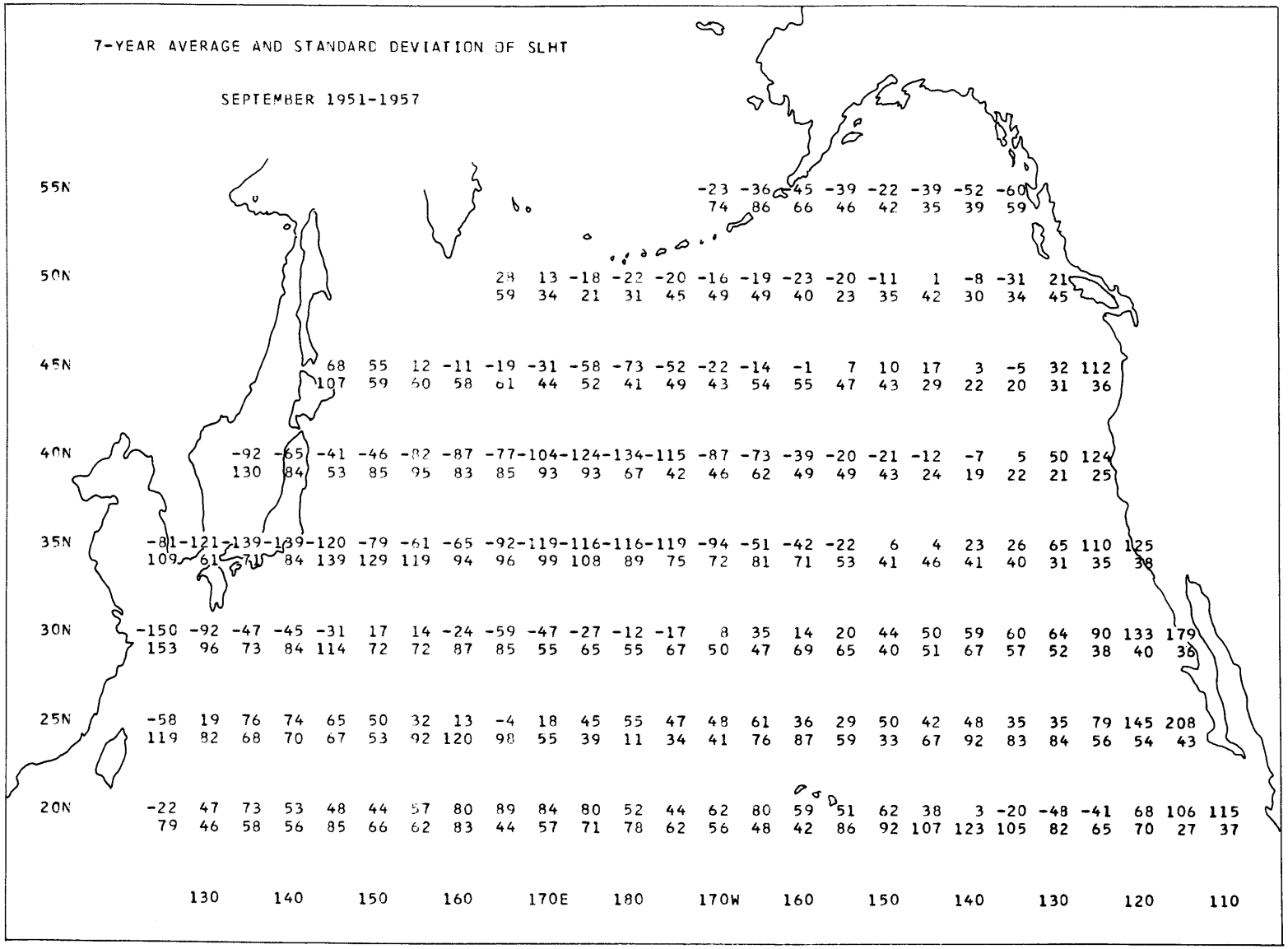

Figure A68. 7-year average values and standard deviations of the total heat transfer. September 1951-1957. (cal/cm^2/day)

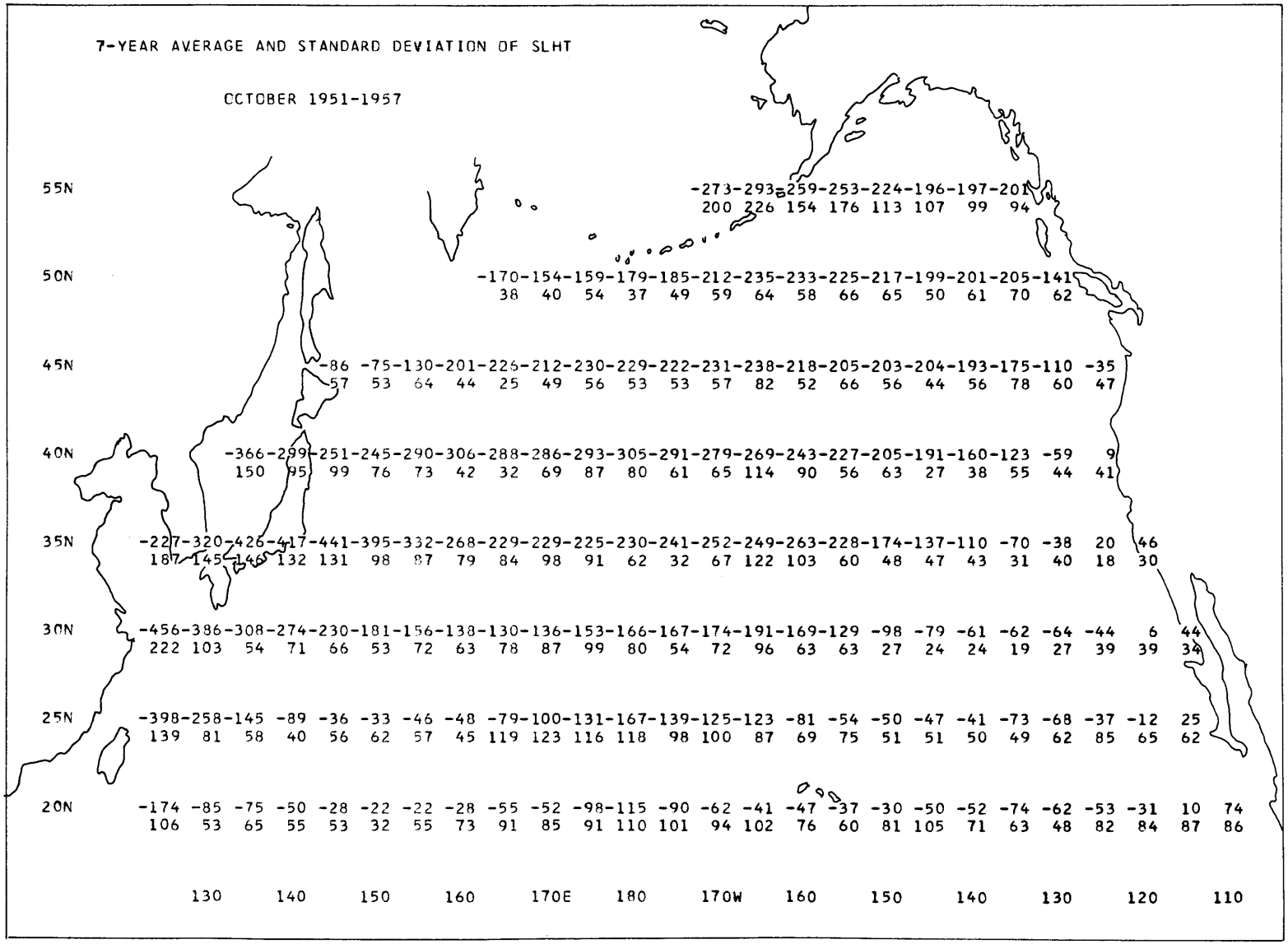

Figure A69. 7-year average values and standard deviations of the total heat transfer. October 1951-1957. (cal/cm^2/day)

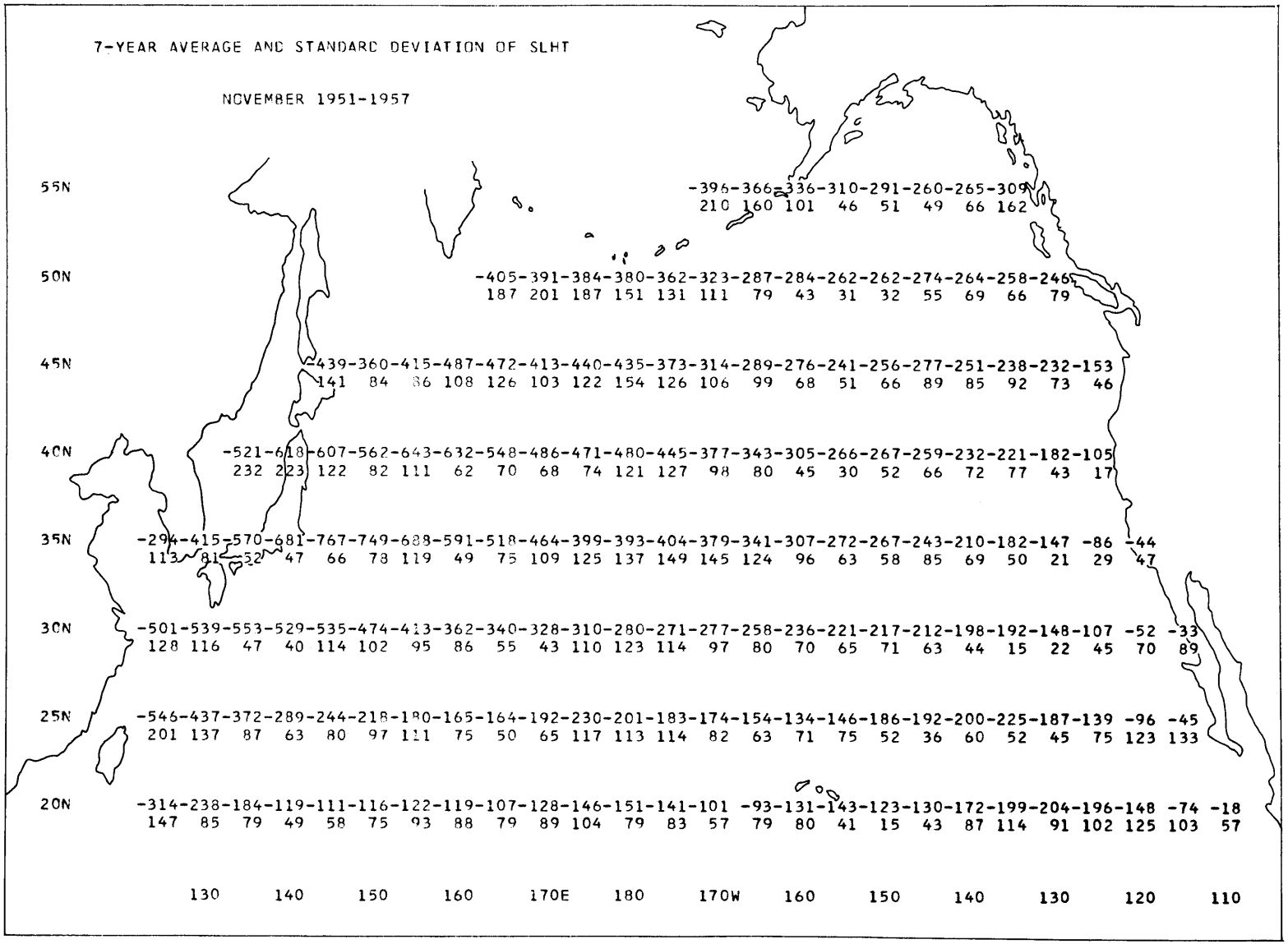

Figure A70. 7-year average values and standard deviations of the total heat transfer. November 1951-1957. (cal/cm^2/day)

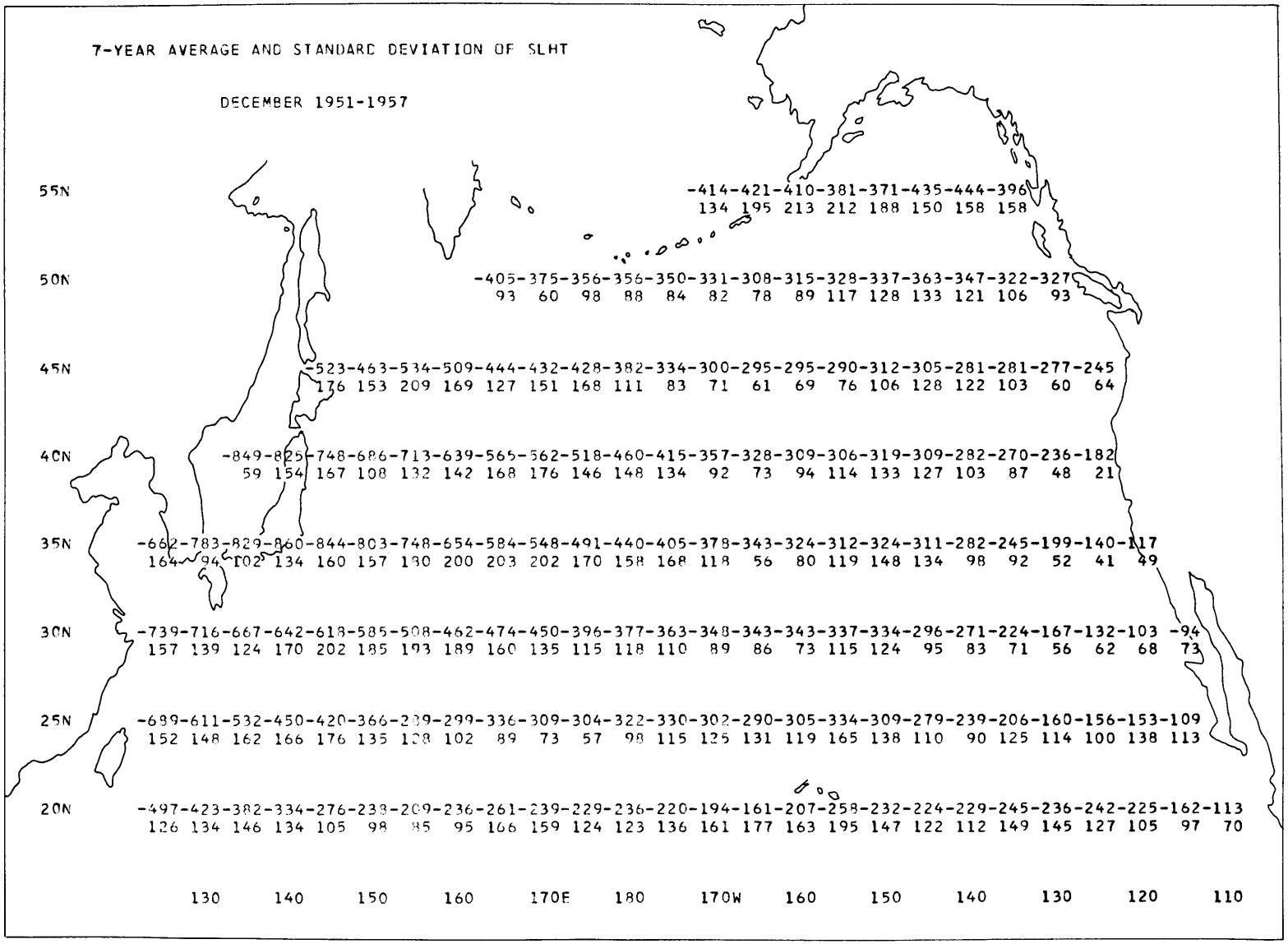

Figure A71. 7-year average values and standard deviations of the total heat transfer. December 1951-1957. (cal/cm^2/day)

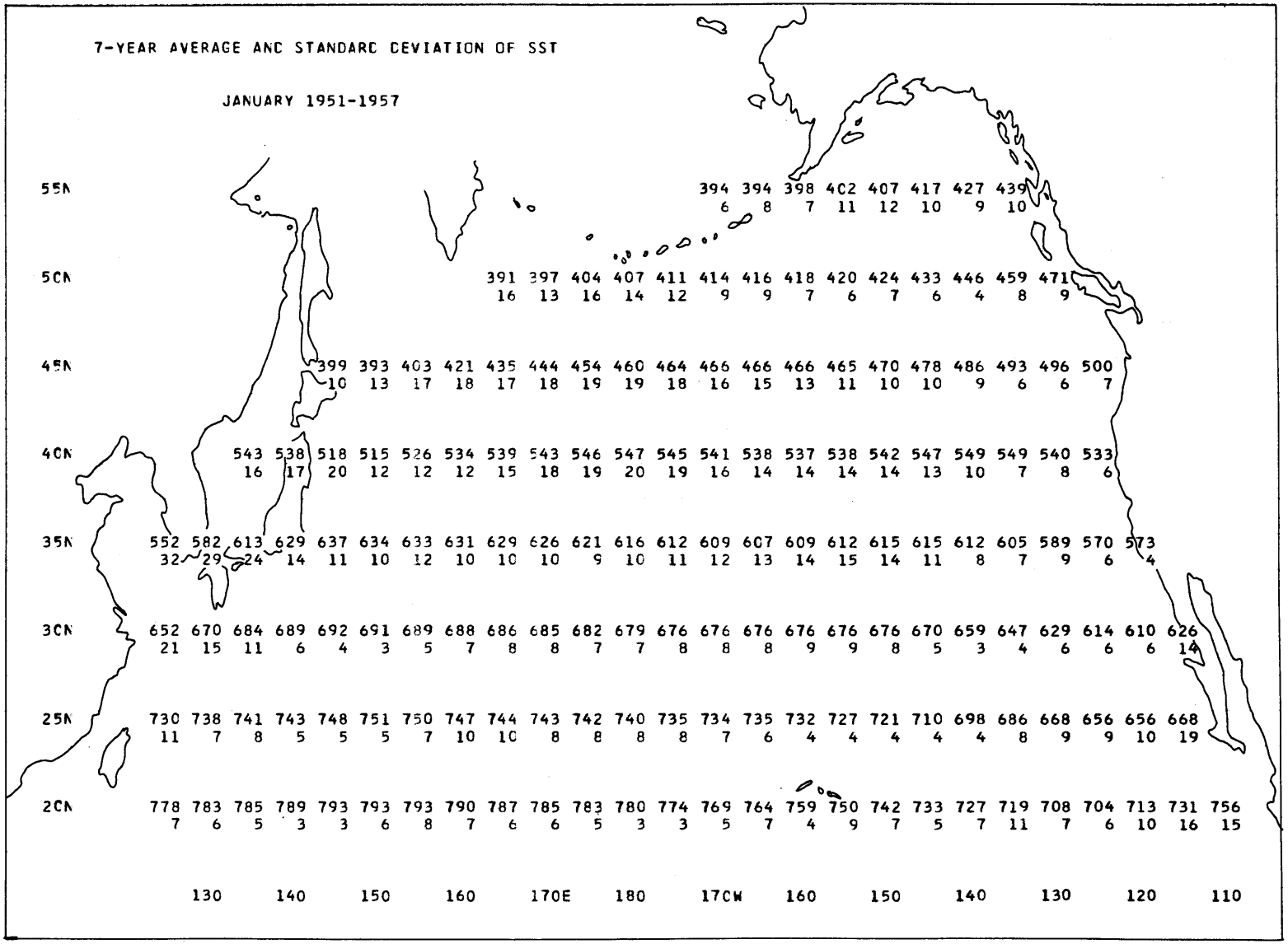

Figure A72. 7-year average values and standard deviations of the sea-surface temperature. January 1951-1957. (^{o}F x 10)

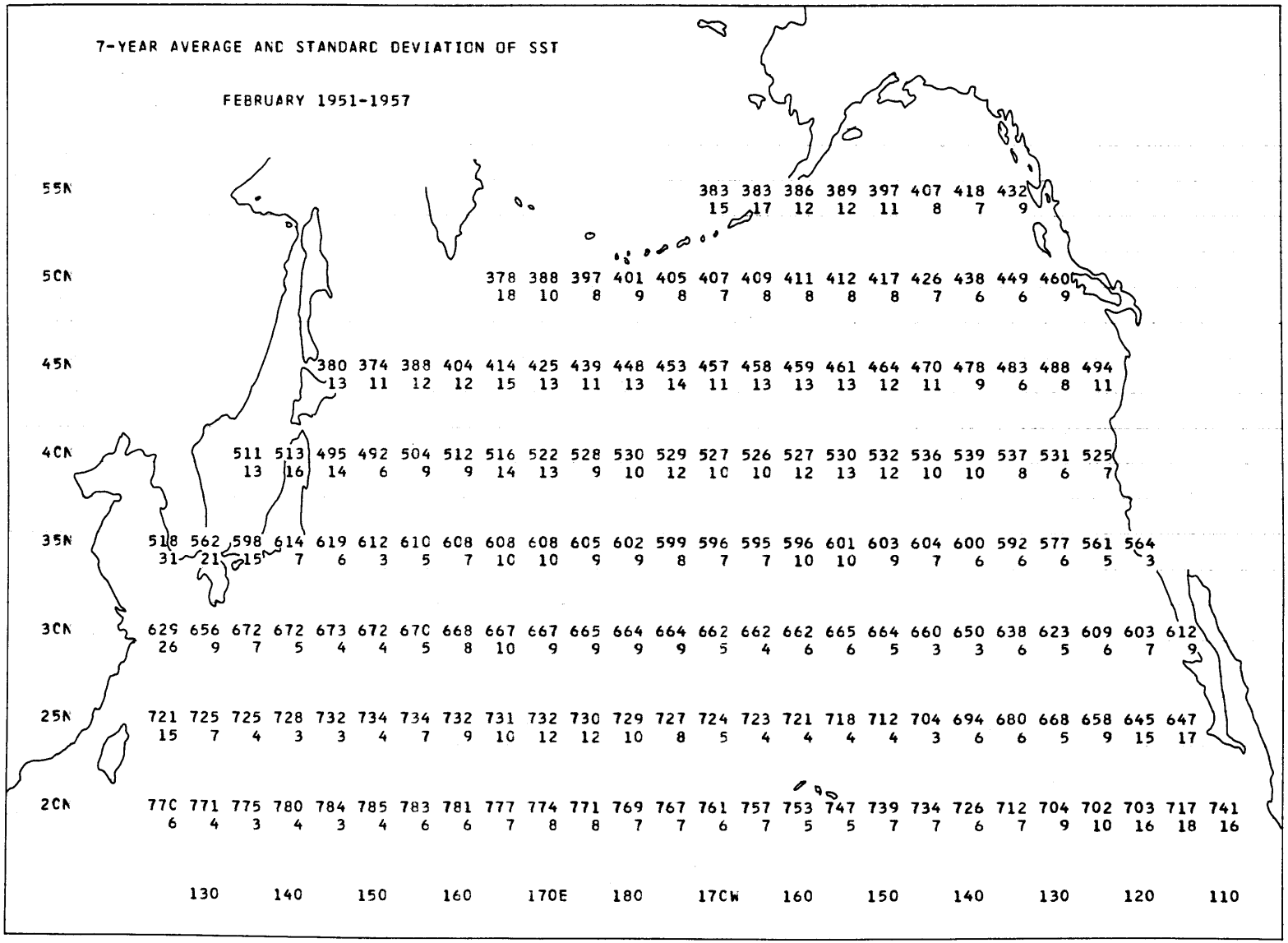

Figure A73. 7-year average values and standard deviations of the sea-surface temperature. February 1951-1957. (^{o}F x 10)

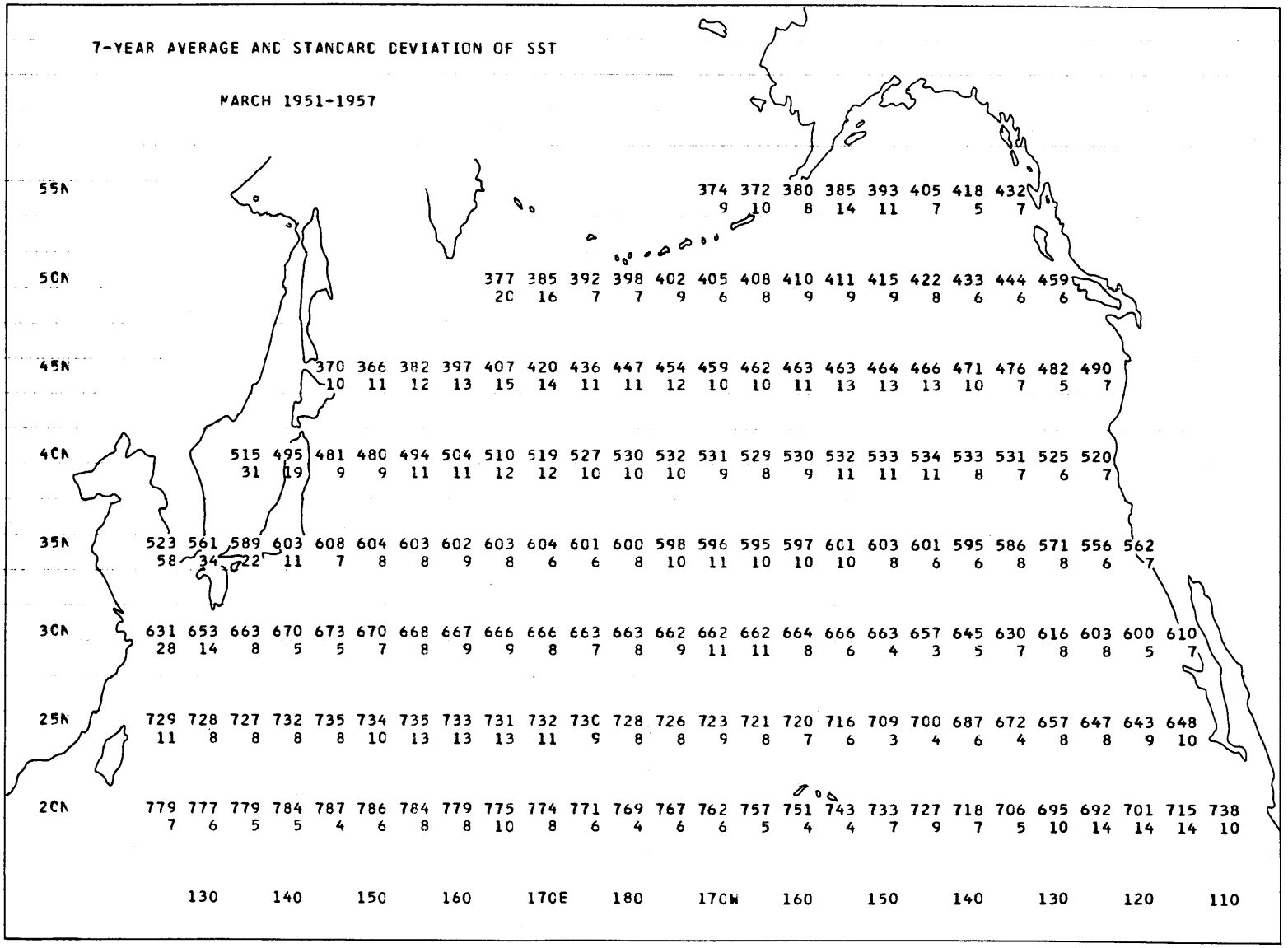

Figure A74. 7-year average values and standard deviations of the sea-surface temperature. March 1951-1957. (^{o}F x 10)

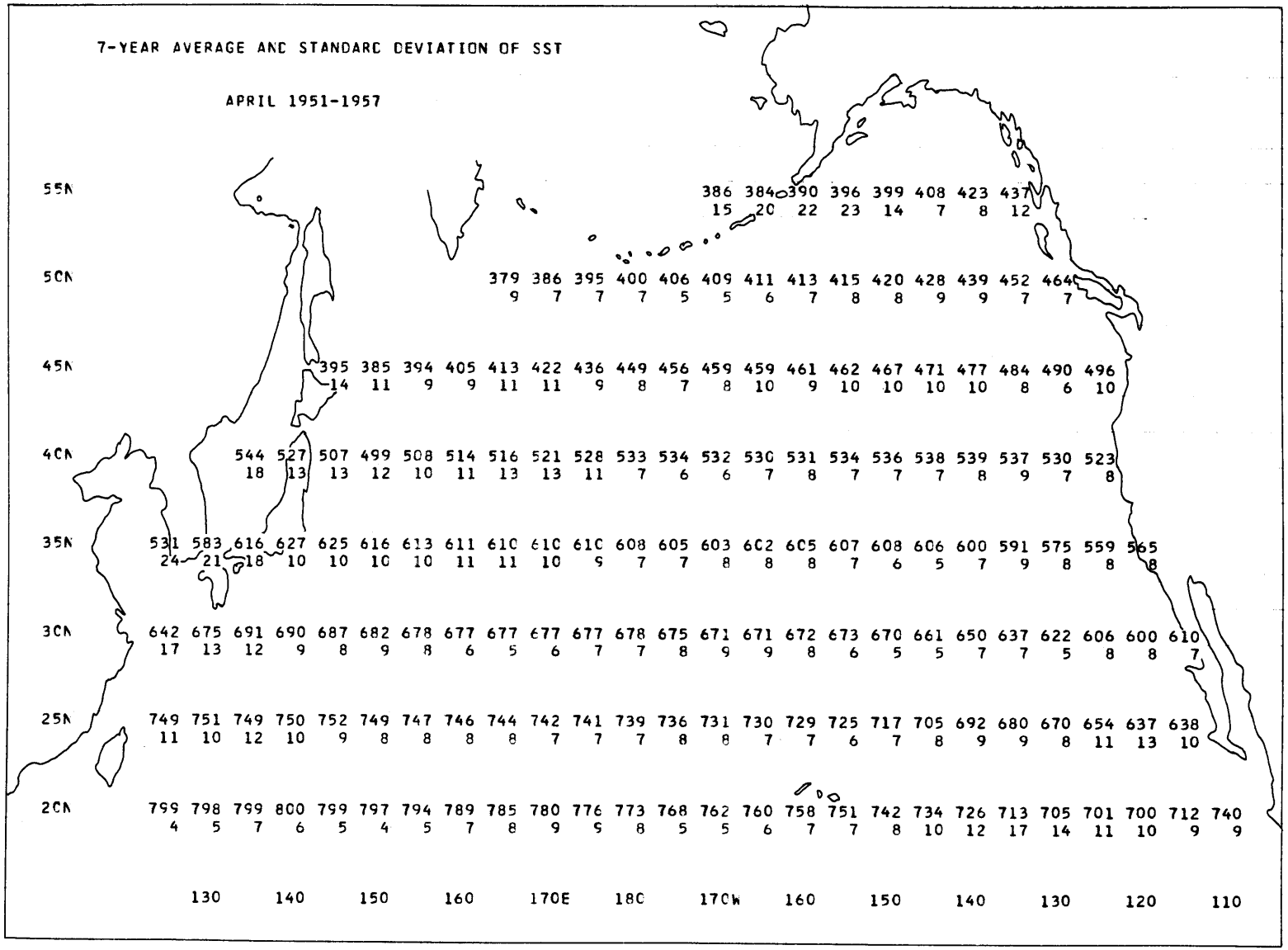

Figure A75. 7-year average values and standard deviations of the sea-surface temperature. April 1951-1957. (^{o}F x 10)

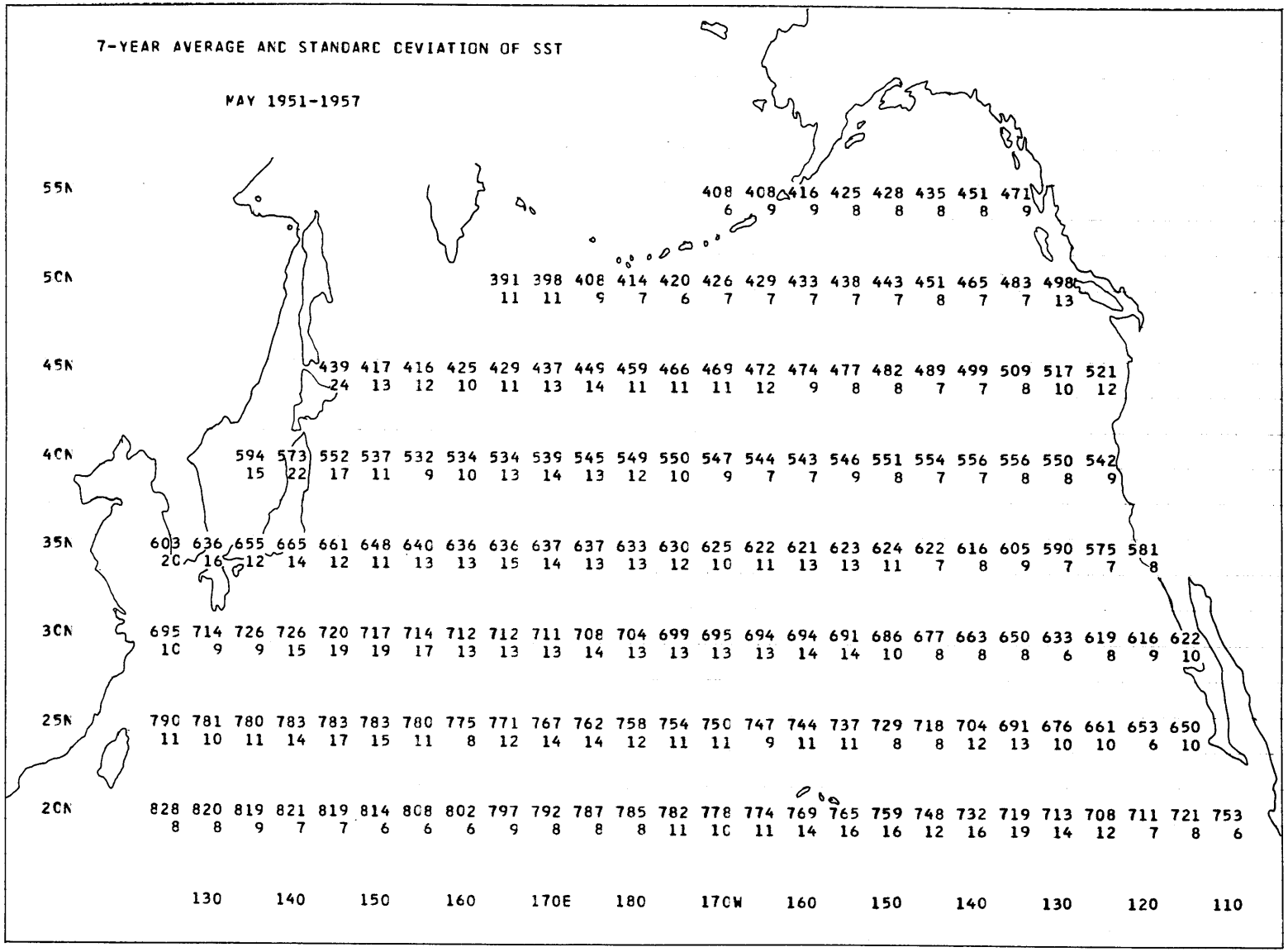

Figure A76. 7-year average values and standard deviations of the sea-surface temperature. May 1951-1957. (^{o}F x 10)

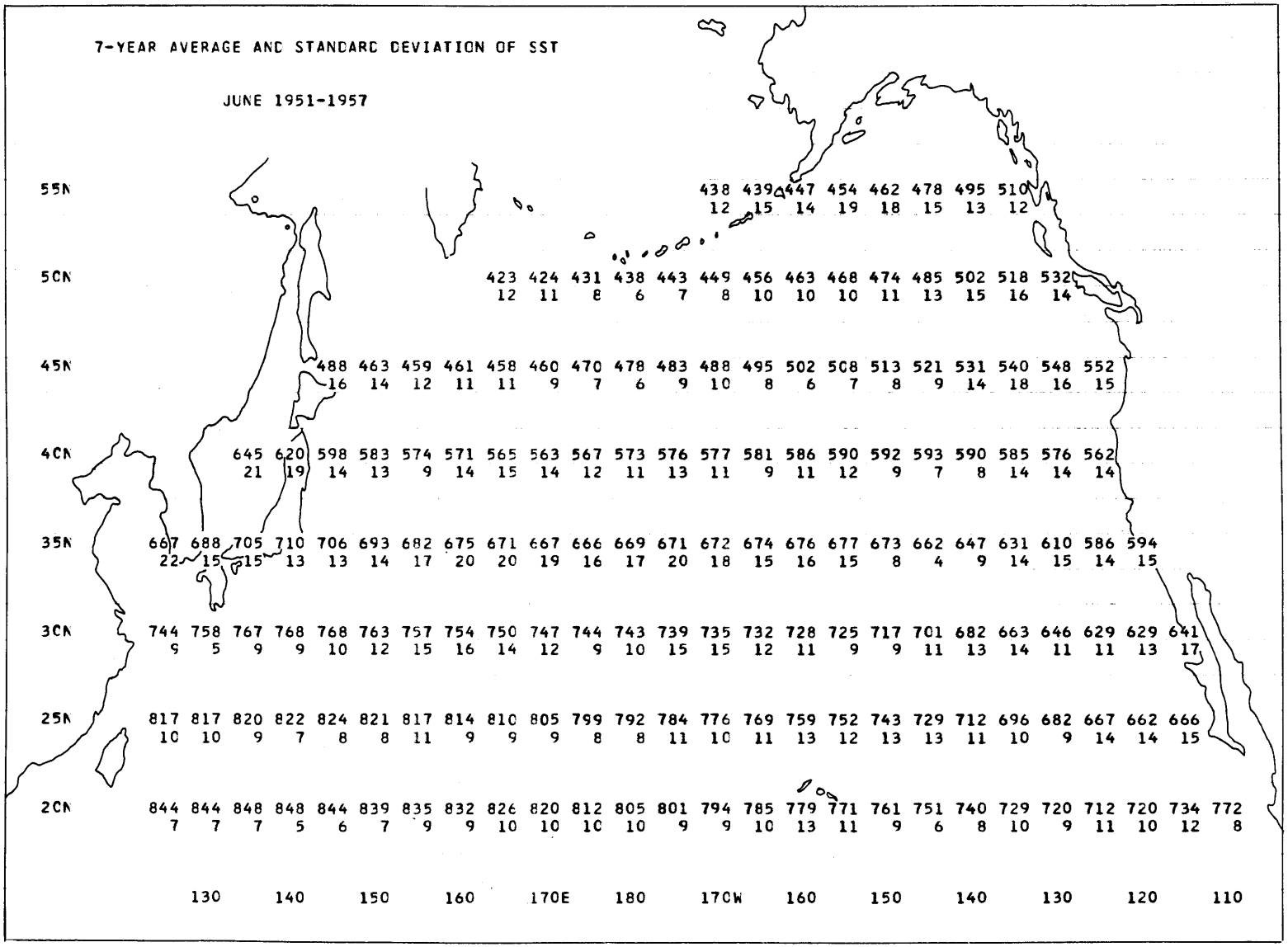

Figure A77. 7-year average values and standard deviations of the sea-surface temperature. June 1951-1957. (^{o}F x 10)

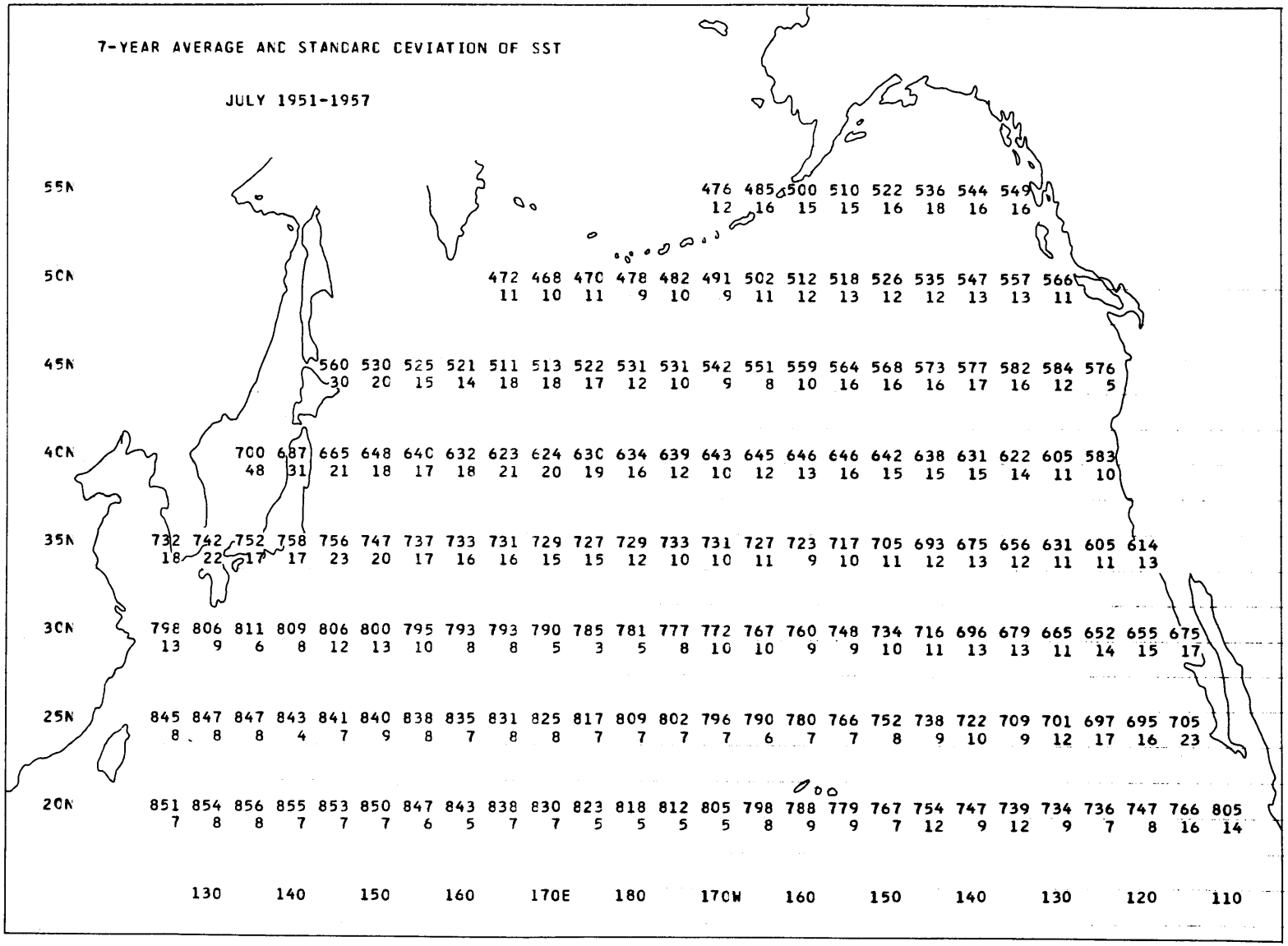

Figure A78. 7-year average values and standard deviations of the sea-surface temperature. July 1951-1957. (^{o}F x 10)

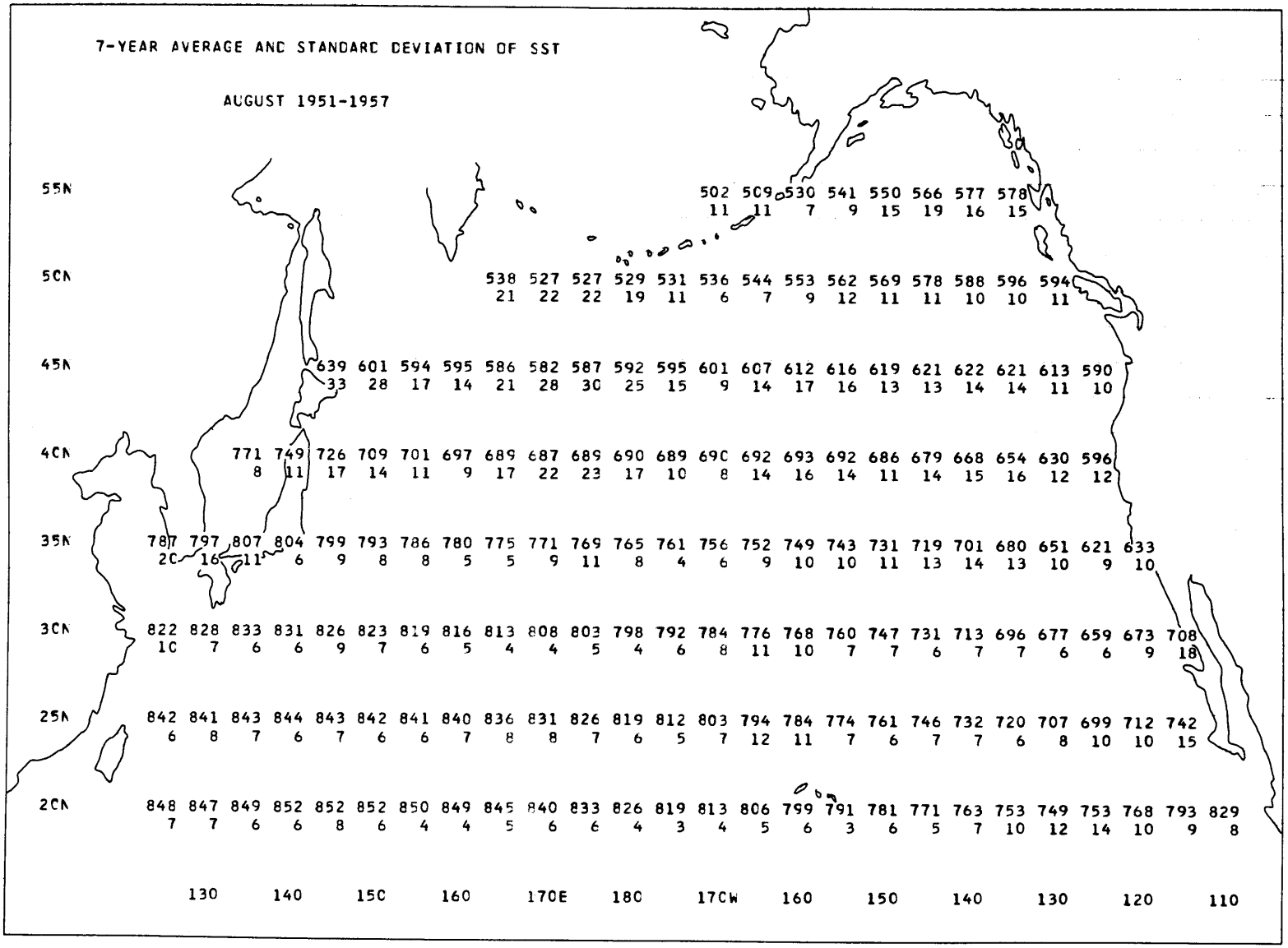

Figure A79. 7-year average values and standard deviations of the sea-surface temperature. August 1951-1957. (^{o}F x 10)

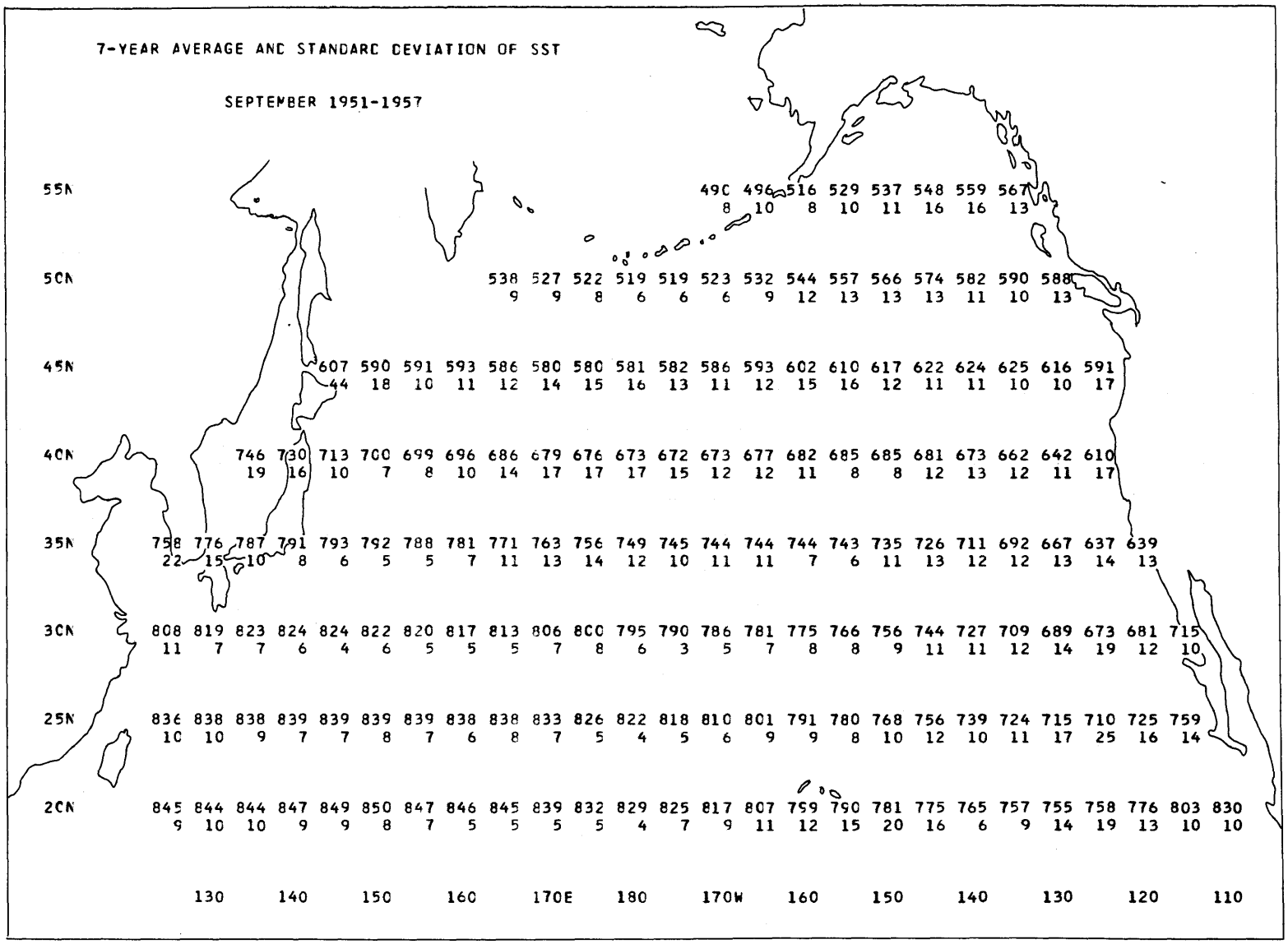

Figure A80. 7-year average values and standard deviations of the sea-surface temperature. September 1951-1957. (°F x 10)

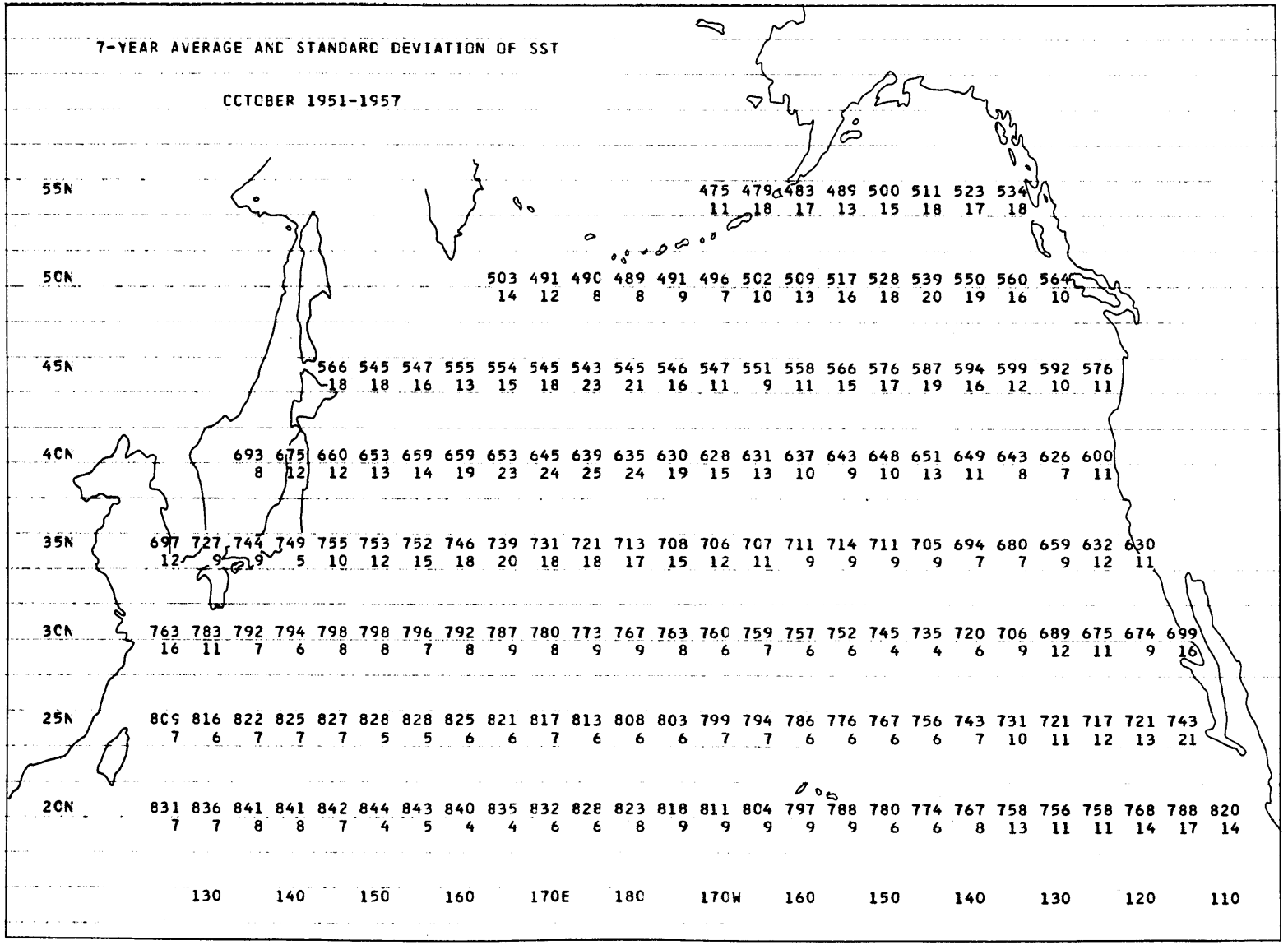

Figure A81. 7-year average values and standard deviations of the sea-surface temperature. October 1951-1957. (^{o}F x 10)

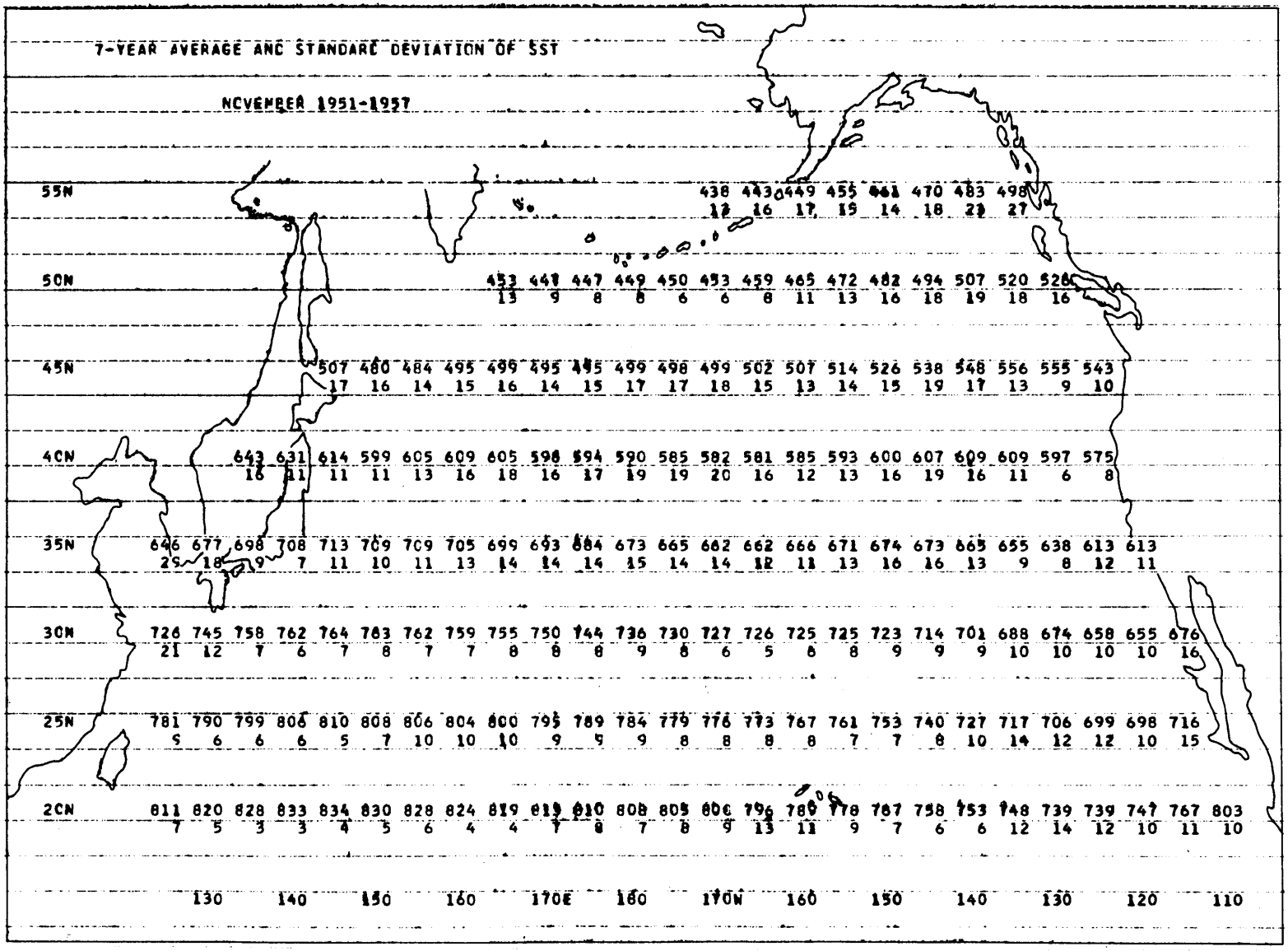

Figure A82. 7-year average values and standard deviations of the sea-surface temperature. November 1951-1957. (^{o}F x 10)

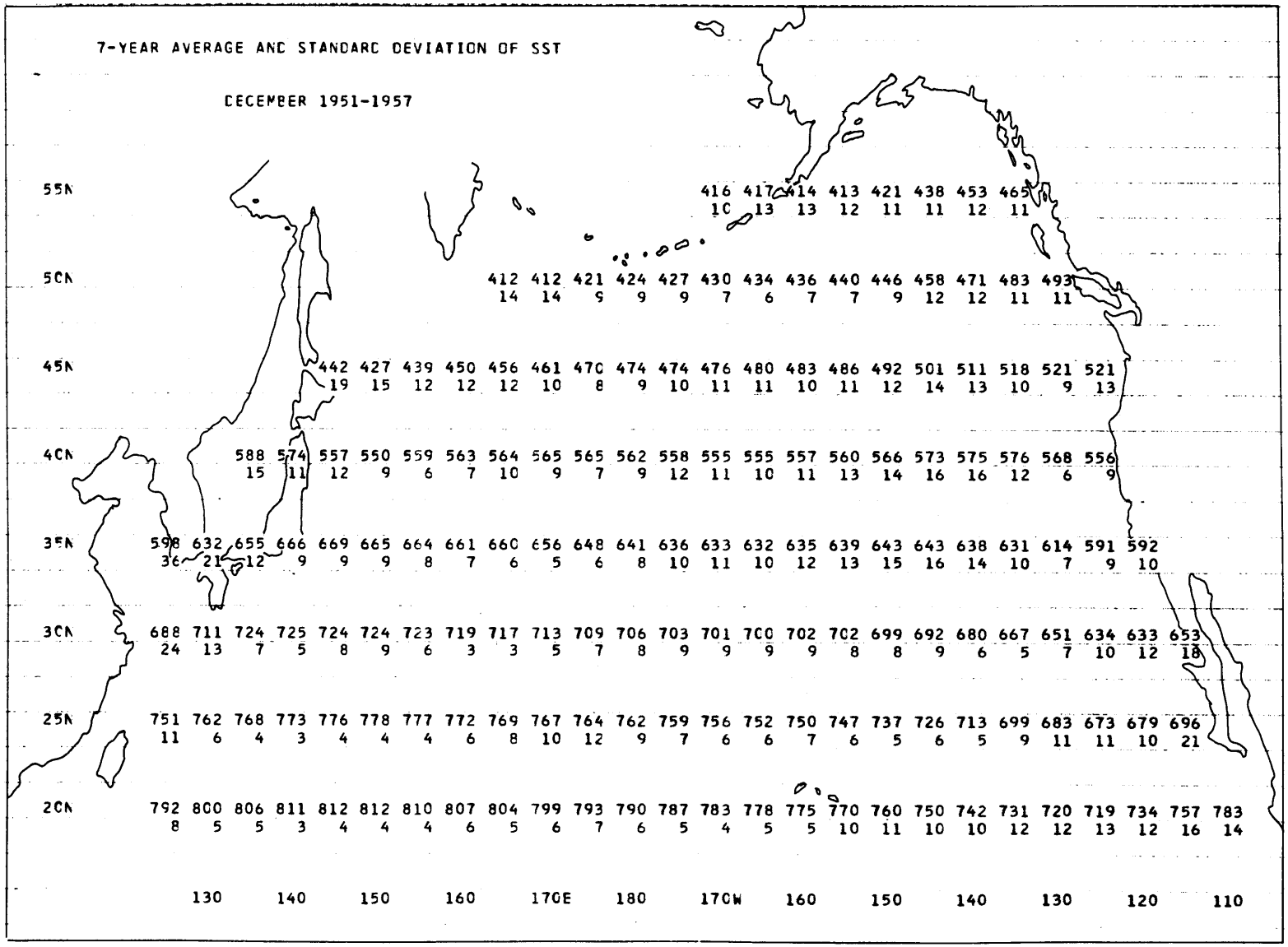

Figure A83. 7-year average values and standard deviations of the sea-surface temperature. December 1951-1957. (^{O}F x 10)

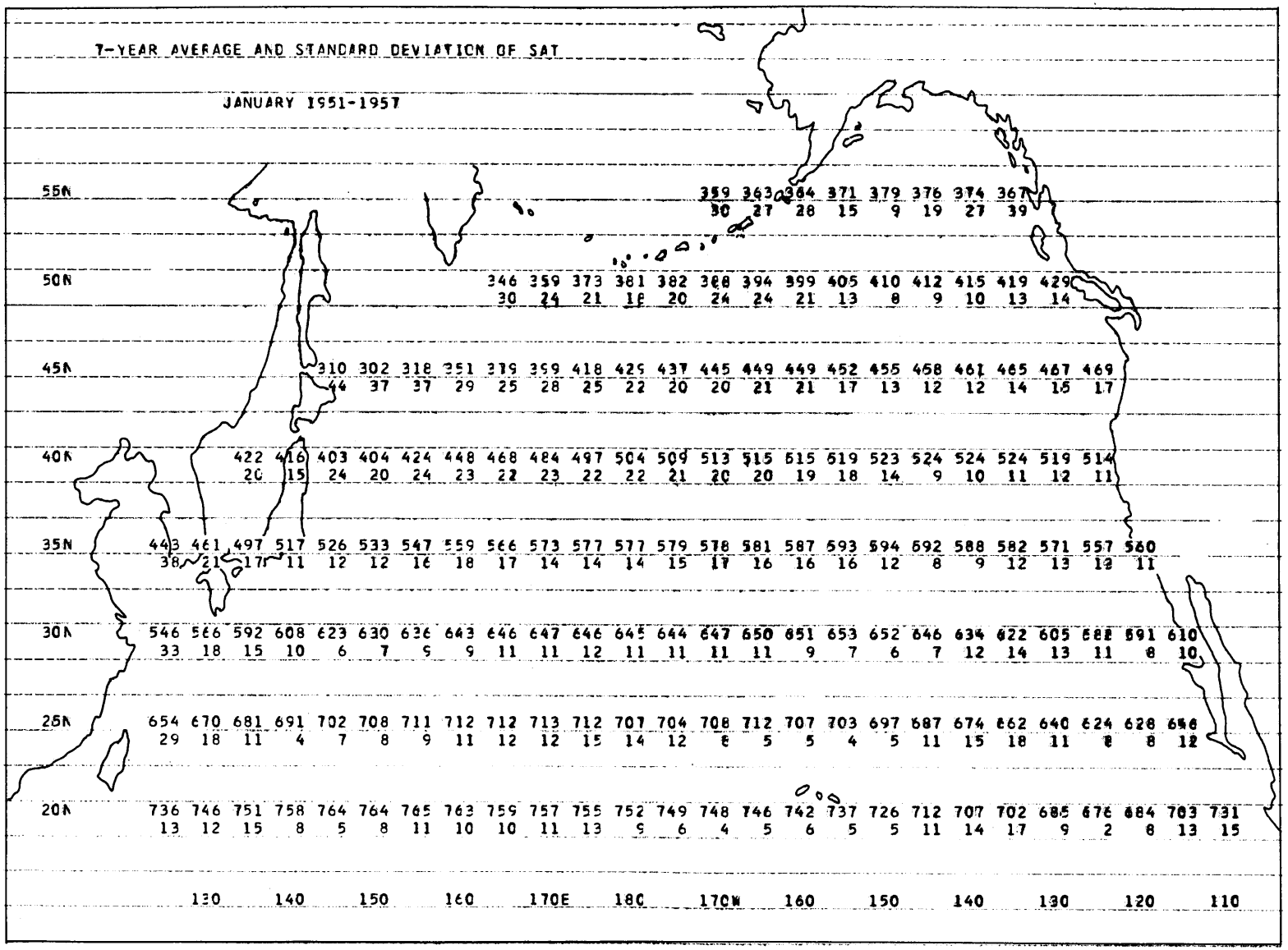

Figure A84. 7-year average values and standard deviations of the surface air temperature. January 1951-1957. (^{o}F x 10)

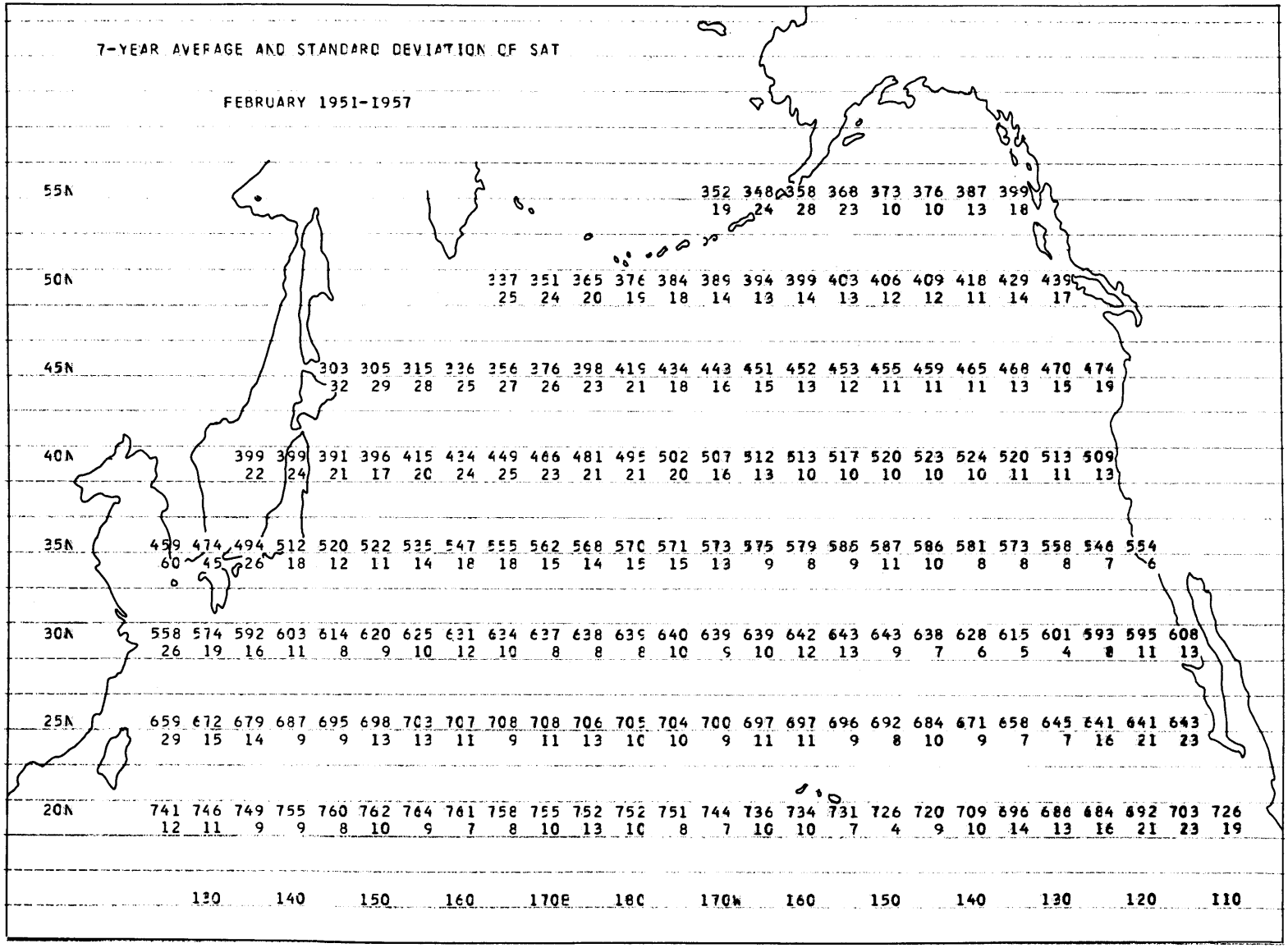

Figure A85. 7-year average values and standard deviations of the surface air temperature. February 1951-1957. (^{o}F x 10)

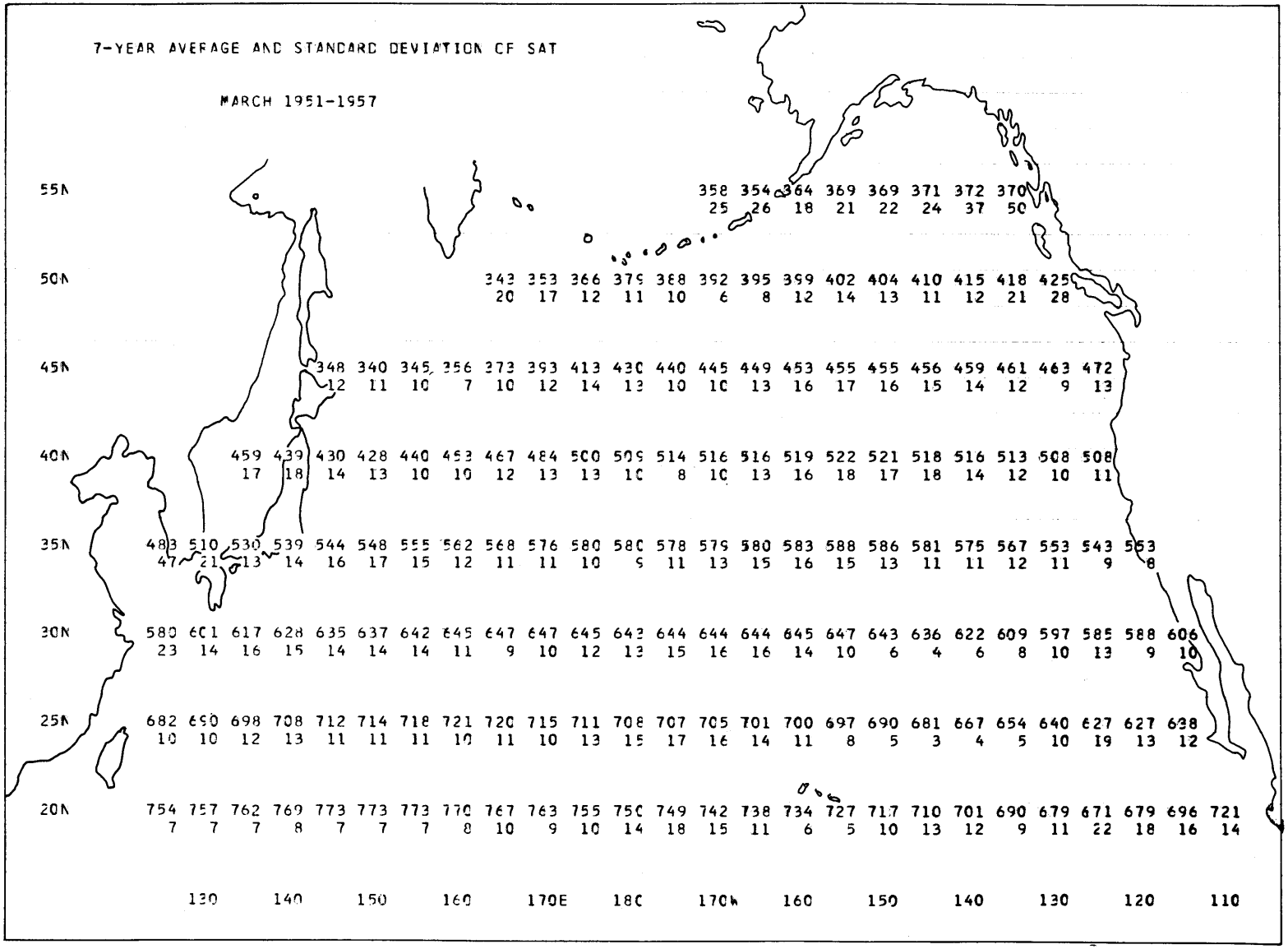

Figure A86. 7-year average values and standard deviations of the surface air temperature. March 1951-1957. (^{o}F x 10)

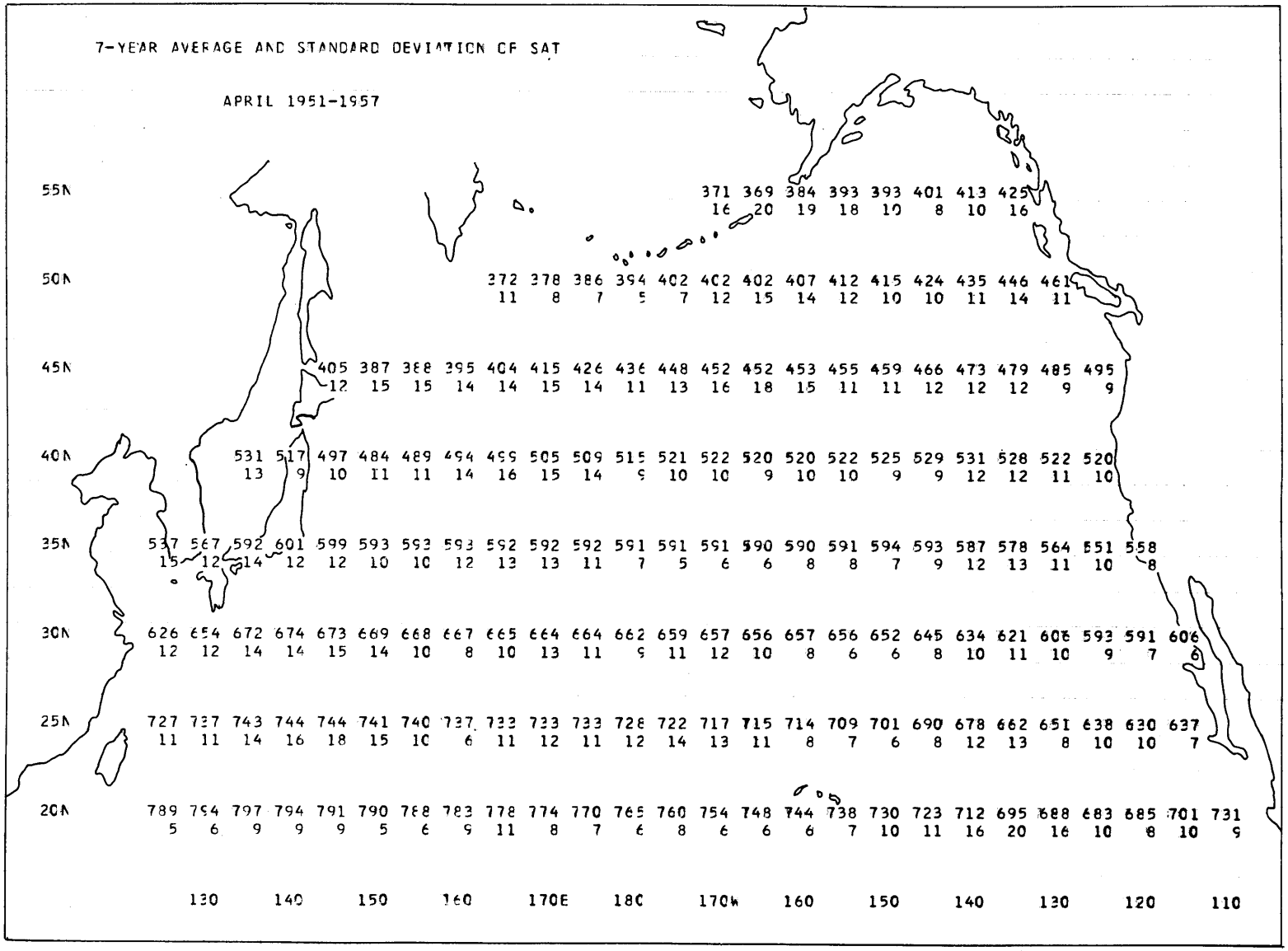

Figure A87. 7-year average values and standard deviations of the surface air temperature. April 1951-1957. (^{o}F x 10)

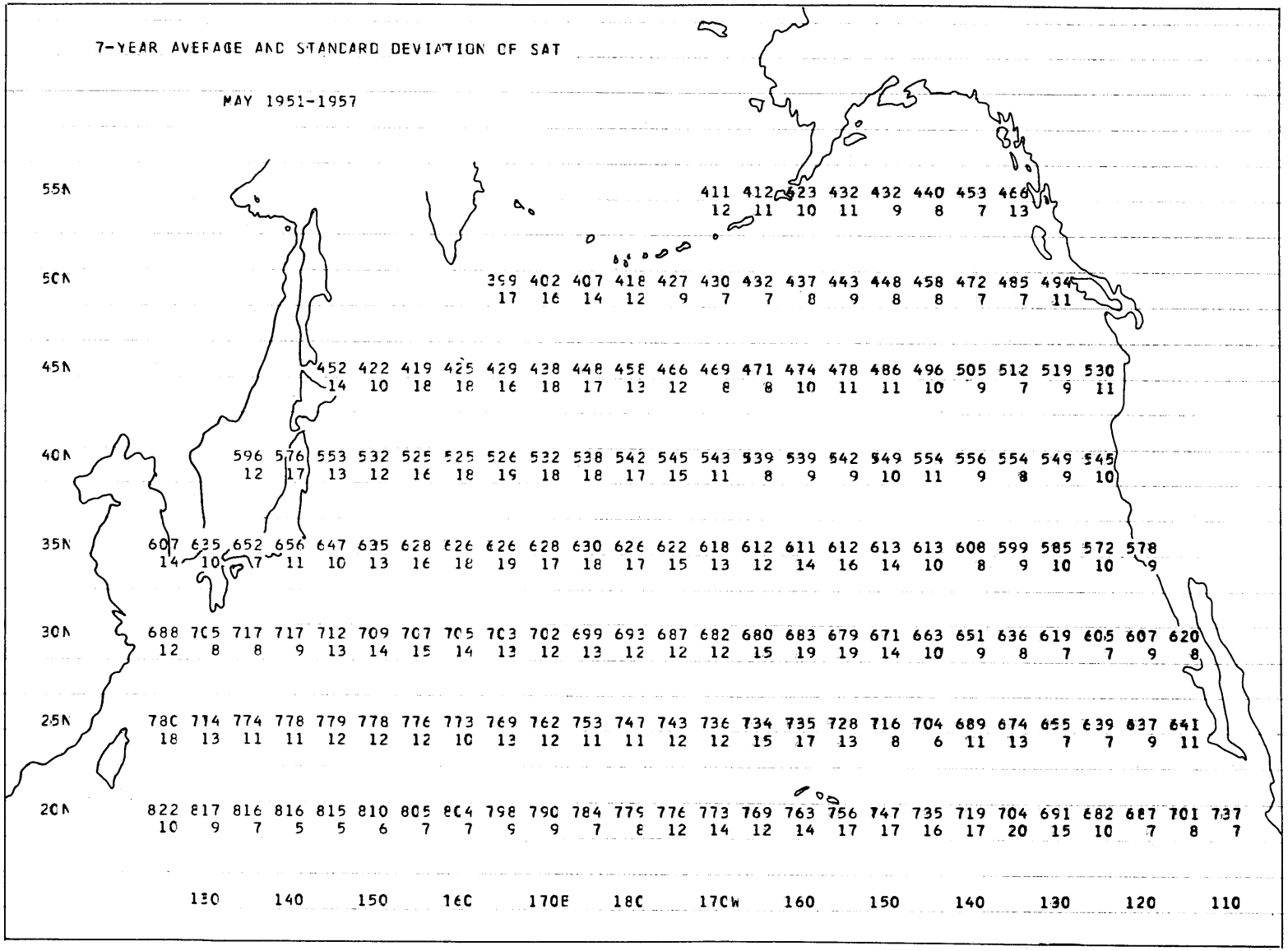

Figure A88. 7-year average values and standard deviations of the surface air temperature. May 1951-1957. (°F x 10)

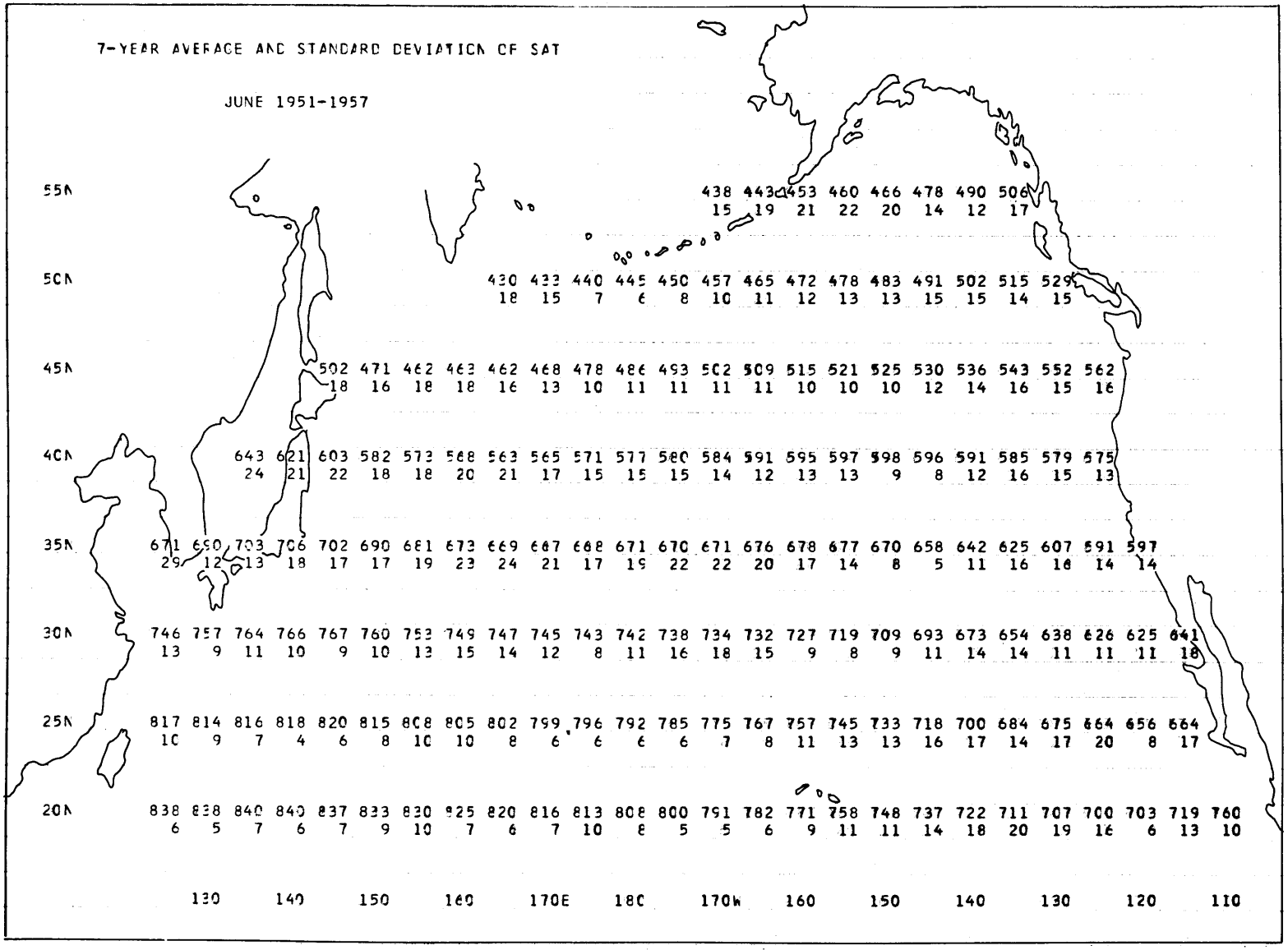

Figure A89. 7-year average values and standard deviations of the surface air temperature. June 1951-1957. (^{o}F x 10)

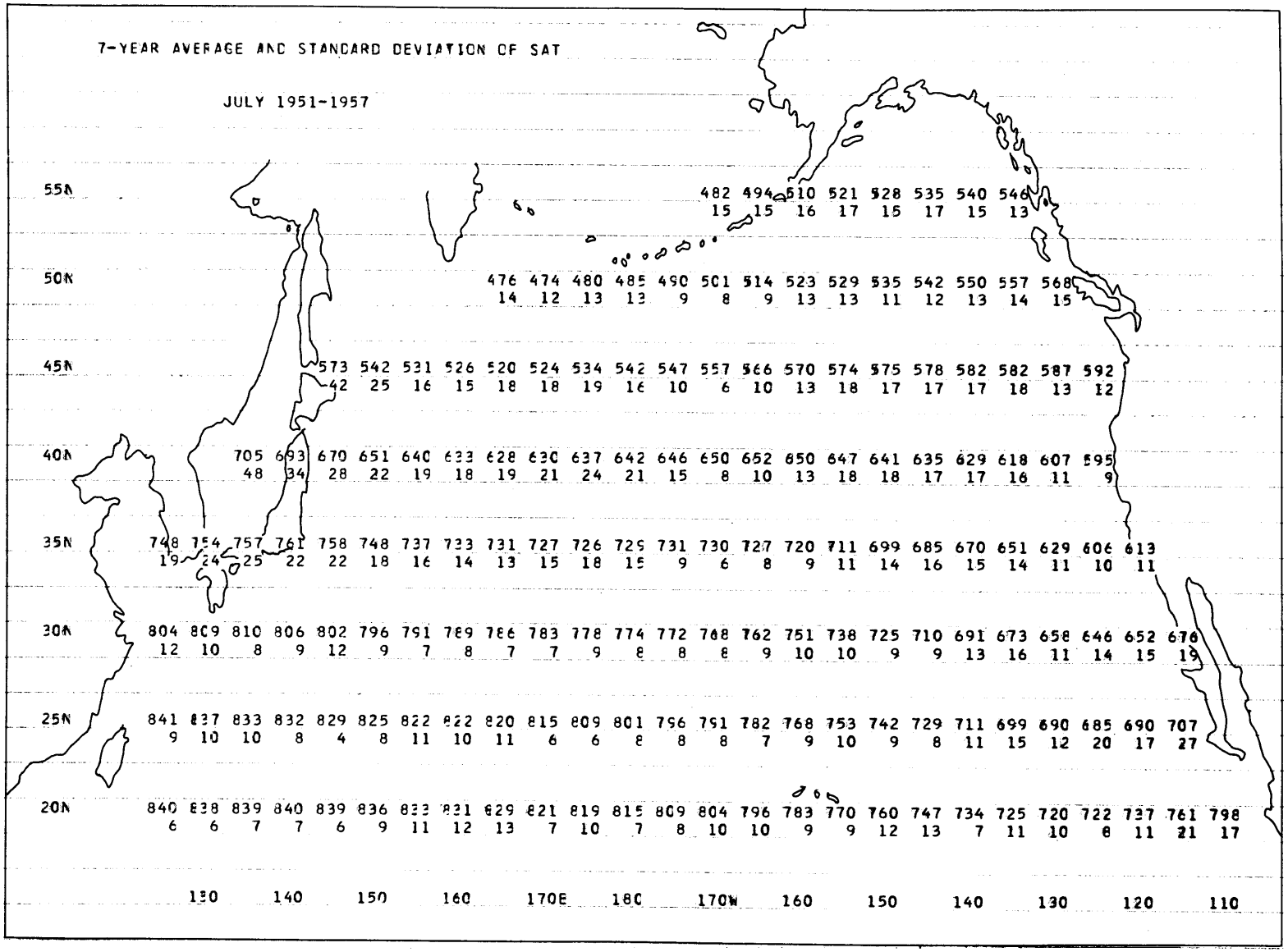

Figure A90. 7-year average values and standard deviations of the surface air temperature. July 1951-1957. (^{o}F x 10)

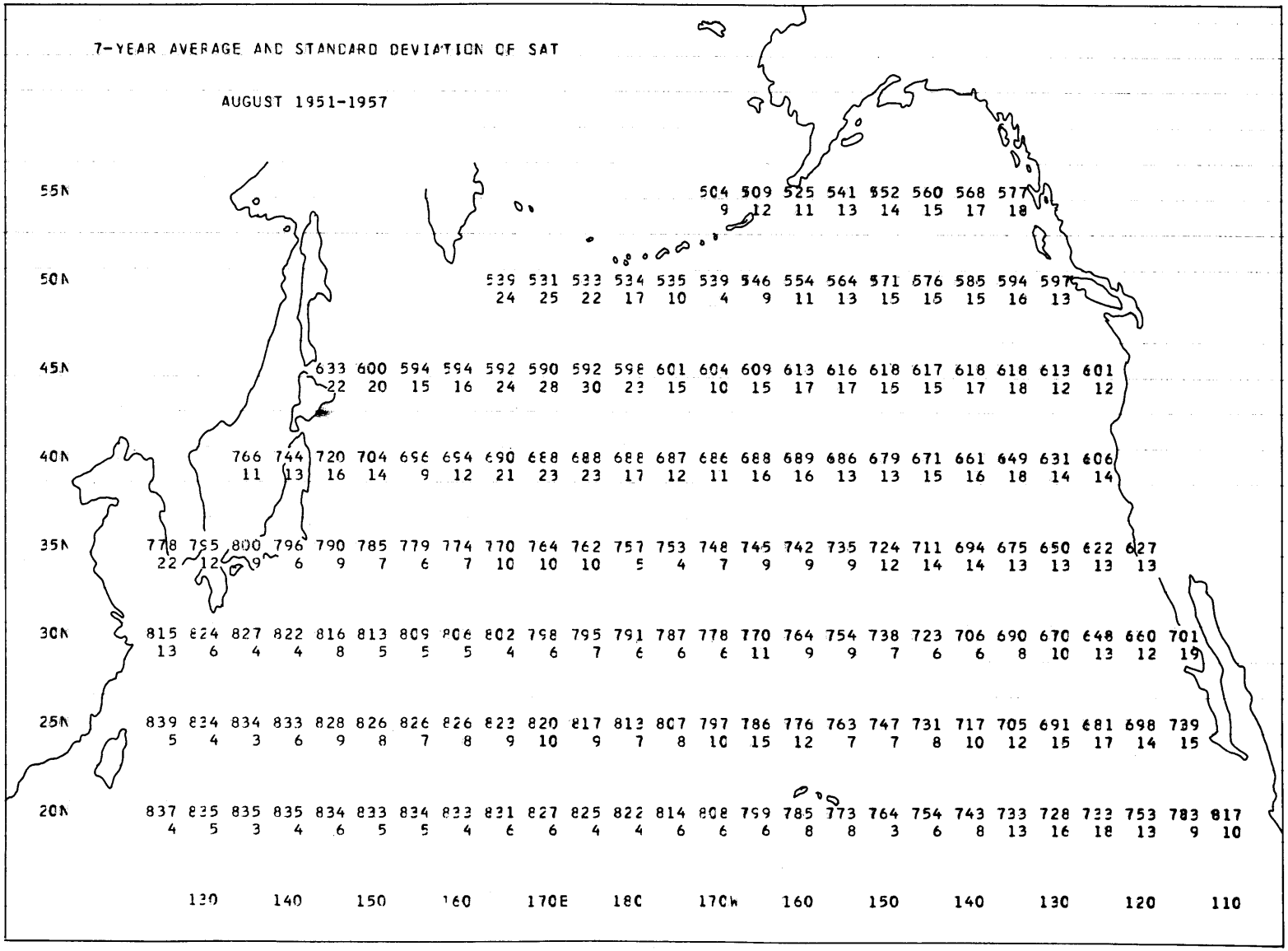

Figure A91. 7-year average values and standard deviations of the surface air temperature. August 1951-1957. (^{o}F x 10)

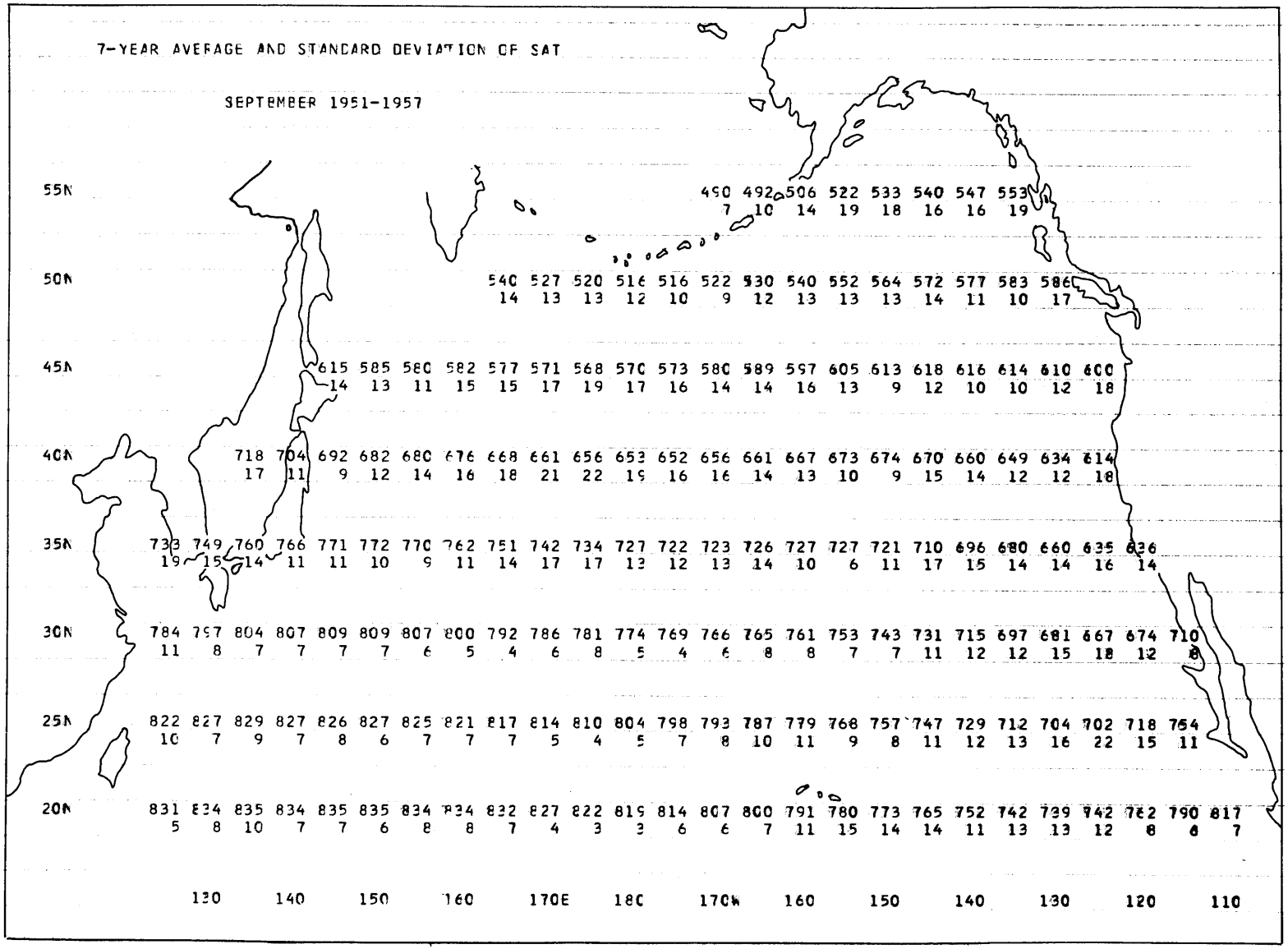

Figure A92. 7-year average values and standard deviations of the surface air temperature. September 1951-1957. (^{o}F x 10)

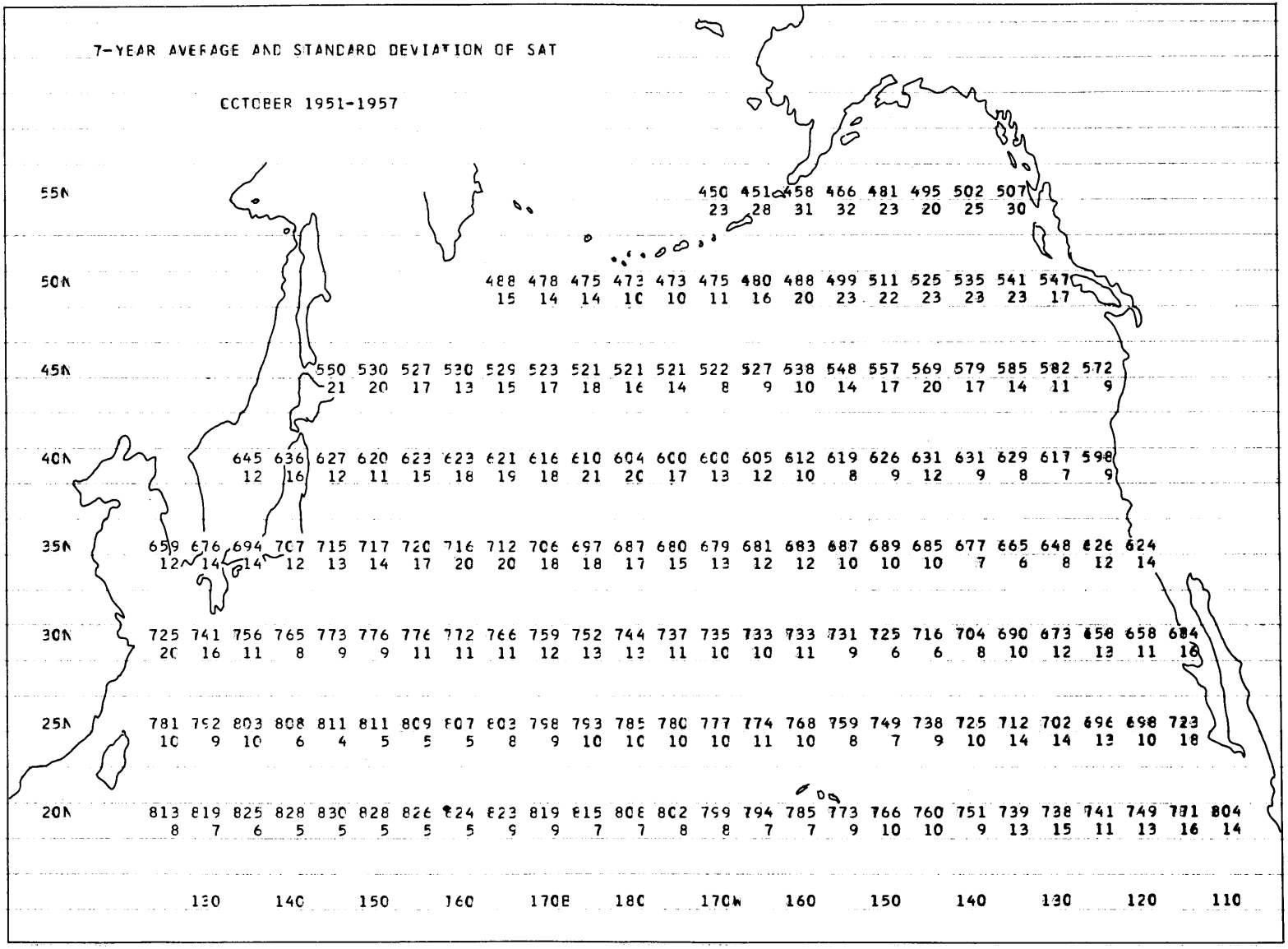

Figure A93. 7-year average values and standard deviations of the surface air temperature. October 1951-1957. (°F x 10)

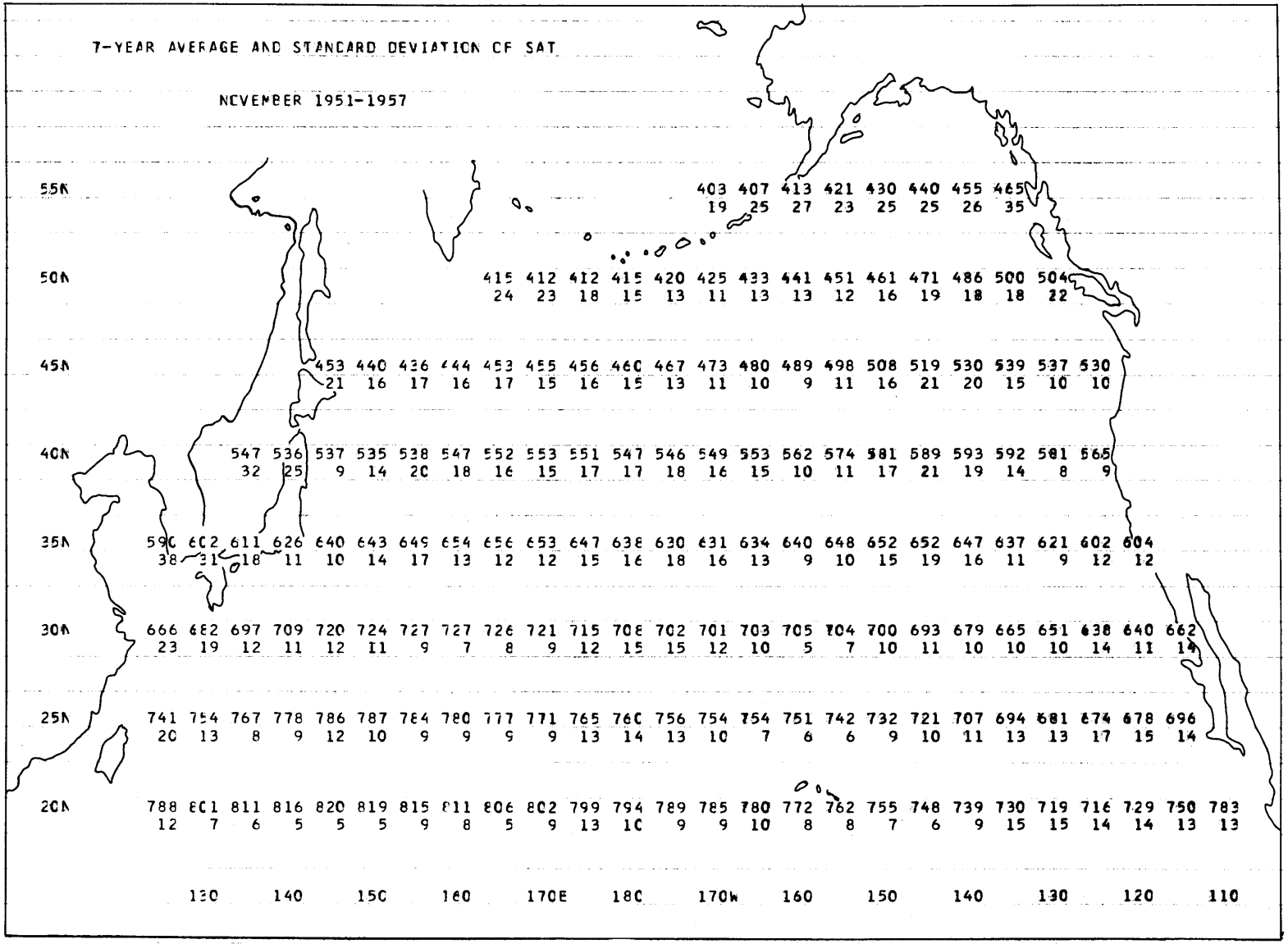

Figure A94. 7-year average values and standard deviations of the surface air temperature. November 1951-1957. (^{o}F x 10)

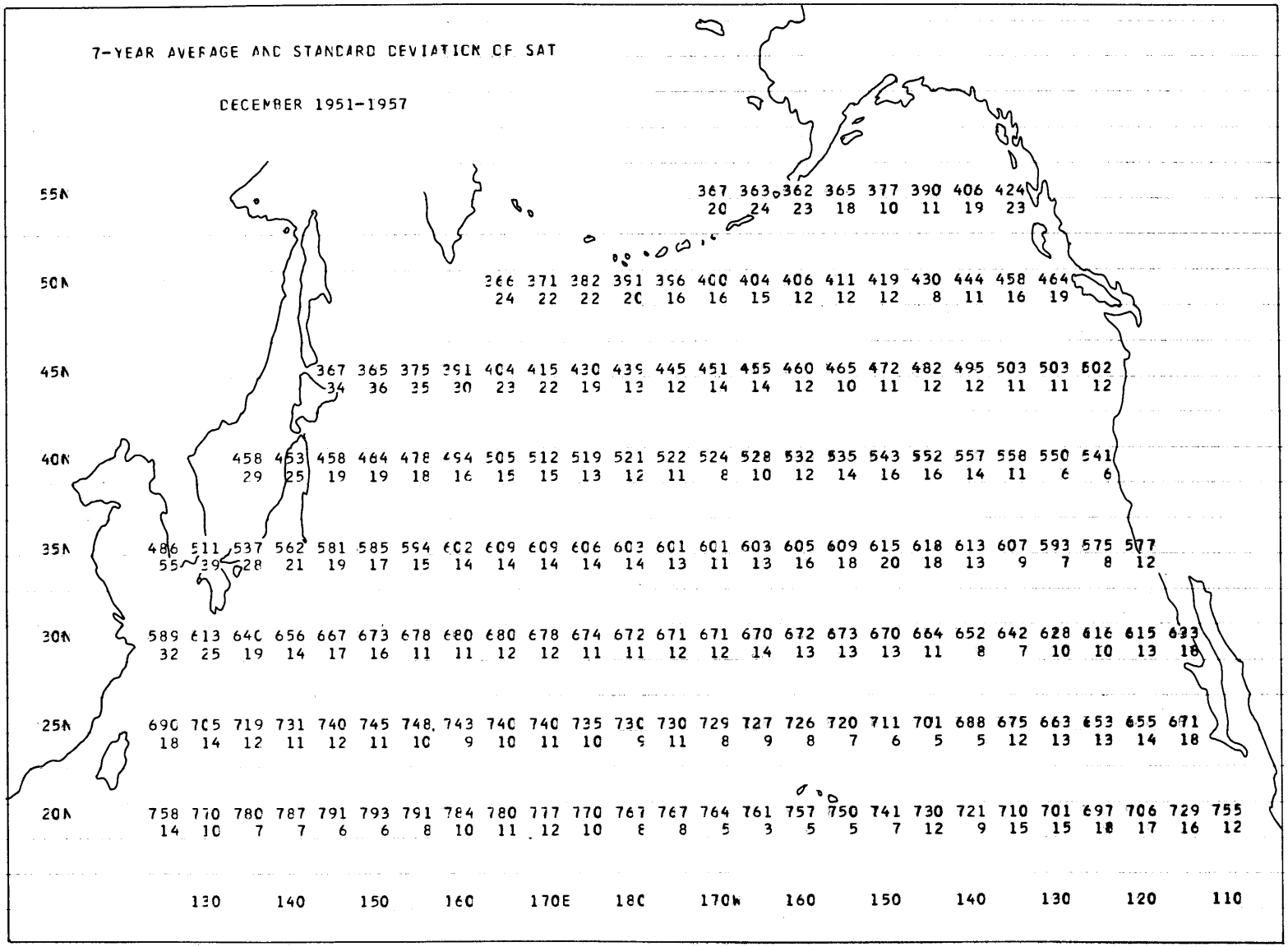

Figure A95. 7-year average values and standard deviations of the surface air temperature. December 1951-1957. (^{o}F x 10)

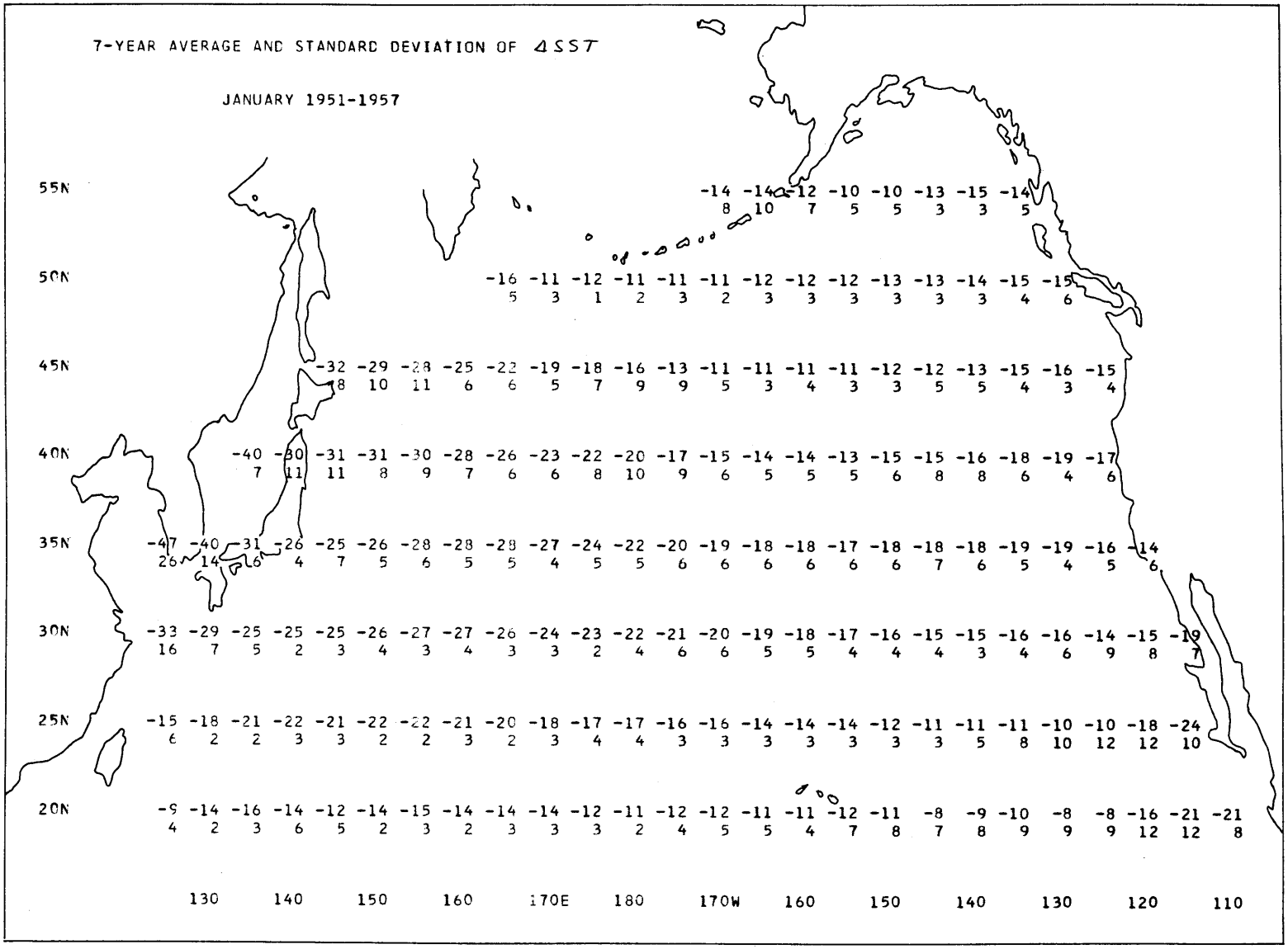

Figure A96. 7-year average values and standard deviations of the change in sea-surface temperature between months. January 1951-1957. (^{o}F x 10)

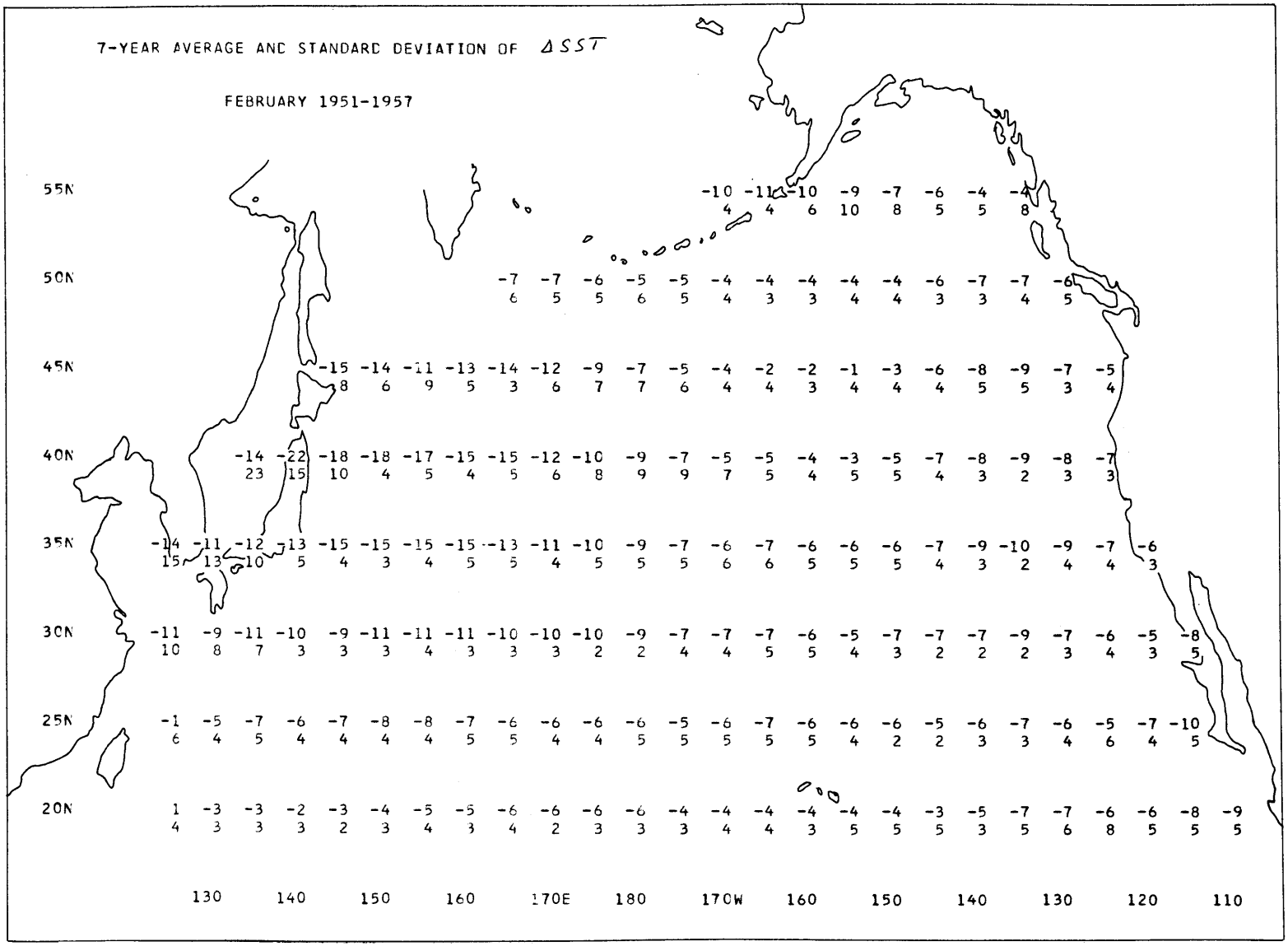

Figure A97. 7-year average values and standard deviations of the change in sea-surface temperature between months. February 1951-1957. (°F x 10)

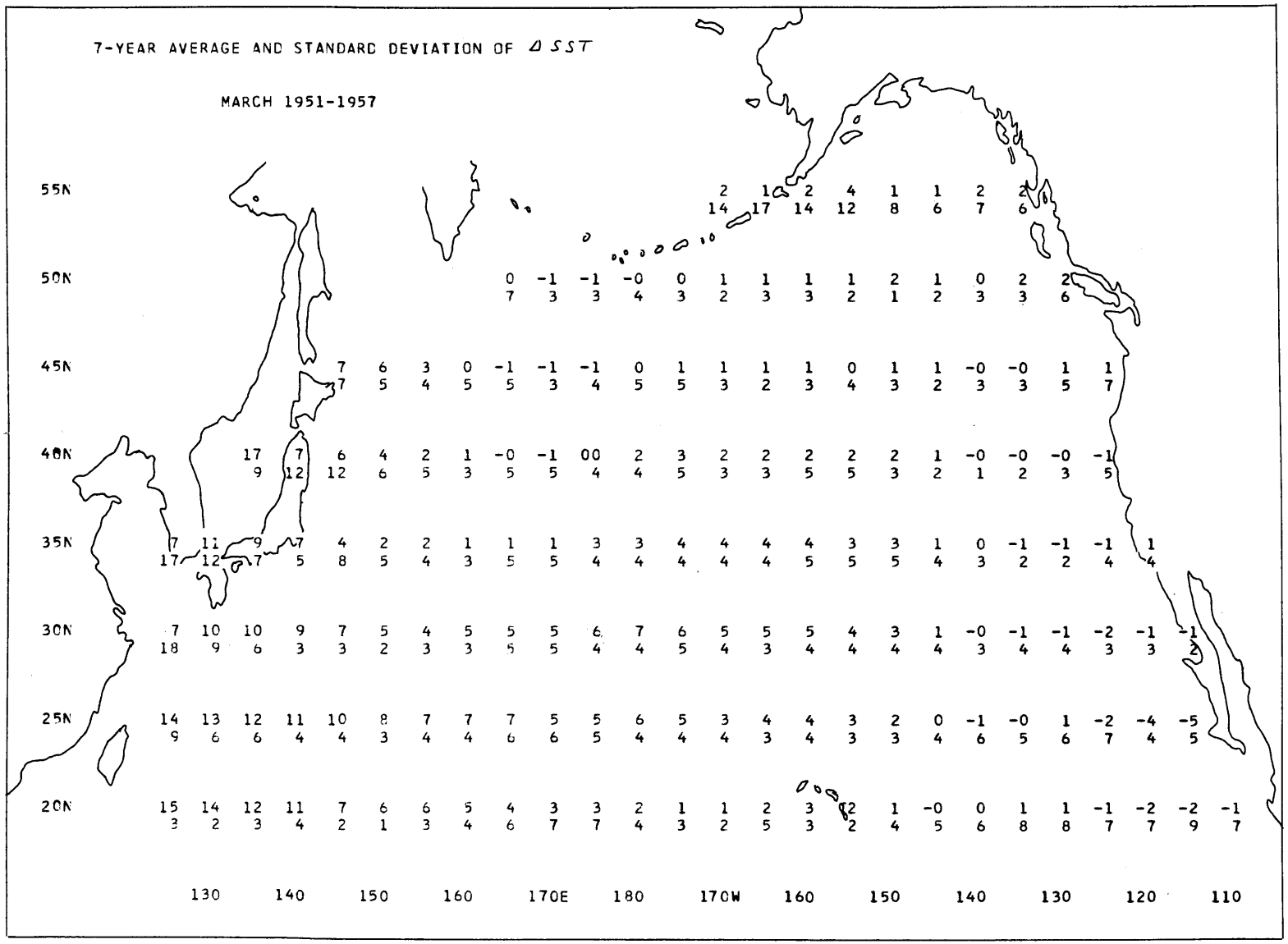

Figure A98. 7-year average values and standard deviations of the change in sea-surface temperature between months. March 1951-1957. (^{o}F x 10)

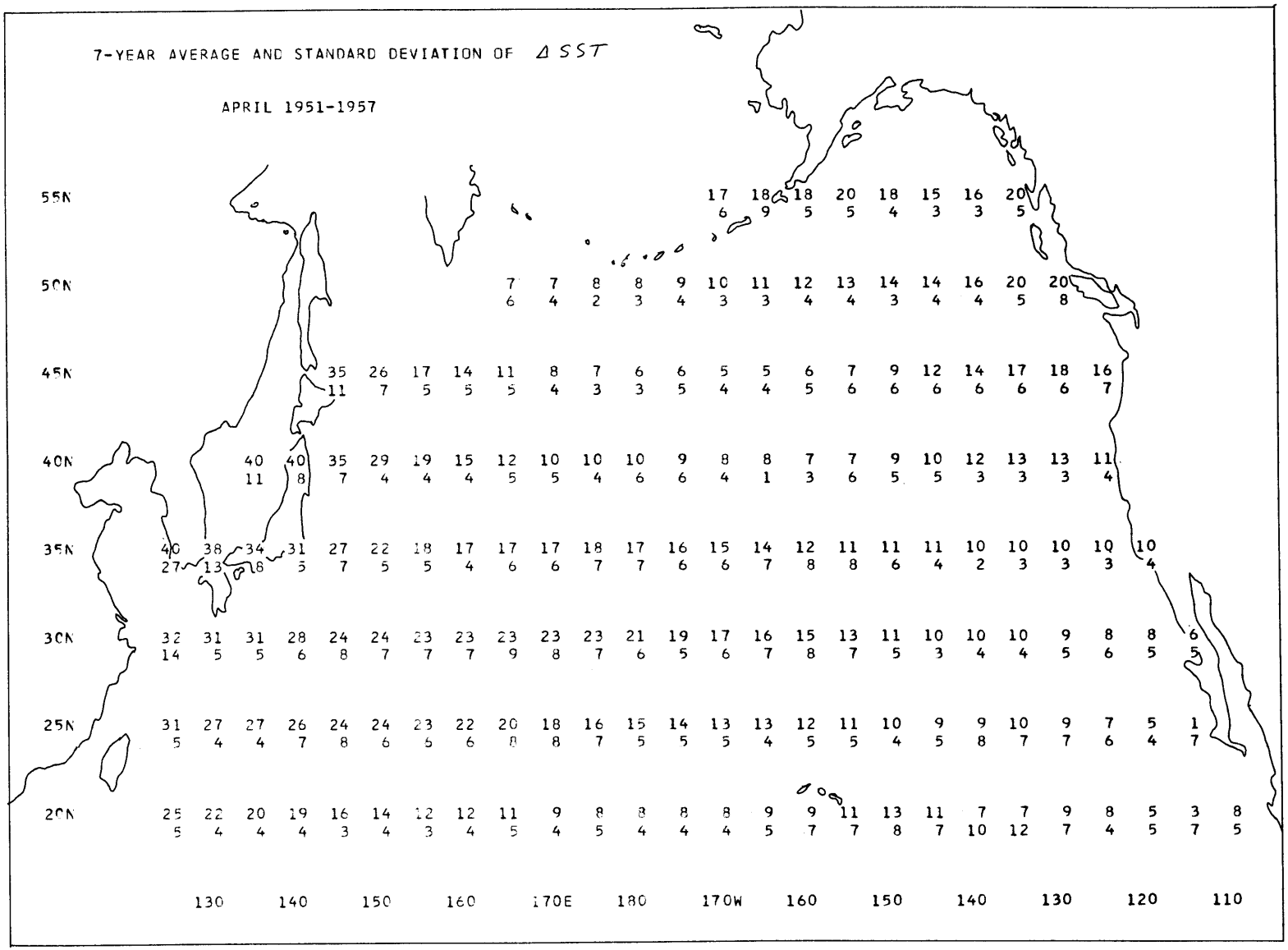

Figure A99. 7-year average values and standard deviations of the change in sea-surface temperature between months. April 1951-1957. (^{o}F x 10)

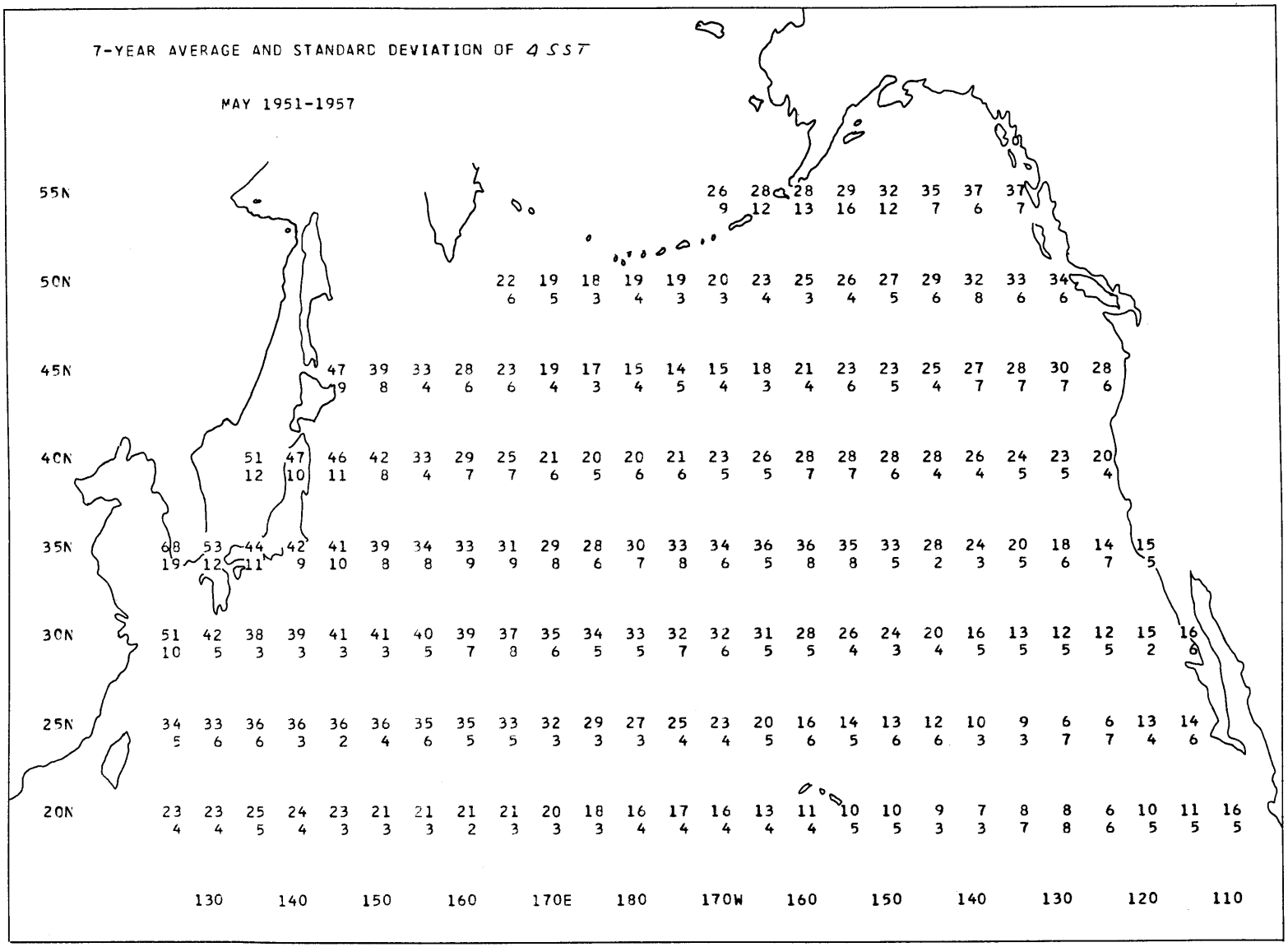

Figure A100. 7-year average values and standard deviations of the change in sea-surface temperature between months. May 1951-1957. (^{o}F x 10)

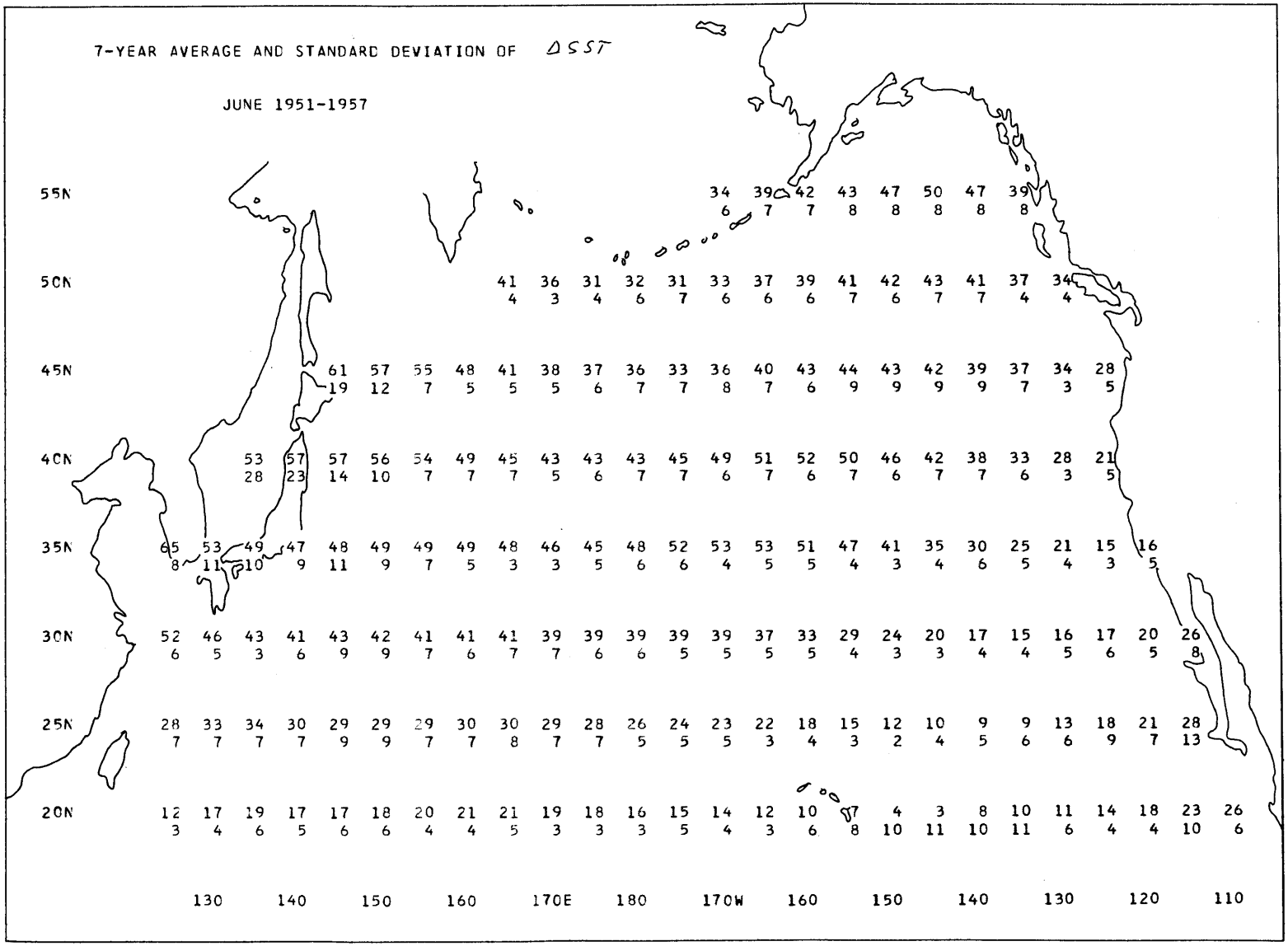

Figure A101. 7-year average values and standard deviations of the change in sea-surface temperature between months. June 1951-1957. (^{o}F x 10)

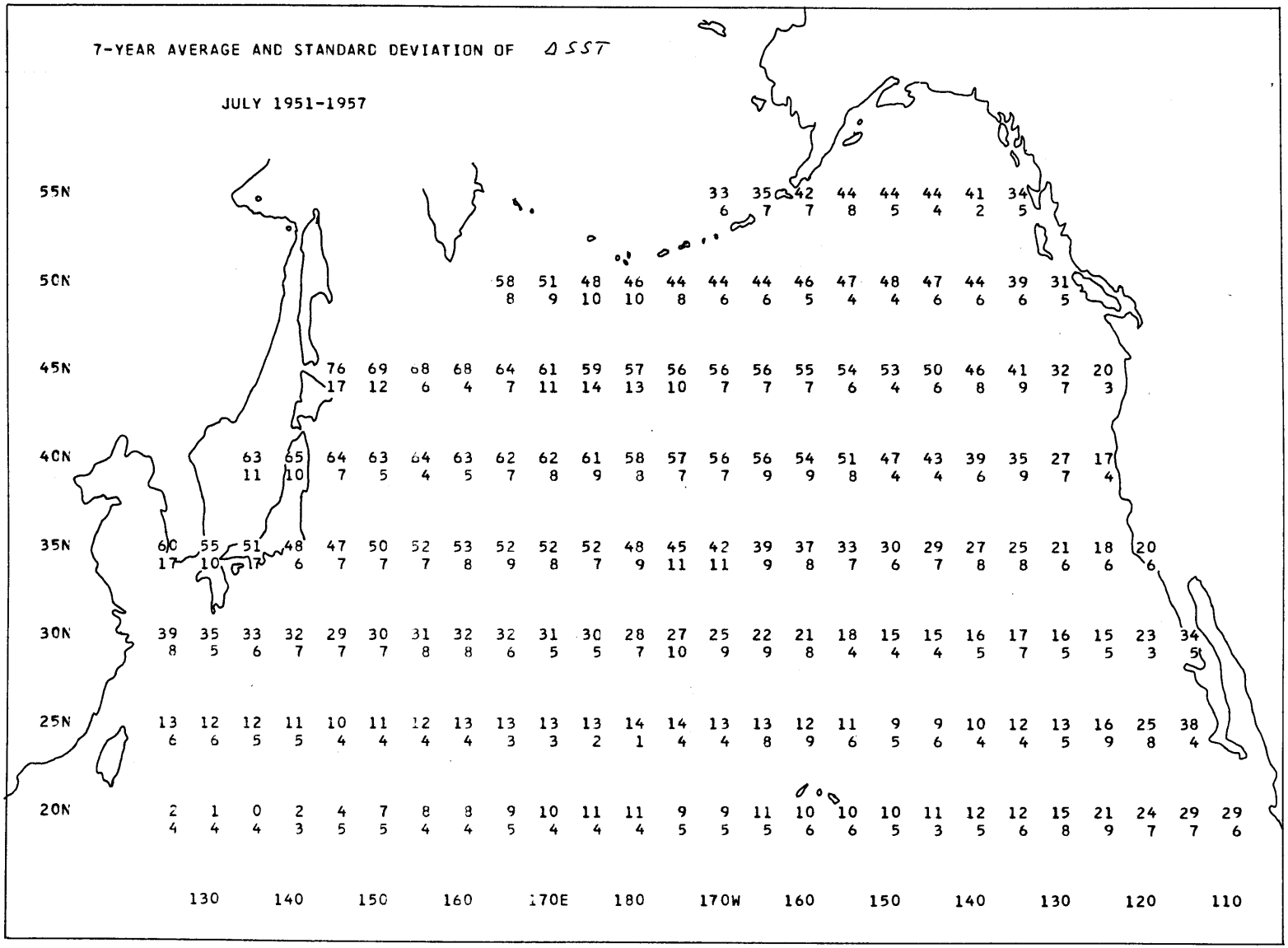

Figure A102. 7-year average values and standard deviations of the change in sea-surface temperature between months. July 1951-1957. (^{o}F x 10)

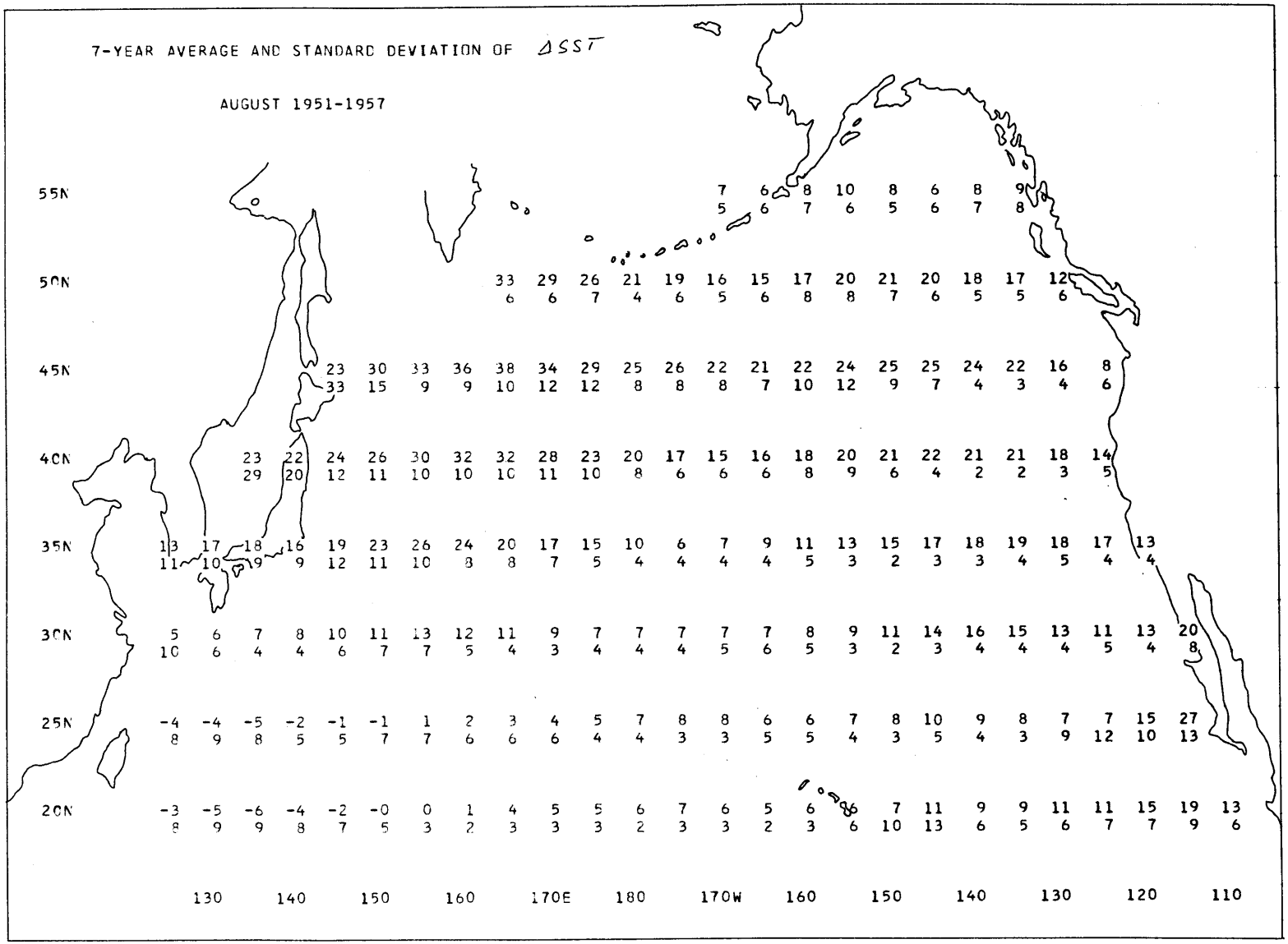

Figure A103. 7-year average values and standard deviations of the change in sea-surface temperature between months. August 1951-1957. (^{o}F x 10)

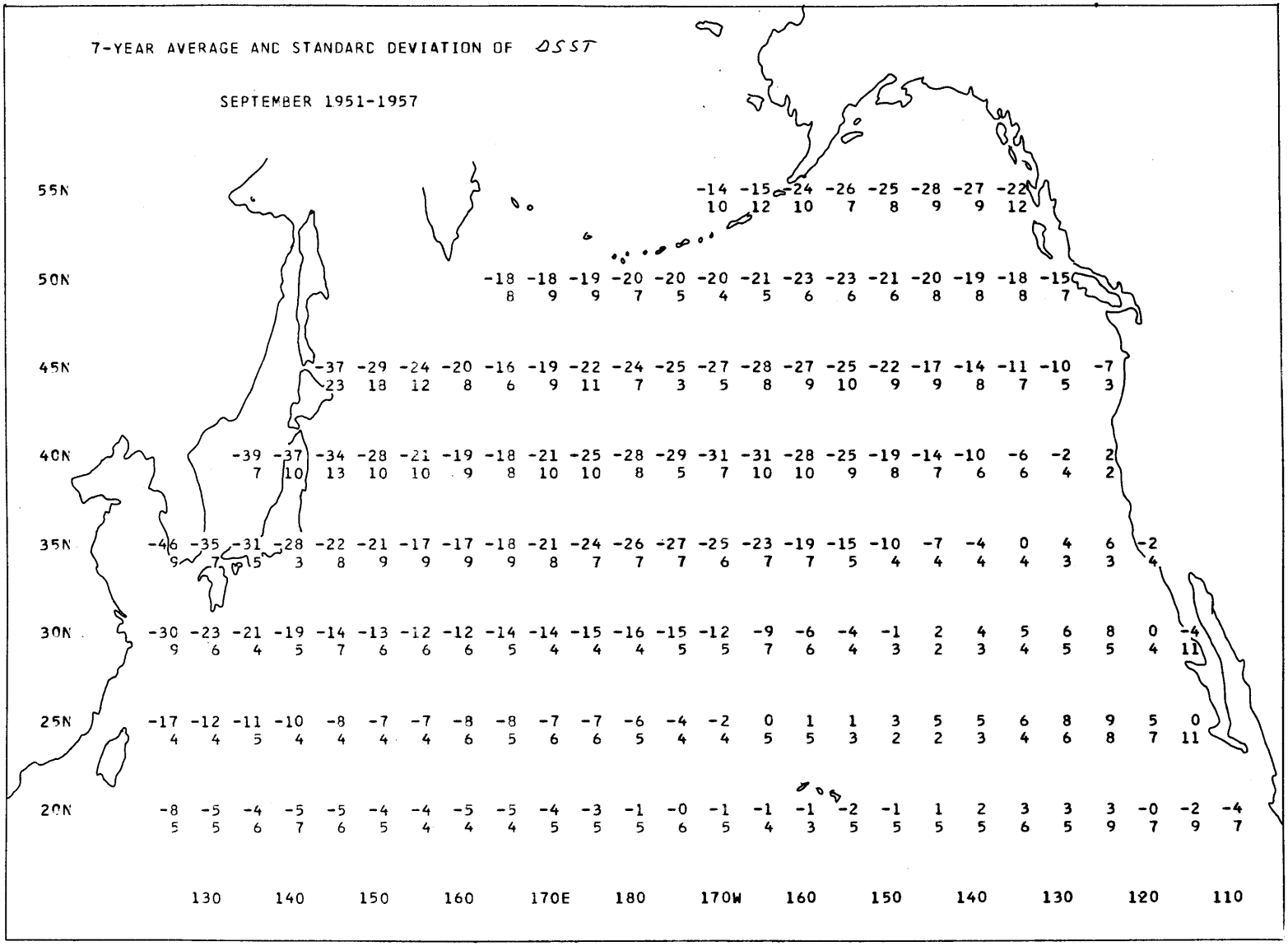

Figure A104. 7-year average values and standard deviations of the change in sea-surface temperature between months. September 1951-1957. (^{o}F x 10)

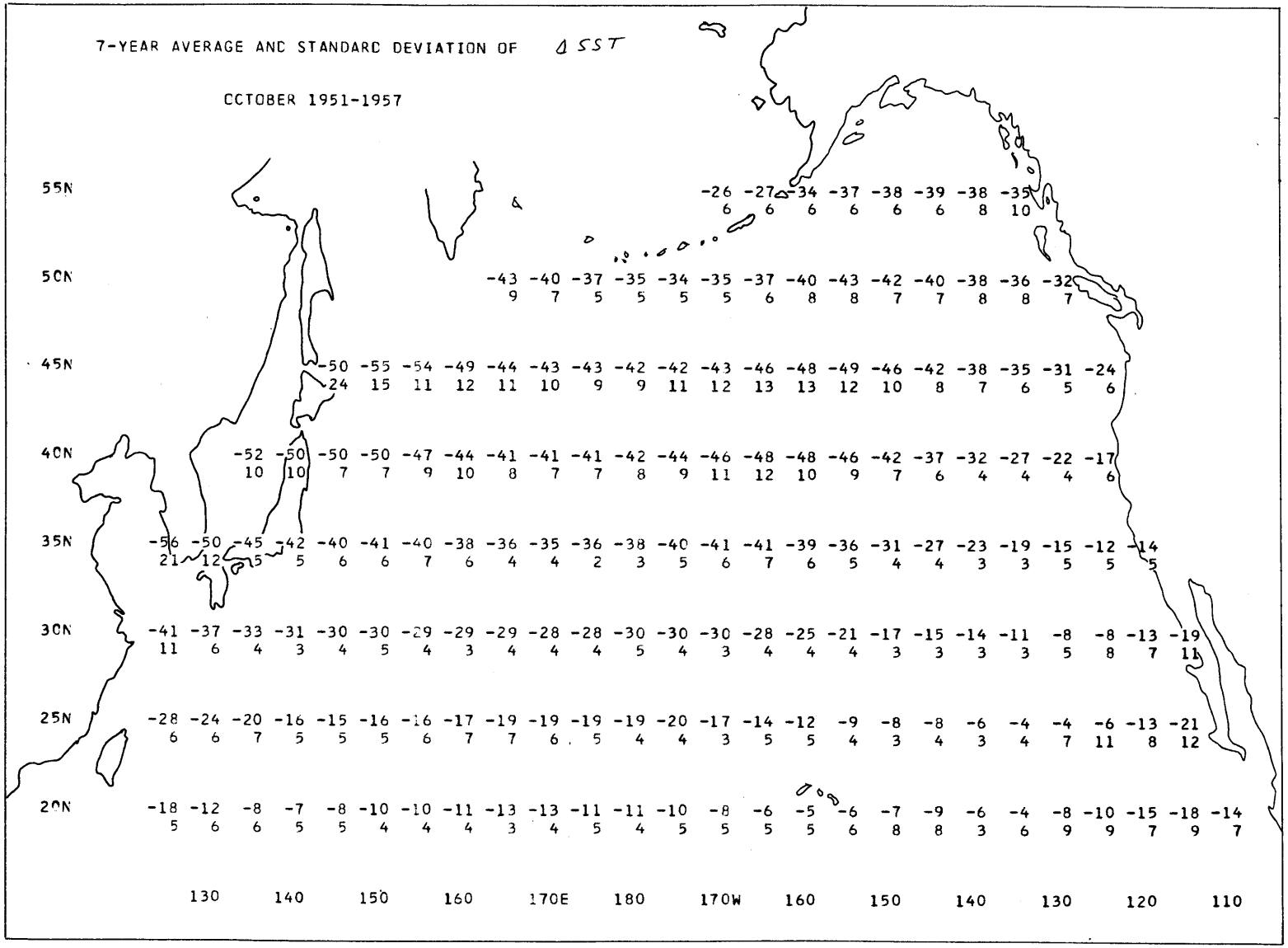

Figure A105. 7-year average values and standard deviations of the change in sea-surface temperature between months. October 1951-1957. (^{o}F x 10)

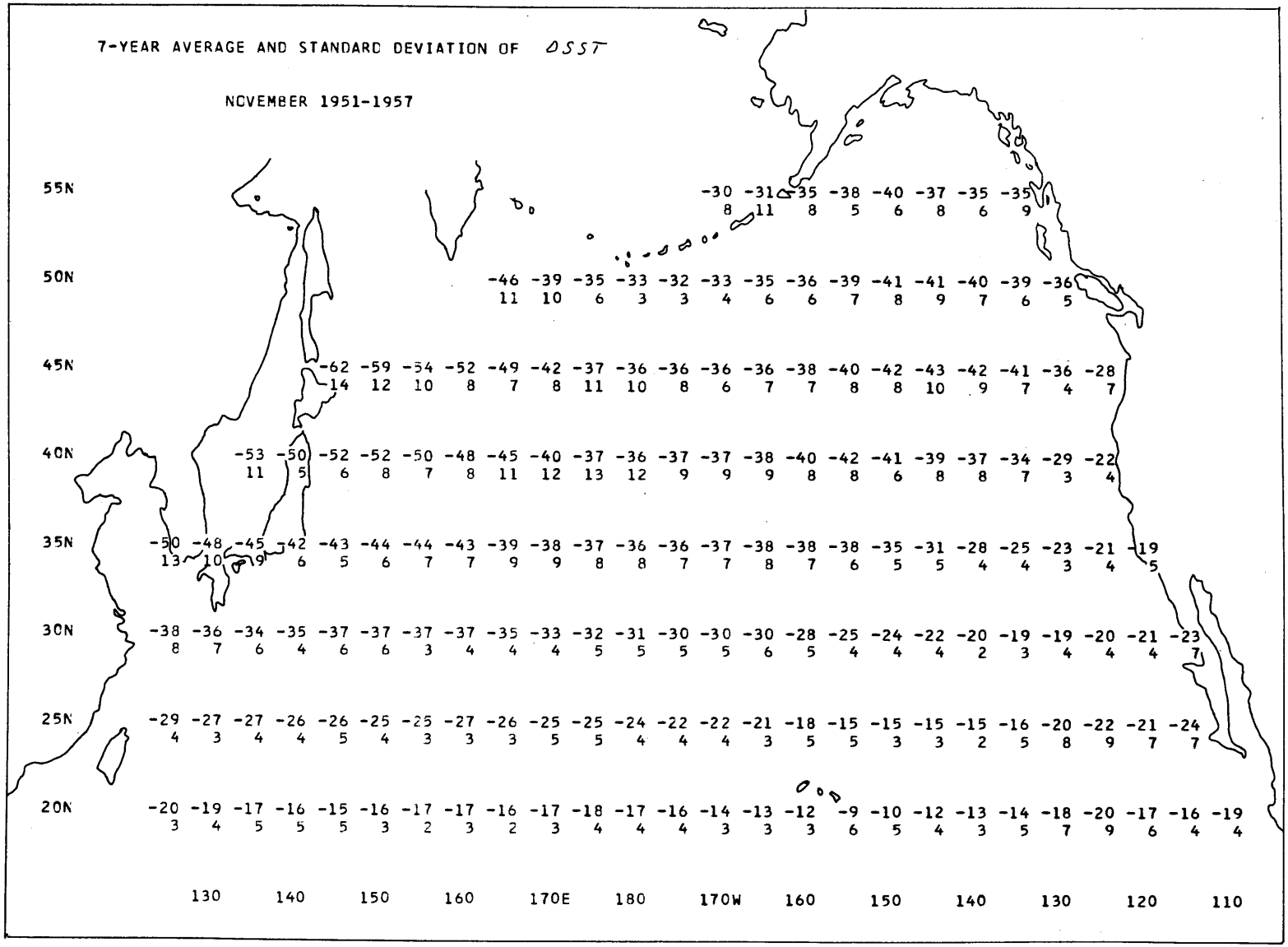

Figure A106. 7-year average values and standard deviations of the change in sea-surface temperature between months. November 1951-1957. (^{o}F x 10)

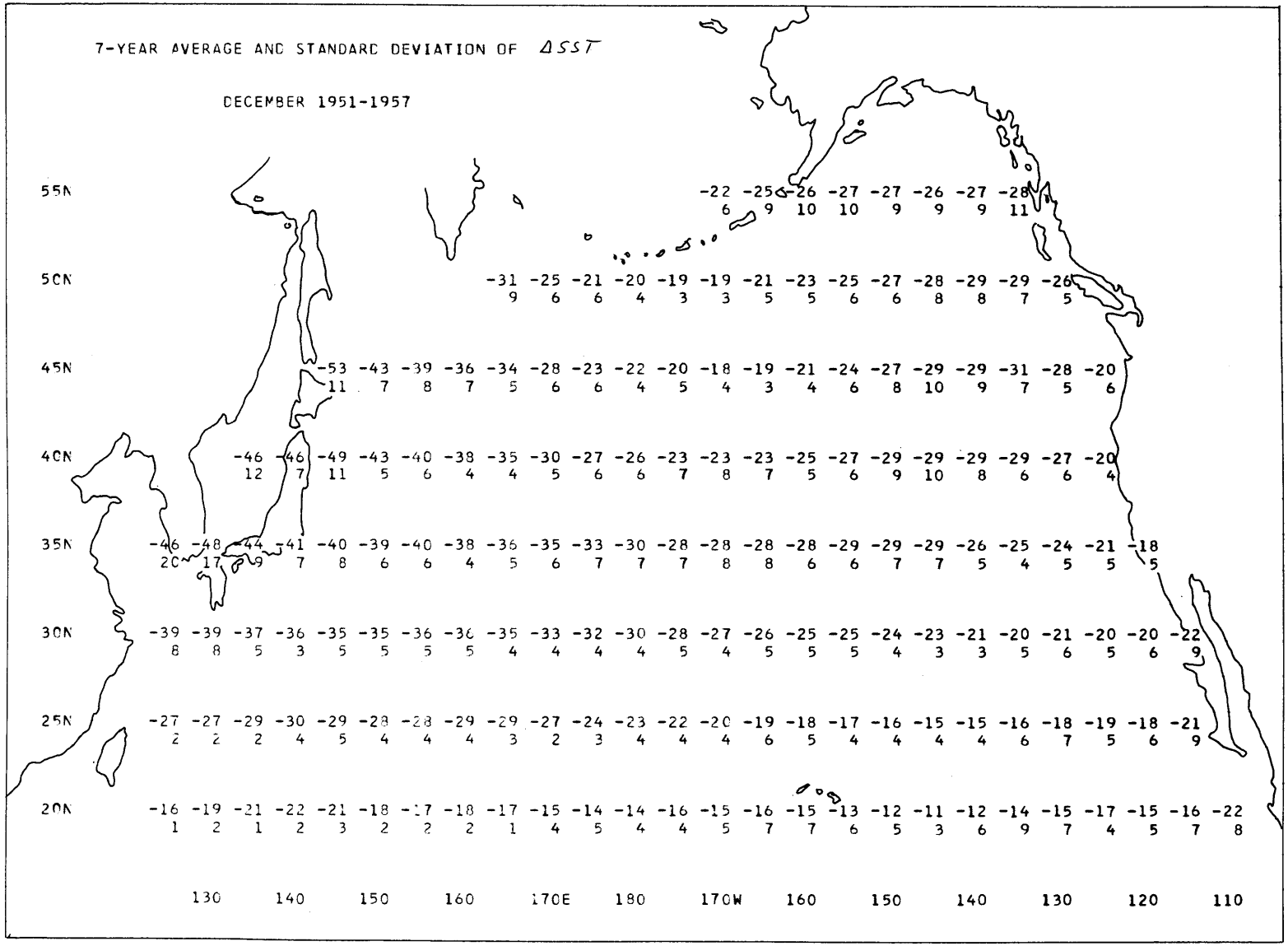

Figure A107. 7-year average values and standard deviations of the change in sea-surface temperature between months. December 1951-1957. (^{o}F x 10)

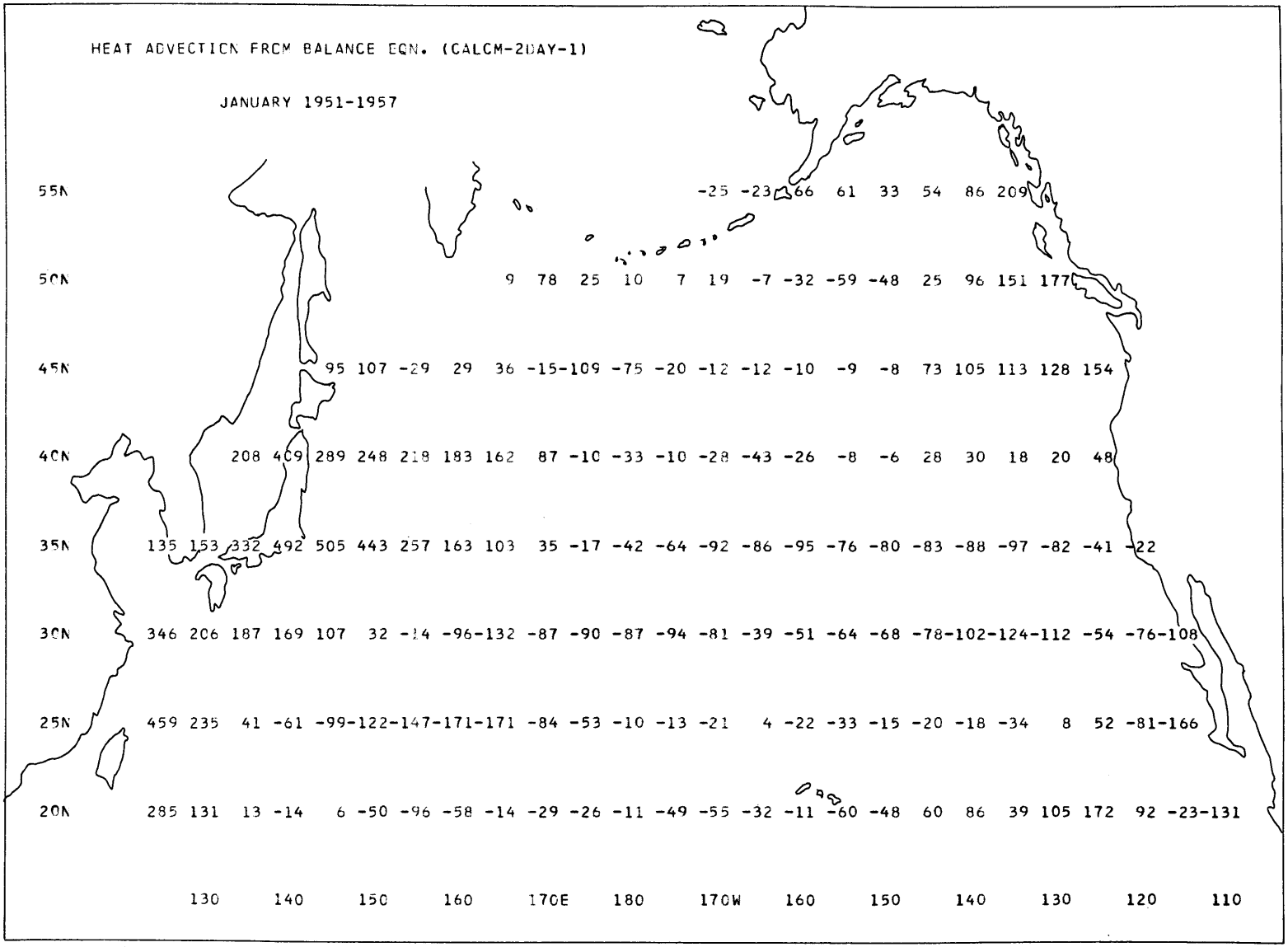

Figure A108. 7-year average values of heat advection determined from the heat balance equation. January 1951-1957. (cal/cm^2/day)

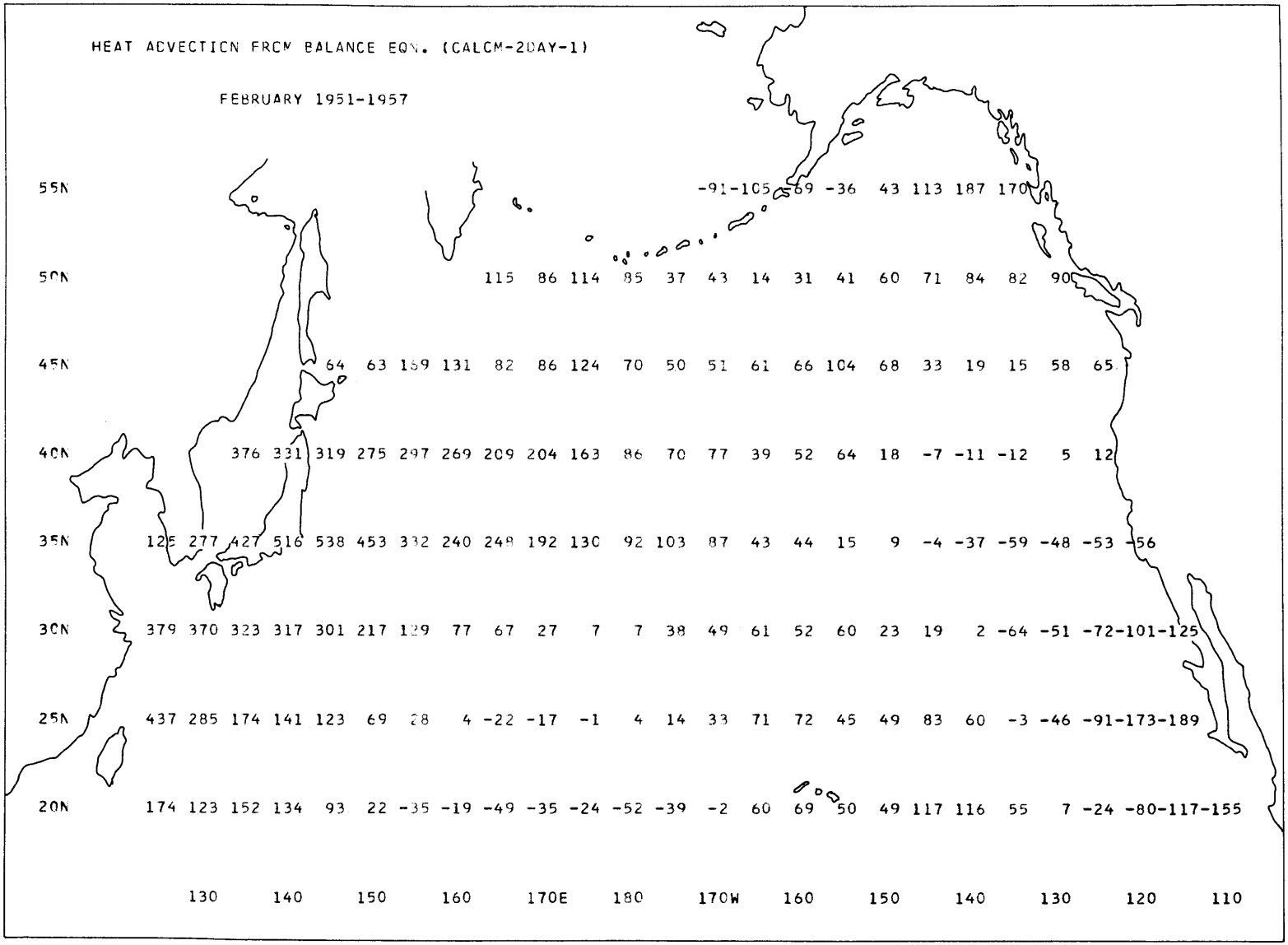

Figure A109. 7-year average values of heat advection determined from the heat balance equation. February 1951-1957. (cal/cm^2/day)

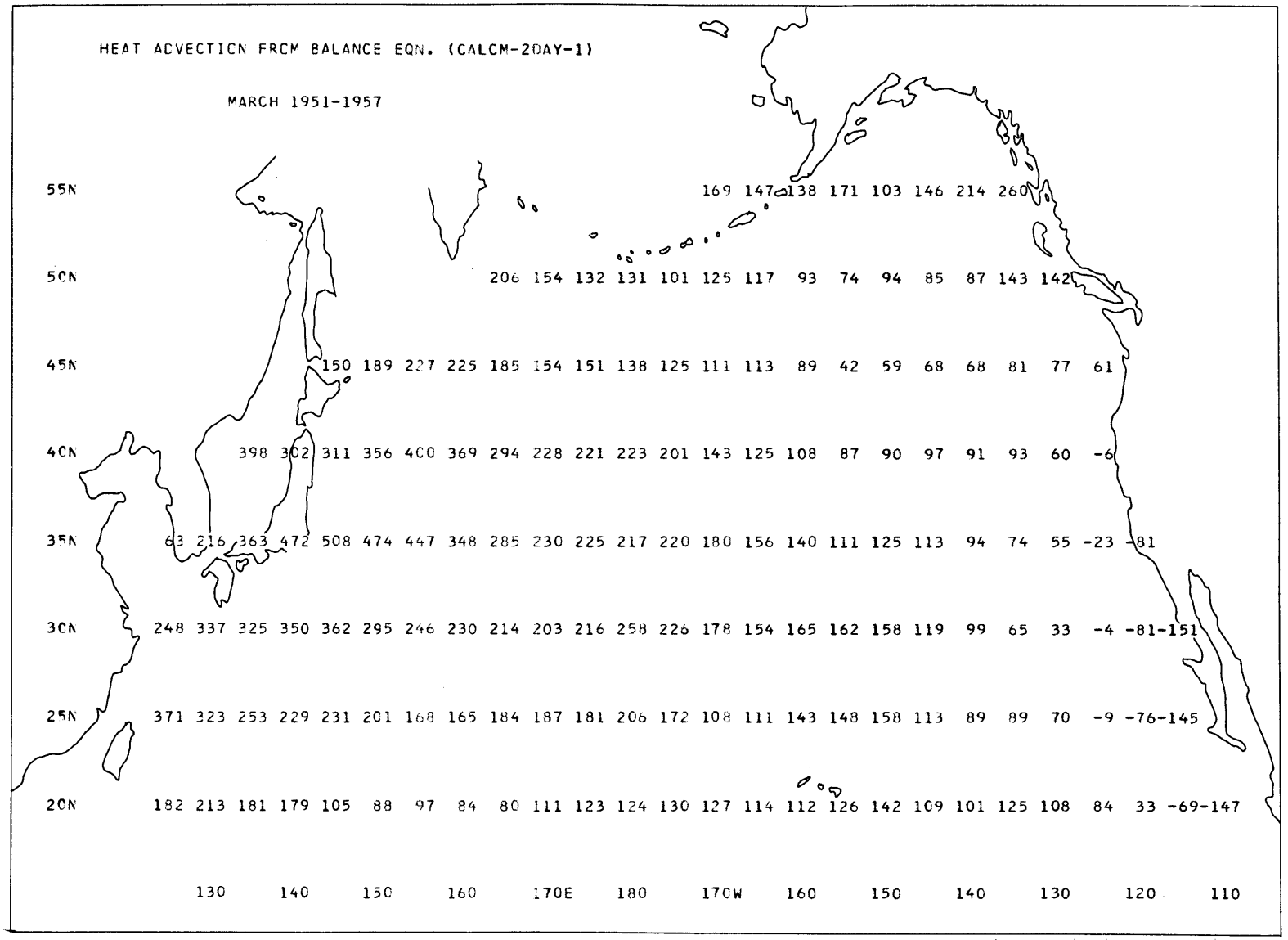

Figure A110. 7-year average values of heat advection determined from the heat balance equation. March 1951-1957. (cal/cm^2/day)

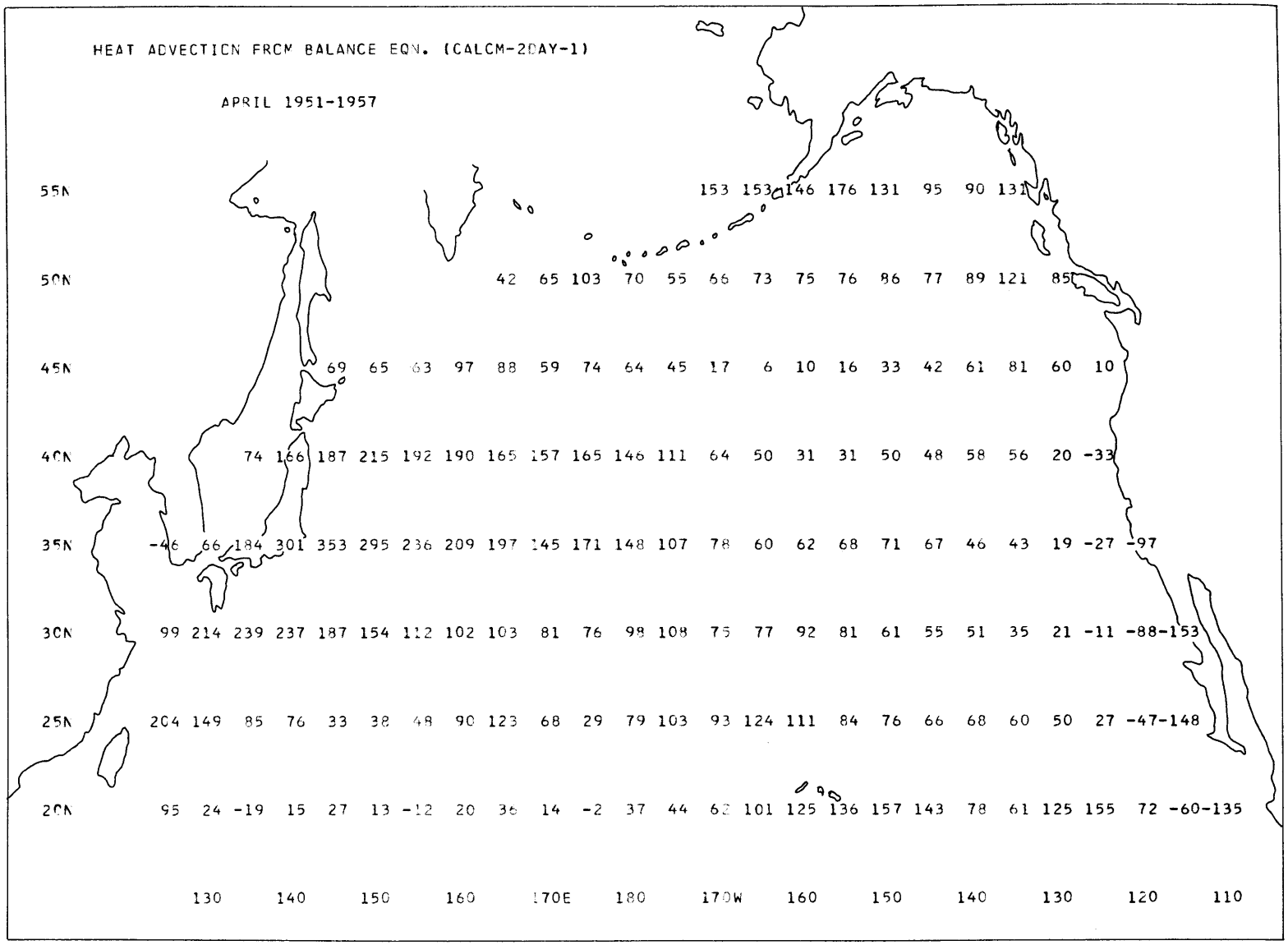

Figure A111. 7-year average values of heat advection determined from the heat balance equation. April 1951-1957. (cal/cm^2/day)

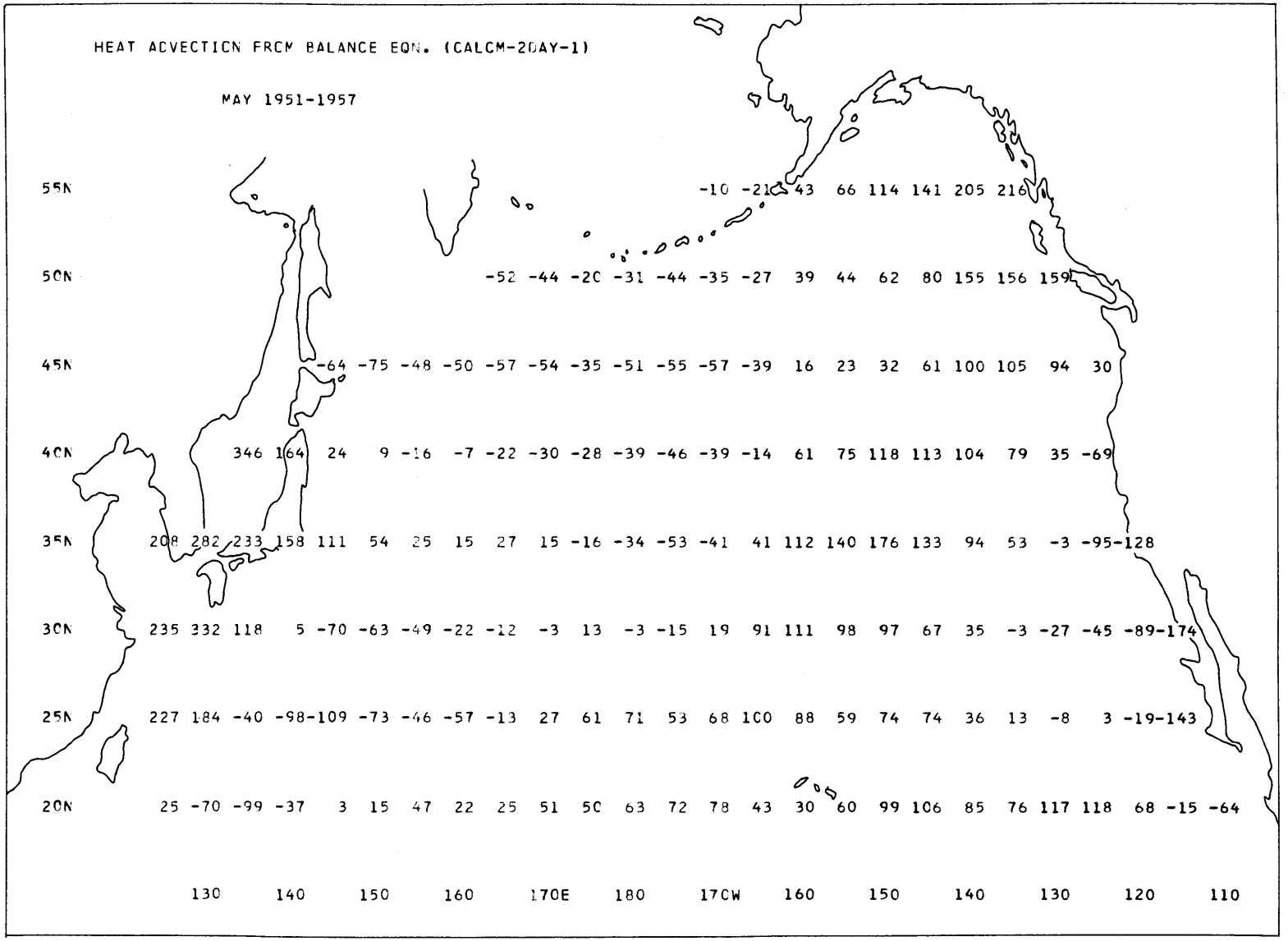

Figure A112. 7-year average values of heat advection determined from the heat balance equation. May 1951-1957. (cal/cm^2/day)

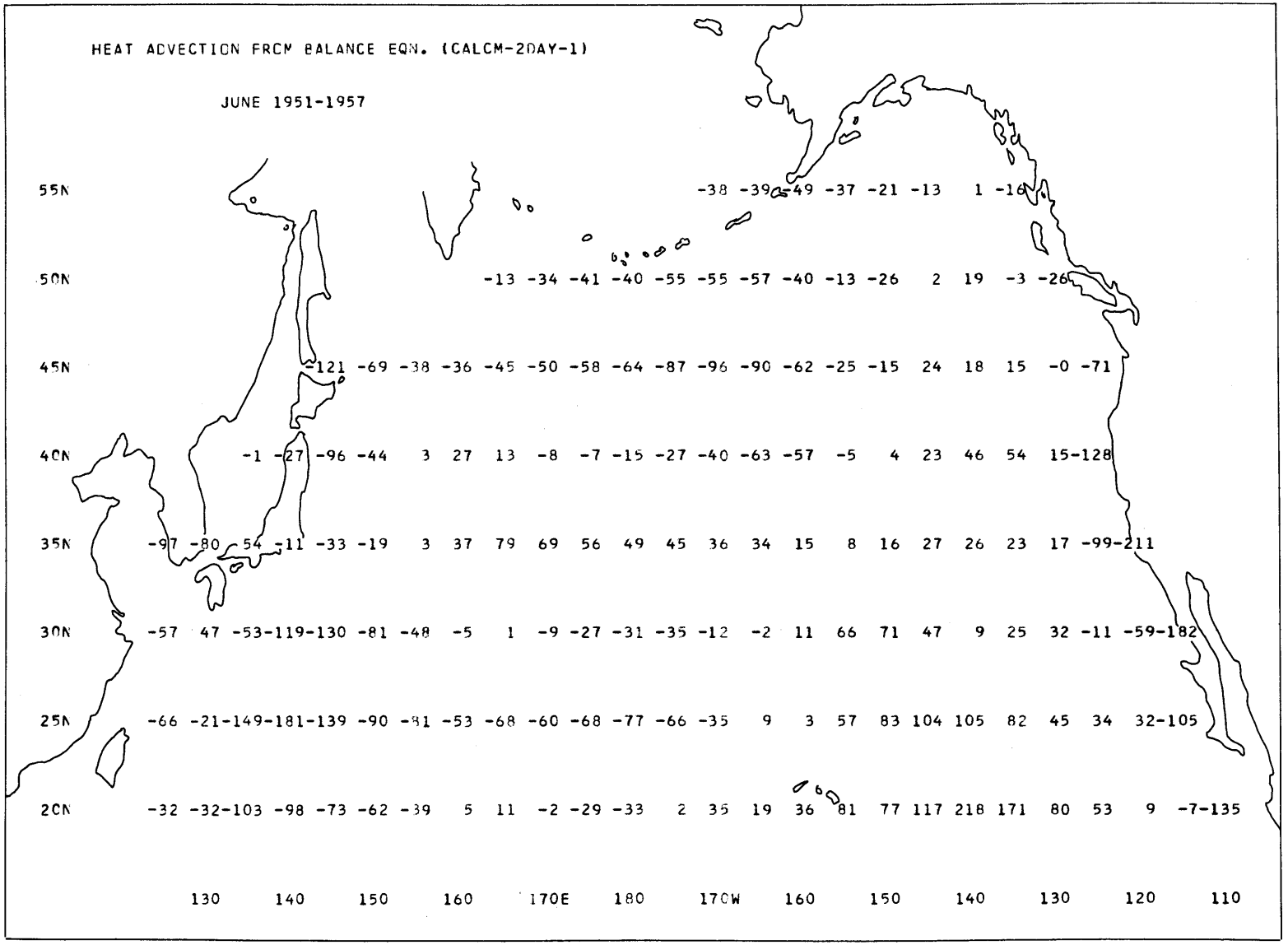

Figure A113. 7-year average values of heat advection determined from the heat balance equation. June 1951-1957. (cal/cm^2/day)

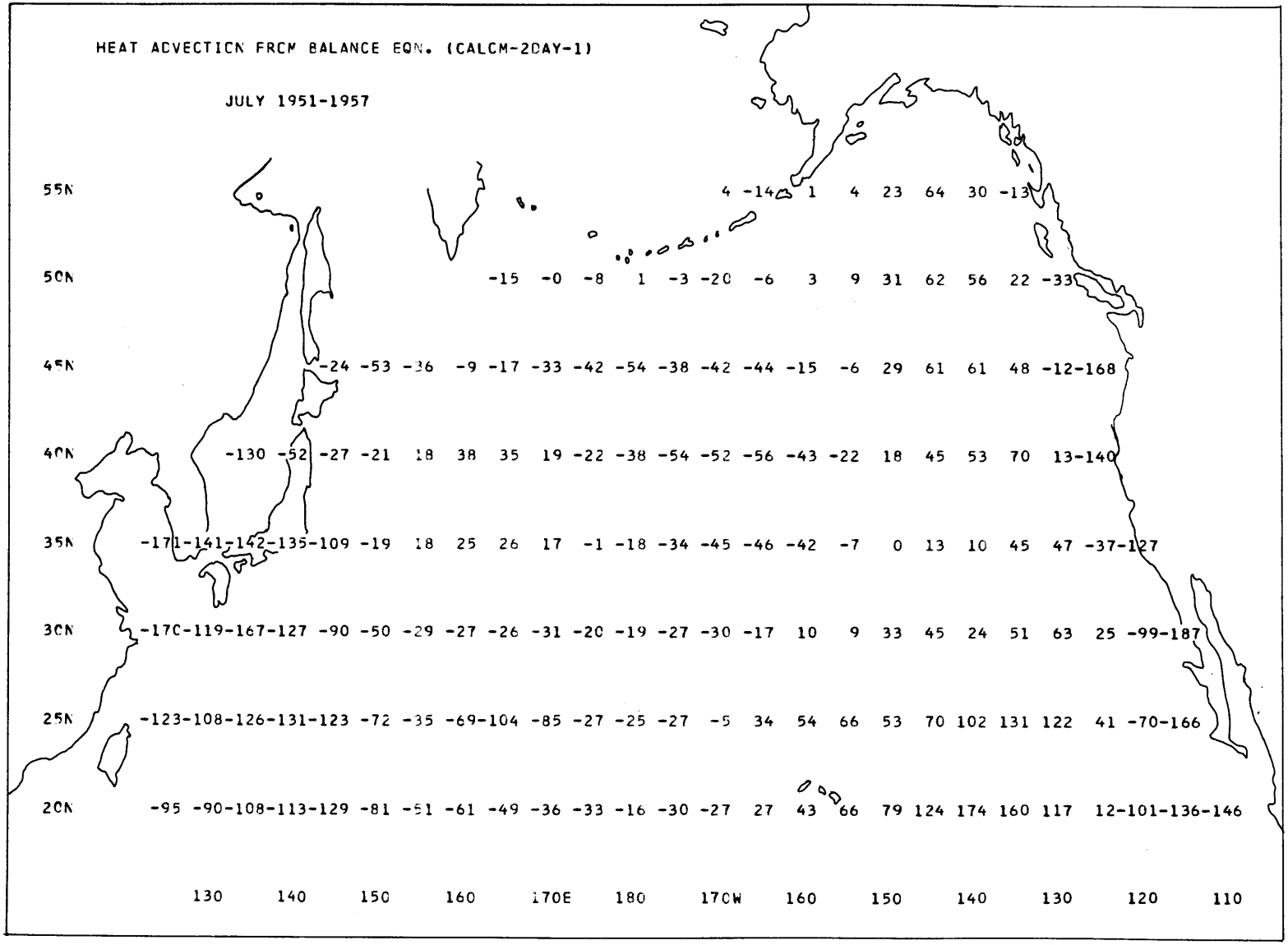

Figure A114. 7-year average values of heat advection determined from the heat balance equation. July 1951-1957. (cal/cm^2/day)

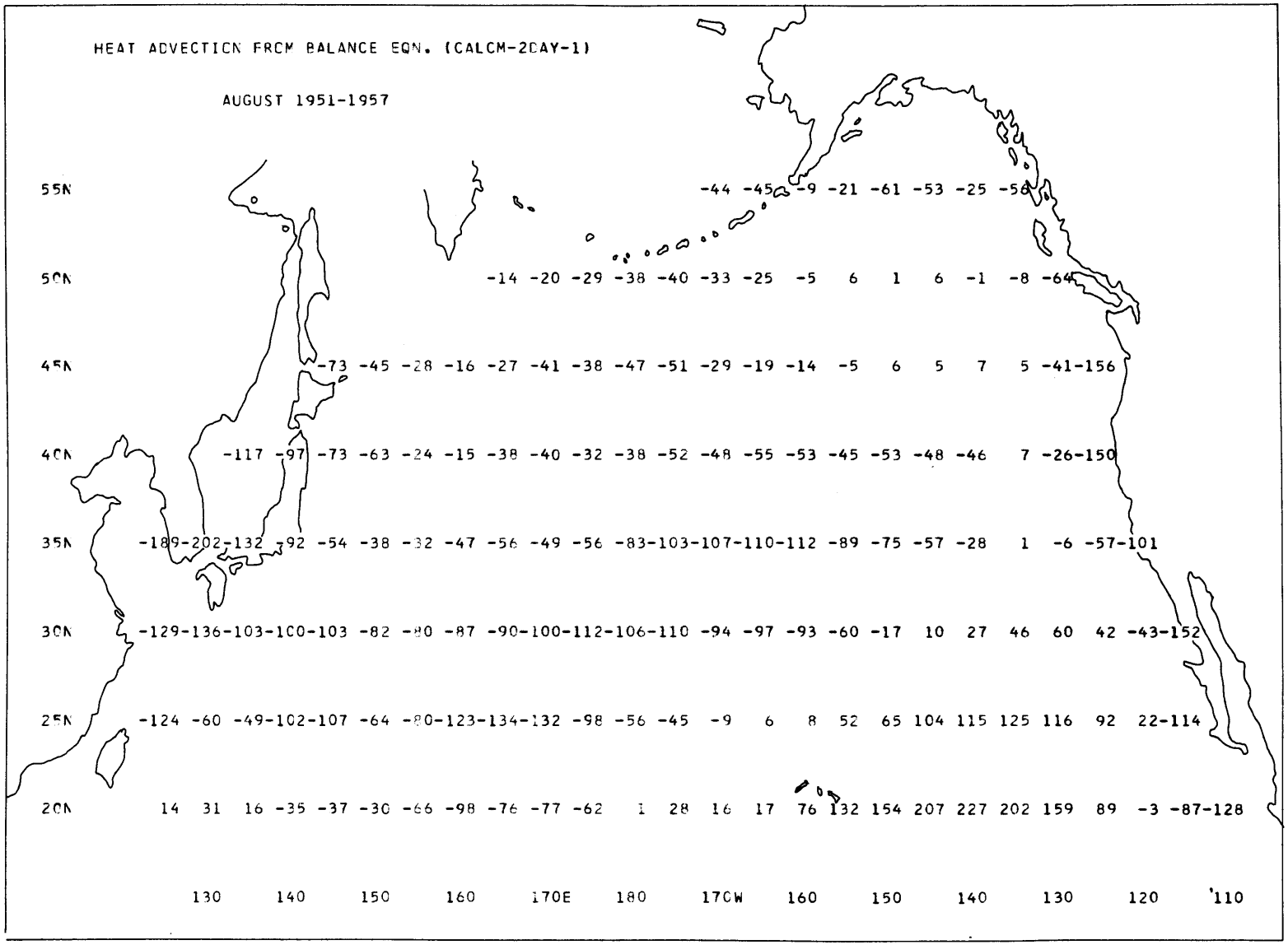

Figure A115. 7-year average values of heat advection determined from the heat balance equation. August 1951-1957. (cal/cm^2/day)

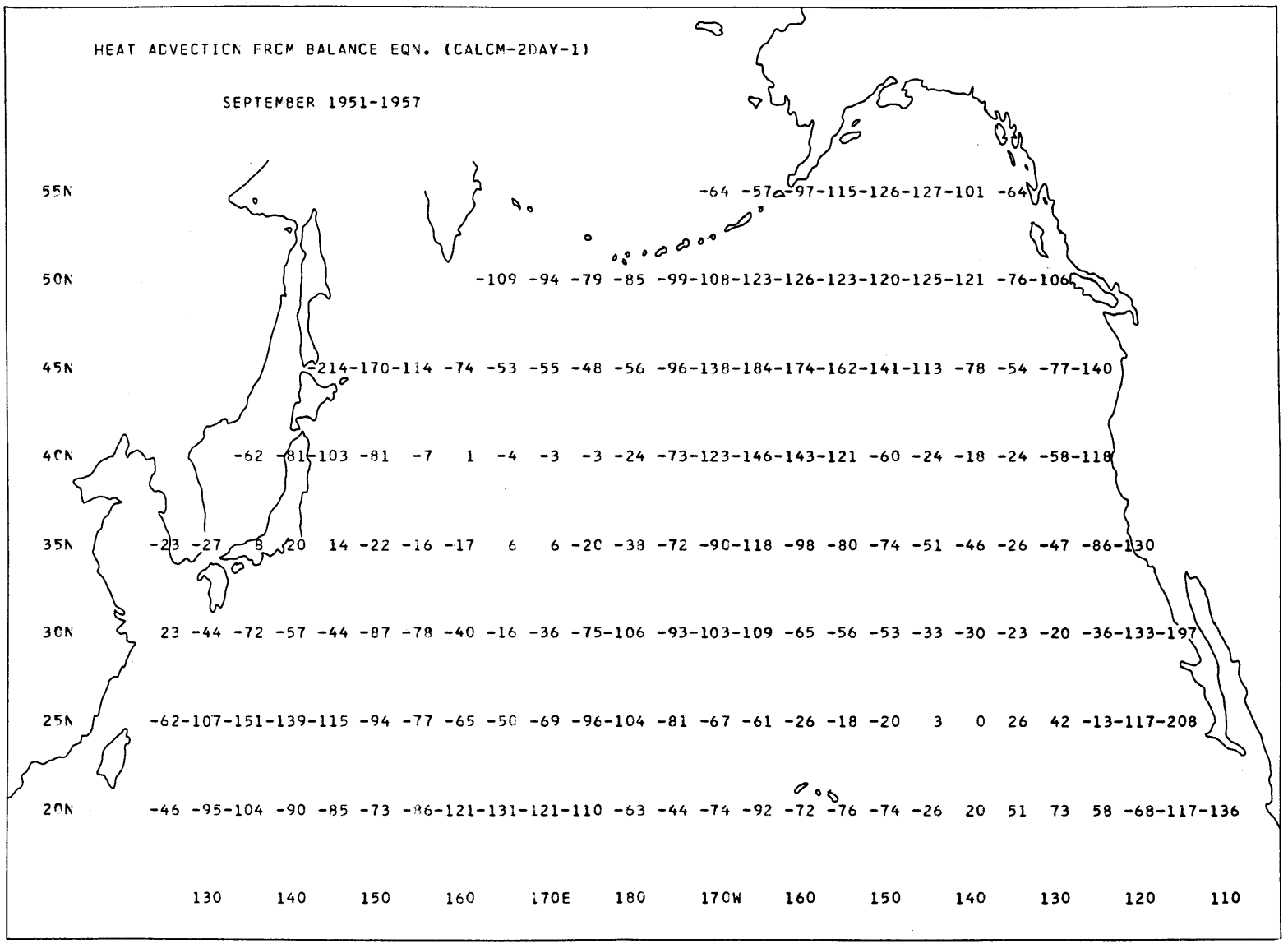

Figure A116. 7-year average values of heat advection determined from the heat balance equation. September 1951-1957. (cal/cm^2/day)

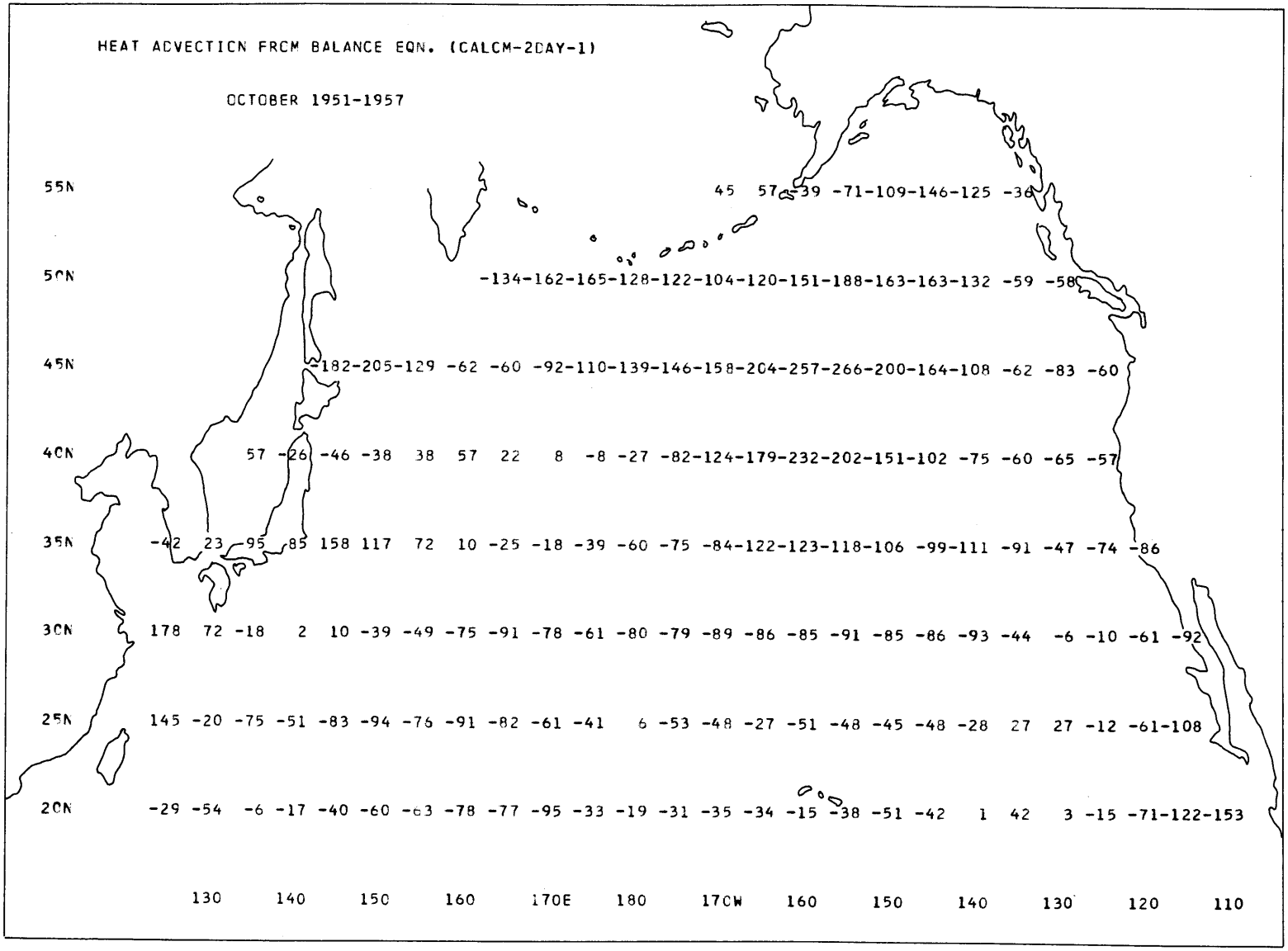

Figure A117. 7-year average values of heat advection determined from the heat balance equation. October 1951-1957. (cal/cm^2/day)

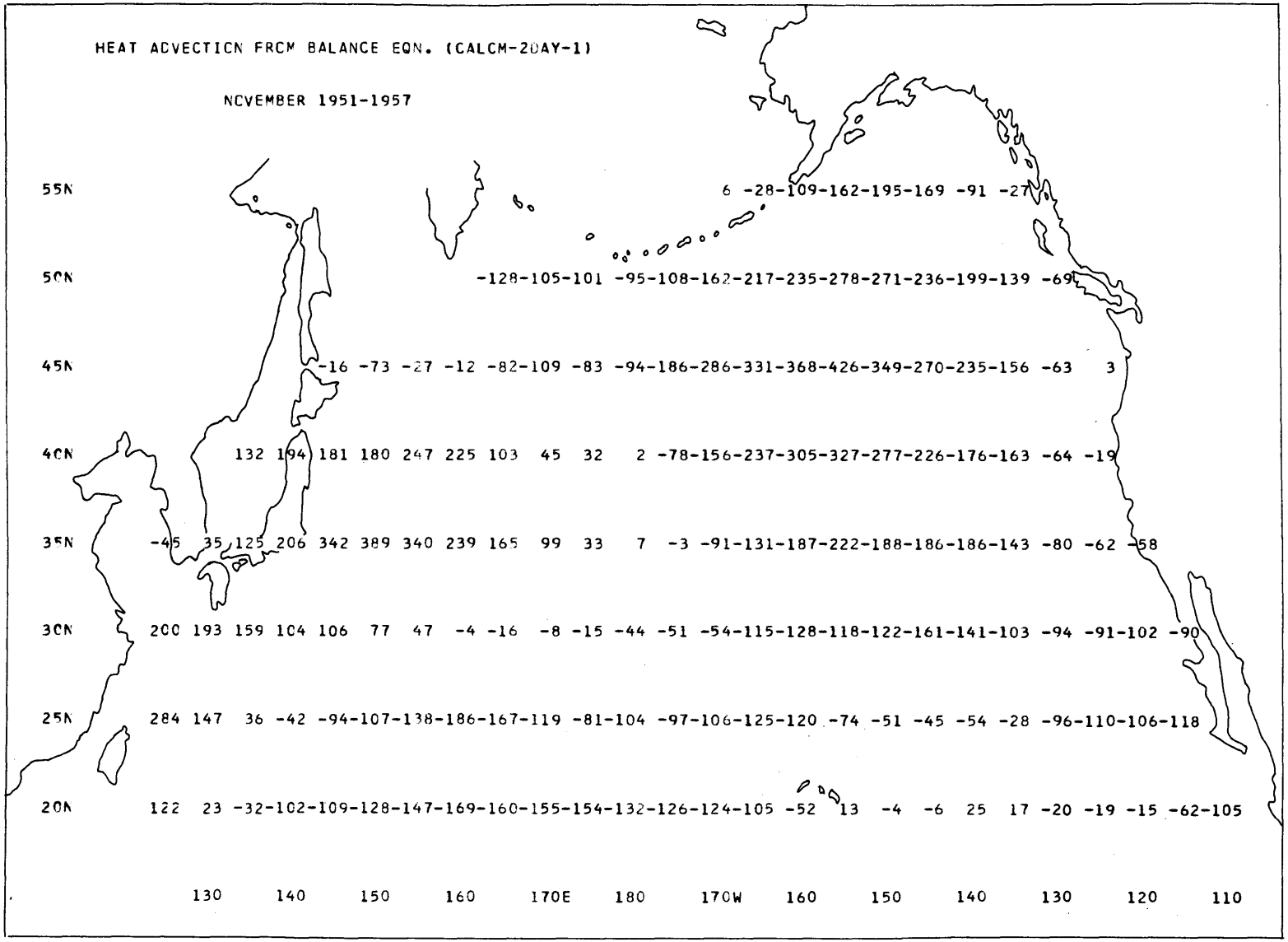

Figure A118. 7-year average values of heat advection determined from the heat balance equation. November 1951-1957. (cal/cm^2/day)

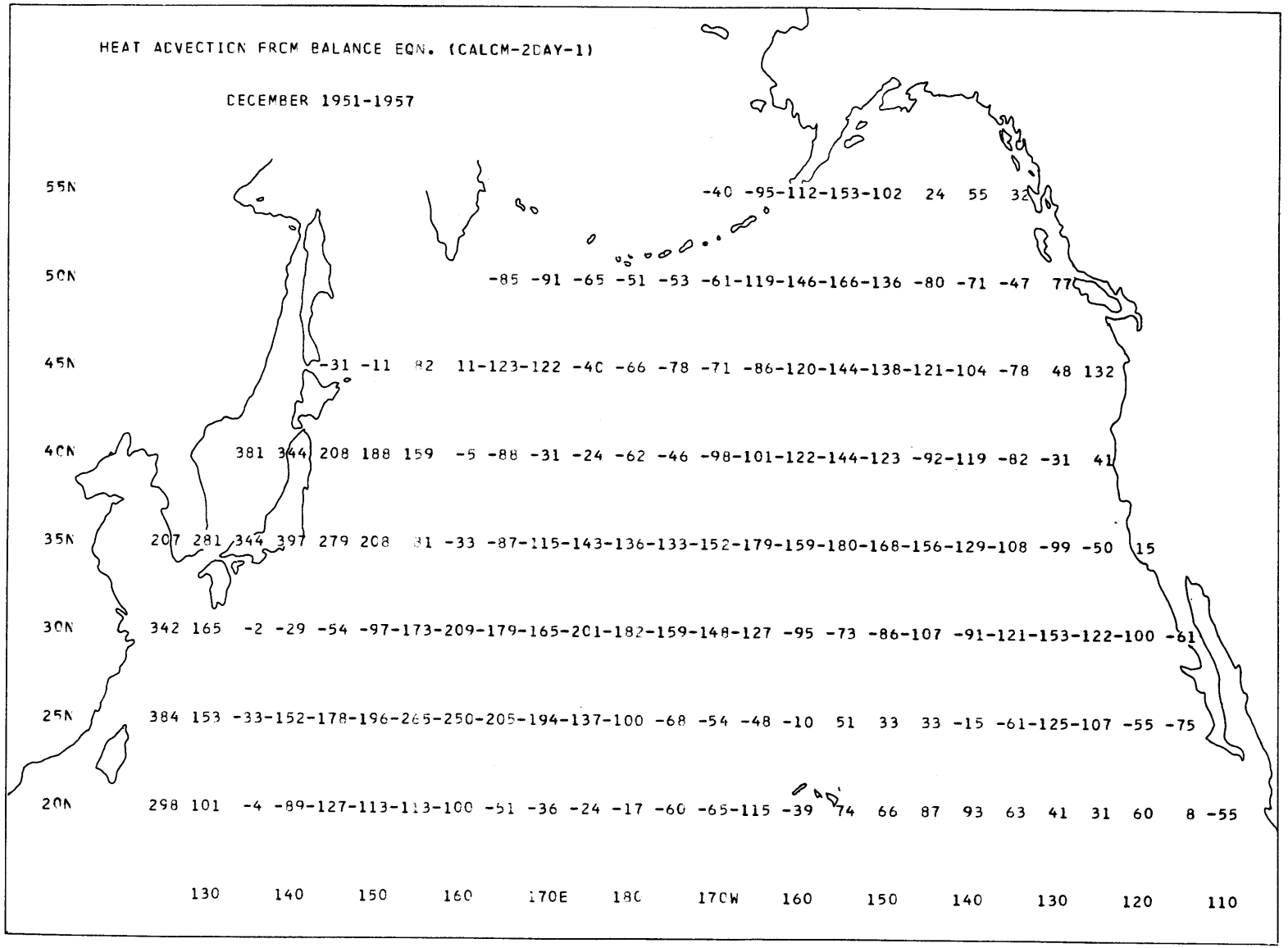

Figure A119. 7-year average values of heat advection determined from the heat balance equation. December 1951-1957. (cal/cm^2/day)